MONASH University

Protein-based functional nanoparticles: Comparison of strategies for design and engineering

Pradeep G. C.

Masters of Pharmacy

A thesis submitted for the degree of *Doctor of Philosophy*

Department of Chemical Engineering

Monash University, Clayton

Australia

May 2018

Copyright notice

Notice 1

This page is intentionally blank

Table of Contents

Abstract

Nanomaterials have been increasingly used in developing new technology and smart materials in several sectors such as biomedicine, energy, and environmental. They may comprise inorganic, organic or biological components and can be fabricated through top-down or bottom-up approaches. Regardless of the components and approaches used to make nanomaterials, each type of nanomaterials has its own strength and weakness. Thus, there is a need to develop efficient strategies to engineer bio- or hybrid (bio-inorganic or bio-organic) functional nanomaterials with improved biocompatibility and strong mechanical and structural properties.

In this thesis, different strategies in designing and engineering protein-based functional nanoparticles have been studied and compared. The strategies include: i) covalent immobilisation of proteins on silica nanoparticles, ii) non-covalent affinity immobilisation of proteins on silica and iron oxide nanoparticles, iii) self-assembly peptide-aided formation of protein-only nanoparticles, iv) combination of self-assembly and affinity adsorption to form clusters of hybrid protein-iron oxide nanoparticles. These engineered protein-based nanoparticles exhibit excellent mechanical and functional properties underpinning the reusable and recovery features.

This thesis comprises four experimental chapters ranging from controlled immobilisation through covalent immobilisation and non-covalent affinity immobilisation to better-controlled functional particles by self-assembly and combination of self-assembly and affinity adsorption. The work promises a platform technology to engineer protein-mediated functional nanoparticles for industrial, biotechnology, and medical applications. In the first experimental chapter of the thesis, Bovine carbonic anhydrase (BCA) was covalently immobilised on the chemically modified surface of mesoporous silica nanoparticles (MSN). The surface density of functional group was diluted to create adequate space between a functional group on the surface of silica particles to reduce the steric effect, enabling efficient immobilisation of BCA. The second experimental chapter includes the non-

covalent affinity immobilisation of two enzymes, BCA and carbonic anhydrase from *Thiomicrospira crunogena* (TmCA). BCA fused with silica binding peptide (BCA-cob) is attached to the surface of unmodified mesoporous silica through affinity binding, while TmCA fused with iron-oxide binding peptide (Mms6-TmCA) facilitates binding of the fusion protein on iron oxide nanoparticles (IONP). In the third chapter, the biological components (proteins and enzyme) are used to produce protein-only nanoparticles facilitated by self-assembly peptides. Two proteins: BCA and green fluorescence protein (GFP) and three peptides ($P_{11}4$, Pep2, and Pep4) are engineered to study the controlled formation of enzymatic and fluorescence nanoparticles. The last experimental chapter extends the concept to engineering nanoparticles into a supra-architecture with tuneable and functional properties, combining self-assembly and affinity binding. Different sizes of iron oxide nanoparticles and variable triggering conditions have been manipulated to achieve desired high hierarchical structures.

In summary, this thesis delivers a comparison of different strategies to produce protein-based functional nanoparticles with attractive properties such as tuneable size and stimuli responsiveness. This research has built a new platform for designing protein-based functional nanomaterials that may have diverse applications in biomedical, health, and environmental sectors.

Declaration

This declaration is to be included in a standard thesis. Students should reproduce this section in their thesis verbatim.

This thesis contains no material which has been accepted for the award of any other degree or diploma at any university or equivalent institution and that, to the best of my knowledge and belief, this thesis contains no material previously published or written by another person, except where due reference is made in the text of the thesis.

Signature: 

Print Name: Pradeep G. C.

Date: 21st May 2018

This page is intentionally blank

Acknowledgments

I would like to express my deepest appreciation and sincere gratitude to my advisors: Dr. Lizhong He, Associate Prof. Victoria Haritos, and Dr. Geoff Dumsday for their continuous support, guidance, and immense knowledge during my Ph.D. research. Special thanks to Ms. Lilyanne Price for connecting me with Dr. Lizhong. I acknowledge New Horizon Research Scholarship on the behalf of Faculty of Engineering, Monash University and CSIRO, Clayton.

Beside my advisors, I am thankful to my thesis committee, Prof. Raman Singh (chairperson), Prof. Wei Shen, and Dr. Yuan Gao (examiners) for their insightful comments, suggestions, and an example to be a good scientist.

This research involves several inputs from the research centers and departments with their innovative techniques and instruments. It would not have been possible without the help and support from wonderful people of these facilities. I would like to thank Dr. David Steer from Biomedical Proteomics facilities in helping me with Mass Spectrometry and Intact Mass analysis results. Big thanks to Drs. Peter Miller, Amelia Liu, Xi Ya Fang, Russell King, Emily Chen, and Tim Williams at Monash Centre for Electron Microscopy for their suggestions, training, and assistance to use scanning and transmission electron microscopes. I thank Drs. Georg Ramn and Adam Costin at Clive and Vera Ramaciotti Centre for Structural Cryo-Electron Microscopy for the necessary training and access to the facilities. I would like to thank Ms. Kim Phu for her help in Micromeritics ASAP 2020, department training, risk assessments, and safe work instructions during my Ph.D. research. I am grateful to my lovely, helpful, and respected senior and current staffs at BEL, Lab 215, and Chemical Engineering department for their constant support, fun, and encouragement during my tenure at Monash University.

I am indebtedness to Dr. Bhuvana Kamath Shanbhag for her assistance from the design of self-assembly peptides to guidance in the experimental parts, interpreting results, and editing of chapter 5. An enormous help from my undergraduate project students Luke Charles McPhail and Sherilyn Roseann to study the covalent immobilisation made it possible to develop into Chapter 3 of this thesis.

Many thanks to Ms. Tayyaba Younas for help in TEM imaging, Mr. Chang Liu for his help to design and ordering of fluorescence protein and Dr. Zhengyang Zhao for advice on the synthesis of silica nanoparticles. I would also like to thank Prof. Rui Nain for the invitation and help during my study at Qingdao Institute of Bioenergy and Bioprocess Technology (QIBEBT), Chinese Academy of Sciences, Qingdao, China. I acknowledge Shenzhen Innova Nanobodi Co., Ltd. for the financial help during my stay at Qingdao, China. My loads of thanks to my Nepali friends in Monash and around the globe for their constant support and interaction.

Finally, yet importantly, I am very grateful to my family members for their moral support during every moment of the Ph.D. life. I am thankful to my parents: Jhapendra Bahadur G.C. and Laxmi G.C. and father-mother in-laws: Chitra Bahadur Pachhain and Shanti Pachhain for their unwavering encouragement, serenity, and trustworthiness without which this Ph.D. would only be my dream. Many thanks to my sweet and beautiful wife Ranjana Pachhain for her incessant love and care and to my extended family Prava G.C. Rishikanta Parajuli, Pashupati G.C., Deepa G.C., Preju, Prayash, Prasish, and Pratikshya who supported and encouraged during the study.

With the saying

"Nothing is pure than parent's love and care"

I would like to dedicate this thesis to my parents

Jhapendra Bahadur G.C. and Laxmi G.C.

This page is intentionally blank

CHAPTER 1

INTRODUCTION

This page is intentionally blank

CHAPTER 1
INTRODUCTION

1.1 Background

Nanomaterials are materials with a single unit size or characteristic length ranging from 1-1000 nm (but typically within 1-100 nm). They exhibit higher biological, chemical, mechanical, and electronic properties (Meier, 1999; Merhari, 2009; Tsuzuki, 2009). They are extensively used in various applications such as electronics, environment, renewable engineering, biomedicine and textile industries as presented in Figure 1.1 (Singh et al., 2016; Tsuzuki, 2009). The global market for nanomaterials was $14.7 B in 2015 and is expected to reach $55 B by 2022, supported by a compound annual growth rate of 20.7% (Global Opportunity Analysis and Industry Forecast, 2014-2022).

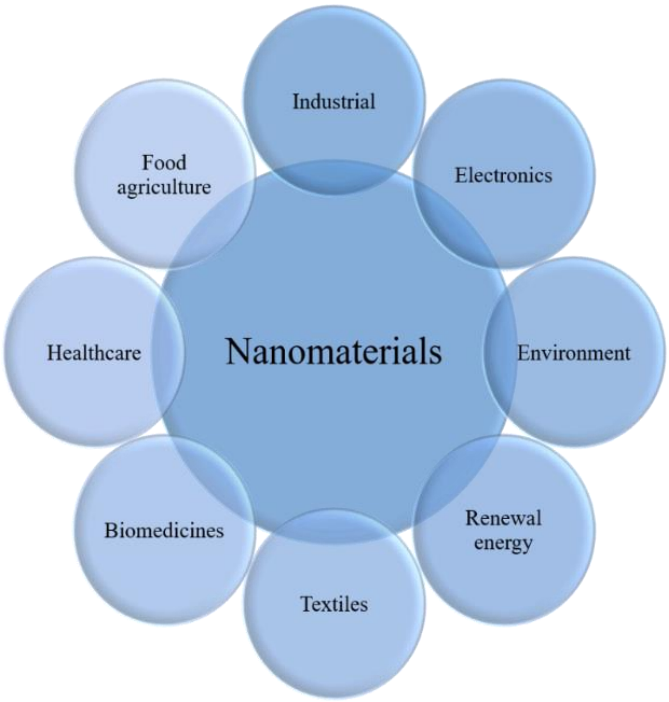

***Figure 1.1**: Application of nanomaterials in different sectors. Reproduced from Tsuzuki et al. (Tsuzuki, 2009).*

Nanomaterials can be composed of inorganic, organic, and biological components. Inorganic and organic nanomaterials such as TiO_2, Al_2O_3, ZrO_2, Fe_3O_4, SiO_2, polymers, diamond, and graphite typically result from the formation of covalent or ionic bonds. These nanomaterials have been used in biomedicine, catalysis, and sensing (De et al., 2008). However, the potential for inorganic nanomaterials is limited due to biocompatibility, toxicity, and environmental issues (Ray et al., 2009). Thus, there has been a concerted effort to seek an alternative way to produce and use nanomaterials by developing biological and hybrid nanomaterials. Bio-nanomaterials can be composed entirely of biological components such as proteins or enzymes. Pure protein nanomaterials are gaining strong interest, as they are environmentally benign, nontoxic and enzyme-based nanomaterials catalyse highly specific reactions and work under mild conditions (Choi et al., 2015; Li et al., 2012).

Currently, covalent immobilisation of proteins onto nanomaterials is one of the most popular approaches for fabricating hybrid nanomaterials using chemically modified inorganic nanoparticles and biological components. Covalent immobilisation binds the protein to the matrix strongly and has a low level of protein loss but can reduce protein activity due to steric hindrance, multipoint attachment occluding the active site, and requires the use of chemicals for the surface modification prior to protein attachment (Homaei et al., 2013). Thus, there a need to improve the approach to protein immobilisation for the efficient protein binding and activity.

The use of self-assembling peptides to assemble protein-based nanoparticles has drawn attention to the potential formation of particles that have biocompatibility, molecular recognition and remain highly stable under conditions such as elevated temperature, and exposure to detergents and other denaturing conditions (Dinca et al., 2008). More recently,

protein-based nanoparticles with tuneable size have been produced by the fusion of self-assembly peptides to enzymes and the use of triggering conditions to control formation and particle size.

In addition, there have been attempts to assemble nanoparticles into higher structures - hierarchically-structured nanomaterials – and in doing so design a new generation of functional materials. These superior architectural forms such as super-lattices (Udayabhaskararao et al., 2017), capsules (Evers et al., 2016), and clusters (Lee et al., 2013) have been synthesised but the materials have limited functionality; i.e. these materials do not exhibit switchable or tuneable properties. Thus, a new approach is needed to design nanomaterials with improved functional properties, greater reusability and recovery efficiency.

1.2 Scope of Research

In this thesis, a new concept is explored enabling customised synthesis of nanomaterials that ensures characteristics such as functional biocatalysis, reusability, tracking and imaging, and a tunable architecture. Here, nanomaterial fabrication includes: enzyme/protein, immobilisation and functionalised particles as illustrated in Figure 1.2.

In this thesis, Bovine Carbonic Anhydrase (BCA) and Green Fluorescent Protein (GFP) were used as exemplary enzymes/protein. BCA is a zinc metalloenzyme that catalyses the interconversion of CO_2 to form bicarbonate and a proton with a turnover rate of up to 10^6 s^{-1} (Kernohan, 1965). GFP is a fluorescent protein used for tracking and imaging of the nanomaterials (Chalfie et al., 1994; Ibraheem & Campbell, 2010). Two forms of inorganic particles were used as supporting bases: silica nanoparticles and iron oxide nanoparticles which are broadly used in nanotechnology. Selective binding of proteins onto these nanoparticles was

achieved using two binding peptides, silica binding peptide and iron oxide binding protein. Additionally, taking a protein-engineering approach, self-assembling peptides were linked to the proteins to produce two different types of functionalised nanoparticles: self-assembling protein nanoparticles and iron oxide nanoclusters. The scope of this thesis covers engineering protein nanomaterials for biocatalytic and functional protein applications.

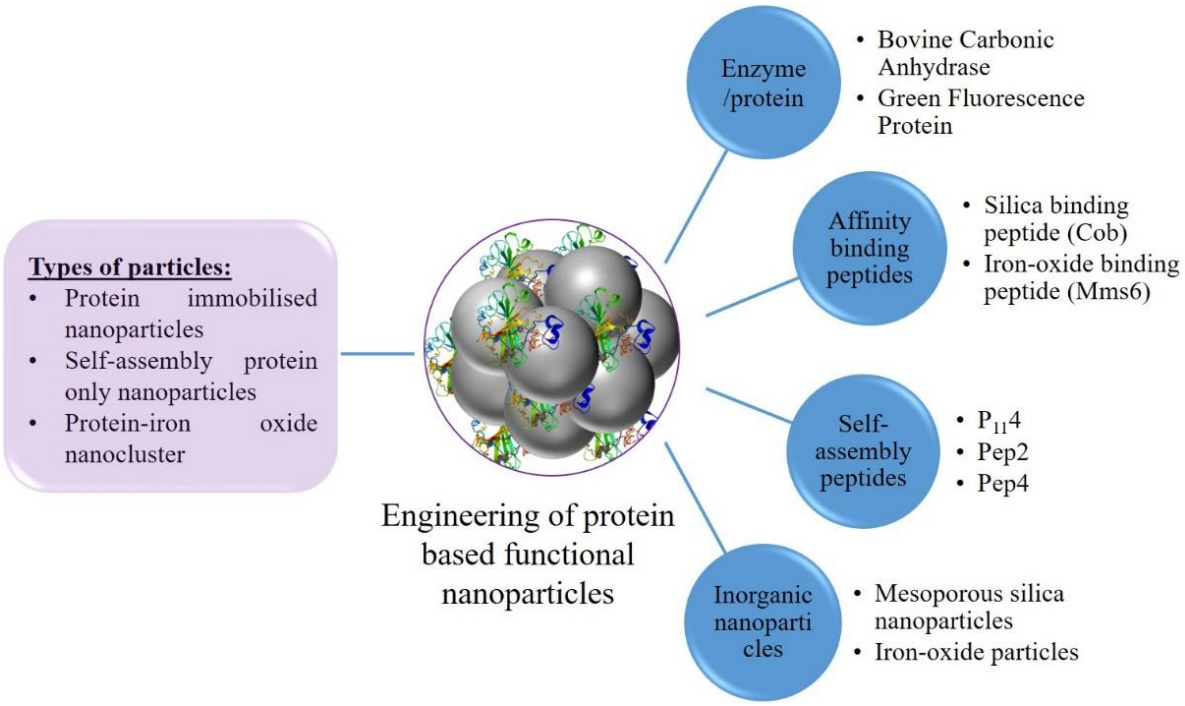

***Figure 1.2**: Diagram illustrating the scope of the research. The diagram illustrates the targeted types of particles (left side) and the components used (left side).*

1.3 Research Objective

This thesis aims to engineer nanomaterials integrating inorganic and/or biological components under controlled/tunable conditions. The major objective of this research is to develop approaches for engineering protein-based nanomaterials that have multi-functional attributes such as being tuneable, trackable, and imageable with the potential for reusability and recovery.

To achieve this goal, a systematic study has been carried out with following aims:

- Optimise the covalent immobilisation of an enzyme on silica nanoparticles
- Deploy surface-binding peptides for non-covalent affinity immobilisation
- Produce self-assembling enzyme and fluorescent protein-based nanoparticles with trackable and imaging properties
- Engineering bifunctional nanoparticle clusters by integrating self-assembly and iron oxide binding peptides together with iron oxide nanoparticles

1.4 Thesis Outline

Chapter 1: Introduction

The first chapter provides the background and motivation for this Ph.D. project. It describes three main aspects, i) problem statement, ii) rationale of the research work and iii) key objectives. It also presents background research on protein-based nanomaterials including the current market and future demand for advanced nanomaterials.

Chapter 2: Literature Review

Chapter two will critically review the current work in the field of nanomaterials and nanotechnology with the focus on the designing and engineering of protein-based nanomaterials. The chapter will first discuss various strategies to produce protein-based nanoparticles using covalent and non-covalent immobilisation. Furthermore, the engineering of nanoparticles from molecular components to nanoparticles and from nanoparticles to higher suprastructure with fine architecture has been reviewed. This chapter also provides a comprehensive understanding of existing protein-based nanomaterials systems (including design, engineering, fusion partners, and functional properties), and identifies the research gap and links these with the aims of this Ph.D. research.

Chapter 3 Effect of Surface Chemistry for Covalent Immobilisation of Carbonic Anhydrase on Mesoporous Silica Nanoparticles

This chapter describes the formation of protein-immobilised nanoparticles via covalent attachment with an emphasis on surface chemistry optimisation of mesoporous silica nanoparticles to improve enzyme immobilisation. For efficient immobilisation, the effect of density of functional groups is studied by introducing spacers between the functional groups to control their surface density. Adequate spaces are created by diluting the functional group using various concentrations of diluent. The various molar concentration of (3-glycidyloxypropyl) trimethoxysilane and trimethoxysilane are used to dilute the surface of the glutaraldehyde-functionalised silica nanoparticles. The catalytic property of engineered protein nanoparticles is evaluated with reuse by comparison with free enzyme and particles without controlled surfaces and then applied to the conversion of CO_2.

Chapter 4 Surface Binding Peptides Enable Facial Preparation of Highly Stable Protein-coated Nanoparticles

Following on from covalent immobilisation, non-covalent affinity immobilisation through surface-binding peptides is studied. In this chapter, BCA and TmCA are fused with silica binding peptide (BCA-cob) and iron oxide binding protein (Mms6-TmCA), respectively. BCA-cob is attached to the surface of unmodified mesoporous silica nanoparticle by the interaction between cob and silica whereas Mms6-TmCA is bound to iron oxide nanoparticles through affinity binding of Mms6. The factors that affect the BCA binding on the surface of inorganic nanoparticles was studied and compared with the wild-type enzyme, and the reusability, recovery, and biocatalytic efficiency of fusion protein is demonstrated.

Chapter 5 Comparisons of Self-assembly Peptides for the Formation of Protein Nanoparticles with Stimuli Responsive Ability

In this chapter, the self-assembly peptide is engineered and three different forms are fused to proteins and tested for the formation of all-protein nanoparticles without the need of a solid-support (as was used in Chapters 3 and 4). Three peptides ($P_{11}4$, Pep2, and Pep4), two different proteins (BCA and GFP), and a single linker (GS) were used to engineer a series of protein-peptide fusion systems. Each self-assembly peptide has 11 amino acid residues with a slight change in an amino acid sequence that are hypothesised to alter the self-assembly mechanism and thus different controlling conditions. The fusion proteins, BCA-$P_{11}4$, BCA-Pep2, and BCA-Pep4 were used to compare self-assembly mechanisms by manipulating pH and addtion of metal ions to drive the self-assembly process. GFP-$P_{11}4$ was used to prepare fluorescent protein nanoparticles, and BCA-$P_{11}4$ was used as a diluent molecule to manipulate the fluorescent intensity of GFP nanoparticles. This chapter describes a platform for engineering protein nanoparticles that have different functionalities and triggerable conditions for particle formation.

Chapter 6 Combining Affinity Binding and Self-assembly Peptides to Engineer Tuneable Iron Oxide Nanoclusters

In this part of the research, proteins are designed to have both surface binding and self-assembly abilities, enabling engineering of nanoparticle clusters with higher ordered suprastructures built around iron oxide nanoparticles (IONP). Enzyme-peptide fusion systems were designed by fusing Mms6c (iron-binding peptide, presented in Chapter 4) and $P_{11}4$ (self-assembly peptide, presented in chapter 5) on either N- or C- termini of the BCA molecule, facilitating dual functions of nanoparticle binding and self-assembly. Variable-sized IONPs (5 to 30 nm) and Mms6c-BCA-$P_{11}4$ were deployed to produce protein-based supra-structured nanomaterials

with self-assembly, tuneable, and enzymatic functionalities. This supra-hierarchical particle clusters provides a platform technology to engineer nanoparticles with highly ordered structures with potential applications in the biotechnology, health, and industrial sectors.

Chapter 7: Conclusion and Future Work

This chapter comprises the main conclusions of this research work. Furthermore, it suggest the future scope of this research area and suggestions of other possible approaches to engineer a higher order of nanomaterials for wide range of application.

1.5 References

Chalfie, M., Tu, G., Euskirchen, G., Ward, W.W., Prasher, D.C. 1994. Green fluorescent protein as a marker for gene expression. *Science*, **263**, 802+.

Choi, J.-M., Han, S.-S., Kim, H.-S. 2015. Industrial applications of enzyme biocatalysis: Current status and future aspects. *Biotechnology Advances*, **33**(7), 1443-1454.

De, M., Ghosh, P.S., Rotello, V.M. 2008. Applications of nanoparticles in biology. *Advanced Materials*, **20**(22), 4225-4241.

Dinca, V., Kasotakis, E., Catherine, J., Mourka, A., Ranella, A., Ovsianikov, A., Chichkov, B.N., Farsari, M., Mitraki, A., Fotakis, C. 2008. Directed three-dimensional patterning of self-assembled peptide fibrils. *Nano Letters*, **8**(2), 538-543.

Evers, C.H., Luiken, J.A., Bolhuis, P.G., Kegel, W.K. 2016. Self-assembly of microcapsules via colloidal bond hybridization and anisotropy. *Nature*, **534**(7607), 364.

Homaei, A.A., Sariri, R., Vianello, F., Stevanato, R. 2013. Enzyme immobilization: an update. *J Chem Biol*, **6**(4), 185-205.

Ibraheem, A., Campbell, R.E. 2010. Designs and applications of fluorescent protein-based biosensors. *Current Opinion in Chemical Biology*, **14**(1), 30-36.

Kernohan, J. 1965. The pH-activity curve of bovine carbonic anhydrase and its relationship to the inhibition of the enzyme by anions. *Biochimica et Biophysica Acta (BBA)-Enzymology and Biological Oxidation*, **96**(2), 304-317.

Lee, S.H., Yu, S.-H., Lee, J.E., Jin, A., Lee, D.J., Lee, N., Jo, H., Shin, K., Ahn, T.-Y., Kim, Y.-W. 2013. Self-assembled Fe_3O_4 nanoparticle clusters as high-performance anodes for lithium ion batteries via geometric confinement. *Nano letters*, **13**(9), 4249-4256.

Li, S., Yang, X., Yang, S., Zhu, M., Wang, X. 2012. Technology prospecting on enzymes: application, marketing and engineering. *Comput Struct Biotechnol J*, **2**, e201209017.

Meier, W. 1999. Nanostructure synthesis using surfactants and copolymers. *Current Opinion in Colloid & Interface Science*, **4**(1), 6-14.

Merhari, L. 2009. *Hybrid nanocomposites for nanotechnology*. Springer.

Ray, P.C., Yu, H., Fu, P.P. 2009. Toxicity and environmental risks of nanomaterials: challenges and future needs. *J Environ Sci Health C Environ Carcinog Ecotoxicol Rev*, **27**(1), 1-35.

Singh, R., Kumar, M., Mittal, A., Mehta, P.K. 2016. Microbial enzymes: industrial progress in 21st century. *3 Biotech*, **6**(2), 174.

Tsuzuki, T. 2009. Commercial scale production of inorganic nanoparticles. *International journal of nanotechnology*, **6**(5-6), 567-578.

Udayabhaskararao, T., Altantzis, T., Houben, L., Coronado-Puchau, M., Langer, J., Popovitz-Biro, R., Liz-Marzán, L.M., Vuković, L., Král, P., Bals, S. 2017. Tunable porous nanoallotropes prepared by post-assembly etching of binary nanoparticle superlattices. *Science*, **358**(6362), 514-518.

This page is intentionally blank

CHAPTER 2

LITERATURE REVIEW

This page is intentionally blank

CHAPTER 2
LITERATURE REVIEW

2.1 Nanomaterials

The definition of nanomaterials varies with different organisations. The International Organisation for Standardisation (ISO/TS80004) classifies nanomaterials as "material with any external dimension in the nanoscale or having an internal structure or surface structure in the nanoscale" and defines nanoscale as "length range approximately from 1 nm to 100 nm" (Boverhof et al., 2015; Lovestam et al., 2010). European Commission defined nanomaterials as "natural, incidental or manufactured materials containing particles, in an unbound state or as an aggregate or as an agglomerate and for 50% or more of the particles in the number size distribution, one or more external dimensions is in the size range of 1 to 100 nm" (Lovestam et al., 2010). These nanomaterials may be in the form of particles, tubes, rods, or fibers. Nanomaterials have the same composition as their bulk counterparts but due to their size exhibit superior physical, chemical, biological, and mechanical properties all of which can be applied in the field of nanotechnology (Meier, 1999; Merhari, 2009).

The notion of nanotechnology emerged when Nobel laureate Professor Richard Feynman gave a lecture "There's Plenty of Room at Bottom" on Dec 29, 1959, at the American Physical Society meeting at California Institute of Technology (Caltech). In his talk, he described the potential of developing a system for deploying individual molecules and atoms. However, only after the discovery of Scanning Tunneling Microscope (STM) and high-resolution transmission microscopy (HRTEM), techniques which were used for imaging fullerenes in 1985 (Kroto et al., 1985) and carbon nanotubes in 1991 (Iijima, 1991), did the era of nanotechnology emerge.

Ever since, there has been a huge interest and innovative research into synthesis, characterisation, and manipulation of nanomaterials.

2.1.1 Synthesis of Nanomaterials

The physical characteristics of nanomaterials such as size, morphology, and surface area play a vital role in their function and application. The prevalence of such characteristic strongly depends on the routes of synthesis. Typically, nanomaterials are produced using two different general approaches, i.e. top down and bottom up (Reithmaier et al., 2009), as illustrated in Figure 2. 1.

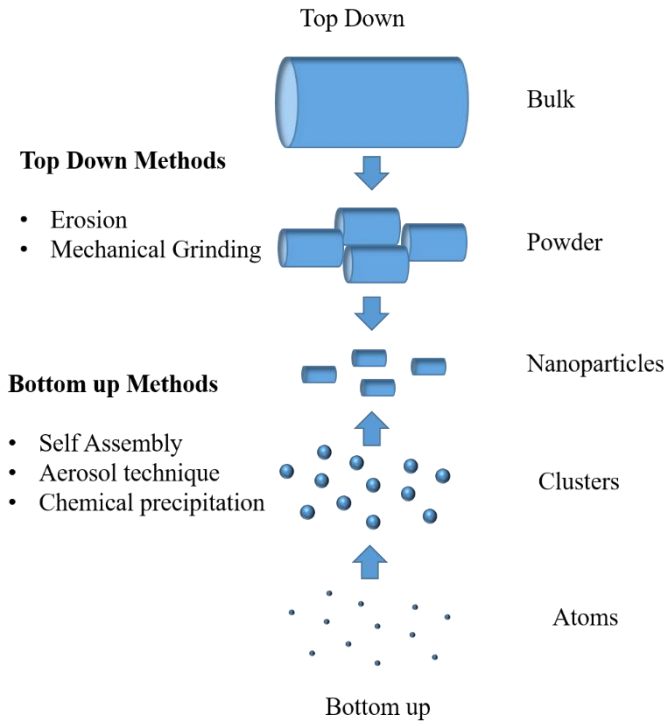

Figure 2.1: *Schematic diagram illustrating two different approaches to synthesise nanomaterials*

a) Top-down approach

Top-down approaches start with bulk materials and relies on physical processes such as mechanical, chemical, electrical or/and thermal methods. Top-down methods use grinding and

erosion to process the bulk materials to fine nanoscale materials. However, the major problems with top-down approaches are the variable nature of surface structures (Cao, 2004), wide particle size distribution, and sometime process is time-consuming (Manh et al., 2009). These problems cause major changes in physical characteristics and surface chemistry of nanomaterials. Additionally, the exposure time and milling speed affect the nanostructure of the final products. The top-down approach has been used for the synthesis of nanomaterials such as magnetic materials (Manh et al., 2009), materials for electronic applications (Chen et al., 2010b), and nanoscale drugs (Basa et al., 2008).

b) Bottom-up approach

Bottom-up approach starts at the atomic-molecular- or nano-scale and rely on individual molecular structures, self-assembly, and dynamic behavior (Meier, 1999; Reithmaier et al., 2009). The bottom-up methods mostly adhere with routes such as self-assembly, aerosol techniques, and chemical precipitation. In most instances, the physical properties of materials are similar in term of chemical compositions, crystallinity, and structures regardless of the synthesis routes. These materials have less defects, similar chemical composition, and better structural ordering.

2.1.2 Types of Nanomaterials

Nanomaterials have been categorized based on shape, size, composition, and functionality. For example, in 1993 Siegel classified nanomaterials into four dimensional structures, zero- (nanocrystals), one (graphene, thin film), two (carbon nanotubes), and three-dimensional (quantum dots or nanoparticles and fullerene nanostructures) (Siegel, 1993). In this work, we have categorized nanomaterials that are relevant to biotechnology research based on composition: inorganic, organic, biological and hybrid nanomaterials.

a) Inorganic and organic nanomaterials

Inorganic and organic nanomaterials have become a focal point in biotechnological applications due to their unique physical properties such as defined size, optical, magnetic, electronic and catalytic properties. Such materials, particularly inorganic nanomaterials are typically synthesised by the co-precipitation of salts mediated by the covalent or metallic bond and orientation of the building blocks. Examples of these nanomaterials include TiO_2, Al_2O_3, ZrO_2, SiO_2, ZnO, CeO_2, MoS_2, polymers, diamond, and graphite which are extensively used in biomedicine, catalysis, and sensing (De et al., 2008).

i) Mesoporous silica nanoparticles

The silica nanoparticles are a major unit in designing and engineering nanostructures for a wide range of application. These particles comprise of porous and nonporous. However, the mesoporous silica nanoparticles (MSN) are of greater interest because of highly ordered structures with larger surface areas. According to IUPAC classification, mesoporous nanoparticles have the pores ranging 2-50 nm and have spherical or cylindrical shapes (Zhang & Cresswell, 2016).

The MSN were first reported with name MCM-X (Mobile Crystalline of Materials) and synthesised by Mobile Corporation laboratories in 1992 (Kresge et al., 1992). This became the starting point to broadly use MSN in the field of research. Even before this, there was a patent in 1971 to synthesise low-density silica using a cationic surfactant (Vincent et al., 1971). In 1998, Zhao et al. (Zhao et al., 1998a; Zhao et al., 1998b) synthesised MSN using a non-ionic triblock surfactant. They gave the name SBA-X (Santa Barbara Amorphous), X refers to specific pore structure and surfactant used for the synthesis. For example, SBA-15 refers using

P123 surfactant to produce hexagonally ordered cylindrical pores and SBA-16 refers using F127 surfactant to produce spherical pores centred in cubic structure.

SBA-15 mesoporous particles synthesised using non-ionic surfactant Pluronic triblock copolymer P123. The surfactant forms micelles that acts as a template to form mesoporous structure while synthesising the particles. They are highly ordered cylindrical pores in hexagonal orders with pore ranges from 2-26 nm (Cao et al., 2009; Zhao et al., 1998a; Zhao et al., 1998b). MSN have variable pore length from 200 nm to several microns (Zhang et al., 2004). MSN have a huge surface area and highly depends on the procedure and applications, and a high value of 838 m^2/g of the particles was reported in literature (Thielemann et al., 2011).

ii) Superparamagnetic iron oxide nanoparticles

The iron oxide nanoparticles are used in wide ranges of applications due to their multivalent oxidation states, low Curie temperature, and high magnetic susceptibility (Faraji et al., 2010; Woo et al., 2004). The most studied particles are Magnetite (Fe_3O_4) and Maghemite (γ-Fe_2O_3) (Gupta & Gupta, 2005). Magnetite is a black ferromagnetic mineral and has both oxidation state of iron Fe (II) and Fe (III). Maghemite is a red-brown ferromagnetic mineral that is deficient in Fe (II). Magnetite is a promising candidate for biomedical application with proven biocompatibility (Schwertmann & Cornell, 1991). The iron oxide nanoparticles (IONP) exhibit quantum size effect showing superparamagnetic property. The superparamagnetism is the unique property of Fe_3O_4 in small, single-domain particles without magnetic memory. In brief, when ferromagnetic particles like iron are reduced in size to less than 40 nm, they appear as single-domain magnetic particles and when placed in an external magnetic field, the particles

develop strong internal magnetisation from exchange coupling of electrons within resulting in a superparamagnetic iron oxide nanoparticle (Lin et al., 2008).

The superparamagnetic iron oxide nanoparticles (SIONP) are synthesised employing physical (aerosol, powder ball milling, gas phase deposition, etc.), chemical (co-precipitation, microemulsion, hydrothermal, chemical, thermal decomposition, etc.), and biological (fungi, bacteria, and protein-mediated) approaches (Mahmoudi et al., 2011b). Several companies such as; Ocean nanotech, Stemcell technologies, Chemical, Micromod, Dexter magnetic technologies, etc. commercially produce the SIONP. SPION are used in biomedical applications such as in vitro cell manipulation, bioseparations, and drug delivery (Chen et al., 2010a; Rozhkova, 2011; Yin & Alivisatos, 2004). The United State and European Union regulation agencies had approved to incorporate SPION in commercial MRI formulation due to the better in vivo contrast (Wang, 2013). These nano size SIONP can be transported in the desired direction by applying magnetic field but does not exhibit magnetic memory allowing them to disperse in the suspension.

iii) Other inorganic nanoparticles

Quantum dots

Quantum dots (QDs) are inorganic nanomaterials with a size between 2-10 nm and produced from the elements of group II-VI or III – V. QDs emits light of tuneable frequencies based on the size, shape, and materials when the electricity or light is supplied (Sabaeian & Khaledi-Nasab, 2012). QDs are composed of core material CdS, CdSe, and CsTe with the shell of ZnS, ZnCd, and CdS (Yong, 2012), (Stachowski et al., 2014). The quantum dot has intrinsic features such as high brightness, variable absorption spectra but narrow emission spectra, and high fluorescent quantum yield which makes the materials applicable for the generation of optical

probes in bioassays (Yong, 2012). However, QDs are highly noxious to the living cells and if injected into the cells, they tends to aggregate and also unknown if QDs are cleared from the body (Alivisatos, 1996; Weng & Ren, 2006).

Gold nanoparticles

The synthesis of gold nanoparticles began when Michael Faraday found that the colloidal gold solutions have different properties compared to bulk gold (Edwards & Thomas, 2007). Gold nanoparticles used in research and biomedical application since they are easy to prepare highly stable and bear higher extinction coefficient. Gold nanoparticles are used in photothermal therapy, photoacoustic imaging, and surface-enhanced resonance spectroscopy (Chandra et al., 2013). However, gold nanoparticles are expensive (use ruthenium for the luminescence) and challenging to use them in drug delivery due to biodistrubition, biocompatibility and pharmacokinetic (Arvizo et al., 2010).

b) Bionanomaterials

Bio-nanomaterials are comprised of natural or synthetic biomolecules and synthesised with the utility of noncovalent interaction for the design and self-assembly or self-organisation of the molecules (Lin & Mao, 2011). Molecular self-assembly or self-organisation is a useful approach to manipulate the morphology, particle size, and shaping of nano-architecture. Biological nanomaterials are formed by a number of non-covalent forces such as electrostatic, van der Waals forces, water-mediated hydrogen bonds, hydrophobic and aromatic π-π interactions (Cavalli et al., 2010). Bio-nanomaterials compromise of protein particles, micelles, vesicles, liposomes, polymersomes, dendrimers, nanocapsules and polymeric nanoparticles (Jesus & Grazu, 2012).

c) Hybrid nanomaterials

Hybrid nanoparticles are produced using two or more different types of nanostructures integrated to enhance physical, chemical and multifunctional features (Kim et al., 2009). The materials are typically a composite of bio and inorganic/organic components and synthesised by the addition of each nanocomposite using a bottom-up approach. Based on the composition, the hybrid nanoparticles are categorised into the inorganic-inorganic, organic-inorganic, and bioinorganic nanoparticles.

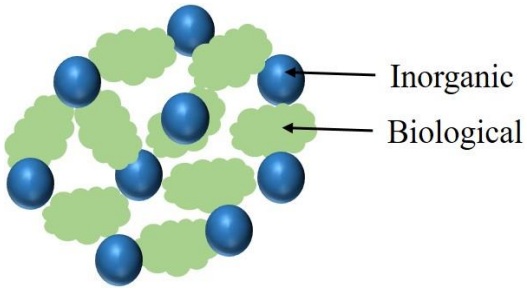

Figure 2.2: *Schematic illustration of hybrid nanoparticles. Self-assembly of hybrid nanoparticles uses inorganic and biological components.*

In general, the components such as inorganic materials are bound to each other using other components such as biological materials proteins, DNA or organic materials like polymers, to enhance the multi-functionality, as illustrated in Figure 2.2.

i) Inorganic-inorganic hybrid nanoparticles

A combination of at least two inorganic nanoparticles is used to produce inorganic hybrid nanoparticles. Inorganic nanoparticles such as quantum dots, iron oxide, and gold nanoparticles are mostly used to produce hybrid nanoparticles and have wide applications in the medical, energy, and biotechnology fields (Kim & Hyeon, 2014; Rao et al., 2006). The hybrid nanoparticles have properties that are developed by engineering composition, structure, shape, and size. For example, the hybrid nanomaterial produced by the deposition of ZnO

nanoparticles on Zn/Se nanosheet is used for the enhanced photocatalytic reduction of CO_2 into methanol using sunlight as a source of the photon (Zhang et al., 2018) (Figure 2.3).

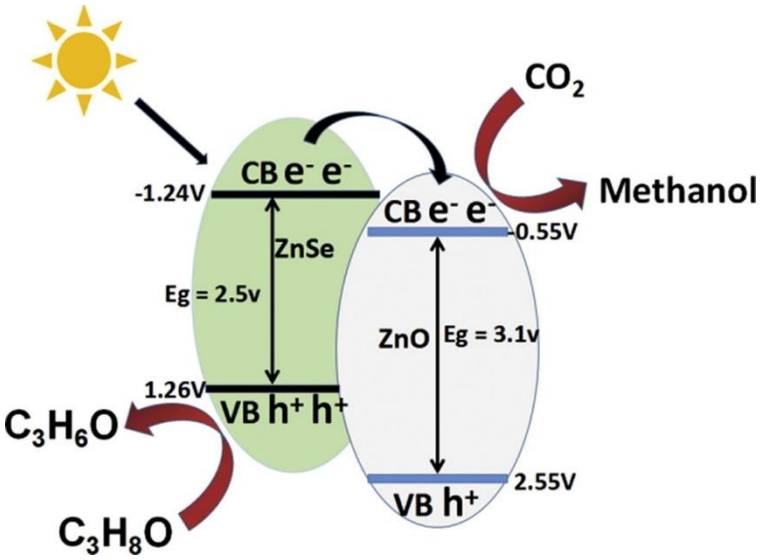

Figure 2.3: *Schematic diagram of CO_2 reduction using ZnO/ZnSe nano composites. This figure was reproduced from Zhang et al. (Zhang et al., 2018).*

Recently, Udayabhaskararao et al. used different size and composition of gold and iron oxide nanoparticles to produce superlattices (Udayabhaskararao et al., 2017). Yang et al. developed systems of mechanised and reactive droplets using gold and iron oxide nanoparticles to produce nanoclusters that are responsive to various stimuli (Yang et al., 2018). These nanoclusters whose formation are tuneable, produced higher hierarchical inorganic structures for various applications (Edel et al., 2013; Kotov, 2017).

ii) Inorganic-organic hybrid nanoparticles

The inorganic-organic hybrid nanoparticles are produced using inorganic and organic components. The inorganic materials normally available in powders or have weak mechanical properties and thus need to be stabilised by the use of organic materials. For example, quantum dots (QDs) are used by conjugating with oligonucleotides (Pathak et al., 2001), phospholipid

(Dubertret et al., 2002), PEG (Polyethylene glycol) (Gao et al., 2004) etc. for development and use in the biomedical applications as shown in Figure 2.4.

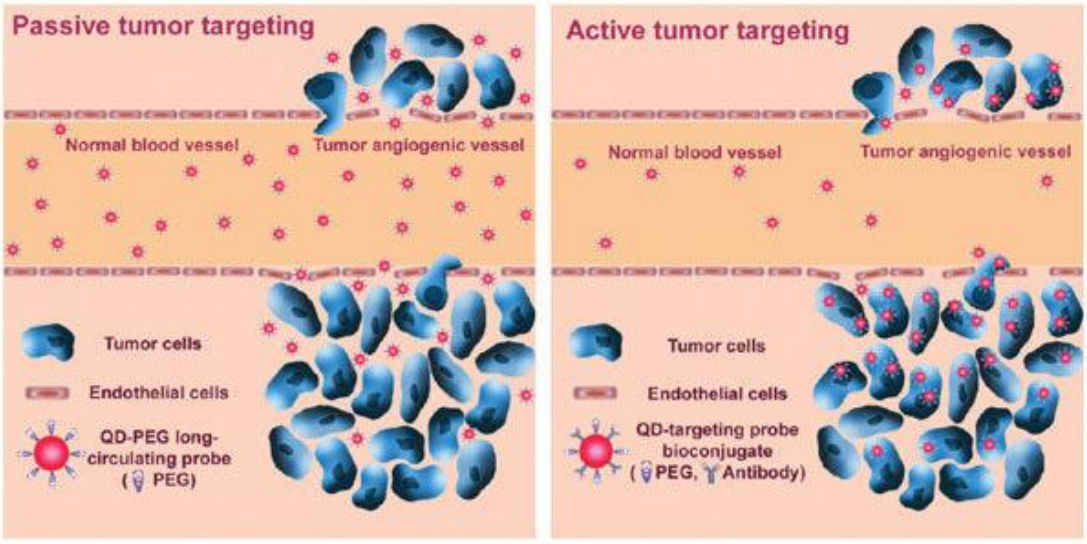

Figure 2.4: *QD-PEG used for retention and permeation in vivo cancer cells through passive and active targeting approach. Here, the QD-PEG hybrid nanomaterials are used to carry tumour-targeting ligands. Figure is reproduced from (Gao et al., 2004)*

iii) Inorganic bio nanoparticles:

Bioinorganic hybrid materials are nano-composites with biological and inorganic components intimately mixed to create a hybrid structure. These hybrid structures are of interest to chemists, physicists, biologists, and material scientists as they enable the development of smart materials that integrate inorganic, organic and biological ideas (Nguyen et al., 2018).

The production of bio-inorganic hybrid materials can be achieved through strategies such as functionalisation: using pre-synthesised functional biomaterials that are compatible with inorganic components via chemical grafting or by embedding in a common solvent to grow a network and in situ generation, through the use of different inducers or/and additives (Sanchez et al., 2011). These hybrid nanomaterials are linked together through simple sol-gel techniques incorporating weaker forces like van der Waals forces, ionic interactions, and hydrogen bond

or through strong covalent bonds via functional groups like alkoxy or carboxyl (Judeinstein & Sanchez, 1996).

The types of materials used in this class can be very diverse. In general, silica nanoparticle-poly-L-lysine and living bacteria (Patwardhan et al., 2003) (Fennouh et al., 2000), calcium carbonate-chitosan and poly(aspartate) (Kato et al., 2002), gold nanoparticles-chitosan (dos Santos et al., 2004), iron oxide-blood exosomes (Qi et al., 2016) and phosphatidylcholine (Burgos-Asperilla et al., 2007), are examples of different types of inorganic-bio nanoparticles used as a carrier molecules tailored for various applications. For example, Qi et al, used superparamagnetic iron oxide-blood exosomes to develop nanoparticle clusters for drug delivery for cancer therapy (Qi et al., 2016), as presented in Figure 2.5. The clusters were loaded with drug doxorubicin and injected into mice as an approach to cancer therapy.

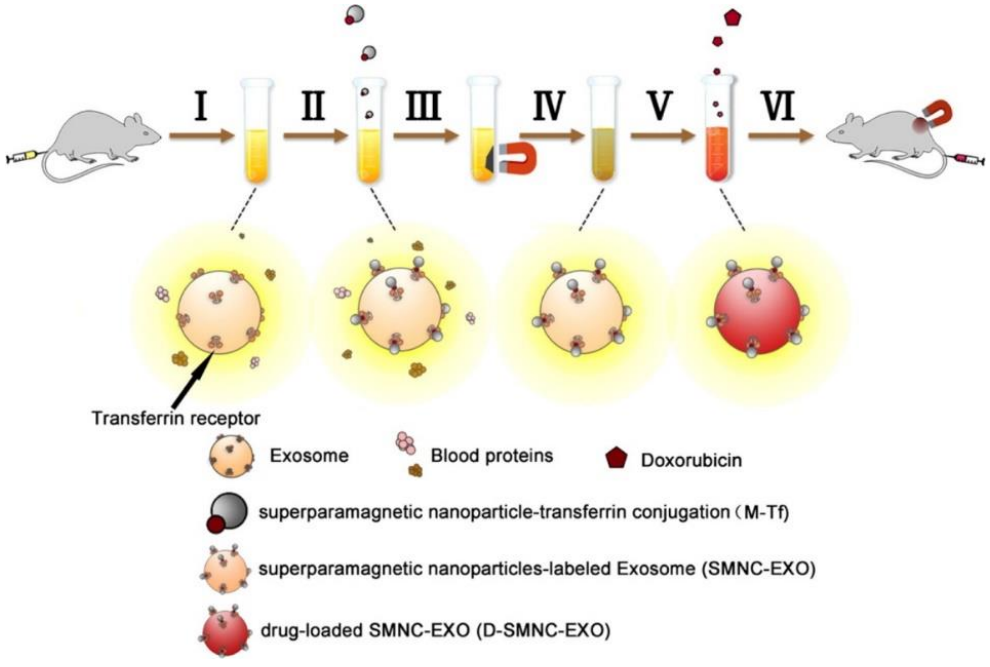

Figure 2.5: *Iron oxide-exosome clusters used to cancer cells. The series of steps includes, i) collection of samples, ii) incubation with transferrin receptor producing iron oxide-exosome clusters, iii) separation of the clusters using magnet, iv) resuspension of clusters, v) doxorubicin loading into the clusters, and vi)injection the clusters into infected mice (tumour). The figure was reproduced from (Qi et al., 2016),*

2.2 Features and Application of Nanomaterials

2.2.1 Surface Area and Reactive Property

Nanomaterials of same composition differs vastly in surface area when compared with large counterparts despite of the same total volume (Figure 2.6). The nanoscale structure with higher surface results in chemically more reactive materials, and some materials that are inert in their bulk state become reactive when produced with nanoscale feature. For example, TiO_2 nanoparticles were found more active compared to large particles during photocatalytic degradation of pollutant (Loryuenyong et al., 2013). The large surface area of nanomaterials has resulted in the development of improved materials with diverse applications including energy storage, separation technologies, product-specific catalysis, biochemical and pharmaceutical separations, construction and manufacturing (Cox, 1999).

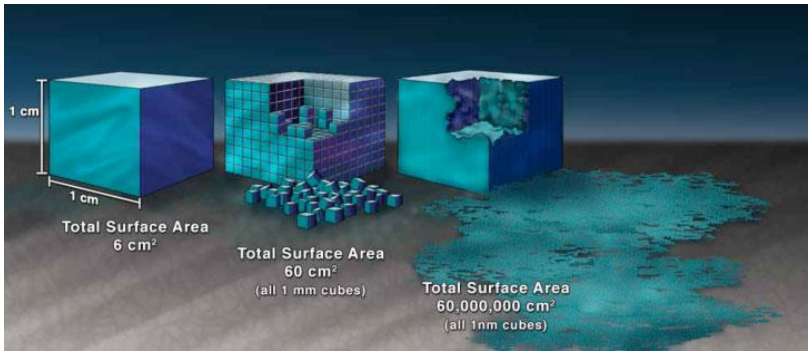

Figure 2.6: *Diagram showing the surface area increase with the change in particle size. Reproduced form Nano.gov (2013)*

2.2.2 Physical Properties

The physical properties such as magnetic properties and colour changes when nanomaterials are reduced to nano-scale. For example, when reduced to a size of less than 40 nm, ferromagnetic iron oxide particles (which can form a permanent magnet and retain magnetic memory) are turned into superparamagnetic nanoparticles (Frenkel, 1930). Unlike their larger-sized counterparts, the magnetic properties of superparamagnetic nanoparticles can be tuned

on and off under the presence and absence of external magnetic field. SIONP have been extensively used for biomedical applications such as in vitro cell manipulation, bioseparations, and drug delivery (Chen et al., 2010a; Rozhkova, 2011; Yin & Alivisatos, 2004). Unlike the white powder in their larger sized format, zinc oxide nanoparticles are transparent in visible wavelength range and used as physical UV filters for UV sunscreen lotions. Rather than absorbance and conversion into heat as chemical filters, the zinc oxide nanoparticles combine reflection, dispersion and adsorption to filter UV light. The color of gold nanoparticles can be blue or red rather than the yellow colour of the bulk material and melt at ~300°C (2.5 nm size) compared with gold slabs (1064°C) (Roy & Goswami, 2017).

2.2.3 Advantages in Biomedicines

The application of nanomaterials in medicine (nano-medicine) may provide treatment for diseases and a number of serious inflammatory or infectious diseases (Roy & Goswami, 2017). Due to their smaller size, the nanomaterials can penetrate the cell membrane and be used as a carrier to deliver molecules into cells (Cavalcanti et al., 2008). Magnetic nanoparticles are used in biology to separate or collect stem cells while quantum dots find application in molecular imaging, tracing, delivery of gene therapies and drugs into stem cells (Wang et al., 2009).

Despite many advantages and features of the nanomaterials, each type of nanomaterial has its own strengths and weakness. For example, inorganic nanomaterials can present serious health effects (Table 2.1), that is, some types of nanoparticles can seriously damage lungs, liver and the nervous system (Ray et al., 2009). As a result, special attention is made in developing strategies to synthesis bio- and/or hybrid bio-inorganic nanomaterials that have better biocompatibility.

Table 2.1: *Potential hazards posed by inorganic nanomaterials.*

Nanomaterials	Possible Risks
Silica and carbon nanoparticles	Acute cirrhosis of lung and liver
Gold, silver and Carbon nanoparticles	Effect on the nervous system
TiO_2, QDs, Carbon nanoparticles	Effect skin through penetration
TiO_2, MnO_2, and carbon nanoparticles	May affect the brain and olfactory nerves
Co, Ni, TiO_2, Al_2O_3 nanoparticles	Toxic to organs such as ears, eyes, skin

This table was reproduced from Ray et al. (Ray et al., 2009).

Biomolecules such as proteins, DNA, RNA, lipids and viruses can self-assemble to form nanomaterials at room temperature under a mild condition and result in biocompatible nanomaterials. Hybrid nanocomposites mimic natural materials but have improved structural and mechanical properties that underpin their biocompatibility and biological functionality (Ruiz-Hitzky et al., 2008). Also, inorganic nanomaterials such as metal oxides and silica can be assembled with biological species to add biological properties to the resultant nanomaterial. If noncovalent interaction is used to build such hybrid materials, the affinity of the biological components to the inorganic material generally determines the stability of hybrid materials.

2.3 Engineering of Bio- and Hybrid Nanomaterials

In general, there is a bio-interface between inorganic or organic surfaces and biological components in engineering of bio- and hybrid nanomaterials. The nano-bio interface, where nanomaterials interact with biological components, contains three dynamically interacting components, i) the nanoparticle surface where physio-chemical composition determines the properties ii) the solid-liquid interface where the nanoparticles and a component of the surrounding medium interact with each other, and iii) the contact zone of solid-liquid interface, where the biological substrate is attached (Nel et al., 2009). The biological response to the nanomaterials occur through the forces such as hydrodynamic, electrodynamic, solvation and

polymer bridging and electrostatic or steric forces at bio-nano interface. As such, the intrinsic characteristics of the nanomaterials such as size, shape, chemical composition, charge, surface modification, crystallinity, hydrophobicity, and wettability plays vital role in shaping the interface (Mahmoudi et al., 2011a; Nel et al., 2009). Interfacial bio-molecular engineering of nanomaterials and biological components has enabled the development of a bio- and hybrid nanomaterials for applications such as biosensors, biomedical and tissue engineering, emulsion processing, and bio-separation (He et al., 2006). Engineering of such materials can use different approaches as reviewed below.

2.3.1 Covalent Immobilisation

Covalent binding of biomolecules to an insoluble matrix is the most extensively researched technique because of the high bond, strong strength, and low or no loss of biomolecules. This immobilisation technique is very stable and normally does not release proteins into the working solution during use. This strong binding is due to the covalent nature of the bonds (as well as multiple binding points) between biomolecules and the carrier matrix. Covalent immobilisation conveys higher thermal, pH, ionic strength, and organic solvent stability of biomolecules because of rigidity and less susceptible to denaturation (Homaei et al., 2013). This mode of immobilisation also results in higher resistance to degradation by proteolysis.

However, to maximise retention of activity or function of the biological component after immobilisation, care must be taken to ensure the functional groups involved in the bioactivity are not bound to or constrained by the support. In some cases, retention of activity can be improved by completing covalent immobilisation reactions in the presence of substrate analogs (Mattiasson & Kaul, 1991). The covalent immobilisations are normally adopted when there is the requirement of the product with high purity without contamination with immobilised

biomolecules. The covalent immobilisation process is facilitated through various coupling reactions as discussed below.

2.3.1.1 Coupling Reactions

Covalent coupling reactions take place between a functional group of nanomaterials and an exposed amino acid group from the protein. The coupling reaction attaches the enzymes to various functional surfaces including; amine, thiol, carboxylate, hydroxyl, aldehyde, and ketone, (Hermanson, 2013a). Covalent coupling reactions complete in two steps, i) functionalisation of the nanoparticles (carrier molecules) with the selected activated group (electrophile), ii) nucleophilic attack of the protein (Figure 2.7).

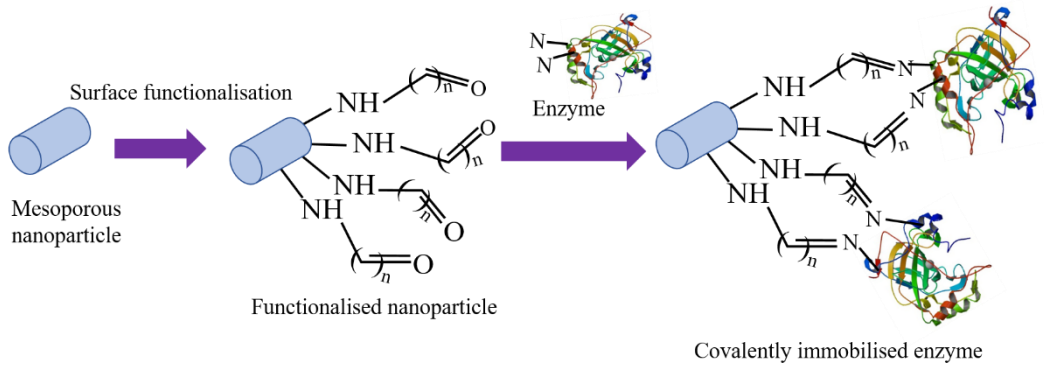

Figure 2.7: *Schematic diagram showing covalent immobilisation of enzyme on functionalised nanoparticles.*

The covalent bond formation depends on the availability and reactivity (nucleophilicity) in various groups of proteins. Normally, amino group in lysine, thiol group in cysteine, and carboxylic group in aspartic and glutamic acids are chosen for the nucleophilic attack on the functionalised carrier molecules and different activated chemicals are responsible for the covalent immobilisation. The nucleophiles are determined on the basis of charge status (called as state of protonation) which mostly follows $-S^-$ > -SH > $-O^-$ > $-NH_2$ > $-COO^-$ > -OH >> -

NH_3^+ order (Hermanson, 2013c). Amines and sulphydryls are nucleophiles that are most frequently involved in covalent immobilisation reactions.

Amine Coupling

Amine coupling reactions are the most widely adopted approach for crosslinking or surface modification (Tsuchiya, 2011). This method proceeds through alkylation or acylation and is robust enough to capture or bind almost all proteins or peptide molecules (Hermanson, 2013a). The amine reactions are rapid with high yield producing stable amide or secondary amide bonds. The type of reactive groups selected will determine the bonds formed (Table 2.2).

Table 2.2: *The major reactions of the amine coupling reactions. This table was reproduced from Hermanson et al. (Hermanson, 2013a)*

Reactive group	Bond formed
Isothiocyanate	Isothiourea
Isocyanate	Isourea
Acyl azide	Amide
NHS ester	Amide
Sulfonyl chloride	Sulfonamide
Epoxide	Secondary amine
Carbonate	Carbamate
Halo acetyl or alkyl halide	Secondary amine
Anhydride	Amide
Glutaraldehyde	Schiff base or secondary amine
Carboxylate	Amide
Tosyl ester	Secondary amine, Sulfonamide, Schiff base
Aldehyde	Secondary amine
Imidoester	Amidine
Fluoro phenyl esters	Amide

The activation agents used for the amine coupling reactions depend on the bond formation required with the protein. The common approach is amide bond or secondary amine formation

using reactive groups such as N-hydroxysuccinimide (NHS) ester, anhydride, acyl azide. The other approaches are carboxylate forming an amide bond and epoxide, glutaraldehyde, aldehyde, Tosyl ester forming a secondary amine.

Some of the most popular amine coupling reactions are mediated through, NHS esters, epoxides, and glutaraldehyde. The amide bond using NHS ester group is achieved through a reaction intermediate formed using activation agents; 1-ethyl-3-(3-dimethylaminopropyl) carbodiimide hydrochloride (EDC) and N-hydroxysuccinimide (NHS) (Hermanson, 2013a). However, amine-coupling reaction go the multiple steps forming ester intermediates. Epoxide reaction involves a primary amine, sulfhydryls, or hydroxyl groups forms a secondary amine, thioester or ether bond. However, most of the ring opening reactions of epoxide occur at alkaline pH (11-12), and the nucleophilic reaction of amine needs at least pH of 9. The use of carbonyl groups like aldehyde reacts with an amine at a wide range of pH. The reaction preferred at low pH, however are efficient at high pH forming Schiff base intermediates.

The use of glutaraldehyde as a functional reagent was first reported by Zahn in 1950s (Zahn, 1955), then followed by the x-ray diffraction studies to prepare stable protein crystals for crystallography (Quiocho & Richards, 1964). The chemical modification of the nanoparticles using glutaraldehyde as cross-linking agent was found chemically and thermally stable (Nimni et al., 1987).

Covalent immobilisation of protein on the surface of nanocarrier using glutaraldehyde as a cross-linking agent takes place in two reactions steps: a) the primary amine (side chains of lysine) reacts with glutaraldehyde producing a Schiff base intermediate (Damink et al., 1995;

Hermanson, 2013b), b) covalent bond formation through nucleophilic attack on glutaraldehyde forming a secondary amine linkage (2. 8).

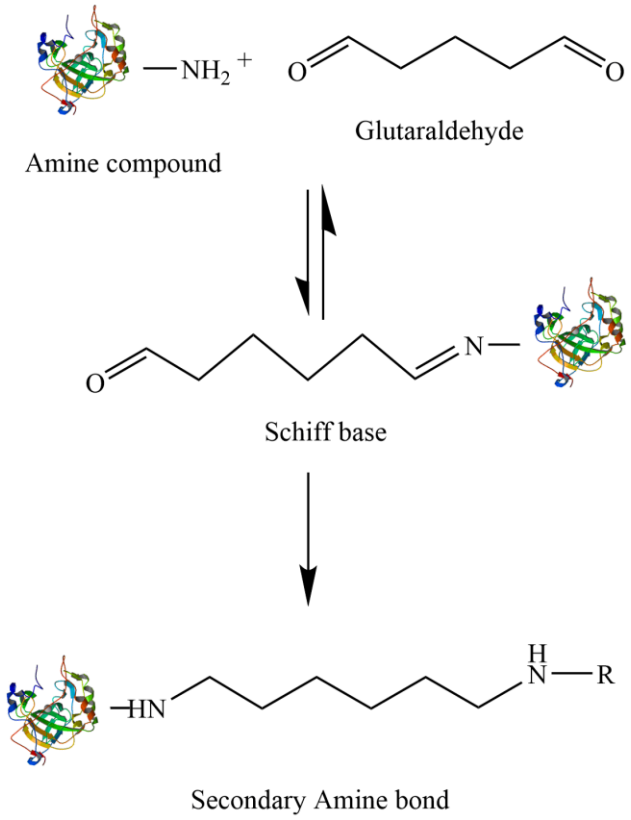

Figure 2.8: *Schematic diagram showing the reaction of glutaraldehyde as a cross-linking agent via a Schiff base intermediate*

2.3.1.2 Surface Chemistry of Covalent Immobilisation

The covalent coupling method increases the half-life and thermal stability of enzymes underpinning the application of enzyme as a reusable biocatalyst. However, the method reduces activity of biomolecules such as enzymes (Crumbliss et al., 1988; Hsieh et al., 2000) due to steric hindrance or poor mass transfer during the reactions. For example, in preparation of immobilised enzymes, overcrowding of enzymes on the surfaces results in less exposed and free active sites for catalysis (Figure 2.9).

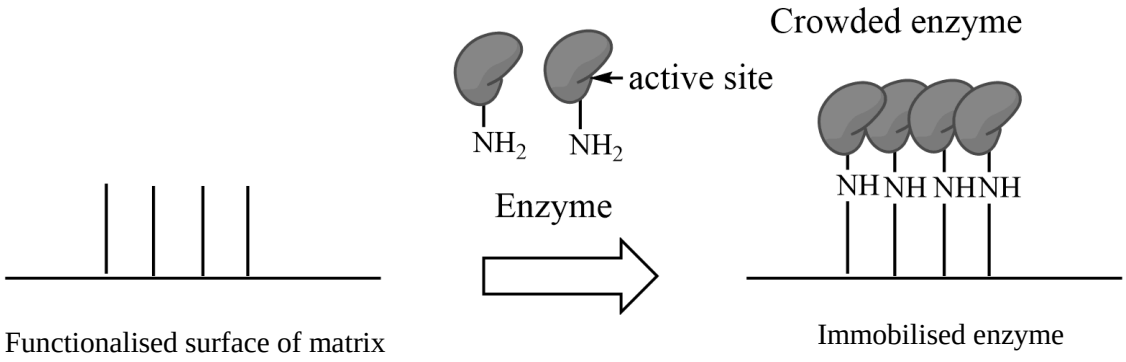

Figure 2.9: *Schematic illustration to show the effect of surface chemistry for covalent immobilisation*

For the efficient covalent immobilisation, the surface of the carrier molecule is desirable to bind enzyme with adequate space between them for proper mass transfer. However, a proper way to subsequentially keep the enzyme with an adequate space is challenging.

2.3.2.3 Advantages and Disadvantages of Covalent Immobilisation

The covalent coupling reaction is a simple method that can be completed under mild reaction conditions and has wide applicability. The binding efficiency is very strong with no or very little leakage of biomolecules. However, the covalent immobilisation uses chemicals as a functional group for surface modification prior to protein attachment that makes the process expensive and sometime toxic. Furthermore, the resulting multipoint attachment of proteins often causes structural changes leading to denaturation and/or loss of activity (Homaei et al., 2013).

2.3.2 Non-covalent Immobilisation

This method has a long history where reusing the agent by adsorbing on the surface of solid such as charcoal and aluminum hydroxide while brewing alcohol (Homaei et al., 2013). Non-covalent immobilisation is a reversible method where the proteins can be attached and detached

from the nanocarrier under certain conditions. Often enzyme activity decays after several cycles and fresh enzymes can be reloaded as required (i.e. the support matrix can be reused). This can make the bioprocess more cost-effective through reuse of the matrix. Non-covalent immobilisation is important for immobilising unstable enzymes and for the bioanalytical applications, such as biosensors (Gupta & Mattiasson, 1992).

Types of Non-covalent Immobilisation

The non- covalent immobilisation of enzymes can be achieved through, a) affinity binding, b) physical adsorption, c) ionic binding, d) hydrophobic adsorption, e) entrapment (encapsulation), and f) cross-linking (Figure 2.10).

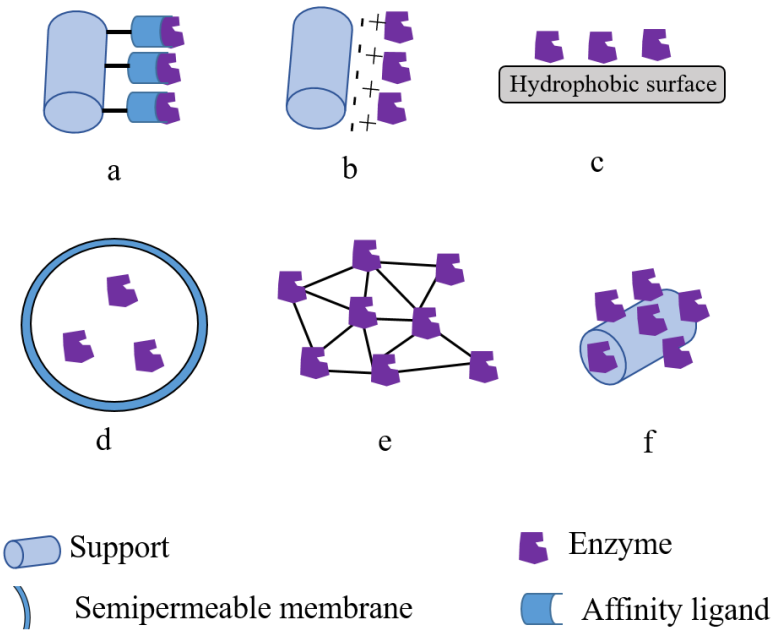

Figure 2.10: *Non-Covalent immobilised enzyme systems; a) affinity binding; b) ionic binding; c) hydrophobic adsorption, d) entrapment (encapsulation), e) cross-linking, f) adsorption*

2.3.2.1 Affinity Binding

Affinity binding causes the attachment of proteins to the matrix using ligands or tags. Affinity tags are usually comprised of exogenous amino acid sequences with high affinities to specific biological or chemical ligands. The ligands or tags are sometimes an existing sequence within the enzymes or artificially fused on terminus (N- or C-) of proteins. The common example of an affinity tag is hexaHis, which is used to selectively purify proteins through binding to immobilised metal ions. Affinity tags are widely used in protein separation and their applications have been extensively reviewed (Arnau et al., 2006; Kimple et al., 2013; Strambio-de-Castillia et al., 2005; Zachariou, 2008).

By including a DNA sequence encoding an affinity tag peptide, the fusion protein construct can be selectively bound to the appropriate ligand. Ideally, the fused affinity tag results in a minimal conformational change to the protein and may improve catalytic efficiency. This improvisation is associated with the active sites not participating during the immobilisation on matrix. Affinity tags may have a positive impact on the biochemical properties of a protein including to; improved protein expression and folding (Rajan et al., 1998) (Kou et al., 2007), prevent proteolysis and protect antigenicity (Tang et al., 1997) (Kou et al., 2007), and improved the solubility (Arnau et al., 2006; Chen et al., 2005). Enzymes immobilised by this method are widely used in biotechnology, diagnostics, and medicines (Abdelhamid et al., 2014; DeLouise & Miller, 2005).

The use of peptide for affinity binding was developed by Brown in 1992, that specifically bind iron oxide particles (Brown, 1992). Followed by the innovative approach, a platform technology was established that enabled the identification of different peptides that are highly specific to inorganic and synthetic materials (Baneyx & Schwartz, 2007; Kriplani & Kay, 2005;

Sarikaya et al., 2003). Researchers have since identified a wide range of peptides that are highly specific to metals and metal oxides (Ikeda & Kuroda, 2011) to produce bioinspired nanohybrids, as summarized in Table 2.3.

More recently, affinity peptides have been used in drug delivery, biocatalysis, bioseparation, material synthesis, etc. Interaction is facilitated through forces such as electrostatic attraction, ionic bonding, van der Waals, and hydrogen bonding (Ikeda & Kuroda, 2011). For example, electrostatic interaction between the negatively charged affinity peptide CCCSSSD and cationic quantum dots was used to modify a cadmium selenide / zinc sulphide mixture and enable incorporation into Quantum Dots (Henry et al., 2011). Furthermore, silica-and iron oxide-binding peptides are used for non-covalent immobilisation via affinity binding tags; together these provide higher binding capacities with the added functionality of enzyme activity.

a) Silica Binding Peptides

There are plentiful cationic peptides used for wide range of affinity interaction using silica as a precursor molecule. Zhou et al studied different silica binding peptides fusing with silk protein to understand the effect of protein sequence chemistry on silicon formation (Zhou et al., 2015). Beside this, Fuchs et al have used Nona arginine (R9) to demonstrate it as a multifunctional tag by fusing with bovine pancreatic ribonuclease (RNase A) (Fuchs & Raines, 2005). The tag enabled strong affinity immobilisation of the fusion protein on glass slides and silica resin but diminished the conformational stability.

Table 2.3: *Affinity binding peptides that have been developed, their corresponding inorganic ligand and potential applications. This table was reproduced from Chockalingam et al. (Chockalingam et al., 2007).*

Peptides	Inorganic nanomaterials	Application of hybrid nanomaterials	References
RRTVKHHVN	Iron oxide	Assembly of nanomachines	(Brown, 1992)
RRSRHH, RSKRGR	Iron oxide	Selection of catalytic antibodies	(Barbas et al., 1993)
MVGGTIWTGKGLGLGLGLGLGAWGPI ILGVVGAGAVYAYMKSRDIESAQSDEEVELRDALA	Iron oxide	Biomineralisation	(Arakaki et al., 2003)
RRRRRRRRR	Silica	Affinity immobilisation	(Fuchs & Raines, 2005)
LSTVQTISPSNH	Iron oxide	Protein-iron nanostructure	(Lower et al., 2008)
QAFPLSNQSLTV	Iron oxide	Multifunctional nanocomposites	(Avery et al., 2009)
CCCSSSD	Cadmium selenide / Zinc sulfide/Quantum dots	Preparation of optical nanomaterials	(Henry et al., 2011)
KSLSRHDHIHHH, RKSLSRHDHIHHH	Silica	Silicification using peptides synthesised chemically or genetically.	(Canabady-Rochelle et al., 2012)
TSNAVHPTLRHL	Palladium	Catalysis	(Coppage et al., 2012)
YAYMKSRDIESAQSDEEVELRDALA	Iron oxide	Biomineralisation	(Feng et al., 2013; Wang et al., 2012)
KLVFF	Gold	Biomolecular scaffold	(Yan et al., 2013)
PKFKFKFKFKFKP	Gold	Material synthesis	(Vinod et al., 2013)

SGRARAQRQSSRGR	Silica	Protein purification	(Abdelhamid et al., 2014; Motomura et al., 2015)
BTA-C_3-GVGVOMe	Copper	Nanowire production	(Gong et al., 2015)
SGSKGSKRRIL, MSPHPHPRHHHT, SSKKSGSYSGSKGSKRRIL	Silica	Controlled Silicification	(Zhou et al., 2015)
CCYKKKKQAGDV	Gold	Drug delivery	(Zhao et al., 2016)
QQTNWSLTVNFKLY	Iron oxide	Diagnostic and therapeutic	(You et al., 2016)
EEEEAAAVVVK-$C_{14}H_{26}$	Silver	Antimicrobial activity	(Pazos et al., 2016)
CALNNDEVDK-FAM	Graphene Oxide	Drug delivery	(Tian et al., 2016)

Later, Abdelhamid et al (Abdelhamid et al., 2014) reported the deposition of silica on the covering of *Bacillus cereus*. This layer was achieved through the accumulation of silica mediated by C-terminal of protein "cob" (Motomura et al., 2015). The C-terminal (SGRARAQRQSSRGR) of cob has highly positive charged residues which enables strong binding affinity with negatively charged silica, Figure 2. 11.

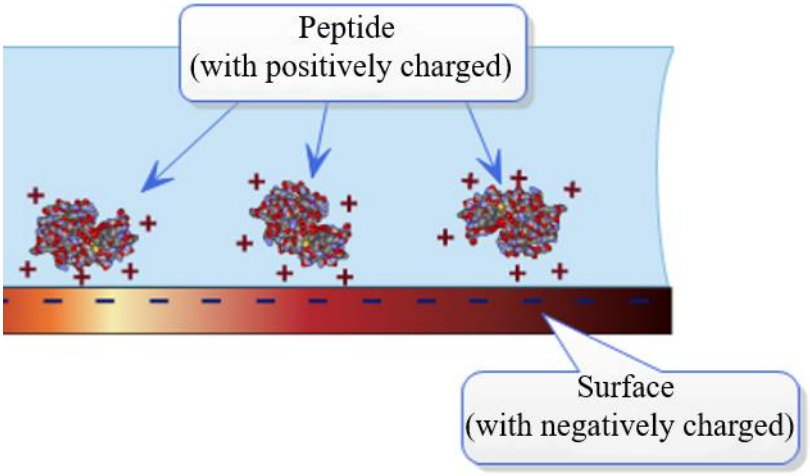

Figure 2.11: *Illustration of non-covalent affinity immobilisation on the surface of negatively charged silica nanoparticles using positively charged peptide such as cob*

The strong binding affinity between the silica particles and peptides is due to the cumulative interactions such as: ionic bond, van der Waals force, hydrogen bonding, and electrostatic interactions (Ikeda & Kuroda, 2011). The Si-tags were found to have the dissociation constants of 0.3 nanomolar in 25 mM Tris-HCl pH 8, 0.5 M NaCl, and 0.5% (v/v) Tween 20 (Ikeda et al., 2009). However, the Si-tag fusion proteins were found to have irreversible binding at higher salt and detergent conditions (Taniguchi et al., 2007). These features of the fusion proteins to have strong affinity under stringent conditions are highly desirable for selective immobilisation.

b) Iron Binding Peptide

Iron binding peptides are extensively studied as molecular building blocks in the field of engineering and nanoscale science. The first short peptide with molecular recognition properties to select iron had been first demonstrated by Brown in 1992 (Brown, 1992) who identified the protein sequences that were able to recognize specific surfaces of the iron. Following this in 1993 Barbas et al. presented an iterative strategy to select metalloantibodies using iron binding peptides (Barbas et al., 1993). Beside this, in 2008 Lower et al. presented work in developing peptide-mediated nanomaterials. However, the peptide had a binding affinity with hematite (Fe_2O_3) (Lower et al., 2008).

Mms6, an amphiphilic protein (Figure 2.12) incoporates iron oxide to form magnetite nanoparticles in vitro similar to those by magnetotactic bacteria (Arakaki et al., 2003). In 2011, Tanaka et al. studied the effect of Mms6 in magnetite formation where the deletion of Mms6 gene resulted in irregular and smaller magnetite crystals (Tanaka et al., 2011).

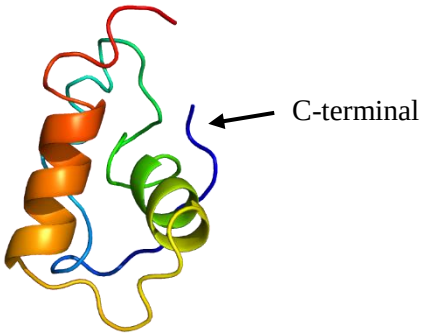

Figure 2.12: *The representative cartoon structure of iron oxide binding protein Mms6. The structure was produced using I-TASSER server (Zhang, 2008).*

Mms6 self-assembles forming a micelle most likely forming an organised octamer structure because of hydrophobic amino acids like glycine, alanine, and valine in the N-terminal region (amino acid: MVGGTIWTGKGLGLGLGLGLGAWGPIILGVVGAGAV). The proteinaceous micelles are stable usually containing 20-40 protein molecules (size of 25-150 nm) as

visualised under cryo-TEM (Kashyap et al., 2014). The C-terminal (Mms6c) has affinity with iron oxide and forms superparamagnetic nanoparticle as the C-terminal is rich in carboxyl groups from glutamic and aspartic acids which chelate iron (Fe^{2+} or Fe^{3+}) (YAYMKSRDIESAQSDEEVELRDALA) (Feng et al., 2013; Wang et al., 2012). However, the binding of Mms6c (C-terminal of Mms6 protein) with iron oxide was inhibited by metal ions such as Ca^{2+}, Mg^{2+} and mildly inhibited in the presence of Ni^{2+}, Cu^{2+}, and Zn^{2+} (Arakaki et al., 2003).

The Mms6c region of Mms6 protein was found to regulate the crystal morphology of magnetite biomineralisation (Arakaki et al., 2003). Biomineralisation is defined as process to deposit minerals by the organism under ambient conditions. The biomineralisation process highly influences the chemical and physical properties of materials with extensive attention in the field of basic and material sciences (Arakaki et al., 2015; Meldrum & Colfen, 2008; Nudelman & Sommerdijk, 2012).

2.3.2.2 Other Types of Non-covalent Immobilisation

i) Ionic Binding

The ionic binding mode is a reversible immobilisation method between two charged molecules; enzyme and matrix. Enzymes can be bound on matrices such as; inorganic materials, polysaccharide derivatives, and synthetic polymers and binding efficiency is dependent on the surface charge density of the matrix. A higher surface charge density results in a large number of immobilised enzymes leading to a minimal change in enzyme conformation. This approach to immobilisation depends on pH, temperature, and enzyme concentration thus special consideration is required to maintain pH and ionic strength to prevent detachment (leakage) of the protein from the immobilisation support (Kayastha & Srivastava, 2001).

ii) Hydrophobic Adsorption

The hydrophobic adsorption is a non-covalent immobilisation technique that essentially relies on entropic interactions based on the hydrophobicity of the matrix and protein. Hydrophobic amino acid side chains interact with the hydrophobic surface of the matrix resulting in multipoint attachment. Variables such as pH, temperature, and salt concentrations can affect the interaction. Proteins will be released from the surface by changing conditions. Hydrophobic interaction has been widely used since the 1980s as a chromatographic technique to purify proteins. Materials such as cross-linked agarose and synthetic copolymer are used (Caldwell et al., 1976). Like ionic binding, maintenance of pH and ionic strength to prevent leakage of protein.

iii) Cross-linking

The cross-linking is one of the most used technique to immobilise enzyme and been commercially launched by CLEA Technologies to produce Cross-linked Enzyme Aggregates (CLEAs). The cross-linking of the enzyme is essentially a matrix-free approach using bi-functional reagents such as glutaraldehyde. This is a simple method but requires high purity enzyme for the preparation of cross-linked enzyme particles (Jegan Roy & Emilia Abraham, 2004). The cross-linking approach causes loss of enzyme activity caused by reduction in mass transport or diffusion of substrate into active sites.

iv) Entrapment (encapsulation)

The immobilisation through entrapment (encapsulation) is available for low molecular substrates and products, enclosing them within the semi-permeable membrane (permanent or temporary) with controlled porosity (1-100 μm) (Das et al., 1997). The substrate and products

can permeate through the polymeric network, which retains the enzyme(s). Enzymes can be entrapped in different configurations including gels (Bernfeld & Wan, 1963) and fibres (Dinelli et al., 1976). However, encapsulation may be limited to smaller molecules that readily diffuse through the encapsulation matrix (Brena et al., 2013) and may be limited by mass transport.

v) Physical Adsorption

Physical adsorption is a simple method to immobilise enzyme on a solid matrix without activation of the surface. Enzymes are attached to various matric such as glass, dextran, alumina, ceramic, etc. via weak interaction; hydrogen bonds and van der Waals forces. The binding forces used in this type of immobilisation can be reversed by changing the environments such as pH and ionic strength (Alloue et al., 2008). This simple method works under mild conditions that are easy to work, however, can be limited by leakage of the enzyme from the immobilisation support.

2.3.2.3 Properties of Affinity Immobilisation

Immobilisation through affinity peptides often results in tight binding, is relatively simple to implement (does not need special skills) and can be completed under mild conditions. The strong binding provides a particle that can be subjected to multiple process cycles without compromising enzyme activity with the added advantage that binding can be reversed by a change in conditions. Furthermore, affinity tags can be used to recover enzymes from the crude lysates without the need for multiple processing steps reducing production costs (Saleemuddin, 1999). However, the carrier (matrix) particles can have a negative impact on mass-transfer due to the formation of an external solid-liquid diffusion barrier and intra-particle barrier (Xiu et al., 2001).

2.3.3 Self-assembly of the Molecular Components into Particles

The term self-assembly was defined by Whiteside and Grazybowski as "an autonomous organisation of components into patterns or structures without human intervention" (Whitesides & Grzybowski, 2002). In addition, Whiteside and Grazybowski classified the self-assembly process into two categories; i) static and ii) dynamic. Static is a highly stable self-assembly process that involves the components at global equilibrium and does not release energy, such as formation of molecular crystals and globular proteins. Dynamic self-assembly involves systems that dissipate energy resulting in the formation of structures from pre-existing components, for example; patterns due to reactions and diffusion of chemicals and biological cells. Regardless the mode of self-assembly, design of individual components to assemble into the preferred structure and function is a key requirement in the application of self-assembly.

2.3.3.1 Mechanisms of Self-assembly

The self-assembly of molecules are attributed to a number of forces such as electrostatic interaction, hydrophobic interaction, hydrogen bonding, ionic bonding, van der Waals forces and π-π interaction (Zhang, 2003). Electrostatic interactions comprise of both attractive and repulsive force between charged amino acid residues in the polypeptide chain. Peptides that self-assemble through electrostatic interactions were used to produce a nanostructure for a pH-responsive anti-cancer drug delivery system (Chen et al., 2015). Hydrophobic interaction depends on the polar and non-polar regions of peptides. In the aqueous solutions, non-polar components will interact forming a cluster to effectively "hide" the hydrophobic domain from water (Fan et al., 2017). Hydrogen bonds are typically found in α-helices and β-sheets that are structural components of nanomaterials. Hydrogen bonding is the electrostatic interaction between the H atom and highly electronegative atoms such as N and O to play an important role in the formation and stabilisation of peptide secondary structures and protein folding. The

interaction involving two aromatic residues in close proximity is known as π-π interaction or π-π stacking. This interaction drives directional growth and results in structures that are robust in aqueous systems due to the hydrophobicity of the aromatic groups. The di-peptide FF enables π-π stacking which is stabilised by hydrogen bonds resulting in the formation of self-assembled structures (Reches & Gazit, 2003). In conclusion, the combination of a number of forces helps to engineer nano-biomaterials as well as influence their interaction with other materials. Molecular-level self-assembly is achieved using biological components as protein, DNA, and peptides (Fan et al., 2017; Ghimire et al., 2017; Zhang & Yan, 2017).

2.3.3.2 Self-assembly of Peptides

Peptides are short chains of amino acid that exhibit biocompatibility and molecular recognition making them attractive as components of nanomaterials. Peptides can be stable under extreme conditions such as high temperatures, detergent exposure, and other denaturing conditions (Dinca et al., 2008). As illustrated in Figure 2.3, peptides can be assembled into different kinds of supermolecular architectures such as nanotubes, fibrils, and vesicular structures. The formation of nanostructures is facilitated by self-assembling peptides such as dipeptides, cyclic, amphiphilic, α-helix, β-sheet resulting in different structures.

The dipeptide, diphenylalanine (FF) has been used to produce various nanostructures and has been recognised as the core motif that drives self-assembly of the amyloid-β-polypeptide segment in Alzheimer's disease (Reches & Gazit, 2003). In 1993 the cyclic peptide Cyclo-(L-Gln-D-Ala-L-Glu-D-Ala)$_2$ was shown to self-assemble into nanotubes that were hypothesised to be stabilised by hydrogen bonding (Ghadiri et al., 1993). Fan et al have reviewed amphiphilic, α-helix, and β-sheet peptides that have been used to synthesis nanostructures with different properties (Fan et al., 2017).

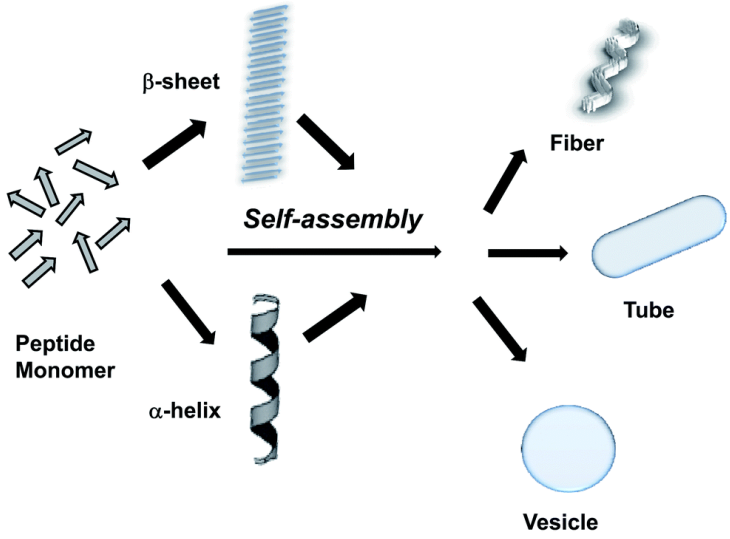

Figure 2.13: *Self-assembly of peptides into the different nanostructure. This figure was reproduced from Panda et al. (Panda & Chauhan, 2014).*

Self-assembling peptides are designed to use in several applications and to respond in various ways to stimuli (Table 2.4). The peptide self-assembly and final structures are tuneable through a change in pH, temperature, metal ion concentrations, and polarity of the solvent. For example, peptides containing charged amino acid residues such as Glutamic acid, Aspartic acid, Lysine, Histidine, and Arginine respond to pH changes forming nanoparticles of different structures.

The surface charge of amino acid residues is highly sensitive to the pH resulting in the formation different nanostructures depending on pH (Sun et al., 2015). For example, the peptide ($P_{11}4$) QQRFEWEFEQQ self-assembled into a β-sheet structure when the pH was reduced and into monomeric structure at higher pH (Aggeli et al., 2003). Self-assembly peptides may be fused to proteins producing self-assembling fusion proteins. Bovine carbonic anhydrase was fused with a $P_{11}4$ containing aromatic amino acids that were also rich glutamic acid (QQRFEWEFEQQ) which resulted in nanoparticles that self-assembled as a result of pH change and the addition of the divalent metal cation Mg^{2+} (Shanbhag et al., 2016).

Table 2.4: *List of stimuli-responsive peptides. This table was reproduced from Chockalingam et al. (Chockalingam et al., 2007)*

Stimuli	Sequences	Conformational change	Application	References
Solvent polarity	ELALKAKAELELKAG	β-sheet to α-helix	Conformational studies	(Mutter & Hersperger, 1990)
Redox state	YLKAMLEAMAKLMAKLMA	α-helix to β-sheet	Conformational studies	(Dado & Gellman, 1993)
Temperature, pH	ADADADADARARARAR	β-sheet to α-helix	Amyloid study	(Zhang & Rich, 1997)
pH	VKVKVKVKVPPTKVKVKVKV	Disordered to β-hairpin	Hydrogels, tissue engineering	(Schneider et al., 2002)
Solvent polarity	FF	Not described	Nanotubes, nanowires, nanoparticles	(Reches & Gazit, 2003)
Calcium	GGXGXDX(L/F/I)X	Disordered to β-roll	Biomaterials	(Ringler & Schulz, 2003)
pH, temperature, salt	VPGXG	Disordered to β-turn	Bioremediation, DNA purification	(Kostal et al., 2003)
pH	QQRFEWEFEQQ	Disordered to β-sheet	Hydrogel formation	(Aggeli et al., 2003)
Zinc	DAEFRHDSGYEVHHQK	Poorly folded helix to well folded irregular 3_{10} helix	Alzheimer disease model	(Zirah et al., 2006)
pH	QQKFQFQFEQQ	β-sheet to nanofibers	Hydrogel formation	(Hudalla et al., 2014)

The slight change in amino acid sequence referred as Pep2 (QQKFQFQFEQQ), Hudalla et al, fused with fluorescence protein producing hydrogel by the change of pH. Recently, Jang et al demonstrated vesicle formation in an aqueous environment with a globular fluorescent protein (mCherry) fused to a glutamic acid-rich peptide (Jang et al., 2017). The vesicle size and structures could be tuned by altering the protein concentration or temperature.

2.3.3.3 Self-assembly of Proteins and DNA

Proteins, under favourable environment self-assemble into various structures such as vesicles, crystals, filaments, gels, fibers, and amorphous aggregates (Dumetz et al., 2008). These structural derivatives have better stability and mechanical strengths with unique physio-chemical properties. The recent advances in site-specific chemical modifications and protein engineering tools have enabled the development of protein sequences that assemble through specific protein interactions providing unique functionalities (Spicer & Davis, 2014). For example, Ghimire et al. produced a bio-hydrogel incorporating glucose oxidase and bovine serum albumin in the presence of ferricyanide (Ghimire et al., 2017). The self-assemble biomaterial had highest current density of 13.2 mA preventing the enzyme from degradation and loading limits. Gao et al., developed a cascade reaction using two fusion enzymes (leucine dehydrogenase and formate dehydrogenase) to synthesise L-leucine-*tert*-leucine and regeneration of the cofactor NADH. After formation of a self-assembling structure, the fusion protein showed better structural stability and co-factor regeneration efficiency (Gao et al., 2014).

DNA is essentially a nanoscale material with 2 nm in diameter and 3.4 nm helical repeat (10.5 base pairs). DNA are used for self-assembly to its simple, stable, and predictable structures. In 1982, Seeman proposed DNA as a molecular structure to fabricate nanomaterials using bottom-up self-assembly approach (Seeman, 1982). Following DNA nanotechnology, several

structures have been fabricated for the applications in therapeutics, drug delivery, biosensors, and nanoelectronic (Li et al., 2009; Zhang & Yan, 2017).

2.3.3.4 Advantages and Disadvantages of Self-assembly of Molecular Components to Particles

The self-assembly of peptides into particles delivers an array of well-defined architecture in biomedical applications for example in drug delivery, therapeutics, and industrial applications (Lakshmanan et al., 2012; Li et al., 2009; Zhang & Yan, 2017). These biological nanoparticles are highly biocompatible and stable under extreme conditions such as high temperatures, detergent exposure, and other denaturing conditions (Dinca et al., 2008). Furthermore, these self-assembled nanostructures are free from the inorganic carrier matrix, designed, and engineered with novel peptide motifs making them responsive to stimuli.

2.3.4 Self-assembly of Higher Order Structures

The self-assembly of nanoparticles into high hierarchical structures at solid-liquid interfaces has opened an avenue for tuneable optical devices, biomedicines, sensors, and energy (Edel et al., 2013; Kotov, 2017). However, application of nanotechnology requires particles that have the right size and contain building blocks that provide a pathway for production of superior architectures (Shipway et al., 2000). Such superior architecture with functionality is desirable to produce using the nanoparticles. However, there is a need to find a way to organize the nanoparticles into controllable architectures. Several researchers have demonstrated the production of higher order structures such as; clusters (Casula et al., 2016; Ge et al., 2007; Kralj & Makovec, 2014; Lee et al., 2013; Liao et al., 2016; Qi et al., 2016; Qiu et al., 2010; Yan et al., 2018; Yang et al., 2018; Zhang et al., 2017), microcapsules (Evers et al., 2016), super lattices (Han et al., 2018; Udayabhaskararao et al., 2017) as described below.

2.3.4.1 Clusters

The self-assembly of the nanoparticles into clusters is the most adopted approach to the synthesis of higher order nanomaterial-based arrays. Ge et al. synthesised a monodispersed magnetite (Fe_3O_4) colloidal cluster ranging in size from 30 to 180 nm (Ge et al., 2007) and composed of many single 10 nm magnetite nanoparticles, however, these nano arrays were produced at harsh conditions. In 2010, Qiu et al synthesised spherical iron oxide clusters using an oil in water emulsion and the surfactant cetyltrimethylammonium bromide (CTAB) to stabilise the nanoparticle cluster (Qiu et al., 2010). In 2013, self-assembled iron oxide (Fe_3O_4) clusters were synthesised with functional properties (Lee et al., 2013). The clusters were used as anodes for lithium-ion batteries that enhanced capacity retention, rate capability, and columbic efficiency (Figure 2.14). However, these nanomaterials do not have shape tuneable or/and switchable properties. The availability of various size and shape- tuneable nanoclusters widens the scope of the studies and applications for their biomedicine and energy (Thota & Crans, 2018).

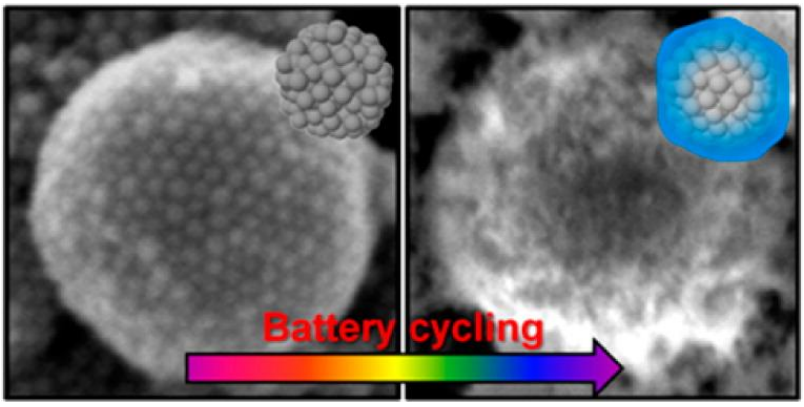

Figure 2.14: *Superparamagnetic Iron Oxide nanoclusters used for lithium-ion batteries. This figure was reproduced from Lee et al. (Lee et al., 2013).*

Clusters have been produced through covalent bonds between carboxyl and amine functionalised IONP (50 nm) (Kralj & Makovec, 2014). With a view to various applications

such as in cancer therapy, magnetic resonance imaging (MRI), and photodynamic therapy, iron oxide nanoclusters were functionalised with poly(dopamine) (Liao et al., 2016), exosomes, (Qi et al., 2016), antigens, (Zhang et al., 2017) and protoporphyrin IX (Yan et al., 2018). However, these particles are not shape-size controllable and are synthesised through chemical modification of iron oxide nanoparticles or coated with chemicals.

Recently, Yang et al. produced a surfactant responsive non-spherical cluster structure (Yang et al., 2018). They produced water/ethylene glycol droplets where gold (6.0 ± 0.7 nm) and iron oxide nanoparticles (12.0 ± 1.2 nm) were suspended near 1, 2 dichlorobenzene-air interfaces. The nanoparticles were then functionalised with hydrophobic (oleic acid) and hydrophilic ligands (11-mercaptoundecanoic acid terminated in a polar COOH head group), to prepare the multi-responsive cluster. The use of droplets with different chemicals and responsiveness controlled the inter-droplet transport and sequences of the chemical. However, production of these kinds of materials required the use of chemicals (e.g. surfactants), which may not be compatible with the functional properties of the nanomaterials.

2.3.4.2 Other Structures

a) Microcapsule

Microcapsules are higher ordered structures synthesised from nano-scale components. In 2016, Evers et al. demonstrated microcapsule formation using colloidal particles (Evers et al., 2016). The self-assembling microcapsules were synthesised using colloidal particles and combine properties; mutual attraction, anisotropy, and deformability. The mutual attraction between a hydrophobic polystyrene group and deformability due to hydrophilic polyacrylic acid causes surface groups to rearrange for binding. Anisotropy induces the curvature formation resulting in a well-structured microcapsule around 100 nm in size. However, these snowman-shaped

capsules are produced using polymers and controlling the above-mentioned properties independently is impossible for other materials such as proteins.

b) Super Lattice

A general route to produce nanoparticle arrays with directional interaction and fine adjustment between attractive and repulsive force been resolved to some extent by producing super lattices. Recently, (Udayabhaskararao et al., 2017) used monodispersed gold (Au) and iron oxide (Fe_3O_4) nanoparticles to produce a binary nanoparticle super lattice. The monodispersed particles were assembled at a diethylene-glycol-air interface to produce two-component nanoparticle arrays, which after selective etching resulted in super lattices, as shown in Figure 2.15.

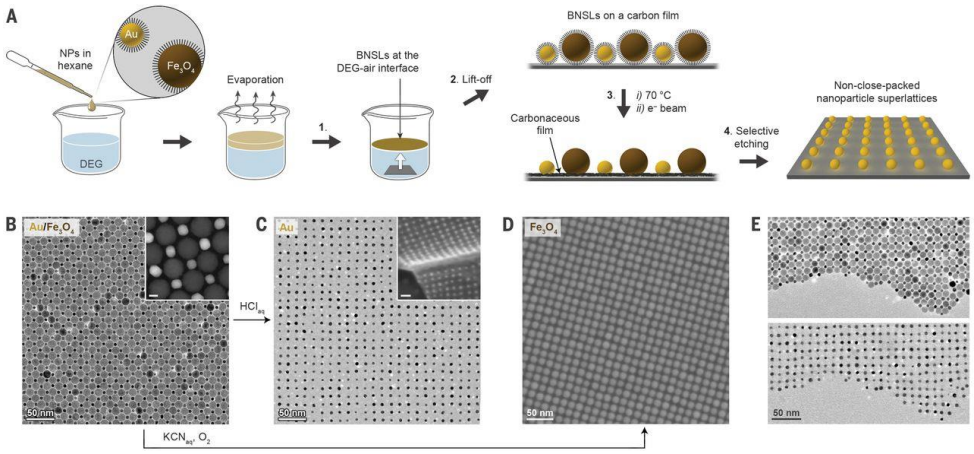

Figure 2.15: *Preparation of a nanoparticle array. A) Schematic illustration to produce a non-closed packed nanoparticle super lattice, B) TEM images of Au/Fe_3O_4 nanoparticle array, C) TEM images of Au nanoparticles array obtained by the selective removal of Fe_3O_4, D) TEM images of Fe_3O_4 nanoparticles array obtained by the selective removal of Au, E) Edge of a super lattice before (top) and after (bottom) Fe_3O_4 etching. This figure was reproduced from (Udayabhaskararao et al., 2017).*

These binary super lattices were transformed to nano-allotropes, which could be tuned to generate different sizes by altering the ratio of gold and iron oxide nanoparticles. This approach

keeps the nanoparticles with an adequate space but was produced under harsh environment and lacks the functional properties.

A "pomegranate-like" super lattice was produced from carbon-coated iron oxide (Fe_3O_4) nanoparticles (Han et al., 2018). The spherical component of the super lattice was produced via emulsion-based self-assembly using the surfactant dodecyltrimethylammonium bromide (DTAB). This material was used for high-performance lithium batteries for energy storage. Even though these types of lattices exhibit electrochemical functionality, they do not have shape tuneable or/and switchable properties.

2.3.4.3 Properties of Self-assembly of Higher Order Structures

The nanoparticles self-assemble into higher order structures through different routes to develop functional materials. These higher ordered structures called nanoparticle arrays has recently emerged as a platform to use in optoelectronics, drug delivery, sensors, catalysis, and energy (Kotov, 2017). The nanoparticle array is self-healing, self-assemble under proper conditions, non-degrading, and easily renewable (Edel et al., 2013). However, they are limited by their production in highly specific systems, the imbalance between the attractive and repulsive force during self-assembly, fabricating in harsh conditions, and functional properties (Udayabhaskararao et al., 2017; Yang et al., 2018).

2.4.5 Rational Design of Bio and Hybrid Nanomaterials

2.4.1 Biological Components

a) Carbonic Anhydrase (CA)

To study the synthesis of bio nano-materials, it is desirable to select well characterized and previously studied enzyme. Bovine carbonic anhydrase (BCA) and carbonic anhydrase from

Thiomicrospira crunogena (TmCA) were chosen for its well-studied monomeric crystal structure, smaller size, and simple assays to test activity. They have a high-level expression in *E. coli*, underpinning the carbon dioxide hydration properties.

BCA, originated from enterocytes (bovine) and TmCA originated from a sulphur-oxidizing gammaproteobacterium, are zinc-containing metalloenzyme that catalysed the reversible reaction for carbon dioxide hydration (Equation 1) (Mahon et al., 2015; Sly & Hu, 1995). Carbonic anhydrase is able to convert CO_2 to bicarbonate with catalytic efficiency (k_{cat}/K_M $M^{-1}s^{-1}$) approximately (BCA) 1.1 $*10^7$ and (TmCA) $1.2*10^8$ (Silverman & Lindskog, 1988), (Mahon et al., 2015)

$$CO_2 + H_2O \xleftrightarrow{CA} HCO_3^- + H^+ \qquad \text{(Eq. 1)}$$

BCA was purified in 1933 from erythrocytes (Meldrum & Roughton, 1933) and carbon dioxide fixation was studied on 1940 (Bradfield, 1947). By 1994, five carbonic anhydrases from prokaryotic cells have been purified, however recent studies suggest that the enzyme is widely distributed among prokaryotes (Smith et al., 1999). TmCA has the >30% amino acid sequences similarity with BCA however has a high T_M 72 °C compared with BCA (56 °C). The stability is postulated to contribute due to the presence of intramolecular disulfide bonds. Both the enzymes are considered as promising candidate for carbon capture and sequestration application in research and industry due to its higher CO_2 hydration efficiency at mild environment (Bond et al., 2001).

Mechanism of Carbonic Anhydrase for Carbon Dioxide Hydration

Carbon dioxide is converted into bicarbonate in the presence of water with the production of proton through two step ping-pong mechanism. Figure 2.16.

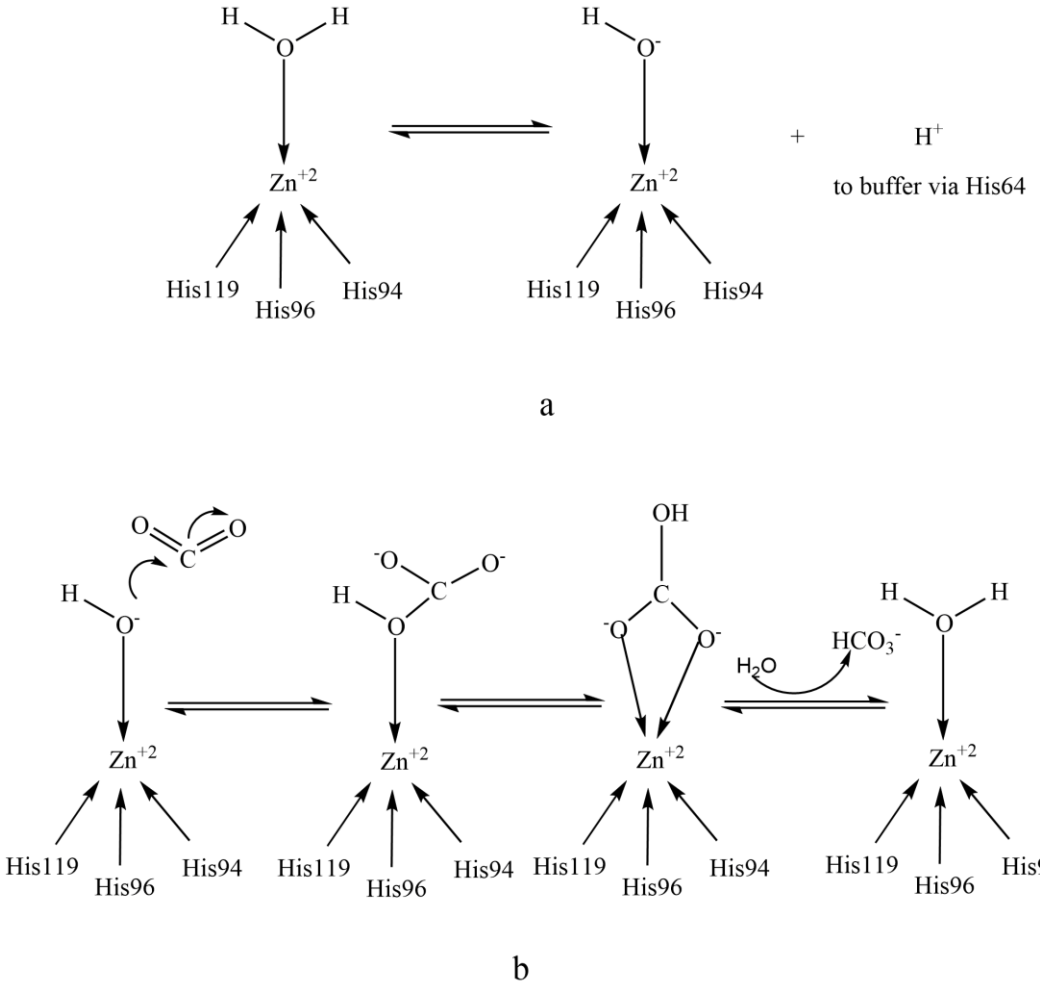

Figure 2.16: *Mechanism of CO_2 hydration reaction. a: Zn^{2+} ion abstracts a proton from a surrounding water molecule, creating a hydroxide ion that is negatively charged; b: The negatively charged molecule attaches the partially positive carbon atom on the solubilized CO_2 molecule to form HCO_3^- ion*

CA hydrolyses water to capture hydroxyl and release a proton (shown in Figure 2. 16a) lowering the pKa value of water ~14 to 7.0. This reaction is mediated by the zinc ions (Lewis acid). The second step is the nucleophilic attack (hydroxyl group) on the carbonyl bond (shown in Figure 2.16b) to produce bicarbonate and CA. During the reaction, the CO_2 rich and

deficiency sites occurs hydration and dehydration reactions (Cowan et al., 2003; Duda et al., 2001; Elder et al., 2004). This carbon-capturing enzyme is used as one of the environmentally friendly approaches to minimize carbon dioxide from the atmosphere. Moreover, BCA is targeted for drug design, carbon dioxide sensor, and as metabolon (Imtaiyaz Hassan et al., 2013).

b) Green fluorescent protein

The human interest in fluorescent protein was dated to first century when the Roman philosopher Pliny the Elder described the glowing jellyfish in the Mediterranean Sea (Greb, 2012). He described the emitted light could be used as a torch. In 1955 Davenport and Nicol first explained the occurrence of fluorescent compound in the organ of *Aequorea victoria* jellyfish (Davenport & Nicol, 1955). However, it was Nobel laureate Professor Osamu Shimomura to unravel the science behind the fluorescence was actually due to green fluorescence protein (GFP) (Shimomura et al., 1962). In 1992, GFP was cloned with complete gene sequence and led the way to expression in organisms (Prasher et al., 1992).

The crystal structure of GFP showed that the chromophore (*p*-hydroxybenzylideneimida-zolinone) is a tri-peptide that consist serine, tyrosine, and glycine residues at 65-67 position in the sequence. This tripeptide undergoes cyclisation and oxidisation with an intramolecular rearrangement forming chromophore; however, extensive mutagenesis studies suggested that the glycine (G67) as a critical chromophore (Heim et al., 1994; Tsien, 1998). Furthermore, by the mutation of the amino acid sequences of the wild-type GFP, a new fluorescent protein with different colour such as blue, cyan, red, yellow-green, etc. were achieved. This in vivo fluorescent chromophore formation has opened a new platform to study the biological system

permitting the visualisation and tracking the intercellular localisation of the construct (Tsien, 1998).

GFP is biocompatible to use for the various biological application as a model protein (fusion tag) and fused with the protein of interest to extract the expanded knowledge of cellular dynamics and interactions (Snapp, 2005). The GFP thus can be used as a functional protein and been used in a wide range of application from the biosensor, drug delivery, imaging, and tracking of the nano-biomaterials (Chalfie et al., 1994; Ibraheem & Campbell, 2010; Snapp, 2005).

c) Linker Selection

The linker serves to connect the two different protein moieties maintaining the cooperative inter-domain interactions (Gokhale & Khosla, 2000) or preserving the biological activity (Ikebe et al., 1998). The appropriate linker selection is an indispensable element for the successful engineering of fusion protein. Direct fusion (without linker) of functional domain with the protein of interest may lead to undesirable outcomes such as; misfolding of fusion protein (Zhao et al., 2008), reduced bioactivity (Bai & Shen, 2006), or/and low protein production (Amet et al., 2008). Therefore, the rational linker design or selection to link the protein of interest with the functional peptide is important.

The fusion proteins typically need three components a) protein of interest, b) functional peptide, and c) linker molecule. The linker molecule is possible to keep on both terminus (N- and/or C-) terminus of the protein, as shown in Figure 3.17. For example, two peptides were fused by linker on both terminals of protein, Figure 3.17d similar to alcohol dehydrogenase enzyme with

α-helix peptides on both terminus that can self-assembly to form hydrogel without compromising enzymatic activity (Wheeldon et al., 2009).

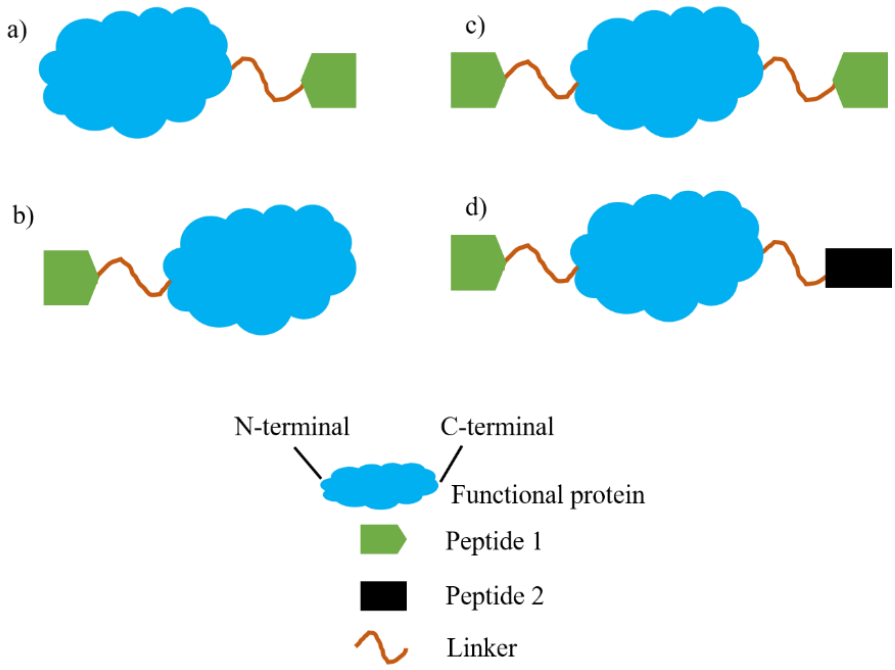

Figure 2.17: *The graphical representation of different fusion protein design based on the location of linker. a) C-terminus, b)N-terminus, c) both N-and C- terminus, d) N- and C-terminus with different functional peptides*

The insertion site of the linker (N- and C- terminal) during the molecular design is based on the protein structure and the distance of the terminal from the active site of the protein. This careful design and selection would help to prevent the interference in the catalytic properties of the protein. For example, while designing fusion protein (BCA-$P_{11}4$), the linker was kept on the C-terminal of bovine carbonic anhydrase to ensure the self-assembly peptide (-$P_{11}4$) lies far from the entrance of the active site. The active site of bovine carbonic anhydrase is closer to N-terminus compared to C-terminus (Shanbhag et al., 2016).

There are varieties of linkers with different amino acid sequences that have been used for recombinant protein fusion, as listed below (Table 2.6). The linkers such as KESGSVSSEQLAQFRSLD and EGKSSGSGSESKST were used for the production of a bioactive single chain variable fragment (scFv) (Bird et al., 1988).

Table 2.6: *Summary of different types of linkers used for the fusion protein*

Linker	Fusion protein	Application	References
KESGSVSSEQLAQFRSLD, EGKSSGSGSESKST	scFv	Increase stability and flexibility	(Bird et al., 1988)
$(Gly)_8$	Myc-Est2p	Increase stability and flexibility	(Sabourin et al., 2007)
$(Gly)_6$	Albumin-ANF	Increase stability and flexibility	(de Bold et al., 2012)
(GGGGS)n (n=1, 2, 4)	PGA-rTHS	Improve stability, flexibility, and biological activity	(Bergeron et al., 2009)
$(GGGGS)_3$	HBsAg preS1	Increase stability and flexibility	(Hu et al., 2004)
GGGGS	HAS-IFN-α2b	Improve biological activity	(Zhao et al., 2008)
$(EAAAK)_n$ (n=1-3)	Beta-Glucanase –Xylanase	Increase expression	(Lu & Feng, 2008)
PAPAP	HAS-IFN-α2b	Improve biological activity	(Zhao et al., 2008)
AEAAAKEAAAKA	HAS-IFN-α2b	Improve biological activity	(Zhao et al., 2008)
VSQTSKLTRAETVFPDV	FIX-albumin	Enable targeting	(Schulte, 2009)
$A(EAAAK)_4ALEA(EAAAK)_4A$	G-CSF-Tf and hGH-Tf	Alter the pK	(Chen et al., 2011)

Sabourin et al designed a linker of eight Glycine (Gly)8 to construct fusion protein for easy protein detection (Sabourin et al., 2007). The linker (Gly)8 was found stable against proteolytic enzyme digestion and highly improved the in vivo functionality whereas (Gly)6 was used to produce human serum albumin (de Bold et al., 2012). The helix forming linker (EAAAK)n were found stable but rigid with the formation of intra-segment hydrogen bones (Amet et al., 2008).

Application of the linker is desirable upon the application of the fusion proteins. However, based on several fusion systems, the linker size (length) varies from 2 to 31 amino acids which are optimised to eliminate any impose on the conformation or interactions of linked partner (Reddy Chichili et al., 2013). Likewise, the linker length was kept considering the substrate molecule effectively interact with an enzyme (Washida et al., 2001). The most preferred linker providing better flexibility, solubility, and improving biological activity is the combination of non-polar Glycine (Gly) and polar Serine (Ser) (GS linker) (Argos, 1990). The GS linker is smaller where Ser maintains the stability of linker forming hydrogen bonds with water. This reduces the interaction between linker and protein. The GS linker has the sequences $(Gly\text{-}Gly\text{-}Gly\text{-}Gly\text{-}Ser)_n$, where 'n' is the copy number used to achieve optimised linker. In this work, the unstructured GS linker $(GGGGS)_2$ was chosen, as shown in Figure 2. 18.

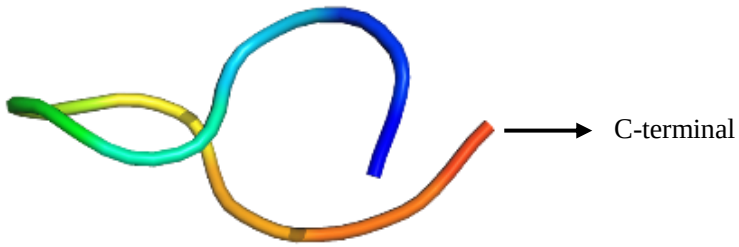

Figure 2.18: *The representative cartoon structure of GS linker. The structure was produced using I-TASSER server (Zhang, 2008).*

2.4.2 Summary

In summary, several methods have been explored in the literature to engineer nanomaterials. In general, nanomaterials are synthesised through top-down or bottom-up approaches using inorganic, organic, and biological components. Inorganic nanoparticles are mechanically stable and bear unique physical and chemical properties while organic nanoparticles constitute of liposomes, micelles, and other organic compounds have attractive biocompatibilities for

therapeutic and drug delivery. The biological nanoparticles are protein/peptide or RNA/DNA-based materials that are highly biocompatible, environmentally friendly, and sustainable technology. The hybrid nanoparticles produced by the integration of inorganic-organic-inorganic-biological components achieved super mechanical and structural properties retaining their individual components properties. Regardless of the types and approaches to engineer nanoparticles, each type has its own strengths and weaknesses. As a result, there is a strong need to engineer bio and hybrid (bio-inorganic) nanoparticles with improved structural features and properties such as attractive biocompatibility and strong mechanical properties.

There are various strategies to engineer bio- and hybrid nanoparticles. Covalent immobilisation has been extensively studied to bind the biological components such as enzymes on the surface of chemically modified inorganic nanoparticles to developing hybrid (bio- and inorganic) nanoparticles. Covalent immobilisation causes multipoint attachment of proteins on the surface of carrier molecular which results in strong binding and low-leakage. However, covalent immobilisation usually reduces protein activity due to steric effects. The use of unmodified inorganic materials through non-covalent affinity immobilisation is the other approach to produce hybrid nanomaterial integrating inorganic and biological components. This approach uses an affinity peptide to bind on the surface of inorganic nanoparticles without using any chemicals to functionalise the surface of inorganic nanoparticles. The affinity binding peptides can also be fused to the desired protein molecule using recombinant technology. The engineering of these hybrid nanoparticles is relatively simple and environmentally friendly, and uses only mild conditions.

The carrier-free approach to engineer nanoparticles is based on biological components such as peptides, DNA, and proteins with self-assembly peptides. The protein particles exhibit higher

biocompatibility, molecular recognition, and self-assembly properties by changing the parameters such as; pH, temperature, and ionic strength. The self-assembling peptides are found highly stable under harsh conditions such as elevated temperature, in the presence of detergents, and other denaturing conditions in literature.

Also, there are strong interests in engineering hybrid nanoparticles with the higher hierarchical nanostructure. There have been several routes and methodologies to produce such architecture using inorganic and organic materials such as Fe_3O_4, Au, and polymers. Such high order structures include capsules, super lattices, and clusters of different sizes. However, these higher order structures still lack important feature such as tuneable size and they require complicated chemistry during fabrication. A new strategy in developing hybrid nanoparticles to tackle the aforementioned challenges is essential to increase the horizon of applications and will be one key question to be addressed in this thesis.

Based on literature review in this chapter, this thesis has identified comparison of different strategies to engineer hybrid and bio-nanoparticles as the central research topic. It will develop and compare four different approaches; i) chemical immobilisation, ii) affinity immobilisation, iii) self-assembly of designed peptides, and iv) combination of affinity adsorption and assembly as detailed in the following chapters.

2.4 References

Abdelhamid, M.A.A., Motomura, K., Ikeda, T., Ishida, T., Hirota, R., Kuroda, A. 2014. Affinity purification of recombinant proteins using a novel silica-binding peptide as a fusion tag. *Applied Microbiology and Biotechnology*, **98**, 5677-84.

Aggeli, A., Bell, M., Carrick, L.M., Fishwick, C.W., Harding, R., Mawer, P.J., Radford, S.E., Strong, A.E., Boden, N. 2003. pH as a trigger of peptide β-sheet self-assembly and reversible switching between nematic and isotropic phases. *Journal of the American Chemical Society*, **125**(32), 9619-9628.

Alivisatos, A.P. 1996. Semiconductor clusters, nanocrystals, and quantum dots. *Science*, **271**(5251), 933-937.

Alloue, W.A.M., Destain, J., El Medjoub, T., Ghalfi, H., Kabran, P., Thonart, P. 2008. Comparison of *Yarrowia lipolytica* lipase immobilization yield of entrapment, adsorption, and covalent bond techniques. *Applied biochemistry and biotechnology*, **150**(1), 51-63.

Amet, N., Lee, H.-F., Shen, W.-C. 2008. Insertion of the designed helical linker led to increased expression of Tf-based fusion proteins. *Pharmaceutical Research*, **26**(3), 523.

Arakaki, A., Shimizu, K., Oda, M., Sakamoto, T., Nishimura, T., Kato, T. 2015. Biomineralization-inspired synthesis of functional organic/inorganic hybrid materials: organic molecular control of self-organization of hybrids. *Organic & Biomolecular Chemistry*, **13**(4), 974-989.

Arakaki, A., Webb, J., Matsunaga, T. 2003. A novel protein tightly bound to bacterial magnetic particles in *Magnetospirillum magneticum* Strain AMB-1. *Journal of Biological Chemistry*, **278**(10), 8745-8750.

Argos, P. 1990. An investigation of oligopeptides linking domains in protein tertiary structures and possible candidates for general gene fusion. *Journal of Molecular Biology*, **211**(4), 943-958.

Arnau, J., Lauritzen, C., Petersen, G.E., Pedersen, J. 2006. Current strategies for the use of affinity tags and tag removal for the purification of recombinant proteins. *Protein Expression and Purification*, **48**(1), 1-13.

Arvizo, R., Bhattacharya, R., Mukherjee, P. 2010. Gold nanoparticles: opportunities and challenges in nanomedicine. *Expert Opin Drug Deliv*, **7**(6), 753-63.

Avery, K.N., Schaak, J.E., Schaak, R.E. 2009. M13 Bacteriophage as a biological scaffold for magnetically recoverable metal nanowire catalysts: combining specific and nonspecific interactions to design multifunctional nanocomposites. *Chemistry of Materials*, **21**(11), 2176-2178.

Bai, Y., Shen, W.-C. 2006. Improving the oral efficacy of recombinant granulocyte colony stimulating factor and transferrin fusion protein by spacer optimization. *Pharmaceutical Research*, **23**(9), 2116-2121.

Baneyx, F., Schwartz, D.T. 2007. Selection and analysis of solid-binding peptides. *Current Opinion in Biotechnology*, **18**(4), 312-317.

Barbas, C.F., Rosenblum, J.S., Lerner, R.A. 1993. Direct selection of antibodies that coordinate metals from semisynthetic combinatorial libraries. *Proceedings of the National Academy of Sciences*, **90**(14), 6385-6389.

Basa, S., Muniyappan, T., Karatgi, P., Prabhu, R., Pillai, R. 2008. Production and in vitro characterization of solid dosage form incorporating drug nanoparticles. *Drug Development and Industrial Pharmacy*, **34**(11), 1209-1218.

Bergeron, L.M., Gomez, L., Whitehead, T.A., Clark, D.S. 2009. Self-renaturing enzymes: Design of an enzyme-chaperone chimera as a new approach to enzyme stabilization. *Biotechnology and Bioengineering*, **102**(5), 1316-1322.

Bernfeld, P., Wan, J. 1963. Antigens and enzymes made insoluble by entrapping them into lattices of synthetic polymers. *Science*, **142**(3593), 678-679.

Bird, R., Hardman, K., Jacobson, J., Johnson, S., Kaufman, B., Lee, S., Lee, T., Pope, S., Riordan, G., Whitlow, M. 1988. Single-chain antigen-binding proteins. *Science*, **242**(4877), 423-426.

Bond, G.M., Stringer, J., Brandvold, D.K., Simsek, F.A., Medina, M.-G., Egeland, G. 2001. Development of integrated system for biomimetic CO_2 sequestration using the enzyme carbonic anhydrase. *Energy & Fuels*, **15**(2), 309-316.

Boverhof, D.R., Bramante, C.M., Butala, J.H., Clancy, S.F., Lafranconi, M., West, J., Gordon, S.C. 2015. Comparative assessment of nanomaterial definitions and safety evaluation considerations. *Regulatory Toxicology and Pharmacology*, **73**(1), 137-150.

Bradfield, J. 1947. Plant carbonic anhydrase. *Nature*, **159**(4040), 467-467.

Brena, B., Gonzalez-Pombo, P., Batista-Viera, F. 2013. Immobilization of enzymes: a literature survey. *Methods Mol Biol*, **1051**, 15-31.

Brown, S. 1992. Engineered iron oxide-adhesion mutants of the *Escherichia coli* phage lambda receptor. *Proceedings of the National Academy of Sciences*, **89**(18), 8651-8655.

Burgos-Asperilla, L., Darder, M., Aranda, P., Vázquez, L., Vázquez, M., Ruiz-Hitzky, E. 2007. Novel magnetic organic–inorganic nanostructured materials. *Journal of Materials Chemistry*, **17**(40), 4233-4238.

Caldwell, K.D., Axén, R., Wall, M.B., Porath, J. 1976. Immobilization of enzymes based on hydrophobic interaction. I. Preparation and properties of a β-amylase adsorbate. *Biotechnology and Bioengineering*, **18**(11), 1573-1588.

Canabady-Rochelle, L.L.S., Belton, D.J., Deschaume, O., Currie, H.A., Kaplan, D.L., Perry, C.C. 2012. Bio-inspired silicification of silica-binding peptide silk protein chimeras: comparison of chemically and genetically produced proteins. *Biomacromolecules*, **13**(3), 683-690.

Cao, G. 2004. Introduction. in: *Nanostructures and Nanomaterials*, Imperial College Press pp. 1-14.

Cao, L., Man, T., Kruk, M. 2009. Synthesis of ultra-large-pore SBA-15 silica with two-dimensional hexagonal structure using triisopropylbenzene as micelle expander. *Chemistry of Materials*, **21**(6), 1144-1153.

Casula, M.F., Conca, E., Bakaimi, I., Sathya, A., Materia, M.E., Casu, A., Falqui, A., Sogne, E., Pellegrino, T., Kanaras, A.G. 2016. Manganese doped-iron oxide nanoparticle clusters and their potential as agents for magnetic resonance imaging and hyperthermia. *Physical Chemistry Chemical Physics*, **18**(25), 16848-16855.

Cavalcanti, A., Shirinzadeh, B., Freitas Jr, R., Hogg, T. 2008. Nanorobot architecture for medical target identification. . *Nanotechnology*, **15103**.

Cavalli, S., Albericio, F., Kros, A. 2010. Amphiphilic peptides and their cross-disciplinary role as building blocks for nanoscience. *Chemical Society Reviews*, **39**(1), 241-263.

Chalfie, M., Tu, G., Euskirchen, G., Ward, W.W., Prasher, D.C. 1994. Green fluorescent protein as a marker for gene expression. *Science*, **263**, 802+.

Chandra, P., Singh, J., Singh, A., Srivastava, A., Goyal, R.N., Shim, Y.B. 2013. Gold nanoparticles and nanocomposites in clinical diagnostics using electrochemical methods. *Journal of Nanoparticles*, **2013**, 12.

Chen, B., He, X.-Y., Yi, X.-Q., Zhuo, R.-X., Cheng, S.-X. 2015. Dual peptide functionalized albumin based nanoparticles with pH-dependent self-assembly behavior for drug delivery. *ACS applied materials & interfaces*, **7**(28), 15148-15153.

Chen, H., Xu, Z., Xu, N., Cen, P. 2005. Efficient production of a soluble fusion protein containing human beta-defensin-2 in *E. coli* cell-free system. *Journal of Biotechnology*, **115**(3), 307-315.

Chen, H., Yeh, J., Wang, L., Khurshid, H., Peng, N., Wang, A.Y., Mao, H. 2010a. Preparation and control of the formation of single core and clustered nanoparticles for biomedical applications using a versatile amphiphilic diblock copolymer. *Nano Research*, **3**(12), 852-862.

Chen, X., Lee, H.-F., Zaro, J.L., Shen, W.-C. 2011. Effects of receptor binding on plasma half-life of bifunctional transferrin fusion proteins. *Molecular Pharmaceutics*, **8**(2), 457-465.

Chen, Z., Cao, Y., Qian, J., Ai, X., Yang, H. 2010b. Facile synthesis and stable lithium storage performances of Sn- sandwiched nanoparticles as a high capacity anode material for rechargeable Li batteries. *Journal of Materials Chemistry*, **20**(34), 7266-7271.

Chockalingam, K., Blenner, M., Banta, S. 2007. Design and application of stimulus-responsive peptide systems. *Protein Eng Des Sel*, **20**(4), 155-61.

Coppage, R., Slocik, J.M., Briggs, B.D., Frenkel, A.I., Naik, R.R., Knecht, M.R. 2012. Determining peptide sequence effects that control the size, structure, and function of nanoparticles. *ACS nano*, **6**(2), 1625-1636.

Cowan, R., GE, J.J., QIN, Y.J., McGregor, M., Trachtenberg, M. 2003. CO_2 capture by means of an enzyme based reactor. *Annals of the New York Academy of Sciences*, **984**(1), 453-469.

Cox, D.M. 1999. High surface area materials. in: *Nanostructure Science and Technology*, Springer, pp. 49-66.
Crumbliss, A., McLachlan, K., O'Daly, J., Henkens, R. 1988. Preparation and activity of carbonic anhydrase immobilized on porous silica beads and graphite rods. *Biotechnology and bioengineering*, **31**(8), 796-801.
Dado, G.P., Gellman, S.H. 1993. Redox control of secondary structure in a designed peptide. *Journal of the American Chemical Society*, **115**(26), 12609-12610.
Damink, L.O., Dijkstra, P.J., Van Luyn, M., Van Wachem, P., Nieuwenhuis, P., Feijen, J. 1995. Glutaraldehyde as a crosslinking agent for collagen-based biomaterials. *Journal of materials science: materials in medicine*, **6**(8), 460-472.
Das, N., Prabhakar, P., Kayastha, A.M., Srivastava, R.C. 1997. Enzyme entrapped inside the reversed micelle in the fabrication of a new urea sensor. *Biotechnology and Bioengineering*, **54**(4), 329-332.
Davenport, D., Nicol, J. 1955. Luminescence in hydromedusae. *Proceedings of the Royal Society of London B: Biological Sciences*, **144**(916), 399-411.
de Bold, M.K., Sheffield, W.P., Martinuk, A., Bhakta, V., Eltringham-Smith, L., de Bold, A.J. 2012. Characterization of a long-acting recombinant human serum albumin-atrial natriuretic factor (ANF) expressed in Pichia pastoris. *Regulatory Peptides*, **175**(1), 7-10.
De, M., Ghosh, P.S., Rotello, V.M. 2008. Applications of nanoparticles in biology. *Advanced Materials*, **20**(22), 4225-4241.
DeLouise, L.A., Miller, B.L. 2005. Enzyme immobilization in porous silicon: Quantitative analysis of the kinetic parameters for Glutathione-S-transferases. *Analytical Chemistry*, **77**(7), 1950-1956.
Dinca, V., Kasotakis, E., Catherine, J., Mourka, A., Ranella, A., Ovsianikov, A., Chichkov, B.N., Farsari, M., Mitraki, A., Fotakis, C. 2008. Directed three-dimensional patterning of self-assembled peptide fibrils. *Nano Letters*, **8**(2), 538-543.
Dinelli, D., Marconi, W., Morisi, F. 1976. Fiber-entrapped enzymes. in: *Methods in Enzymology*, Vol. 44, Academic Press, pp. 227-243.
dos Santos, D.S., Goulet, P.J., Pieczonka, N.P., Oliveira, O.N., Aroca, R.F. 2004. Gold nanoparticle embedded, self-sustained chitosan films as substrates for surface-enhanced Raman scattering. *Langmuir*, **20**(23), 10273-10277.
Dubertret, B., Skourides, P., Norris, D.J., Noireaux, V., Brivanlou, A.H., Libchaber, A. 2002. In vivo imaging of quantum dots encapsulated in phospholipid micelles. *Science*, **298**(5599), 1759-1762.
Duda, D., Tu, C., Qian, M., Laipis, P., Agbandje-McKenna, M., Silverman, D.N., McKenna, R. 2001. Structural and kinetic analysis of the chemical rescue of the proton transfer function of carbonic anhydrase II. *Biochemistry*, **40**(6), 1741-1748.
Dumetz, A.C., Chockla, A.M., Kaler, E.W., Lenhoff, A.M. 2008. Protein phase behavior in aqueous solutions: crystallization, liquid-liquid phase separation, gels, and aggregates. *Biophysical Journal*, **94**(2), 570-583.
Edel, J.B., Kornyshev, A.A., Urbakh, M. 2013. Self-assembly of nanoparticle arrays for use as mirrors, sensors, and antennas. *ACS Nano*, **7**(11), 9526-9532.
Edwards, P.P., Thomas, J.M. 2007. Gold in a metallic divided state—from Faraday to present day nanoscience. *Angewandte Chemie International Edition*, **46**(29), 5480-5486.
Elder, I., Han, S., Tu, C., Steele, H., Laipis, P.J., Viola, R.E., Silverman, D.N. 2004. Activation of carbonic anhydrase II by active-site incorporation of histidine analogs. *Archives of biochemistry and biophysics*, **421**(2), 283-289.
Evers, C.H., Luiken, J.A., Bolhuis, P.G., Kegel, W.K. 2016. Self-assembly of microcapsules via colloidal bond hybridization and anisotropy. *Nature*, **534**(7607), 364.
Fan, T., Yu, X., Shen, B., Sun, L. 2017. Peptide self-assembled nanostructures for drug delivery applications. *Journal of Nanomaterials*, **2017**.
Faraji, M., Yamini, Y., Rezaee, M. 2010. Magnetic nanoparticles: synthesis, stabilization, functionalization, characterization, and applications. *Journal of the Iranian Chemical Society*, **7**(1), 1-37.

Feng, S., Wang, L., Palo, P., Liu, X., Mallapragada, S.K., Nilsen-Hamilton, M. 2013. Integrated self-assembly of the Mms6 magnetosome protein to form an iron-responsive structure. *Int J Mol Sci*, **14**(7), 14594-606.

Fennouh, S., Guyon, S., Livage, J., Roux, C. 2000. Sol-gel entrapment of *Escherichia coli*. *Journal of Sol-Gel Science and Technology*, **19**(1-3), 647-649.

Frenkel, J. 1930. J. Frenkel and J. Dorfman, Nature 126, 274 (1930). *Nature*, **126**, 274.

Fuchs, S.M., Raines, R.T. 2005. Polyarginine as a multifunctional fusion tag. *Protein Sci*, **14**(6), 1538-44.

Gao, X., Cui, Y., Levenson, R.M., Chung, L.W.K., Nie, S. 2004. In vivo cancer targeting and imaging with semiconductor quantum dots. *Nature Biotechnology*, **22**, 969.

Gao, X., Yang, S., Zhao, C., Ren, Y., Wei, D. 2014. Artificial multienzyme supramolecular device: highly ordered self-assembly of oligomeric enzymes in vitro and in vivo. *Angewandte Chemie International Edition*, **53**(51), 14027-14030.

Ge, J., Hu, Y., Biasini, M., Beyermann, W.P., Yin, Y. 2007. Superparamagnetic magnetite colloidal nanocrystal clusters. *Angewandte Chemie International Edition*, **46**(23), 4342-4345.

Ghadiri, M.R., Granja, J.R., Milligan, R.A., McRee, D.E., Khazanovich, N. 1993. Self-assembling organic nanotubes based on a cyclic peptide architecture. *Nature*, **366**, 324.

Ghimire, A., Pattammattel, A., Maher, C.E., Kasi, R.M., Kumar, C.V. 2017. Three-dimensional, enzyme biohydrogel electrode for improved bioelectrocatalysis. *ACS applied materials & interfaces*, **9**(49), 42556-42565.

Gokhale, R.S., Khosla, C. 2000. Role of linkers in communication between protein modules. *Current Opinion in Chemical Biology*, **4**(1), 22-27.

Gong, R., Li, F., Yang, C., Wan, X. 2015. Inclusion of Cu nano-cluster 1D arrays inside a C3-symmetric artificial oligopeptide via co-assembly. *Nanoscale*, **7**(48), 20369-20373.

Greb, C. 2012. Fluorescent proteins-from the beginnings to the nobel prize.

Gupta, A.K., Gupta, M. 2005. Synthesis and surface engineering of iron oxide nanoparticles for biomedical applications. *Biomaterials*, **26**(18), 3995-4021.

Gupta, M.N., Mattiasson, B. 1992. Unique applications of immobilized proteins in bioanalytical systems. *Methods Biochem Anal*, **36**, 1-34.

Han, D., Guo, G., Yan, Y., Li, T., Wang, B., Dong, A. 2018. Pomegranate-like, carbon-coated Fe_3O_4 nanoparticle superparticles for high-performance lithium storage. *Energy Storage Materials*, **10**, 32-39.

He, L., Dexter, A.F., Middelberg, A.P. 2006. Biomolecular engineering at interfaces. *Chemical engineering science*, **61**(3), 989-1003.

Heim, R., Prasher, D.C., Tsien, R.Y. 1994. Wavelength mutations and posttranslational autoxidation of Green Fluorescent Protein. *Proceedings of the National Academy of Sciences of the United States of America*, **91**(26), 12501-12504.

Henry, E., Dif, A., Schmutz, M., Legoff, L., Amblard, F., Marchi-Artzner, V., Artzner, F. 2011. Crystallization of fluorescent quantum dots within a three-dimensional bio-organic template of actin filaments and lipid membranes. *Nano letters*, **11**(12), 5443-5448.

Hermanson, G. 2013a. The reactions of bioconjugation. *Bioconjugate techniques*, **3**, 229-258.

Hermanson, G.T. 2013b. Chapter 5 - Homobifunctional Crosslinkers. in: *Bioconjugate Techniques (Third edition)*, Academic Press. Boston, pp. 275-298.

Hermanson, G.T. 2013c. Chapter 13 - Silane Coupling Agents. in: *Bioconjugate Techniques (Third edition)*, (Ed.) G.T. Hermanson, Academic Press. Boston, pp. 535-548.

Homaei, A.A., Sariri, R., Vianello, F., Stevanato, R. 2013. Enzyme immobilization: an update. *J Chem Biol*, **6**(4), 185-205.

Hsieh, H.-J., Liu, P.-C., Liao, W.-J. 2000. Immobilization of invertase via carbohydrate moiety on chitosan to enhance its thermal stability. *Biotechnology letters*, **22**(18), 1459-1464.

Hu, W., Li, F., Yang, X., Li, Z., Xia, H., Li, G., Wang, Y., Zhang, Z. 2004. A flexible peptide linker enhances the immunoreactivity of two copies HBsAg preS1 (21–47) fusion protein. *Journal of Biotechnology*, **107**(1), 83-90.

Hudalla, G.A., Sun, T., Gasiorowski, J.Z., Han, H., Tian, Y.F., Chong, A.S., Collier, J.H. 2014. Gradated assembly of multiple proteins into supramolecular nanomaterials. *Nature materials*, **13**(8), 829.

Ibraheem, A., Campbell, R.E. 2010. Designs and applications of fluorescent protein-based biosensors. *Current Opinion in Chemical Biology*, **14**(1), 30-36.
Iijima, S. 1991. Helical microtubules of graphitic carbon. *Nature*, **354**, 56.
Ikebe, M., Kambara, T., Stafford, W.F., Sata, M., Katayama, E., Ikebe, R. 1998. A hinge at the central helix of the regulatory light chain of myosin is critical for phosphorylation dependent regulation of smooth muscle myosin motor activity. *Journal of Biological Chemistry*, **273**(28), 17702-17707.
Ikeda, T., Hata, Y., Ninomiya, K.-i., Ikura, Y., Takeguchi, K., Aoyagi, S., Hirota, R., Kuroda, A. 2009. Oriented immobilization of antibodies on a silicon wafer using Si-tagged protein A. *Analytical Biochemistry*, **385**(1), 132-137.
Ikeda, T., Kuroda, A. 2011. Why does the silica-binding protein "Si-tag" bind strongly to silica surfaces? Implications of conformational adaptation of the intrinsically disordered polypeptide to solid surfaces. *Colloids and Surfaces B: Biointerfaces*, **86**(2), 359-363.
Imtaiyaz Hassan, M., Shajee, B., Waheed, A., Ahmad, F., Sly, W.S. 2013. Structure, function and applications of carbonic anhydrase isozymes. *Bioorganic & Medicinal Chemistry*, **21**(6), 1570-1582.
Jang, Y., Choi, W.T., Heller, W.T., Ke, Z., Wright, E.R., Champion, J.A. 2017. Engineering globular protein vesicles through tunable self-assembly of recombinant fusion proteins. *Small*, **13**(36).
Jegan Roy, J., Emilia Abraham, T. 2004. Strategies in making cross-linked enzyme crystals. *Chemical Reviews*, **104**(9), 3705-3722.
Jesus, M., Grazu, V. 2012. *Nanobiotechnology: inorganic nanoparticles vs organic nanoparticles*. Elsevier.
Judeinstein, P., Sanchez, C. 1996. Hybrid organic–inorganic materials: a land of multidisciplinarity. *Journal of Materials Chemistry*, **6**(4), 511-525.
Kashyap, S., Woehl, T.J., Liu, X., Mallapragada, S.K., Prozorov, T. 2014. Nucleation of iron oxide nanoparticles mediated by Mms6 protein in situ. *ACS Nano*, **8**(9), 9097-9106.
Kato, T., Sugawara, A., Hosoda, N. 2002. Calcium carbonate–organic hybrid materials. *Advanced Materials*, **14**(12), 869-877.
Kayastha, A.M., Srivastava, P.K. 2001. Pigeonpea (Cajanus cajan L.) urease immobilized on glutaraldehyde-activated chitosan beads and its analytical applications. *Applied Biochemistry and Biotechnology*, **96**(1), 41-53.
Kim, J., Piao, Y., Hyeon, T. 2009. Multifunctional nanostructured materials for multimodal imaging, and simultaneous imaging and therapy. *Chemical Society Reviews*, **38**(2), 372-390.
Kim, T., Hyeon, T. 2014. Applications of inorganic nanoparticles as therapeutic agents. *Nanotechnology*, **25**(1), 012001.
Kimple, M.E., Brill, A.L., Pasker, R.L. 2013. Overview of affinity tags for protein purification. *Curr Protoc Protein Sci*, **73**, Unit 9 9.
Kostal, J., Mulchandani, A., Gropp, K.E., Chen, W. 2003. A temperature responsive biopolymer for mercury remediation. *Environmental science & technology*, **37**(19), 4457-4462.
Kotov, N.A. 2017. The art of empty space. *Science*, **358**(6362), 448-448.
Kou, G., Shi, S., Wang, H., Tan, M., Xue, J., Zhang, D., Hou, S., Qian, W., Wang, S., Dai, J., Li, B., Guo, Y. 2007. Preparation and characterization of recombinant protein ScFv(CD11c)-TRP2 for tumor therapy from inclusion bodies in *Escherichia coli*. *Protein Expression and Purification*, **52**(1), 131-138.
Kralj, S., Makovec, D. 2014. The chemically directed assembly of nanoparticle clusters from superparamagnetic iron-oxide nanoparticles. *RSC Advances*, **4**(25), 13167-13171.
Kresge, C.T., Leonowicz, M.E., Roth, W.J., Vartuli, J.C., Beck, J.S. 1992. Ordered mesoporous molecular sieves synthesized by a liquid-crystal template mechanism. *Nature*, **359**, 710.
Kriplani, U., Kay, B.K. 2005. Selecting peptides for use in nanoscale materials using phage-displayed combinatorial peptide libraries. *Current Opinion in Biotechnology*, **16**(4), 470-475.
Kroto, H.W., Heath, J.R., O'Brien, S.C., Curl, R.F., Smalley, R.E. 1985. C60: Buckminsterfullerene. *Nature*, **318**, 162.
Lakshmanan, A., Zhang, S., Hauser, C.A. 2012. Short self-assembling peptides as building blocks for modern nanodevices. *Trends in biotechnology*, **30**(3), 155-165.

Lee, S.H., Yu, S.-H., Lee, J.E., Jin, A., Lee, D.J., Lee, N., Jo, H., Shin, K., Ahn, T.-Y., Kim, Y.-W. 2013. Self-assembled Fe_3O_4 nanoparticle clusters as high-performance anodes for lithium ion batteries via geometric confinement. *Nano letters*, **13**(9), 4249-4256.

Li, H., Carter, J.D., LaBean, T.H. 2009. Nanofabrication by DNA self-assembly. *Materials Today*, **12**(5), 24-32.

Liao, N., Wu, M., Pan, F., Lin, J., Li, Z., Zhang, D., Wang, Y., Zheng, Y., Peng, J., Liu, X. 2016. Poly (dopamine) coated superparamagnetic iron oxide nanocluster for noninvasive labeling, tracking, and targeted delivery of adipose tissue-derived stem cells. *Scientific Reports*, **6**, 18746.

Lin, M.M., Kim, D.K., Haj, A.J.E., Dobson*, J. 2008. Development of superparamagnetic iron oxide nanoparticles (SPIONS) for translation to clinical applications. *IEEE Transactions on NanoBioscience*, **7**(4), 298-305.

Lin, Y., Mao, C. 2011. Bio-inspired supramolecular self-assembly towards soft nanomaterials. *Front Mater Sci*, **5**(3), 247-265.

Loryuenyong, V., Buasri, A., Pochana, J., Hosawangwong, S., Thaisaung, S., Sooksaen, P. 2013. Synthesis of anatase TiO_2 nanoparticles by template sol–gel method and its application in photocatalytic degradation of organic pollutants. *Advanced Science Letters*, **19**(10), 2919-2922.

Lovestam, G., Rauscher, H., Roebben, G., Klüttgen, B.S., Gibson, N., Putaud, J.-P., Stamm, H. 2010. Considerations on a definition of nanomaterial for regulatory purposes. *Joint Research Centre (JRC) Reference Reports*, 80004-1.

Lower, B.H., Lins, R.D., Oestreicher, Z., Straatsma, T.P., Hochella Jr, M.F., Shi, L., Lower, S.K. 2008. In vitro evolution of a peptide with a hematite binding motif that may constitute a natural metal-oxide binding archetype. *Environmental science & technology*, **42**(10), 3821-3827.

Lu, P., Feng, M.-G. 2008. Bifunctional enhancement of a β-glucanase-xylanase fusion enzyme by optimization of peptide linkers. *Applied Microbiology and Biotechnology*, **79**(4), 579-587.

Mahmoudi, M., Lynch, I., Ejtehadi, M.R., Monopoli, M.P., Bombelli, F.B., Laurent, S. 2011a. Protein− nanoparticle interactions: opportunities and challenges. *Chemical reviews*, **111**(9), 5610-5637.

Mahmoudi, M., Sant, S., Wang, B., Laurent, S., Sen, T. 2011b. Superparamagnetic iron oxide nanoparticles (SPIONs): development, surface modification and applications in chemotherapy. *Advanced drug delivery reviews*, **63**(1-2), 24-46.

Mahon, B.P., Díaz-Torres, N.A., Pinard, M.A., Tu, C., Silverman, D.N., Scott, K.M., McKenna, R. 2015. Activity and anion inhibition studies of the α-carbonic anhydrase from *Thiomicrospira crunogena* XCL-2 Gammaproteobacterium. *Bioorganic & Medicinal Chemistry Letters*, **25**(21), 4937-4940.

Manh, D.H., Thuan, N.C., Phong, P.T., Hong, L.V., Phuc, N.X. 2009. Magnetic properties of $La_{0.7}Ca_{0.3}MnO_3$ nanoparticles prepared by reactive milling. *Journal of Alloys and Compounds*, **479**(1), 828-831.

Mattiasson, B., Kaul, R. 1991. Determination of coupling yields and handling of labile proteins in immobilization technology. *Bioprocess Technol*, **14**, 161-79.

Meier, W. 1999. Nanostructure synthesis using surfactants and copolymers. *Current Opinion in Colloid & Interface Science*, **4**(1), 6-14.

Meldrum, F.C., Colfen, H. 2008. Controlling mineral morphologies and structures in biological and synthetic systems. *Chemical Reviews*, **108**(11), 4332-4432.

Meldrum, N.U., Roughton, F.J.W. 1933. Carbonic anhydrase. Its preparation and properties. *The Journal of Physiology*, **80**(2), 113-142.

Merhari, L. 2009. *Hybrid nanocomposites for nanotechnology*. Springer.

Motomura, K., Ikeda, T., Matsuyama, S., Abdelhamid, M.A., Tanaka, T., Ishida, T., Hirota, R., Kuroda, A. 2015. The C-terminal zwitterionic sequence of CotB1 is essential for biosilicification of the *Bacillus cereus* spore coat. *J Bacteriol*, **198**(2), 276-82.

Mutter, M., Hersperger, R. 1990. Peptides as conformational switch: medium-Induced conformational transitions of designed peptides. *Angewandte Chemie International Edition*, **29**(2), 185-187.

Nel, A.E., Madler, L., Velegol, D., Xia, T., Hoek, E.M., Somasundaran, P., Klaessig, F., Castranova, V., Thompson, M. 2009. Understanding biophysicochemical interactions at the nano–bio interface. *Nature materials*, **8**(7), 543.

Nguyen, P.Q., Courchesne, N.M.D., Duraj-Thatte, A., Praveschotinunt, P., Joshi, N.S. 2018. Engineered living materials: Prospects and challenges for using biological systems to direct the assembly of smart materials. *Advanced Materials*.

Nimni, M.E., Cheung, D., Strates, B., Kodama, M., Sheikh, K. 1987. Chemically modified collagen: A natural biomaterial for tissue replacement. *Journal of Biomedical Materials Research*, **21**(6), 741-771.

Nudelman, F., Sommerdijk, N.A.J.M. 2012. Biomineralization as an inspiration for materials chemistry. *Angewandte Chemie International Edition*, **51**(27), 6582-6596.

Panda, J.J., Chauhan, V.S. 2014. Short peptide based self-assembled nanostructures: implications in drug delivery and tissue engineering. *Polymer Chemistry*, **5**(15), 4418-4436.

Pathak, S., Choi, S.-K., Arnheim, N., Thompson, M.E. 2001. Hydroxylated quantum dots as luminescent probes for in situ hybridization. *Journal of the American Chemical Society*, **123**(17), 4103-4104.

Patwardhan, S.V., Mukherjee, N., Steinitz-Kannan, M., Clarson, S.J. 2003. Bioinspired synthesis of new silica structures. *Chemical Communications*(10), 1122-1123.

Pazos, E., Sleep, E., Rubert Pérez, C.M., Lee, S.S., Tantakitti, F., Stupp, S.I. 2016. Nucleation and growth of ordered arrays of silver nanoparticles on peptide nanofibers: hybrid nanostructures with antimicrobial properties. *Journal of the American Chemical Society*, **138**(17), 5507-5510.

Prasher, D.C., Eckenrode, V.K., Ward, W.W., Prendergast, F.G., Cormier, M.J. 1992. Primary structure of the *Aequorea victoria* green-fluorescent protein. *Gene*, **111**(2), 229-233.

Qi, H., Liu, C., Long, L., Ren, Y., Zhang, S., Chang, X., Qian, X., Jia, H., Zhao, J., Sun, J. 2016. Blood exosomes endowed with magnetic and targeting properties for cancer therapy. *ACS nano*, **10**(3), 3323-3333.

Qiu, P., Jensen, C., Charity, N., Towner, R., Mao, C. 2010. Oil phase evaporation-induced self-assembly of hydrophobic nanoparticles into spherical clusters with controlled surface chemistry in an oil-in-water dispersion and comparison of behaviors of individual and clustered iron oxide nanoparticles. *Journal of the American Chemical Society*, **132**(50), 17724-17732.

Quiocho, F.A., Richards, F.M. 1964. Intermolecular cross linking of a protein in the crystalline state: Carboxypeptidase-A. *Proceedings of the National Academy of Sciences of the United States of America*, **52**(3), 833-839.

Rajan, S.S., Lackland, H., Stein, S., Denhardt, D.T. 1998. Presence of an N-terminal polyhistidine tag facilitates stable expression of an otherwise unstable N-terminal domain of mouse tissue inhibitor of metalloproteinase-1 in *Escherichia coli*. *Protein Expression and Purification*, **13**(1), 67-72.

Rao, B.C.N.R., Govindaraj, A., Vivekchand, S.R.C. 2006. Inorganic nanomaterials: current status and future prospects. *Annual Reports Section "A" (Inorganic Chemistry)*, **102**(0), 20-45.

Ray, P.C., Yu, H., Fu, P.P. 2009. Toxicity and environmental risks of nanomaterials: challenges and future needs. *J Environ Sci Health C Environ Carcinog Ecotoxicol Rev*, **27**(1), 1-35.

Reches, M., Gazit, E. 2003. Casting metal nanowires within discrete self-assembled peptide nanotubes. *Science*, **300**(5619), 625-627.

Reddy Chichili, V.P., Kumar, V., Sivaraman, J. 2013. Linkers in the structural biology of protein–protein interactions. *Protein Science : A Publication of the Protein Society*, **22**(2), 153-167.

Reithmaier, J., Petkov, P., Kulisch, W., Popov, C. 2009. *Nanostructured materials for advanced technological applications*. Springer Science & Business Media.

Ringler, P., Schulz, G.E. 2003. Self-assembly of proteins into designed networks. *Science*, **302**(5642), 106-109.

Roy, I., Goswami, A. 2017. An introduction to the scope of nanoscience and nanotechnology. in: *Nanobiotechnology*, Anthem Press, pp. 1-30.

Rozhkova, E.A. 2011. Nanoscale materials for tackling brain cancer: recent progress and outlook. *Advanced Materials*, **23**(24), H136-H150.

Ruiz-Hitzky, E., Ariga, K., Lvov, Y.M. 2008. *Bio-inorganic hybrid nanomaterials: strategies, synthesis, characterization and applications*. John Wiley & Sons.
Sabaeian, M., Khaledi-Nasab, A. 2012. Size-dependent intersubband optical properties of dome-shaped InAs/GaAs quantum dots with wetting layer. *Applied Optics*, **51**(18), 4176-4185.
Sabourin, M., Tuzon, C.T., Fisher, T.S., Zakian, V.A. 2007. A flexible protein linker improves the function of epitope-tagged proteins in *Saccharomyces cerevisiae*. *Yeast*, **24**(1), 39-45.
Saleemuddin, M. 1999. Bioaffinity based immobilization of enzymes. *Advances in biochemical engineering/biotechnology*, **64**, 203-226.
Sanchez, C., Belleville, P., Popall, M., Nicole, L. 2011. Applications of advanced hybrid organic-inorganic nanomaterials: from laboratory to market. *Chemical Society Reviews*, **40**(2), 696-753.
Sarikaya, M., Tamerler, C., Jen, A.K.Y., Schulten, K., Baneyx, F. 2003. Molecular biomimetics: nanotechnology through biology. *Nature Materials*, **2**, 577.
Schneider, J.P., Pochan, D.J., Ozbas, B., Rajagopal, K., Pakstis, L., Kretsinger, J. 2002. Responsive hydrogels from the intramolecular folding and self-assembly of a designed peptide. *Journal of the American Chemical Society*, **124**(50), 15030-15037.
Schulte, S. 2009. Half-life extension through albumin fusion technologies. *Thrombosis Research*, **124**, S6-S8.
Schwertmann, U., Cornell, R. 1991. Iron oxides in the laboratory.
Seeman, N.C. 1982. Nucleic acid junctions and lattices. *J Theor Biol*, **99**(2), 237-47.
Shanbhag, B.K., Liu, B., Fu, J., Haritos, V.S., He, L. 2016. Self-assembled enzyme nanoparticles for carbon dioxide capture. *Nano letters*, **16**(5), 3379-3384.
Shimomura, O., Johnson, F.H., Saiga, Y. 1962. Extraction, purification and properties of aequorin, a bioluminescent protein from the luminous hydromedusan, Aequorea. *Journal of Cellular Physiology*, **59**(3), 223-239.
Shipway, A.N., Katz, E., Willner, I. 2000. Nanoparticle arrays on surfaces for electronic, optical, and sensor applications. *ChemPhysChem*, **1**(1), 18-52.
Siegel, R.W. 1993. Synthesis and properties of nanophase materials. *Materials Science and Engineering: A*, **168**(2), 189-197.
Silverman, D.N., Lindskog, S. 1988. The catalytic mechanism of carbonic anhydrase: implications of a rate-limiting protolysis of water. *Accounts of Chemical Research*, **21**(1), 30-36.
Sly, W.S., Hu, P.Y. 1995. Human carbonic anhydrases and carbonic anhydrase deficiencies. *Annu Rev Biochem*, **64**, 375-401.
Smith, K.S., Jakubzick, C., Whittam, T.S., Ferry, J.G. 1999. Carbonic anhydrase is an ancient enzyme widespread in prokaryotes. *Proceedings of the National Academy of Sciences*, **96**(26), 15184-15189.
Snapp, E. 2005. Design and use of fluorescent fusion proteins in cell biology. *Curr Protoc Cell Biol*, **Chapter 21**, Unit 21 4.
Spicer, C.D., Davis, B.G. 2014. Selective chemical protein modification. *Nature communications*, **5**, ncomms5740.
Stachowski, G.M., Bauer, C., Waurisch, C., Bargheer, D., Nielsen, P., Heeren, J., Hickey, S.G., Eychmüller, A. 2014. Synthesis of radioactively labelled CdSe/CdS/ZnS quantum dots for in vivo experiments. *Beilstein journal of nanotechnology*, **5**, 2383.
Strambio-de-Castillia, C., Tetenbaum-Novatt, J., Imai, B.S., Chait, B.T., Rout, M.P. 2005. A method for the rapid and efficient elution of native affinity-purified protein A tagged complexes. *J Proteome Res*, **4**(6), 2250-6.
Sun, L., Fan, Z., Wang, Y., Huang, Y., Schmidt, M., Zhang, M. 2015. Tunable synthesis of self-assembled cyclic peptide nanotubes and nanoparticles. *Soft Matter*, **11**(19), 3822-3832.
Tanaka, M., Mazuyama, E., Arakaki, A., Matsunaga, T. 2011. MMS6 protein regulates crystal morphology during nano-sized magnetite biomineralization in vivo. *Journal of Biological Chemistry*, **286**(8), 6386-6392.
Tang, W., Sun, Z.-Y., Pannell, R., Gurewich, V., Liu, J.-N. 1997. An efficient system for production of recombinant urokinase-type plasminogen activator. *Protein Expression and Purification*, **11**(3), 279-283.

Taniguchi, K., Nomura, K., Hata, Y., Nishimura, T., Asami, Y., Kuroda, A. 2007. The Si-tag for immobilizing proteins on a silica surface. *Biotechnology and Bioengineering*, **96**(6), 1023-1029.
Thielemann, J.P., Girgsdies, F., Schlögl, R., Hess, C. 2011. Pore structure and surface area of silica SBA-15: influence of washing and scale-up. *Beilstein Journal of Nanotechnology*, **2**, 110-118.
Thota, S., Crans, D.C. 2018. *Metal nanoparticles: synthesis and applications in pharmaceutical sciences*. John Wiley & Sons.
Tian, J., Luo, Y., Huang, L., Feng, Y., Ju, H., Yu, B.-Y. 2016. Pegylated folate and peptide-decorated graphene oxide nanovehicle for in vivo targeted delivery of anticancer drugs and therapeutic self-monitoring. *Biosensors and Bioelectronics*, **80**, 519-524.
Tsien, R.Y. 1998. The Green Fluorescent Protein. *Annual Review of Biochemistry*, **67**(1), 509-544.
Tsuchiya, K. 2011. Synthesis of macrocyclic aromatic amines via C-N coupling reaction. *Yuki Gosei Kagaku Kyokaishi/Journal of Synthetic Organic Chemistry*, **69**(2), 169-170.
Udayabhaskararao, T., Altantzis, T., Houben, L., Coronado-Puchau, M., Langer, J., Popovitz-Biro, R., Liz-Marzán, L.M., Vuković, L., Král, P., Bals, S. 2017. Tunable porous nanoallotropes prepared by post-assembly etching of binary nanoparticle superlattices. *Science*, **358**(6362), 514-518.
Vincent, C., E, R.J., D, V.C. 1971. Process for producing low-bulk density silica, Google Patents.
Vinod, T., Zarzhitsky, S., Morag, A., Zeiri, L., Levi-Kalisman, Y., Rapaport, H., Jelinek, R. 2013. Transparent, conductive, and SERS-active Au nanofiber films assembled on an amphiphilic peptide template. *Nanoscale*, **5**(21), 10487-10493.
Wang, L., Prozorov, T., Palo, P.E., Liu, X., Vaknin, D., Prozorov, R., Mallapragada, S., Nilsen-Hamilton, M. 2012. Self-assembly and biphasic iron-binding characteristics of Mms6, a bacterial protein that promotes the formation of superparamagnetic magnetite nanoparticles of uniform size and shape. *Biomacromolecules*, **13**(1), 98-105.
Wang, Y.-X.J. 2013. Quantitative imaging in medicine and surgery: progress and perspective. *Quantitative Imaging in Medicine and Surgery*, **3**(1), 1-4.
Wang, Z., Ruan, J., Cui, D. 2009. Advances and prospect of nanotechnology in stem cells. *Nanoscale research letters*, **4**(7), 593.
Washida, M., Takahashi, S., Ueda, M., Tanaka, A. 2001. Spacer-mediated display of active lipase on the yeast cell surface. *Applied microbiology and biotechnology*, **56**(5-6), 681-686.
Weng, J., Ren, J. 2006. Luminescent quantum dots: a very attractive and promising tool in biomedicine. *Curr Med Chem*, **13**(8), 897-909.
Wheeldon, I.R., Campbell, E., Banta, S. 2009. A chimeric fusion protein engineered with disparate functionalities—enzymatic activity and self–assembly. *Journal of Molecular Biology*, **392**(1), 129-142.
Whitesides, G.M., Grzybowski, B. 2002. Self-assembly at all scales. *Science*, **295**(5564), 2418-2421.
Woo, K., Hong, J., Choi, S., Lee, H.-W., Ahn, J.-P., Kim, C.S., Lee, S.W. 2004. Easy synthesis and magnetic properties of iron oxide nanoparticles. *Chemistry of Materials*, **16**(14), 2814-2818.
Xiu, G.H., Jiang, L., Li, P. 2001. Mass-transfer limitations for immobilized enzyme-catalyzed kinetic resolution of racemate in a fixed-bed reactor. *Biotechnology and Bioengineering*, **74**(1), 29-39.
Yan, J., Pan, Y., Cheetham, A.G., Lin, Y.-A., Wang, W., Cui, H., Liu, C.-J. 2013. One-step fabrication of self-assembled peptide thin films with highly dispersed noble metal nanoparticles. *Langmuir*, **29**(52), 16051-16057.
Yan, L., Amirshaghaghi, A., Huang, D., Miller, J., Stein, J.M., Busch, T.M., Cheng, Z., Tsourkas, A. 2018. Protoporphyrin IX (PpIX)-coated superparamagnetic iron oxide nanoparticle (SPION) nanoclusters for magnetic resonance imaging and photodynamic therapy. *Advanced Functional Materials*.
Yang, Z., Wei, J., Sobolev, Y.I., Grzybowski, B.A. 2018. Systems of mechanized and reactive droplets powered by multi-responsive surfactants. *Nature*.
Yin, Y., Alivisatos, A.P. 2004. Colloidal nanocrystal synthesis and the organic–inorganic interface. *Nature*, **437**, 664.
Yong, K.-T. 2012. Quantum dots for biophotonics. *Theranostics*, **2**(7), 629.

You, F., Yin, G., Pu, X., Li, Y., Hu, Y., Huang, Z., Liao, X., Yao, Y., Chen, X. 2016. Biopanning and characterization of peptides with Fe_3O_4 nanoparticles-binding capability via phage display random peptide library technique. *Colloids and Surfaces B: Biointerfaces*, **141**, 537-545.
Zachariou, M. 2008. *Affinity chromatography: methods and protocols*. Springer Science & Business Media.
Zahn, H. 1955. Bridge reactions in amino acids and fibrous proteins. *Angewandte Chemie International Edition*, **67**, 561-572.
Zhang, F., Yan, H. 2017. DNA self-assembly scaled up. *Nature*, **552**(7683), 34-35.
Zhang, H., Sun, J., Ma, D., Bao, X., Klein-Hoffmann, A., Weinberg, G., Su, D., Schlögl, R. 2004. Unusual mesoporous SBA-15 with parallel channels running along the short axis. *Journal of the American Chemical Society*, **126**(24), 7440-7441.
Zhang, Q., Wei, W., Wang, P., Zuo, L., Li, F., Xu, J., Xi, X., Gao, X., Ma, G., Xie, H.-y. 2017. Biomimetic magnetosomes as versatile artificial antigen-presenting cells to potentiate T-cell-based anticancer therapy. *ACS nano*, **11**(11), 10724-10732.
Zhang, S. 2003. Fabrication of novel biomaterials through molecular self-assembly. *Nature Biotechnology*, **21**, 1171.
Zhang, S., Rich, A. 1997. Direct conversion of an oligopeptide from a β-sheet to an α-helix: a model for amyloid formation. *Proceedings of the National Academy of Sciences*, **94**(1), 23-28.
Zhang, S., Yin, X., Zheng, Y. 2018. Enhanced photocatalytic reduction of CO_2 to methanol by ZnO nanoparticles deposited on ZnSe nanosheet. *Chemical Physics Letters*, **693**, 170-175.
Zhang, X., Cresswell, M. 2016. Chapter 4 - Silica-based amorphous drug delivery systems. in: *Inorganic Controlled Release Technology*, Butterworth-Heinemann. Boston, pp. 93-137.
Zhang, Y. 2008. I-TASSER server for protein 3D structure prediction. *BMC Bioinformatics*, **9**(1), 40.
Zhao, D., Feng, J., Huo, Q., Melosh, N., Fredrickson, G.H., Chmelka, B.F., Stucky, G.D. 1998a. Triblock copolymer syntheses of mesoporous silica with periodic 50 to 300 Angstrom pores. *Science*, **279**(5350), 548-552.
Zhao, D., Huo, Q., Feng, J., Chmelka, B.F., Stucky, G.D. 1998b. Nonionic triblock and star diblock copolymer and oligomeric surfactant syntheses of highly ordered, hydrothermally stable, mesoporous silica structures. *Journal of the American Chemical Society*, **120**(24), 6024-6036.
Zhao, H.L., Yao, X.Q., Xue, C., Wang, Y., Xiong, X.H., Liu, Z.M. 2008. Increasing the homogeneity, stability and activity of human serum albumin and interferon-α2b fusion protein by linker engineering. *Protein Expression and Purification*, **61**(1), 73-77.
Zhao, L., Zhai, J., Zhang, X., Gao, X., Fang, X., Li, J. 2016. Computational design of peptide-Au cluster probe for sensitive detection of α IIb β 3 integrin. *Nanoscale*, **8**(7), 4203-4208.
Zhou, S., Huang, W., Belton, D.J., Simmons, L.O., Perry, C.C., Wang, X., Kaplan, D.L. 2015. Control of silicification by genetically engineered fusion proteins: Silk–silica binding peptides. *Acta biomaterialia*, **15**, 173-180.
Zirah, S., Kozin, S.A., Mazur, A.K., Blond, A., Cheminant, M., Ségalas-Milazzo, I., Debey, P., Rebuffat, S. 2006. Structural changes of region 1-16 of the Alzheimer disease amyloid β-peptide upon zinc binding and in vitro aging. *Journal of Biological Chemistry*, **281**(4), 2151-2161.

This page is intentionally blank

CHAPTER 3

EFFECT OF SURFACE CHEMISTRY FOR COVALENT IMMOBILISATION OF CARBONIC ANHYDRASE ON MESOPOROUS SILICA NANOPARTICLES

This page is intentionally blank

CHAPTER 3
EFFECT OF SURFACE CHEMISTRY FOR COVALENT IMMOBILISATION OF CARBONIC ANHYDRASE ON MESOPOROUS SILICA NANOPARTICLES

3.1 Introduction

One classic group of hybrid bioinorganic nanomaterials is a protein-loaded nanocarrier. This class of bio-nanomaterials includes antibodies-immobilised on nanoparticles for drug delivery, fluorescent protein-conjugated nanoparticles for imaging and tracking, and enzyme-immobilised nanoparticles for biocatalysts. Despite different applications, they share a same principle – proteins are covalently or noncovalent immobilised onto nanocarrier to facilitate their intended functions. This chapter thus choses enzyme immobilisation as an example to study how surface chemistry can affect protein immobilisation including protein activity and stability.

Enzyme immobilisation on nanocarrier has attracted great interests in last decade. The main aim of immobilisation is to increase the reusability, thermal stability, and bio catalytic activity of enzymes (Mateo et al., 2007). There are several approaches such as entrapment (Drevon et al., 2003; Ozdemir, 2009), adsorption (Azari & Nemat-Gorgani, 1999), and covalent coupling (Bhattacharya et al., 2004; Crumbliss et al., 1988; Fei et al., 2016; Vinoba et al., 2012; Zhang et al., 2011) used for immobilisation. The covalent immobilisation approach yields the strongest attachment and highest stability amongst various protein attachment methods with a carrier that has high resistance to degradation. The immobilisation includes the addition of a reactive functional group and then react with the strong nucleophile on the protein. The covalent immobilisation method increases the half-life and thermal stability of enzymes;

however bears steric hindrances and maintaining full enzymatic activity after immobilisation is challenging (Crumbliss et al., 1988; Hsieh et al., 2000).

Previously, covalent immobilisation of the bovine carbonic anhydrase (BCA) on the surface of silica nanoparticles was studied using glutaraldehyde as a functional group (Fei et al., 2016; Vinoba et al., 2012). Glutaraldehyde is used in wide range of pH as a cross-linking agent to produce chemically and thermally stable protein-nanoparticles (Nimni et al., 1987). However, this approach is not significantly great to capture the enzyme or/and limited by the stability. Thus, a better approach is essential for efficient immobilisation. In this chapter, protein-immobilised nanoparticles are studied with an emphasis on surface chemistry optimisation for efficient covalent immobilisation.

Improved enzymatic activity during covalent immobilisation can be achieved by combining two approaches; a) surface optimisation prior to covalent immobilisation and b) use of appropriate inert carrier nanoparticles. The surface optimisation creates an adequate space between the functional groups using various concentrations of diluents to control the surface density. Other is the use of mesoporous silica nanoparticles (MSN, type SBA-15) as carriers. These carrier particles have highly ordered cylindrical hexagonal pores with pore ranges from 2-26 nm (Cao et al., 2009; Zhao et al., 1998a; Zhao et al., 1998b) and a large surface area, up to 838 m^2/g (Thielemann et al., 2011). Additionally, BCA was chosen to study the effect of surface chemistry for efficient covalent immobilisation. BCA has been widely investigated to study the capture and conversion of anthropogenic gas, carbon dioxide (da Costa Ores et al., 2012; J. et al., 2015; Mirjafari et al., 2007). BCA catalyses CO_2 to produce bicarbonate and proton with catalytic efficiency (k_{cat}/K_M $M^{-1}s^{-1}$) approximately $1.1 * 10^7$ (Silverman & Lindskog, 1988) and the reverse reaction at acidic pH. Thus, the optimised surface will provide the

efficient condition for BCA captivity with the improvised catalytic properties and offer a safe, stable, and environmentally benign process for CO_2 capture.

In this chapter, surface chemistry optimisation was undertaken with (3-glycidyloxypropyl) trimethoxysilane (epoxy) or trimethoxysilane (methoxy) as diluent and glutaraldehyde as a cross-linking agent to anchor protein to the particle surface. The silica surfaces were optimised using different mole percentage (mol%) of the functional group (2.5 to 100 mol%) to create optimum space for the covalent binding of BCA with glutaraldehyde. The catalytic property of engineered protein nanoparticles were evaluated by comparison with free enzyme and particles without controlled surfaces underpinning the reusable and CO_2 conversion property. The synthesised MSN were characterised by scanning electron microscopy (SEM), transmission electron microscopy (TEM), and nitrogen adsorption/desorption isotherms.

3.2 Materials and Methods

3.2.1 Materials

E. coli BL21 (DE3) competent cells were purchased from New England Bio labs Inc.-NEB (Wilbury Way Hitchin, UK). Bovine Carbonic Anhydrase (BCA) was synthesised with codon optimisation for bacterial expression and inserted into pET28a by Life Technologies (Germany). Tetraethyl orthosilicate (Si(OC2H5)4, TEOS) (> 99 %), triblock copolymer Pluronic P-123 (P123), Trimethoxysilane (CAS: 2487-90-3), Glutaraldehyde (Grade 1, 25% in H_2O, CAS: 111-30-8), 3-[2-(2-Aminoethylamino)ethyl amino]propyltrimethoxysilane (CAS: 35141-30-1), Toluene (≥99.8%, CAS: 108-88-3), Methanol (≥ 99.9%, CAS: 67-56-1) and Hydrochloric Acid (36.5% - 38%, CAS: 7647-01-0) were purchased from Sigma Aldrich. All the reagents used for the experiments were of standard grades.

3.2.2 Bacterial Transformation, Expression, and Purification

BCA was cloned between *NcoI* and *XhoI* restriction sites in a pET28a expression vector. The vector was transformed into *E. coli* BL21 (DE3) competent cells (New England Biolabs Inc.) adopting NEB transformation protocol. The transformed cells were grown in YT media (kanamycin 50 µg/mL) at 37 °C for 4 h and protein expression was autoinduced using lactose (0.2% w/v) at 20 °C for 18 h. After induction, the cells were harvested and centrifuged at 16221×g, 15 min at 4 °C, then resuspended in lysis buffer (50 mM Tris-HCl pH 8.0, 50 mM NaCl, 1 mM EDTA, 0.5% Triton-X 100) for 20 min then lysed using a sonicator (Q sonicator – Q125, Daintree scientific). The cell pellets were sonicated inside an icebox for 5 min (5 sec on and 20 sec off mode). The soluble recombinant proteins were recovered from cell debris by centrifugation (16221×g) for 30 min at 4 °C.

The recombinant protein was purified using Ni-affinity chromatography (ID 0.78cm ×11.75 cm) with a Bio-Rad BioLogic Duoflow^{TM} Chromatography system. Proteins were eluted from the resin with a linear gradient from 0 to 200 mM imidazole in 10 mM Tris-HCl, 0.5 NaCl (pH 8.0) buffer. The purified protein was desalted into 10 mM phosphate buffer pH 8.0 using Sephadex G-25 (16.7 cm × I.D. 16.7 cm). The purity of the protein was analysed by SDS-PAGE (Laemmli, 1970).

3.2.3 Protein Concentration and Measurement of Enzyme Activity

Protein concentration was determined at 280 nm using Beer's Lambert equation, where ε at Abs 0.1% (=1 g/l) = 1.740 $M^{-1}cm^{-1}$. BCA activity was analysed by measuring esterase activity (Verpoorte et al., 1967). Briefly, 1 mM *p*-nitro phenylacetate (*p*NPA) prepared in 50 mM Tris-HCl, 0.5 M NaCl, pH 8.0 and 50 µL of appropriately diluted purified BCA was incubated in microplate at 37 °C. The reaction was monitored at 15 min intervals using a spectrophotometer

(Tecan Infinite 200 PRO). The amount of *p*-nitrophenoxide ion released on hydrolysis of *p*-nitro phenylacetate (*p*NPA) was measured at 410 nm. A control contained all reagents except enzyme and carbonic anhydrase activity was confirmed using the Wilbur-Anderson titration method which measures the pH change due to the formation of carbonic acid (Wilbur & Anderson, 1948).

3.2.4 Synthesis and Characterization of Silica Nanoparticles

MSN were synthesised using tetraethylorthosilicate (TEOS), as a precursor, as previously described (Yu et al., 2002; Zhao et al., 2013). Briefly, in 150 mL of HCl (2 M), 5 g of Pluronic-123 and 5 g of KCl was added and stirred (280 rpm for 4 h) to allow micelle formation. Then 10.4 g of silica precursor (TEOS) was added to the mixture and stirred for 7 min. Then, the reaction mixture was kept in static condition for 24 h. All the reactions were performed at 37.5 °C. The pore size was regulated by subjecting the reaction mixture to hydrothermal treatment in an oven at 130 °C for 24 h to achieve highly ordered mesoporous structures. The mesoporous particles were washed with MiliQ water, filtered, and collected for drying at 60 °C for 12 h. HCl-ethanol (0.1 M HCl) extraction of detergents was achieved by mixing the dried particles into 180 mL of HCl-ethanol and refluxing at 80 °C for 24 h with stirring at 350 rpm. After extensive washing, MSN were dried at 50 °C overnight.

3.2.5 Electron Microscopy and Surface Area Measurement

MSN were analysed by TEM and SEM. For TEM, the particles were suspended in isopropanol and sonicated for 5 mins. The copper grid with a holey carbon film (300-mesh copper, EM Resolution, United Kingdom) was immersed in the solution for particles loading. The grid was dried and samples were viewed using a TEM at 200 kV (FEI, Tecnai G2 T20 TWIN LaB6) and electron micrographs were recorded using CCD camera and Gatan “Digital Micrograph”

software. For SEM, the silica particles were smeared on carbon tape and coated with iridium. The images were taken using an FEI NOVA 450 electron microscope.

MSN were analysed by N_2 adsorption/desorption at -195.85 °C (Micromeritics ASAP 2020 analyzer). Briefly, the MSN were degassed for 24 hrs at 200 °C under vacuum <5 mmHg. Then, the samples were loaded into ASAP 2020 to calculate surface area (Brunauer-Emmett-Teller, BET), pore size distribution (Barrett-Joyner-Halenda, BJH), and pore volume. BET surface and pore volumes were calculated at a relative pressure range of $P/P_0 = 0.065 \sim 0.28$ and (P/P_0) of 0.99, respectively.

3.2.6 Modifying Surface Chemistry of MSN

The effect of surface chemistry for covalent immobilisation was studied using diluents, a) (3-glycidyloxypropyl) trimethoxysilane (epoxy) or b) trimethoxysilane (methoxy) with glutaraldehyde as a crosslinking agent between particle and enzyme. The aldehyde-functionalised epoxy diluent (AFED) surface particles were prepared in multiple steps as shown in Figure 3.1. Firstly, 3-[2-(2-Aminoethylamino) ethyl amino] propyltrimethoxysilane at the final mol % concentration (2.5-100) was added to (3-glycidyloxypropyl) trimethoxysilane (45 µM in 1.5 mL) and mixed with MSN (100 mg) then stirred (250 rpm) at 37 °C overnight to chemically modify the surface, Figure 3.1a and 3.1b. After chemical attachment, ring opening reaction of the epoxy group was performed (resulting in –OH groups) by adding 0.05 M HCl to the reaction mixture (Parker & Isaacs, 1959), Figure 3.1c. The ring opening reaction was performed to avoid multipoint attachment or/and competition for epoxy groups during the amine coupling reaction used to attach BCA. The silica particles were recovered by discarding the supernatant by centrifugation at 16221×g for 15 min. The nanoparticles were washed sequentially three times with toluene and methanol (5 mL each

time), and dried overnight at 55 °C. The amine group in 3-[2-(2-aminoethyl amino) ethyl amino] propyltrimethoxysilane was converted to an aldehyde group for hydrazone linkage to the protein—a type of Schiff base (Hermanson, 2013), by the addition of 2% (w/v) glutaraldehyde in 10 mM phosphate buffer, pH 8. The mixture was incubated in shaking condition for 60 min at 250 rpm then washed three times with 10 mM phosphate buffer (5 mL each time wash), and dried at 55 °C overnight.

The aldehyde functionalised methoxy diluent (AFMD) particles were prepared under the same conditions as those used for aldehyde functionality with epoxy diluent functionalised particles formation completed as shown in Figure 3.2. In brief, 3-[2-(2-Aminoethylamino) ethyl amino] propyltrimethoxysilane (final mol% concentration 2.5- 100) was added to trimethoxysilane (45 µM in 1.5 mL) and mixed with MSN (100 mg) then stirred (250 rpm) at 37 °C overnight resulting in chemical modification of the surface, Figure 3.2a and 3.2b. These surfaces did not undergo the ring opening reaction and glutaraldehyde was used as a crosslinking agent as described in earlier.

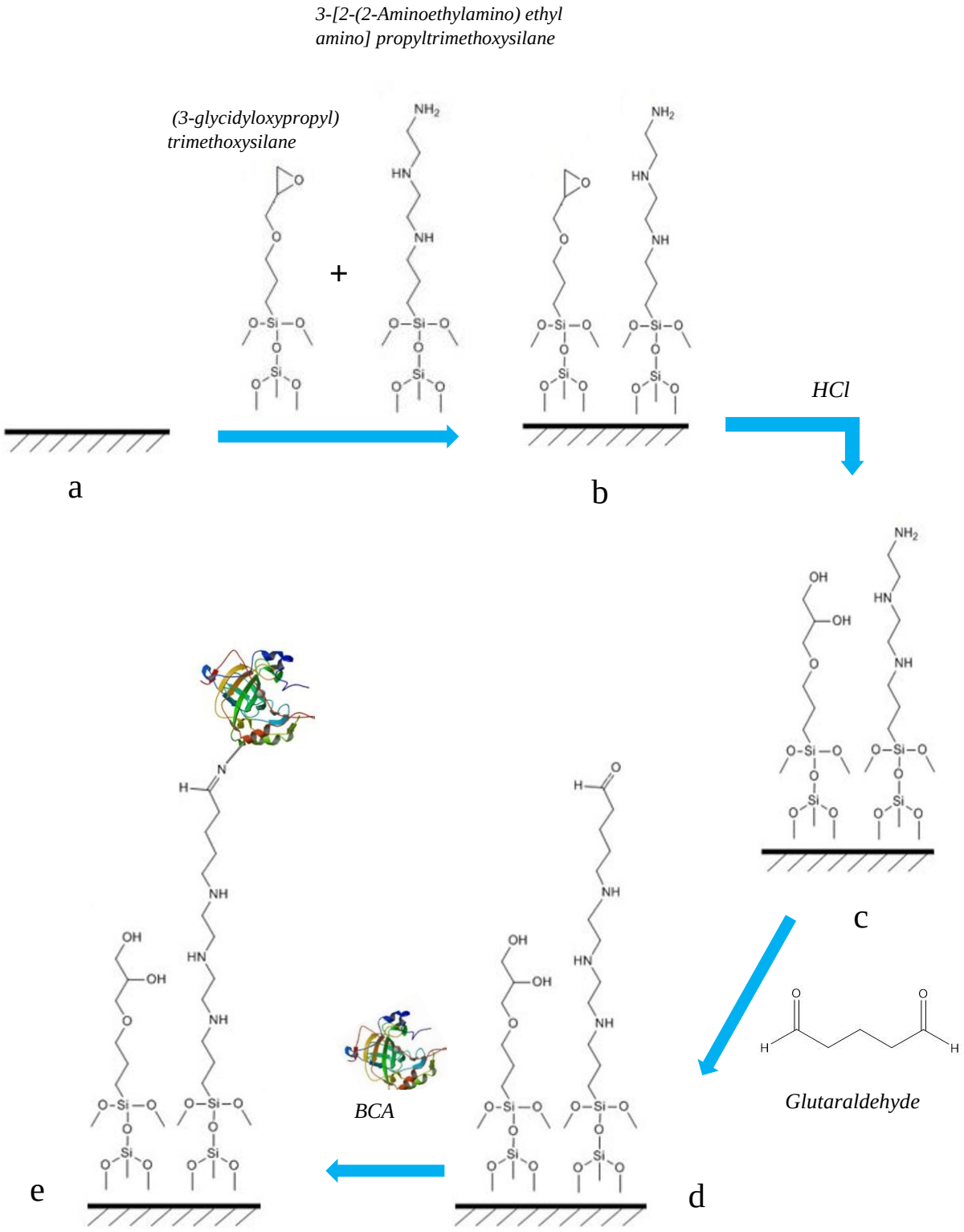

Figure 3.1: *Illustration of the mechanism of covalent immobilisation of BCA on Aldehyde Functionalised Epoxy Diluent (AFED) MSN. a) surface of MSN, b) chemical modification of surface by 3-[2-(2-Aminoethylamino) ethyl amino] propyltrimethoxysilane and (3-glycidyloxypropyl) trimethoxysilane, c) epoxy surface conversion into hydroxyl group through ring opening reaction using HCl, d) MSN with glutaraldehyde on the surface, e) covalent immobilisation of BCA on AFED MSN.*

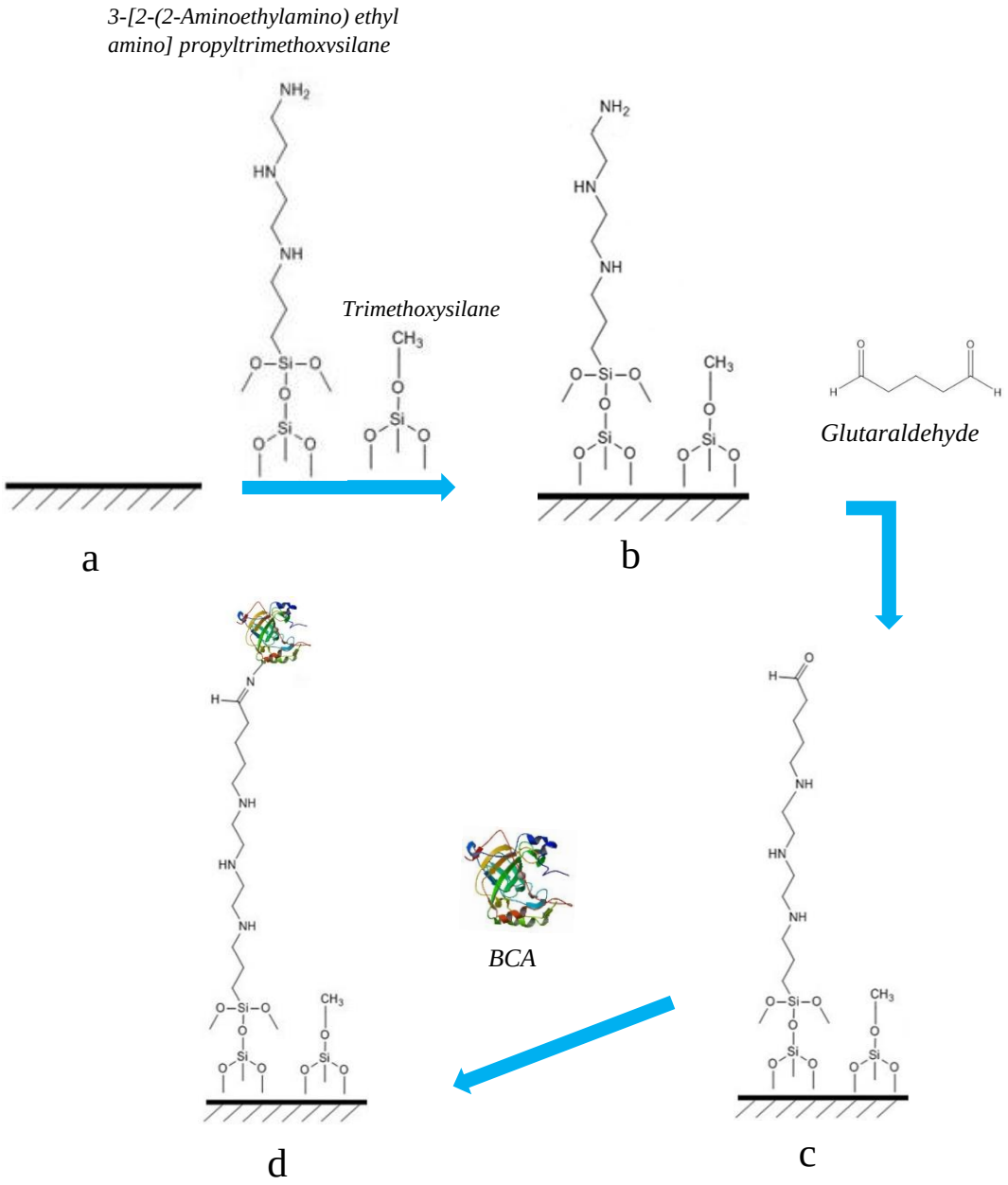

Figure 3.2: *Illustration of the mechanism of covalent immobilisation of BCA on Aldehyde Functionalised Methoxy Diluent (AFMD MSN. a) surface of MSN, b) chemical modification of surface by 3-[2-(2-Aminoethylamino) ethyl amino] propyltrimethoxysilane and Trimethoxysilane, c) MSN with glutaraldehyde on the surface, d) covalent immobilisation of BCA on AFMD MSN*

3.2.7 Immobilisation of BCA on Functionalised MSN

BCA was immobilised on MSN by a covalent coupling method (Zhang et al., 2011; Zhao et al., 2013) using glutaraldehyde as the crosslinking agent Figure 3.1e and 3.2d. In brief, 500 µL of 1 mg/mL of BCA solution in buffer (10 mM phosphate buffer pH 8.0) was mixed with 10

mg of the glutaraldehyde functionalised MSN, followed by gentle vortexing. The mixtures were then shaken (250 rpm) overnight at 37°C. The BCA-immobilised mesoporous nanoparticles (hereafter referred at BCA-nanoparticles) were centrifuged at 16221 ×g at 4°C for 15 min. The BCA nanoparticles were washed three times with 2 mL of 10 mM phosphate buffer, 1 M NaCl, pH 8. The supernatant was collected after each wash. Unreacted epoxy or aldehyde groups were blocked by the addition of 1 ml of ethanolamine solution (1 M). The BCA-nanoparticles were washed three times using phosphate buffer and resuspended in 10 mM phosphate buffer pH 8. BCA-nanoparticles with final 0.5 mg/mL BCA was prepared and stored as stock for further characterisation. The protein concentration of each surface's supernatant was measured for mass balance. A control sample without functionalised nanoparticles was also prepared.

3.2.8 Thermal Stability and Reusability of BCA-nanoparticles

The thermal stability of BCA-nanoparticles was tested by incubating the particles (50 µL, 1 mg/mL) for 2 hr at three different temperatures (25, 40, and 70°C) and the residual activity was compared to free enzyme using the pNPA hydrolysis method (section 2.2).

The reusability of BCA-nanoparticles were analysed by measuring hydratase activity using the Wilbur-Anderson method (Wilbur & Anderson, 1948). In brief, 100 µL of chilled buffer (50 mM HEPES, pH 8 and 50 mM sodium sulfate) was added to an Eppendorf tube. Then, 50 µL of 0.05% bromothymol blue dye was added to the solution. To this solution, 10 µL of ice-cold immobilised BCA enzyme (1 mg/mL) was added. A pH probe was inserted into the tube to monitor pH. The hydratase reaction was initiated by the addition of 250 µL of chilled carbon dioxide saturated water. The rate of pH change from pH 8 to 7.45 was monitored. Five cycles

of the Wilbur-Anderson assay were performed to show the reusability of BCA-nanoparticles. A control sample was measured under the same conditions by replacing enzyme with buffer.

3.3 Results and Discussion

3.3.1 Characterisation of MSN

The synthesized MSN were found to have BET surface area of 442 ± 2.21 m^2/g as measured by N_2 desorption, Figure 3.3a. The particles exhibited a highly ordered mesostructure as shown in TEM images, Figure 3.3b. The SEM analysis of the nanoparticles showed short nano rod shaped structure of about 750 nm in length, as shown in Figure 3.3c. However, the SEM image did not clearly showed the well dispersed particles. This may be due to the unsuitable method of sample preparation procedure. The MSN sample was prepared by smearing directly (without dilution and sonication) on the carbon tape by using a spatula and coated with iridium. The relative standard deviation was 0.125, calculated as the ratio of standard deviation (SD) and mean (M) of the particles. These nanoparticles has an average pore diameter of about 8.7 as analysed by BJH adsorption that are suitable carrier molecule to immobilise large molecules such as BCA which has an average diameter of 3.8 nm (Wanjari et al., 2012). The internal hollow structure of MSN can be fully utilised for efficient immobilisation.

a

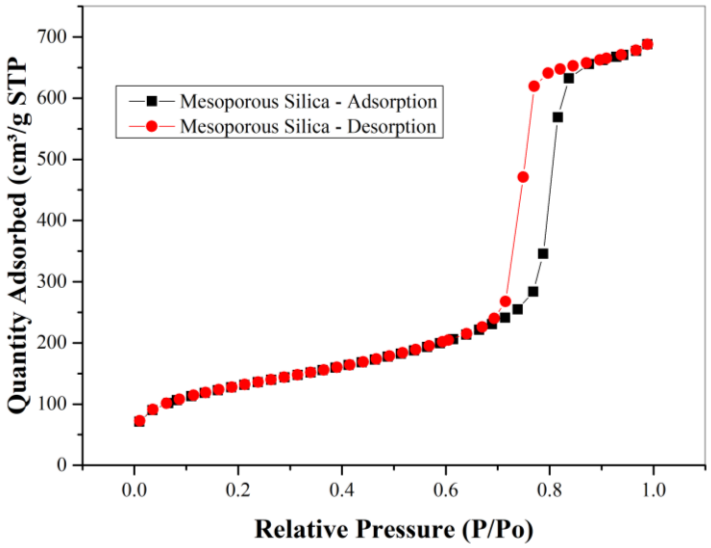

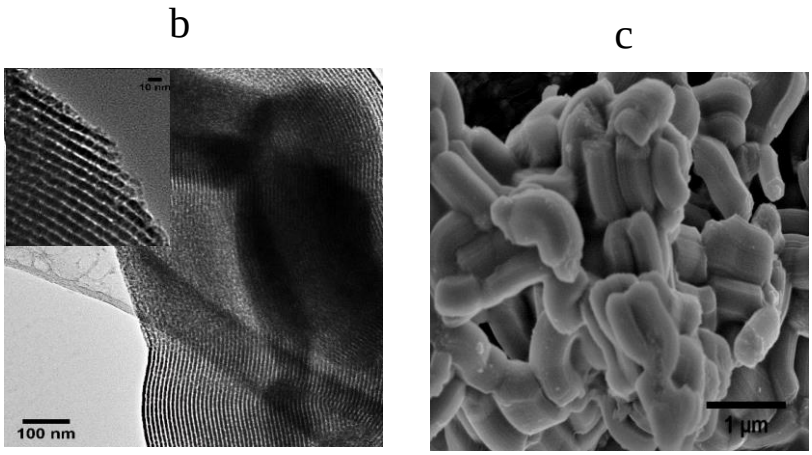

Figure 3.3: *Characterisation of mesoporous silica nanoparticles. a) Nitrogen sorption isotherms, b) TEM image of nanopores, c) SEM of silica nanoparticles*

3.3.2 Purification and Immobilisation of BCA on MSN

BCA was purified using Ni-affinity column chromatography (Figure 3.4a) to a high level of purity as determined by SDS-PAGE, Figure 3.4b. Purified BCA appeared as a single band with a molecular weight of 28 kDa.

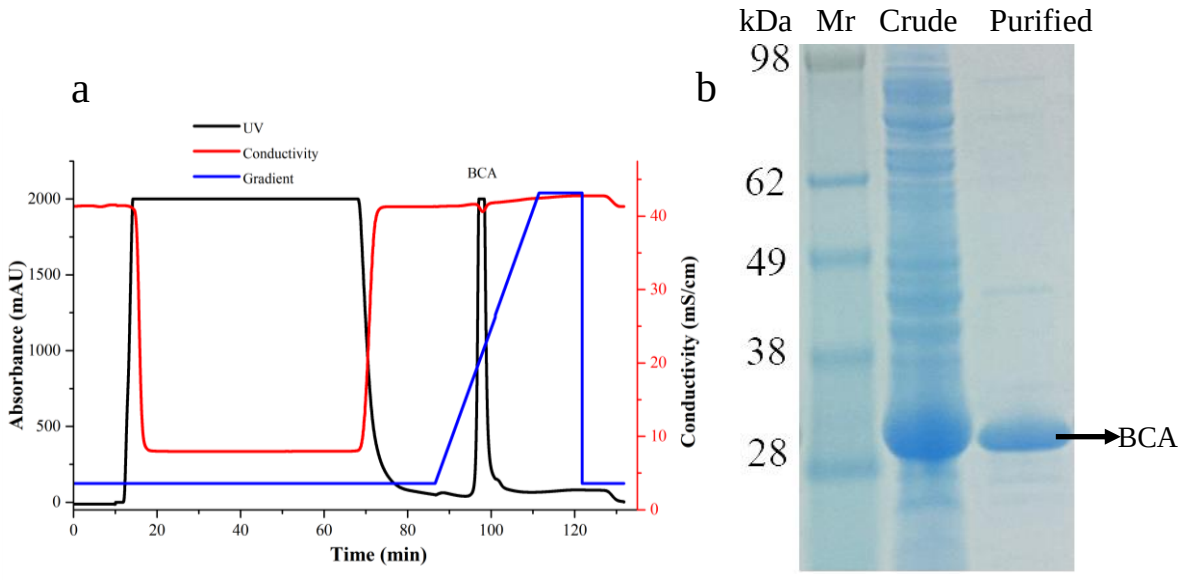

Figure 3.4: *Purification of BCA: a) chromatograph of Ni-affinity purification of BCA. Proteins in solution were absorbed at 280 nm as presented in the chromatography. b) SDS-PAGE gel showing crude and purified BCA. Lanes Mr, protein molecular weight marker (Invitrogen); Crude: crude lysate before purification; Purified; purified BCA. Blue arrow; BCA.*

The purified proteins were immobilised on MSN with different surface chemistries. Interestingly, all these surfaces showed a higher percentile of glutaraldehyde-immobilised enzyme compared to surfaces without diluent, as shown in Figure 3.5. The methoxy diluent AFMD particles bound 87% of BCA (178 mg/g of silica) at 20 mol% dilution and the AFED particles, 88% of BCA (180 mg/g) was immobilised at 50 mol% dilution. This loading is significantly improved in comparison to recent work by Vinoba et al. (116 mg/g of BCA on the surface of MSN) (Vinoba et al., 2012). The dilution on the surface of MSN kept an adequate space between the functional groups (glutaraldehyde) so that covalent immobilisation of BCA was improved. This controlled mode of immobilisation reduced the multi-point attachment of enzyme providing adequate space for increased enzyme capture. The higher loading capacities suggest that the diluted surfaces are better for efficient immobilisation of BCA on the surface of MSN.

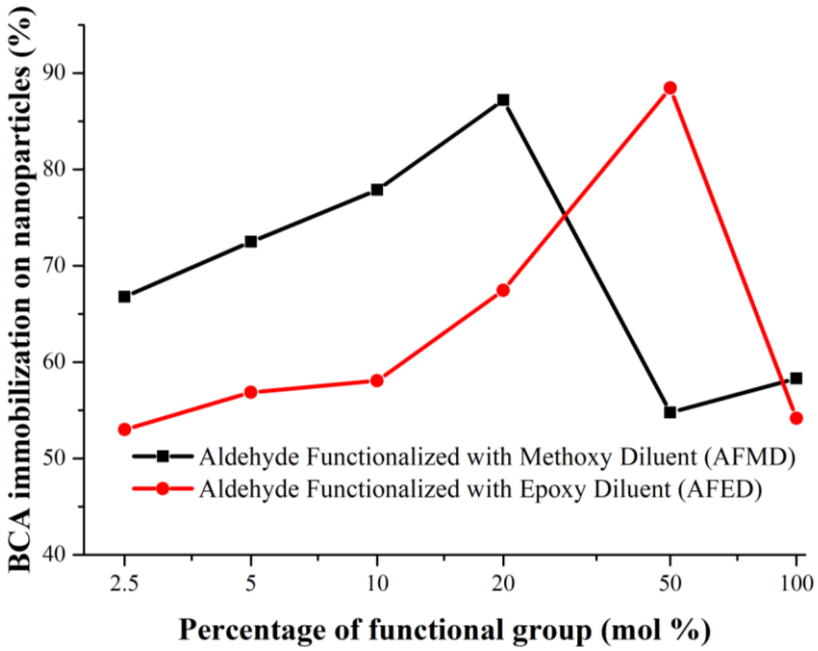

Figure 3.5: *Effect of surface chemistry on covalent immobilisation of BCA on aldehyde functionalised MSN. Two different surfaces (AFMD and AFMD) were prepared using functional groups at various mole percentages (2.5 to 100 mol %)*

3.3.3 Effect of Surface Chemistry on Enzymatic Activity

BCA immobilised onto the aldehyde-functionalised silica nanoparticles retained activity based on pNPA hydrolysis, as shown in Figure 3.6. BCA immobilised with both surface chemistry (AFED and AFMD) showed the highest activity at 20 mol% despite the highest immobilisation of protein at 50 mol% on AFED particles. The low enzymatic activity at 50 mol% compared to that at 20% may be due to the poor mass transfer of substrate due to the steric hindrance from the higher amount of protein (Veronese, 2001).

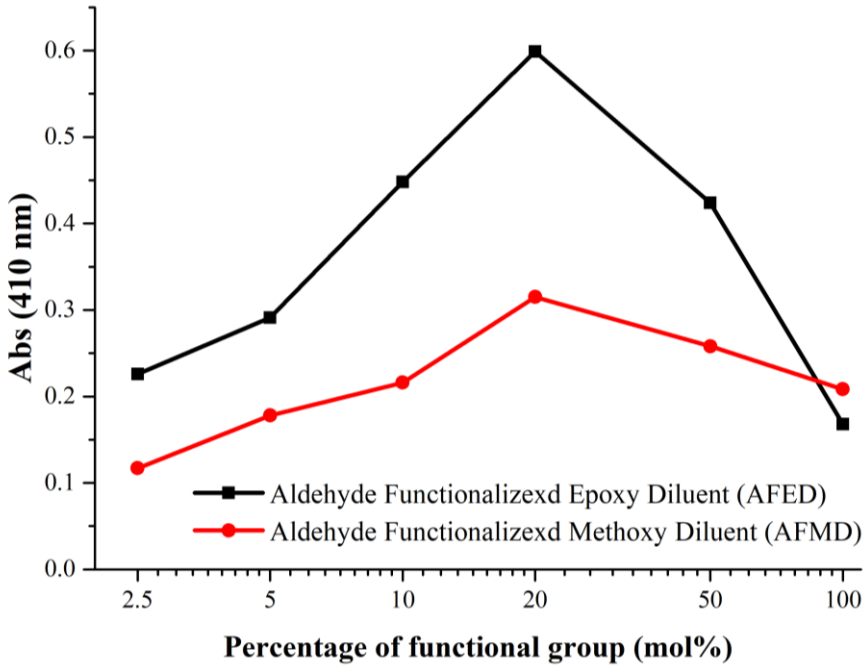

Figure 3.6: *The effect of surface chemistry on enzymatic activity determined using the esterase assay. The assay using p-NPA as the substrate producing p-nitrophenol and measured at absorbance 410 nm*

3.3.4 Effect of the Surface on Thermal Stability and Reusability of BCA-nanoparticles

BCA-nanoparticles were found stable and reusable. The immobilised enzymes were highly stable and retained activity after incubation 2 h at 70 °C, a temperature 5-10 °C above its normal denaturation temperature when in solution. At this temperature, the enzyme immobilised on

AFMD particles and AFED retained 90 and 56% of residual activity, respectively, whereas the free enzyme lost almost 90% of its original activity (Figure 3.7). The diluted surface showed better stability at a higher temperature compared to recent work by Fei et al., who found BCA immobilised on the surface of aldehyde functionalised (without dilution) MSN retained 85% activity at after incubation at 50 °C (Fei et al., 2016). The stability of BCA immobilised on silica supports is well known to improve thermal stability of the enzyme (Abdel-Naby, 1993; Vinoba et al., 2011) and a phenomenon that has been attributed to the steric constraints that MSN imposes on the structure of BCA making denaturation more difficult (Forsyth et al., 2013). BCA immobilised on AFMD was more stable at 70 °C compared to AFED surface particles. However, the reason behind this improved stability was not clear and further research on protein-silica interface during the covalent bond is essential to understand the mechanism.

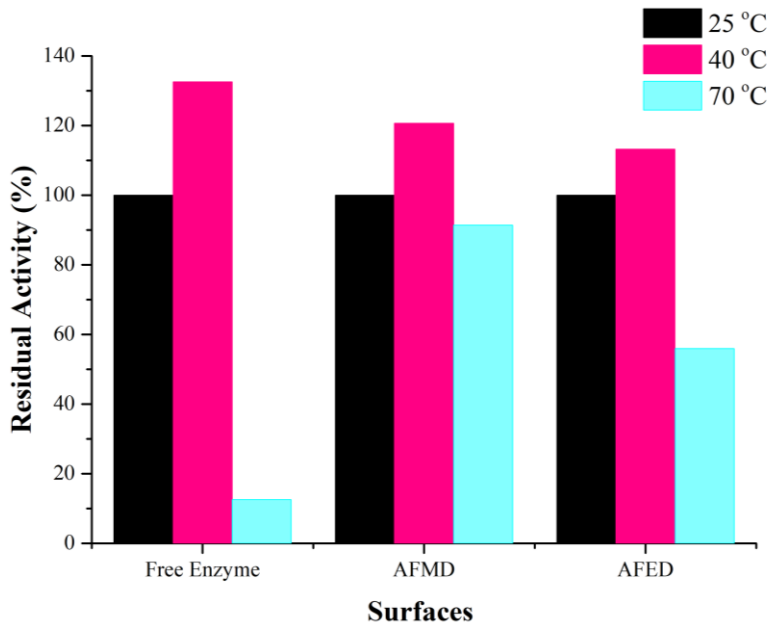

Figure 3.7: *Thermal stability of the BCA-nanoparticles. BCA was incubated at 25, 40, and 70 °C for 2 h and residual activities were determined using the pNPA assay under standard conditions. AFMD: aldehyde functionalisation with methoxy diluent, AFED: aldehyde functionalisation with epoxy diluent.*

The BCA immobilised particles were found reusable as determined using the Wilbur Anderson assay, which is an indicator of carbon dioxide capture. BCA covalently immobilised on AFMD and AFED was active and reused five times without a reduction in enzymatic activity. The reusability of the immobilised particles at 20 mol% on AFMD and AFED surfaces is shown in Figure 3.8a and 3.8b, respectively.

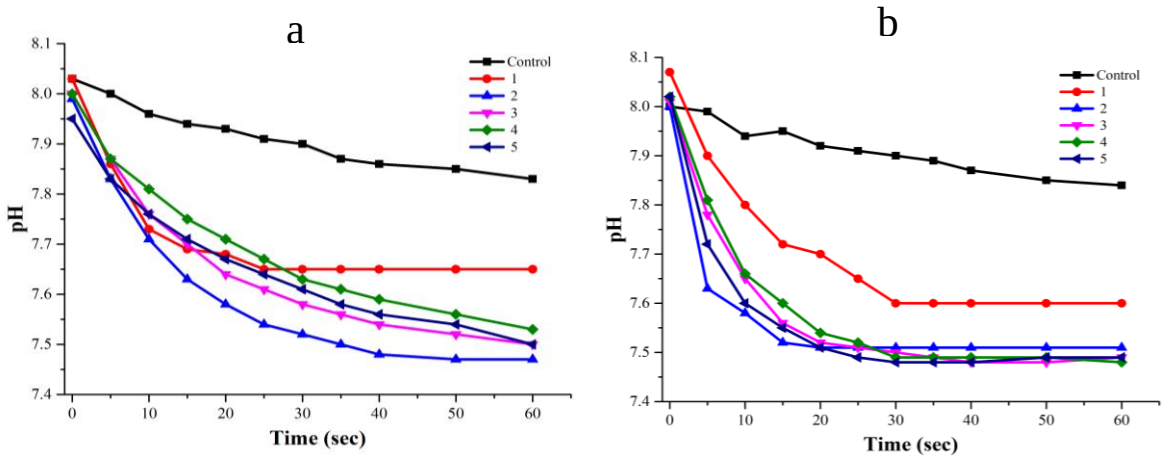

Figure 3.8: *Effect of surface treatment on activity and reusability of BCA-nanoparticles for CO_2 capture, a) AFMD and b) AFED. The immobilised enzymes were reused five times (AFMD/AFED 1-5) and CO_2 capture analysed using the Wilber-Anderson assay. AFMD; aldehyde functionalisation with methoxy diluent, AFED, aldehyde functionalisation with epoxy diluent. The reusability of different surface was performed using the Wilbur Anderson assay to monitor the change in pH with respect to time.*

The immobilised enzyme took nearly 60 secs to reduce the pH from 8.0 to 7.45 ± 0.2, whereas the control (non-functionalized silica nanoparticles) only reduced from pH 8.0 to 7.84 ± 0.3 over the same time. The reusability of the surfaces at different diluent mol% were also evaluated and showed similar results (data not shown). Surprisingly, during the first cycle (Wilbur Anderson assay) the pH decreased to only 7.65 in 60 seconds. The reason for this observation is not known but the non-specific protein (physical adsorption) on the surface of aldehyde functionalised MSN may have resulted in the steric hindrance limiting proper access

of the substrate to the BCA active site. The ability of carbon dioxide capture was improved and stabilised after the first cycle (Figure 3.8). A highly stable and reusable enzyme biocatalyst was produced through the controlled covalent immobilisation of BCA on the surface of MSN. The methodology described herewith provides a platform technology for the development of hybrid enzyme-inorganic materials that enable reuse of enzymes, which not only reduces the cost of enzyme-mediated carbon dioxide capture, but also other processes that require low cost enzyme solutions.

3.4 Summary

In this chapter, BCA was successfully expressed in *E. coli* BL21 (DE3) cells and purified using Ni-affinity chromatography. The purified protein was immobilised covalently to the surface of MSN using glutaraldehyde (2.5- to 100- mol%) as a crosslinking agent with the addition of a lateral spacer. The spacer was created by using two different diluents (3-glycidyloxypropyl) trimethoxysilane (epoxy) and trimethoxysilane (methoxy). The silica surface having epoxy and methoxy at 20 mol percent of the functional group to the surface showed a better enzyme immobilisation level compared with silica lacking diluent treatment. The immobilised BCA was found to be more stable than free enzyme; immobilisation on the methoxy-treated surface exhibited greater stability than the epoxy-treated surface. Furthermore, the silica-immobilised enzymes were recovered and reused five times without compromising CO_2 hydration activity as determined by the Wilbur-Anderson assay. Therefore, an optimised surface provides a platform for the efficient covalent immobilisation of industrial enzymes such as BCA as functional nanoparticles with attractive features such as reusability and high recovery without compromising enzyme activity. However, such convenient approach still requires tedious chemical modification of surface. In the following chapter, a method that does not need surface modification will be developed and presented.

3.5 References:

Abdel-Naby, M.A. 1993. Immobilization of *Aspergillus niger* NRC 107 xylanase and β-xylosidase, and properties of the immobilized enzymes. *Applied Biochemistry and Biotechnology*, **38**(1), 69-81.

Azari, F., Nemat-Gorgani, M. 1999. Reversible denaturation of carbonic anhydrase provides a method for its adsorptive immobilization. *Biotechnology and bioengineering*, **62**(2), 193-199.

Bhattacharya, S., Nayak, A., Schiavone, M., K Bhattacharya, S. 2004. Solubilization and concentration of carbon dioxide: novel spray reactors with immobilized carbonic anhydrase. *Biotechnology and bioengineering*, **86**(1), 37-46.

Cao, L., Man, T., Kruk, M. 2009. Synthesis of ultra-large-pore SBA-15 silica with two-dimensional hexagonal structure using triisopropylbenzene as micelle expander. *Chemistry of Materials*, **21**(6), 1144-1153.

Crumbliss, A., McLachlan, K., O'Daly, J., Henkens, R. 1988. Preparation and activity of carbonic anhydrase immobilized on porous silica beads and graphite rods. *Biotechnology and bioengineering*, **31**(8), 796-801.

da Costa Ores, J., Sala, L., Cerveira, G.P., Kalil, S.J. 2012. Purification of carbonic anhydrase from bovine erythrocytes and its application in the enzymic capture of carbon dioxide. *Chemosphere*, **88**(2), 255-259.

Drevon, G.F., Urbanke, C., Russell, A.J. 2003. Enzyme-containing Michael-adduct-based coatings. *Biomacromolecules*, **4**(3), 675-682.

Fei, X., Chen, S., Liu, D., Huang, C., Zhang, Y. 2016. Comparison of amino and epoxy functionalized SBA-15 used for Carbonic Anhydrase immobilization. *Journal of Bioscience and Bioengineering*, **122**(3), 314-321.

Forsyth, C., Yip, T.W.S., Patwardhan, S.V. 2013. CO_2 sequestration by enzyme immobilized onto bioinspired silica. *Chemical Communications*, **49**(31), 3191-3193.

Hermanson, G.T. 2013. Chapter 5 - Homobifunctional Crosslinkers. in: *Bioconjugate Techniques (Third edition)*, Academic Press. Boston, pp. 275-298.

Hsieh, H.-J., Liu, P.-C., Liao, W.-J. 2000. Immobilization of invertase via carbohydrate moiety on chitosan to enhance its thermal stability. *Biotechnology letters*, **22**(18), 1459-1464.

J., Y.J.K., W., S.G., Frank, C., E., K.S. 2015. The use of carbonic anhydrase to accelerate carbon dioxide capture processes. *Journal of Chemical Technology & Biotechnology*, **90**(1), 3-10.

Laemmli, U.K. 1970. Cleavage of structural proteins during the assembly of the head of bacteriophage T4. *Nature*, **227**(5259), 680-685.

Mateo, C., Palomo, J.M., Fernandez-Lorente, G., Guisan, J.M., Fernandez-Lafuente, R. 2007. Improvement of enzyme activity, stability and selectivity via immobilization techniques. *Enzyme and microbial technology*, **40**(6), 1451-1463.

Mirjafari, P., Asghari, K., Mahinpey, N. 2007. Investigating the application of enzyme carbonic anhydrase for CO_2 sequestration purposes. *Industrial & Engineering Chemistry Research*, **46**(3), 921-926.

Nimni, M.E., Cheung, D., Strates, B., Kodama, M., Sheikh, K. 1987. Chemically modified collagen: A natural biomaterial for tissue replacement. *Journal of Biomedical Materials Research*, **21**(6), 741-771.

Ozdemir, E. 2009. Biomimetic CO_2 sequestration: 1. Immobilization of carbonic anhydrase within polyurethane foam. *Energy & Fuels*, **23**(11), 5725-5730.

Parker, R.E., Isaacs, N.S. 1959. Mechanisms of epoxide reactions. *Chemical Reviews*, **59**(4), 737-799.

Silverman, D.N., Lindskog, S. 1988. The catalytic mechanism of carbonic anhydrase: implications of a rate-limiting protolysis of water. *Accounts of Chemical Research*, **21**(1), 30-36.

Thielemann, J.P., Girgsdies, F., Schlögl, R., Hess, C. 2011. Pore structure and surface area of silica SBA-15: influence of washing and scale-up. *Beilstein Journal of Nanotechnology*, **2**, 110-118.

Veronese, F.M. 2001. Peptide and protein PEGylation: a review of problems and solutions. *Biomaterials*, **22**(5), 405-417.

Verpoorte, J.A., Mehta, S., Edsall, J.T. 1967. Esterase activities of human carbonic anhydrases B and C. *Journal of Biological Chemistry*, **242**(18), 4221-4229.

Vinoba, M., Bhagiyalakshmi, M., Jeong, S.K., Yoon, Y., II, Nam, S.C. 2012. Immobilization of carbonic anhydrase on spherical SBA-15 for hydration and sequestration of CO_2. *Colloids and Surfaces B: Biointerfaces*, **90**, 91-96.

Vinoba, M., Kim, D.H., Lim, K.S., Jeong, S.K., Lee, S.W., Alagar, M. 2011. Biomimetic sequestration of CO_2 and reformation to $CaCO_3$ using bovine carbonic anhydrase immobilized on SBA-15. *Energy & Fuels*, **25**(1), 438-445.

Wanjari, S., Prabhu, C., Satyanarayana, T., Vinu, A., Rayalu, S. 2012. Immobilization of carbonic anhydrase on mesoporous aluminosilicate for carbonation reaction. *Microporous and Mesoporous Materials*, **160**, 151-158.

Wilbur, K.M., Anderson, N.G. 1948. Electrometric and colorimetric determination of carbonic anhydrase. *Journal of Biological Chemistry*, **176**(1), 147-154.

Yu, C., Fan, J., Tian, B., Zhao, D., Stucky, G.D. 2002. High yield synthesis of periodic mesoporous silica rods and their replication to mesoporous carbon rods. *Advanced materials*, **14**(23), 1742-1745.

Zhang, S., Zhang, Z., Lu, Y., Rostam-Abadi, M., Jones, A. 2011. Activity and stability of immobilized carbonic anhydrase for promoting CO_2 absorption into a carbonate solution for post-combustion CO_2 capture. *Bioresource Technology*, **102**(22), 10194-10201.

Zhao, D., Feng, J., Huo, Q., Melosh, N., Fredrickson, G.H., Chmelka, B.F., Stucky, G.D. 1998a. Triblock copolymer syntheses of mesoporous silica with periodic 50 to 300 Angstrom pores. *Science*, **279**(5350), 548-552.

Zhao, D., Huo, Q., Feng, J., Chmelka, B.F., Stucky, G.D. 1998b. Nonionic triblock and star diblock copolymer and oligomeric surfactant syntheses of highly ordered, hydrothermally stable, mesoporous silica structures. *Journal of the American Chemical Society*, **120**(24), 6024-6036.

Zhao, Z., Tian, J., Wu, Z., Liu, J., Zhao, D., Shen, W., He, L. 2013. Enhancing enzymatic stability of bioactive papers by implanting enzyme-immobilized mesoporous silica nanorods into paper. *Journal of Materials Chemistry B*, **1**(37), 4719-4722.

This page is intentionally blank

CHAPTER 4

SURFACE BINDING PEPTIDES ENABLE FACIAL PREPARATION OF HIGHLY STABLE PROTEIN-COATED NANOPARTICLES

This page is intentionally blank

CHAPTER 4
SURFACE BINDING PEPTIDES ENABLE FACIAL PREPARATION OF HIGHLY STABLE PROTEIN-COATED NANOPARTICLES

4.1 Introduction:

The optimisation of surface chemistry in Chapter 3 has facilitated efficient covalent immobilisation of BCA on the chemically modified MSN, delivering protein-coated nanoparticles with reasonably good enzymatic activities. However, the covalent coupling approach needs chemical modification prior to the protein attachment making the preparation process expensive while decreasing functionalities such as the activity. The loss of activity is attributed to covalent multi-point attachment of proteins onto the particle surface, causing protein denaturation and steric hindrance (Ozdemir, 2009). Thus, there is need to explore non-covalent immobilisation using unmodified nanoparticles as carriers while achieving a high stability of functional nanoparticles at the same time.

In this chapter, we propose to achieve a high capacity adsorption of the enzyme without compromising enzymatic activity through the combination of two methods. One method is the use of carrier molecules such as mesoporous silica nanoparticles (MSN) and iron oxide nanoparticles (IONP). The advantage of using MSN has been demonstrated in chapter 3 and we include IONP as another example in this chapter. The second method is the use of affinity binding peptides (cob and Mms6) to facilitate a strong noncovalent binding of enzymes onto nanoparticles.

We have chosen two binding peptides: a) silica binding peptide - cob and b) iron oxide binding peptide - Mms6 to target MSN and IONP, respectively. Cob has highly positive arginine

residues that facilitate strong binding affinity with negatively charged silica nanoparticles (Ikeda & Kuroda, 2011). This affinity mode of immobilisation allows better steric accessibility of their active sites with the substrate and increases the interaction between the immobilised protein and the substrate molecules without compromising the enzymatic activity (Ikeda et al., 2009). Mms6 had been found for the process of biomineralisation and well-studied to form magnetite (Fe_3O_4) nanoparticles in vitro in a Magnetotactic bacterium (*M. magneticum* AMB-1) (Arakaki et al., 2003a). The c-terminal of the protein with a high content of carboxyl and hydroxyl group such as glutamic and aspartic acids are capable of chelating iron (Fe^{2+} or Fe^{3+}) (Feng et al., 2013a; Wang et al., 2012). As shown in the following section, the strong binding affinity of BCA-cob with silica made the immobilisation almost irreversible that made enzyme to be reused without losing enzymatic activity. Interestingly, both engineered fusion proteins were recovered in a single step from crude lysate. The immobilised proteins were found active and BCA-cob has reusable and thermostable properties, underpinning the development of a sustainable technology to capture carbon dioxide. While the results in this chapter are focused on BCA-cob and MSNs, preliminary data of Mms6 and IONPs will be briefly discussed.

4. 2 Materials and Methods

4.2.1 Bacterial Transformation, Protein Expression, and Purification

In this chapter 4 recombinant proteins BCA, BCA-cob, TmCA, and Mms6-TmCA were designed and produced. The amino acid sequences of the proteins are present below. In general, silica binding peptide (cob, amino acid sequences: GRARAQRQSSRGR) (Abdelhamid et al., 2014) was fused to BCA on C-termini. In contrast, iron oxide binding peptide (Mms6, amino acid sequences: MVGGTIWTGKGLGLGLGLGLGAWGPIILGVVGAGAVYAYMKSRDIE SAQSDEEVELRDALA) (Arakaki et al., 2003b) was fused to TmCA on the N-termini., GS-linker (amino acid sequences- GGGGSGGGGS) was used to link peptides and proteins. The

fusion BCA-cob and Mms6-TmCA were synthesized between *NcoI* and *XhoI* restriction sites into pET28a expression plasmids by GenScript (Piscataway, NJ, USA). The plasmids were then transformed into *E. coli* BL21 (DE3) competent cells (New England Biolabs Inc.) following NEB transformation protocol.

Amino acid sequences of the fusion proteins

BCA

GMSHHWGYGKHNGPEHWHKDFPIANGERQSPVDIDTKAVVQDPALKPLALVYGEA
TSRRMVNNGHSFNVEYDDSQDKAVLKDGPLTGTYRLVQFHFHWGSSDDQGSEHTV
DRKKYAAELHLVHWNTKYGDFGTAAQQPDGLAVVGVFLKVGDANPALQKVLDAL
DSIKTKGKSTDFPNFDPGSLLPNVLDYWTYPGSLTTPPLLESVTWIVLKEPISVSSQQM
LKFRTLNFNAEGEPELLMLANWRPAQPLKNRQVRGFPK

BCA-cob

GMSHHWGYGKHNGPEHWHKDFPIANGERQSPVDIDTKAVVQDPALKPLALVYGEA
TSRRMVNNGHSFNVEYDDSQDKAVLKDGPLTGTYRLVQFHFHWGSSDDQGSEHTV
DRKKYAAELHLVHWNTKYGDFGTAAQQPDGLAVVGVFLKVGDANPALQKVLDAL
DSIKTKGKSTDFPNFDPGSLLPNVLDYWTYPGSLTTPPLLESVTWIVLKEPISVSSQQM
LKFRTLNFNAEGEPELLMLANWRPAQPLKNRQVRGFPKGGGGSGGGGSGSGRARA
QRQSSRGR

TmCA

MGSSHHHHHHSSGLVPAGSHMANNVAAPLIDLGAEAKKQAQKSAATQSAVPEKES
ATKVAEKQKEPEEKAKPEPKKPPHWGYFGEEGPQYWGELAPEFSTCKTGKNQSPIN
LKPQTAVGTTSLPGFDVYYRETALKLINNGHTLQVNIPLGSYIKINGHRYELLQYHFH

TPSEHQRDGFNYPMEMHLVHKDGDGNLAVIAILFQEGEENETLAKLMSFLPQTLKK
QEIHESVKIHPAKFFPADKKFYKYSGSLTTPPCSEGVYWMVFKQPIQASVTQLEKMH
EYLGSNARPVQRQNARTLLKSWPDRNRANTVYEFY

Mms6-TmCA

MGSSHHHHHHSSGLVPRGSHMVGGTIWTGKGLGLGLGLGLGAWGPIILGVVGAGA
VYAYMKSRDIESAQSDEEVELRDALAGGGGSGGGGSANNVAAPLIDLGAEAKKQA
QKSAATQSAVPEKESATKVAEKQKEPEEKAKPEPKKPPHWGYFGEEGPQYWGELAP
EFSTCKTGKNQSPINLKPQTAVGTTSLPGFDVYYRETALKLINNGHTLQVNIPLGSYI
KINGHRYELLQYHFHTPSEHQRDGFNYPMEMHLVHKDGDGNLAVIAILFQEGEENE
TLAKLMSFLPQTLKKQEIHESVKIHPAKFFPADKKFYKYSGSLTTPPCSEGVYWMVF
KQPIQASVTQLEKMHEYLGSNAR PVQRQNARTLLKSWPDRNRANTVYEFY

The expression and purification were carried out under the similar conditions as described in chapter 3. In brief, the transformed cells were expressed on YT media through auto-induction at 20 °C for 20 hours. Kanamycin (50 µg/mL) antibiotic was used to prevent microbial infection. The expressed cells were lysed and purified using Ni-affinity column chromatography (5 cm × I.D. 1 cm). Note that Mms6-TmCA expressed cells were lysed and purified under mild denaturation condition using 1% sodium dodecyl sulfate (SDS) or 8 M urea to disrupt the micelles formed by the hydrophobic residues in the N-terminus of Mms6 (Ma et al., 2017). The eluting conditions for the proteins used in this study are summarized in Table 4.1. The purified proteins were desalted into a desalting buffer using Sephadex G-25 (16.7 cm × I.D. 1.76 cm) and purity was analysed by SDS-PAGE and protein sequence was confirmed by mass spectrometry.

Table 4.1: *Elution conditions for proteins used in this study*

Proteins	Elution type	Elution condition	Desalting buffer
BCA	Gradient	0 to 200 mM imidazole in 10 mM Tris-HCl, 0.5 M NaCl, pH 8	10 mM Tris-HCl, pH 8
BCA-cob	Gradient	0 to 200 mM imidazole in 10 mM Tris-HCl, 0.5 M NaCl, pH 8	10 mM Tris-HCl, pH 8
TmCA	Gradient	0 to 200 mM imidazole in 10 mM Tris-HCl, 0.5 M NaCl, pH 8	10 mM phosphate, pH 8
Mms6-TmCA	Gradient	0 to 200 mM imidazole in 20 mM Tris-HCl, 0.1 M NaCl, 1% SDS, pH 8 or 8 M Urea	10 mM phosphate, pH 8

4.2.2 Protein Concentration and Enzyme Activity

The protein concentration was determined by absorbance at 280 nm (Verpoorte et al., 1967) with extinction coefficient determined from amino acids. Enzyme activity was analyzed under the same condition as in chapter 3, using esterase activity measuring the *p*-nitrophenoxide ion released on hydrolysis of *p*-nitro phenylacetate (*p*NPA) by absorbance at 410 nm.

4.2.3 Synthesis and Characterisation of Nanoparticles

IONP was synthesised through chemical co-precipitation reaction method under alkaline condition (Lapresta-Fernández et al., 2011; Ma et al., 2009). Briefly, 0.86 g of $FeCl_2.H_2O$ and 1.4 g of $FeCl_3$ were dissolved on 40 mL of deaerated deionised water under N_2 atmosphere. The mixture was vigorously stirred and heated to 80 °C followed by the dropwise addition of 5 mL of ammonium hydroxide resulting black precipitate. The precipitate was stirred for 30 minutes allowing the growth of iron oxide nanocrystals. Then, 2g of citric acid in 5 mL of miliQ water was added dropwise and stirred for 90 min. All the experiments were performed under Nitrogen atmosphere. After the solution was cool, the magnetic black principate washed three times with N_2 purged miliQ water and recovered each times using a magnet. The

concentrated IONP was dispersed on 100 mL of N_2 purged miliQ water and used as stock for the further experiments.

MSNs was synthesized using the same method as Chapter 3. They were however independently characterized using TEM, SEM, and N_2 adsorption/desorption, and pore size distribution.

4.2.4 BCA Adsorption on MSN

The adsorption of BCA-cob and Wt-BCA on MSN was determined as explained (Liu et al., 2012). In brief, different concentration of BCA-cob and Wt-BCA at 10 mM Tris-HCl, pH 8.0, were mixed with 5 mg of particles in an Eppendorf tube. The solution mixtures were incubated (shaking condition, 250 rpm) for 12 hours at 20 °C to achieve the maximum binding affinity. Then the solution mixtures were centrifuged at 10000 *g for 5 min and the supernatants were collected. Protein concentration before and after binding was a determination by measuring the absorbance at 280 (theoretical extinction coefficient 50420 M^{-1} cm^{-1}) using Tecan (infinite® 200 PRO, Life science). The binding affinity of BCA-cob and WT-BCA were calculated based on the amount of enzyme in the solution before and after the binding.

4.2.5 Immobilisation and Desorption of BCA-cob on MSN

The immobilisation of purified recombinant BCA-cob (3.81 mg) on MSN was performed by mixing 30 mg of MSN in 1.5 mL of binding buffer (10 mM Tris-HCl, pH 8.0). The mixture was incubated under shaking condition (250 rpm) for 1 hour at room temperature. The immobilised BCA-cob on MSN were recovered by centrifugation at 16221 ×g for 5 min, suspended on the binding buffer and analysed by SDS-PAGE. The dissociation of BCA-cob from silica particles were analysed by washing particles for 3 hrs under different ionic strength solutions. The solutions used were; 2 M $MgCl_2$, 2 M $CaCl_2$, 5 M NaCl, 1 N HCl, 50 mM CHES

buffer pH 9 and 10. Then, the particles were washed with binding buffer, collected, and analyzed by SDS-PAGE.

4.2.6 Reusability of Immobilised BCA-cob

The reusability of the immobilised BCA-cob was studied at 4 °C unless stated. The reusability of immobilised BCA-cob was studied and compared with Wt-BCA by hydratase assay using Wilbur-Anderson method (Wilbur & Anderson, 1948). Briefly, 15 mL falcon tube containing 0.5 mL of HEPES and sodium sulfate buffer (50 mM, pH 7.9), 50 µL bromothymol blue dye (0.1 % w/v), and 50 µg/mL of protein (BCA and BCA-cob) were mixed well. The pH probe was inserted into the reaction mixture. The addition of 0.5 mL of saturated CO_2 solution into the reaction mixture (2 mL) will initiate the enzymatic reaction. The time to displace hydrogen ion concentration in the reaction mixture from pH 7.9 to 7.6 had been recorded in seconds. Five cycles of Wilbur-Anderson assay were performed to show the reusability of BCA-cob and Wt-BCA. The immobilised enzymes were recovered each time after centrifugation at 10000 g for 5 min. The hydratase activity was calculated and presented in Wilbur-Anderson Unit (WU) using formula (Tc-Te)/Te, here Tc; time to change the pH to 7.6 by control whereas Te; time to change the pH to 7.6 by the enzyme. A control was run along with the reaction without any enzymes (silica particles).

4.2.7 Single-step Recovery of Mms6-TmCA and BCA-cob from Crude Lysate

IONP and MSN were used to recover Mms6-TmCA and BCA-cob, respectively from the crude lysate. The recombinant *E. coli* BL21 (DE3) cells expressing Mms6-TmCA (0.012 g), BCA-cob (0.1 g wet cell mass), and BCA (0.06 g wet cell mass) protein were suspended in lysis buffer (OD600-20). However, the Mms6-TmCA cells were lysed with the lysis buffer contained with 1% SDS to disrupt the micelles. The cell-free lysate was prepared as explained

above in bacterial transformation and purification section. The single step recovery of Mms6-TmCA was performed by mixing 5 mL of crude lysate and IONP (concentrated 500 µL) for 20 min at room temperature under shaking condition (150 rpm). A magnet was used to recover Mms6-TmCA immobilised particles and resuspended in 200 µL of 10 mM phosphate buffer pH. 8. The recovery of Mms6-TmCA was analysed by SDS-PAGE

The single step recovery of BCA-cob and Wt-BCA were performed by mixing 1.5 mL of soluble crude lysate with silica particles (30 mg). The solution mixtures were incubated at room temperature for 60 minutes under shaking condition (250 rpm). Then, the particles were collected by centrifugation at 10000 g for 5 min. The recovered particles were washed three times with 5 mL of 10 mM Tris/HCl, 0.5 M NaCl, pH 8. The immobilised particles were suspended on 10 mM Tris-HCl, pH 8 and analyzed by SDS-PAGE. The activity of crude BCA-cob attached to silica particles (crude-Si- BCA-cob was determined using Wilbur-Anderson method (Wilbur & Anderson, 1948) as described.

4.2.8 Carbon Dioxide Capture by BCA-cob

The carbon dioxide captured experiments were performed at 4 °C unless stated. The efficiency of CO_2 capture by BCA-cob was determined by the change in pH from 7.85 to 7.45. In brief, 0.127 mg/mL of BCA-cob was mixed with 50 mM of HEPES and sodium sulfate. Then 500 µL of saturated carbon dioxide added to the mixture of 2 mL solution causes the drop-in pH. The time will be recorded for BCA-cob to drop the pH from 7.85 to 7.45. As a control buffer (10 mM Tris-HCl, pH 8) was run under standard condition.

4.3 Results and Discussion:

4.3.1 Structure, Expression, and Purification

In this research, we used TmCA and BCA fused with iron oxide and silica binding peptide linked by a GS linker, Figure 4.1. The fusion protein Mms6-TmCA binds with iron oxide due to the presence of amino acids (Aspartic acid, Glutamic acid in Mms6) that are capable of complexation with iron (Wang et al., 2012). Whereas, BCA-cob binds to silica particles due to affinity adsorption of peptide present at the c-terminal of BCA.

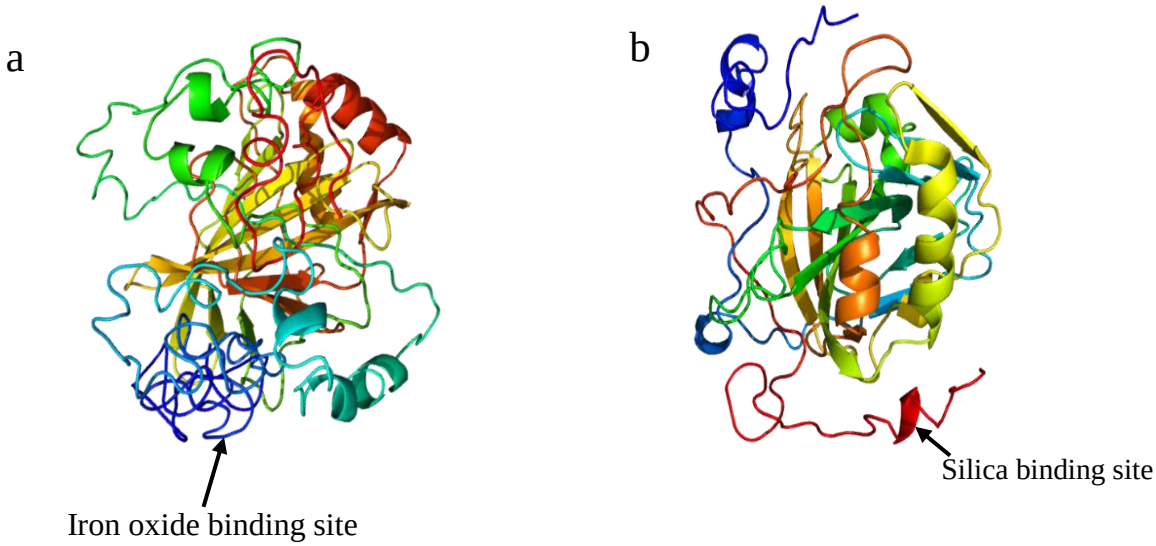

Figure 4.1: *A representative cartoon shaped structure of the fusion protein. a) Mms6-TmCA with Mms6 targeting iron oxide surface and b) BCA-cob with peptide cob targeting silica surface. The structures were produced using I-TASSER server (Zhang, 2008).*

The engineered proteins were expressed in *E.coli BL21* (DE3) and analysed by SDS-PAGE as shown in Figure 4.2 (not BCA). The proteins were well expressed by auto induction and most of the proteins were recovered in soluble fraction when analysed by the gel. The uninduced (seed) cultures did not show any dominant band in the respective size proteins and on adding of lactose have enough expressed protein (induced). The expression was compared with the empty expression plasmid (pET28).

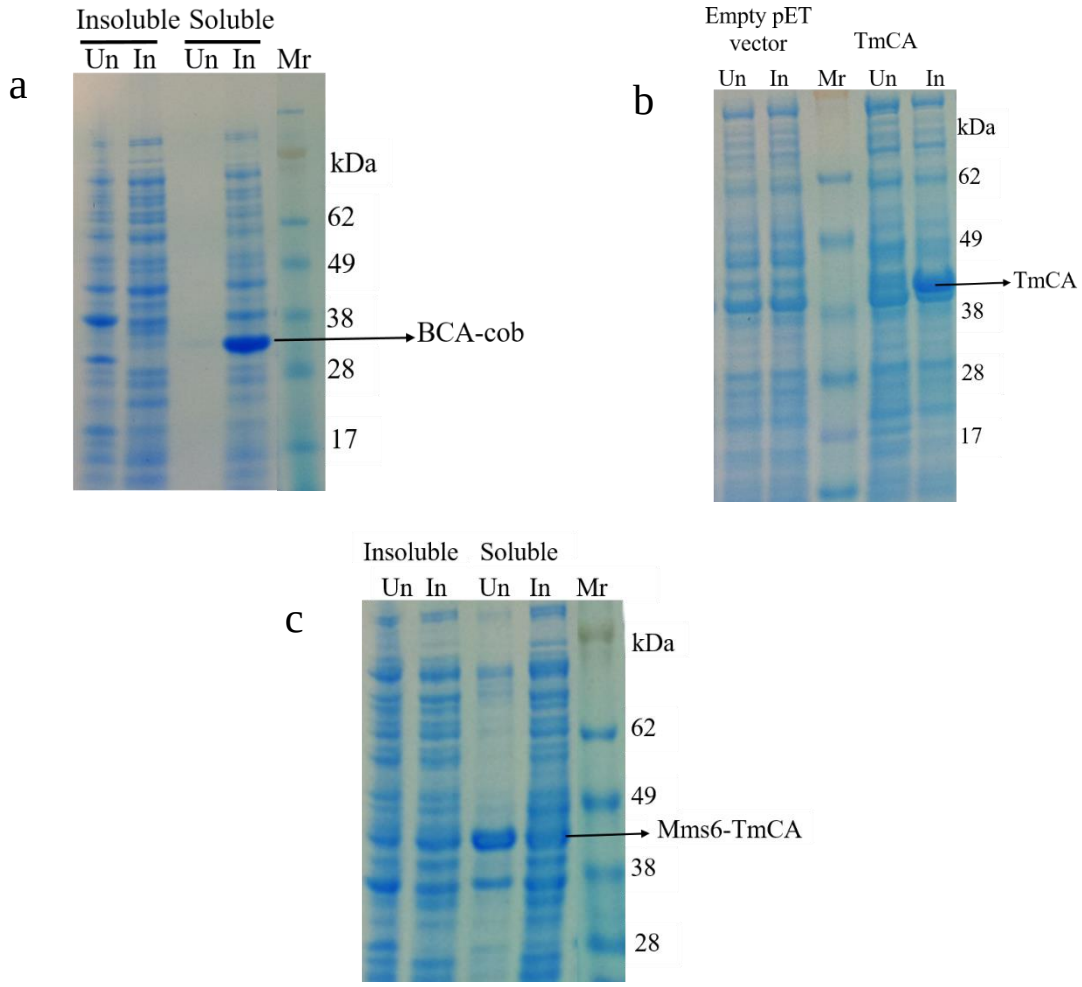

***Figure 4.2**: Expression of recombinant protein: a) BCA-cob, b) TmCA, and c) Mms6-TmCA. Mr, protein marker, Un; uninduced, In; induced samples. Soluble means the proteins were extracted in lysis buffer and insoluble represent the proteins in the cell debris after cell lysis. Empty pET vector is without the recombinant protein sequence. An arrow showed the expressed protein.*

The proteins were purified through Ni-affinity chromatography. The purification chromatography of fusion proteins BCA-cob, TmCA, and Mms6-TmCA are shown in Figure 4.3. The presence of histidine in the recombinant proteins enable the binding with the Ni^{2+} charged sepharose beads which were eluted by the increase in imidazole concentration (gradient method). However, the fusion protein Mms6-TmCA was purified under denaturation condition using 1% SDS and 8 M urea. The denaturation condition was required to disturb the

micelles formations due to the presence of hydrophobic residues in the iron oxide binding peptides (Mms6) (Feng et al., 2013b; Ma et al., 2017) . The purified proteins were desalted into 10 mM Tris-HCl, pH 8 (BCA and BCA-cob) and 10 mM phosphate buffer pH 8 (Mms6 and Mms6-TmCA) for the further characterisation.

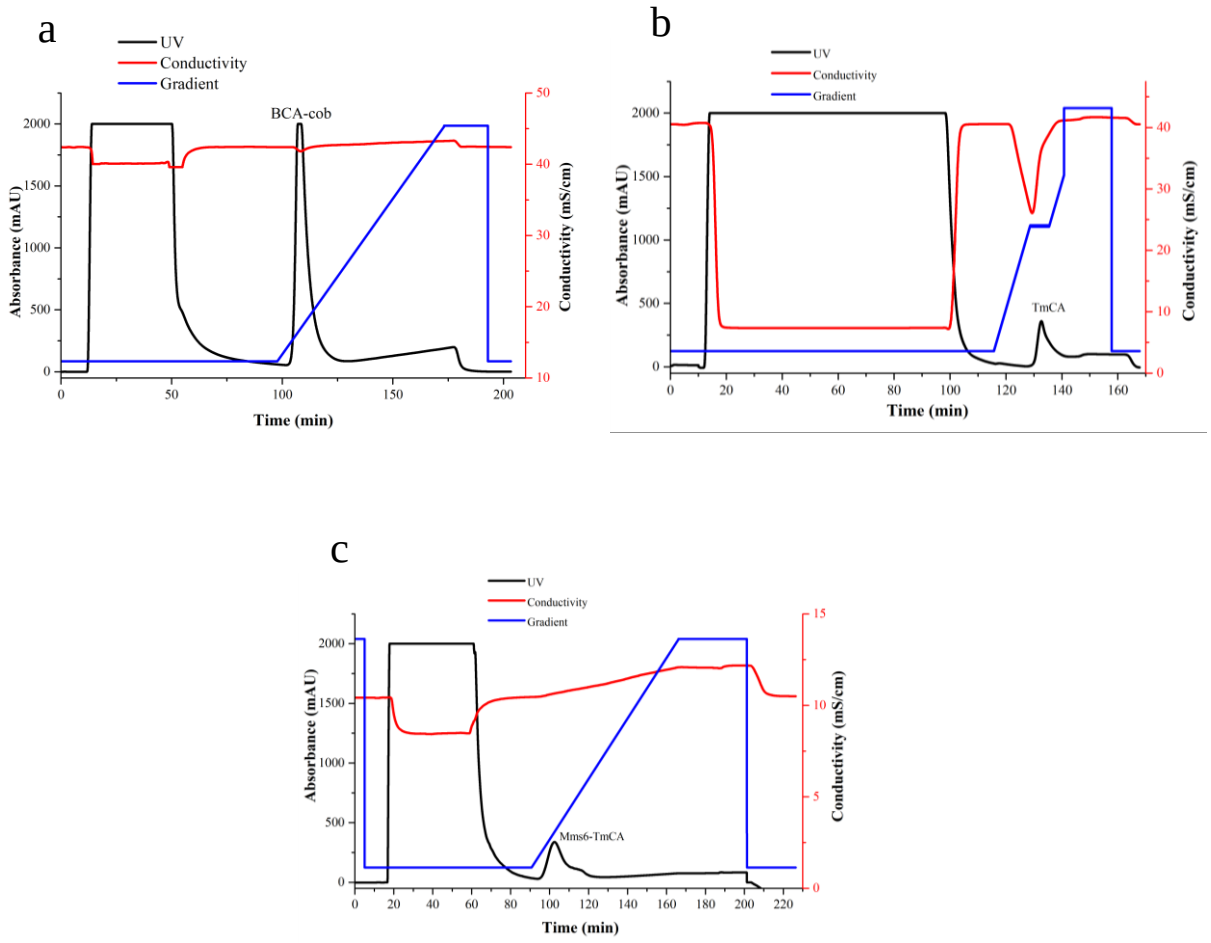

***Figure 4.3**: Chromatography profile of Ni-affinity purification of recombinant fusion protein; a) BCA-cob, b) TmCA, and c) Mms6-TmCA. Proteins in solution were absorbed at 280 nm as presented in the chromatography.*

The purified proteins were analysed by SDS-PAGE (Figure 4.4). The recombinant proteins BCA, BCA-cob, TmCA, and Mms6-TmCA appeared as a single band to their respective molecule weight (Da) in the gel: BCA (MW 29170), BCA-cob (MW 31413), TmCA (MW 35726), and Mms6-TmCA (MW 42483).

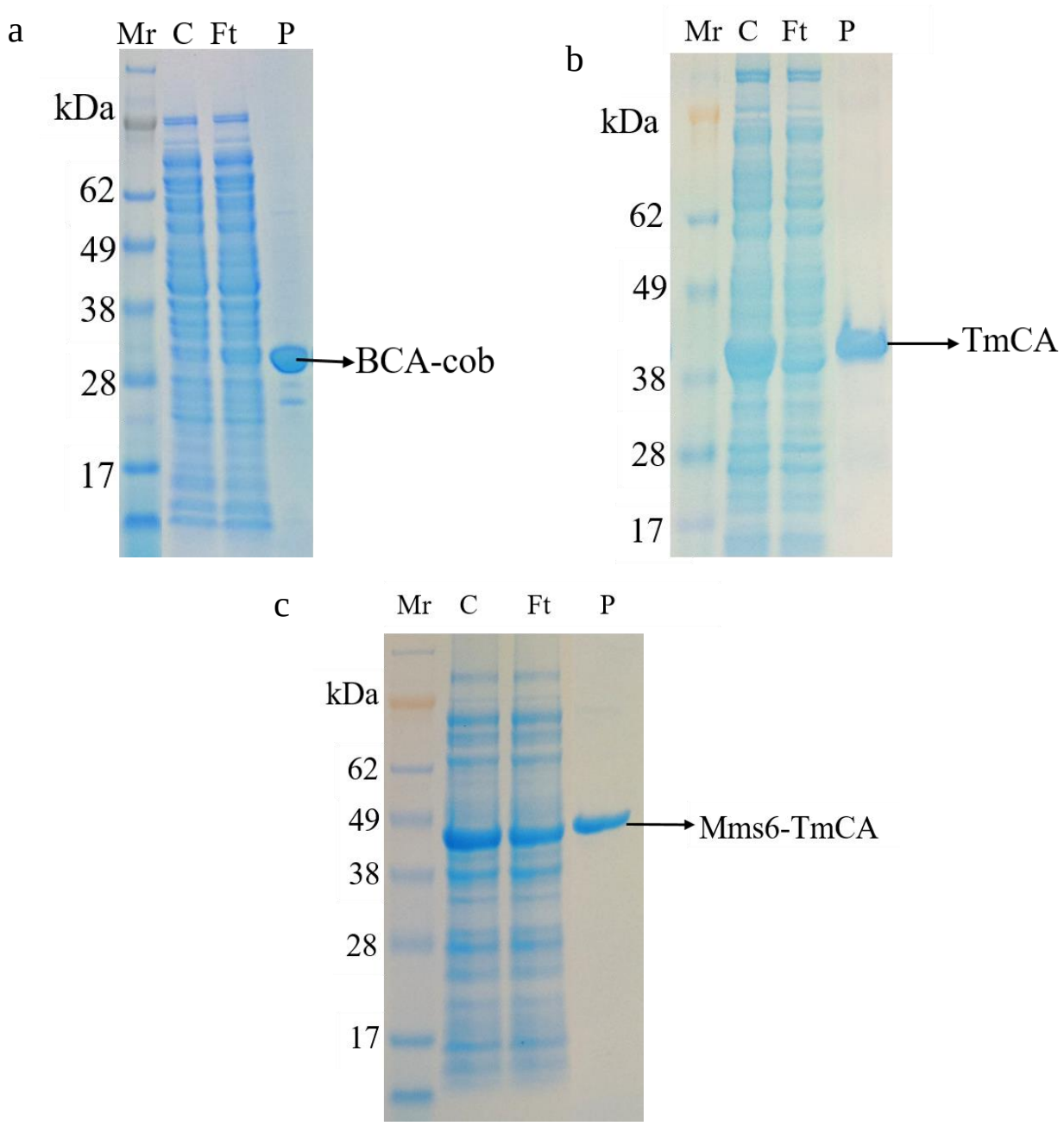

***Figure 4.4**: SDS-PAGE analysis of purified protein, a) BCA-cob, b) TmCA, and c) Mms6-TmCA. Mr, protein marker; C, crude lysate; Ft, flow through the column, P, purified protein*

4.3.2 Characterisation of MSNs and IONP

The SEM and TEM images of the MSN showed the highly ordered mesoporous structure with straight and connected pore channels of about 1 micron in size length (Figure 4.5). The BET surface area of MSN was found 469.3 m^2/g and have the BJH adsorption of average pore width of 8.6 nm. The MSN bearing high surface area and pore volume enabled the high cargo carrying

capacity for the lower molecular biocatalyst. The enzyme BCA with a molecular size of 3.8 nm (Wanjari et al., 2012) bears proper access to utilize the internal hollow structure of the mesoporous particles for binding. The TEM images of the IONP clearly showed the very uniform distribution of nanoparticles with an average size of 10 nm as shown in Figure 4.5c. The nanoparticles appeared monodispersed and relatively spherical crystals (insert figure 4.5c).

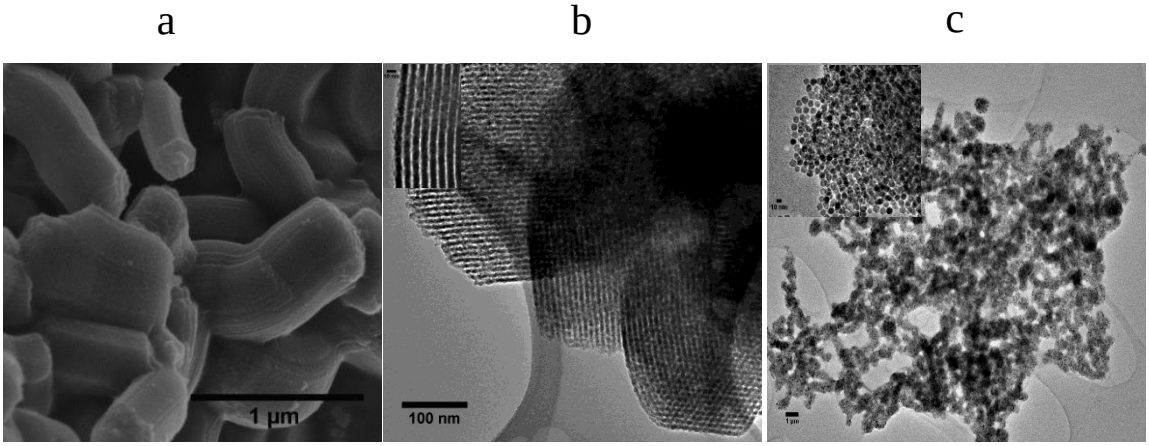

Figure 4.5*: Characterisation of MSN and IONP. (a) SEM image and (b) TEM image of MSN. MSNs were prepared using the same method as chapter 3, but independently here using a different batch. c) TEM images of IONP. The TEM images were taken in a holey carbon grid whereas for SEM, MSN were smeared on carbon tape.*

4.3.3 Adsorption of enzyme on MSNs

The adsorption of the BCA-cob was carried out at 10 mM Tris-HCl pH 8 which is a typical pH used for CO_2 capture (Shanbhag et al., 2016). Additionally, at pH 8 the estimated charge of the silica binding peptide (cob) was estimated to be +5.5 (Estimated using PROTEIN CALCULATOR v3.4.), enabling sufficient binding of peptide onto negative silica surface. The adsorption of BCA-cob and WT-BCA on the MSN is shown in Figure 4.6. Initially, the adsorption of the enzymes increased with increasing the enzyme concentration then reached to a maximum value as presented by Langmuir isotherm. The isotherms for BCA-cob and WT-BCA as described by Langmuir isotherm with maximum adsorption capacity, q_m, was 750.2 ±

26 and 331 ± 20 µg/mg, respectively. Whereas the dissociation constant, K_d, was 130.8 ± 24 and 960.8 ± 14 µg/mL for BCA-cob and WT-BCA, respectively.

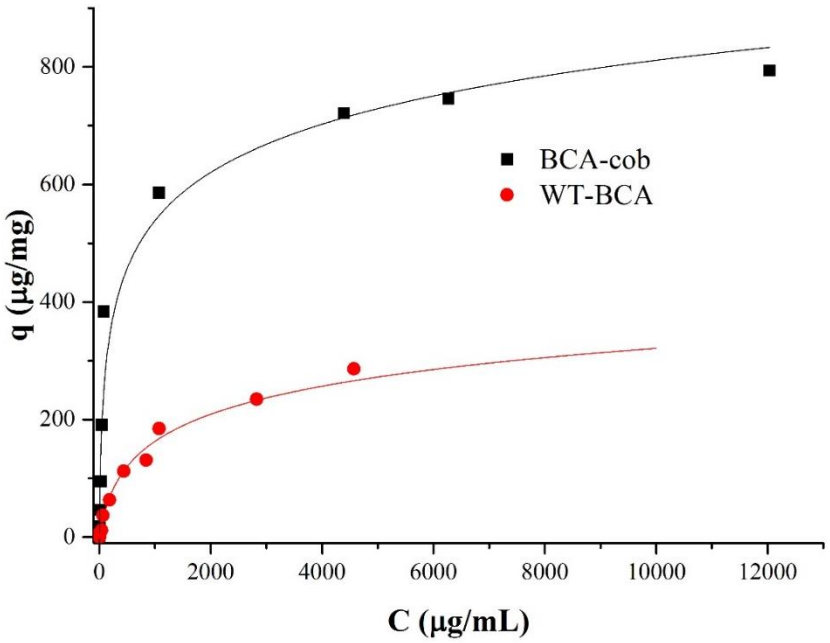

***Figure 4.6**: Adsorption isotherm of (■) BCA-cob (●) WT- BCA in 10 mM Tris-HCl, pH 8.0. Affinity immobilisation of proteins on the surface of MSN.*

The large q_m and low K_d values suggest a higher adsorption capacity and stronger binding affinity of BCA-cob with MSN than WT-BCA. The higher adsorption of the fusion protein may be attributed to (i) the silica-tag peptide (cob) attached on the c-terminal of the protein, (ii) smaller size of BCA-cob protein, and (ii) large internal surface of the MSN (Fan et al., 2003). The peptide cob is a highly basic peptide that binds strongly with the silica surfaces through the collective forces, such as electrostatic binding, Van der Waal forces, ionic bond, and hydrogen bonding (Ikeda & Kuroda, 2011). The smaller size protein (about 3.8 nm) can utilize the internal hollow structure and surface of the silica nanoparticles. Additionally, the nanorods (~ 1 µm) size length particles possess more entrances with short pore channel (Ding et al., 2013), which enabled BCA-cob high capacity adsorption. BCA-cob (31 kDa protein) has a high adsorption capacity, q_m = 750 µg/mg on MSN, higher than the reported value of 533 µg/mg for adsorption of lysosome (14 kDa) on MSN (Fan et al., 2003).

4.3.4 Adsorption stability and dissociation of immobilised BCA-cob

The recombinant BCA-cob was immobilised on MSN and followed by analysis of their adsorption stability on the particles. The immobilised BCA-cob was recovered at higher capacity from working solution as shown in Figure 4.7 (lane 1 and lane 2). This affinity mode of immobilisation is an easy and simple method that involves mixing protein with silica nanoparticles in binding buffer (10 mM Tris-HCl, pH 8.0). This method of immobilisation is due to the strong electrostatic binding between the highly basic cob and negatively charged silanol groups on the silica surfaces (Abdelhamid et al., 2014; Ikeda & Kuroda, 2011; Ikeda et al., 2010).

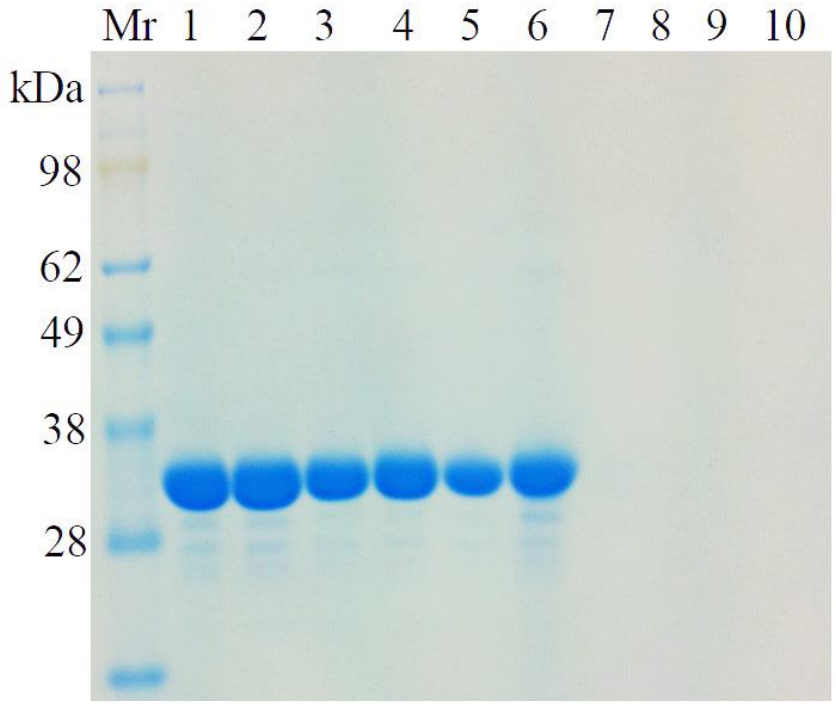

Figure 4.7: *SDS-PAGE showing the elution conditions of BCA-cob. Purified BCA-cob was immobilised on mesoporous silica nanoparticles and eluted by washing the particles using the following solution. Silica particles were recovered by centrifugation then analyzed by SDS-PAGE. Purified BCA-cob (lane 1), immobilised in 10 mM Tris/HCl, pH 8 (lane 2), 2 M $MgCl_2$ (lane 3), 2 M $CaCl_2$ (lane 4), 5 M NaCl (lane 5), 1 N HCl (lane 6), supernatant 2 M $MgCl_2$ (lane 7), 2 M $CaCl_2$ (lane 8), 5 M NaCl (lane 9), 1 N HCl (lane 10). Lane Mr, Protein molecular marker.*

However, at higher ionic strength or/and basic pH, the electrostatic interaction will be significantly reduced because of the competition between the buffer ions and proteins for the adsorption on the silica surfaces (Ikeda & Kuroda, 2011). But surprisingly BCA-cob binds irreversibly with silica surface at high ionic strength such as; 2 M $MgCl_2$, 2 M $CaCl_2$, 5 M NaCl, 1 N HCl (Figure 4.7, lane 3-6, respectively) when ran through the SDS-PAGE gel recovering all the BCA-cob. Additionally, unbound proteins when separated from the MSN were not detected on the gel (Figure 4.7, lane 6-10). This phenomenon is against the work done by T. Ikeda et al. (Ikeda et al., 2010). This strong binding mechanism is still not well understood but may be due to the communal forces such as Van der Waal forces, ionic bond, and hydrogen bonding (Ikeda & Kuroda, 2011). This irreversible affinity immobilisation will be useful for the oriented immobilisation and may achieve good steric accessibility of the active sites for the carbon dioxide capture and conversion.

4.3.5 Reusability of Immobilised BCA-cob

The fusion protein immobilised using silica tag on MSN showed the highest reusability without compromising the residual activity (Figure 4.8). The affinity tagged fusion protein, BCA-cob (pure and crude lysate) showed the hydratase activity when reused for five times without compromising the residual activities. The immobilised fusion protein BCA-cob pure and BCA-cob crude possessed the residual activity of 30 and 25 WU, respectively when reused for five times. Moreover, the reusability of immobilised BCA-cob was compared with the Wt-BCA and found the residual activity of Wt-BCA almost decayed (2 WU) when reused for five times. The physically adsorbed Wt-BCA on MSN lost the protein during each reaction step ultimately requiring the reload of protein.

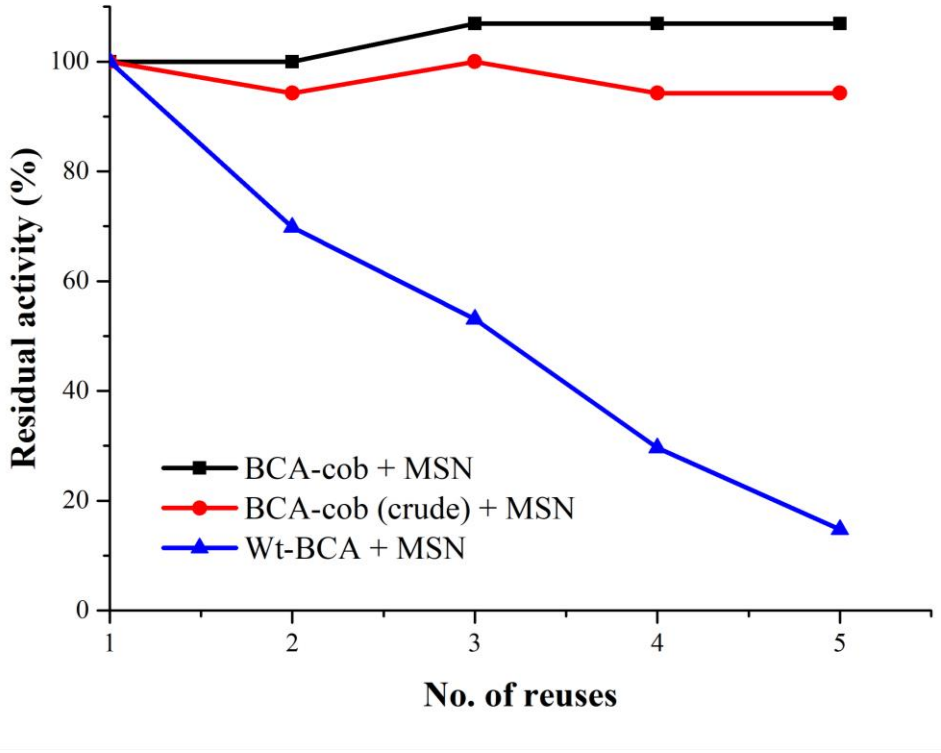

***Figure 4.8**: Residual activities of immobilised BCA-cob. Wilbur-Anderson assay was performed to find the residual activities for five times and compared with WT-BCA. After each assay, the particles were recovered by centrifugation and reused.*

4.3.6 Single Step Recovery of BCA-cob and Mms6-TmCA

The BCA-cob protein was recovered in a single step from the crude lysate using MSN as a matrix and analysed by SDS-PAGE, as shown in Figure 4.9. The strong binding affinity of Si-tag with silica nanoparticles made the fusion protein to fully recover from the crude lysate as compared to Wt- BCA. This positive result is highly comparable with the staphylococcal protein A with silica binding peptides on the c-terminal (Ikeda et al., 2010). The single step recovery of BCA-cob using silica particle can achieve similar purity as Ni-affinity purification of the protein (Figure 4.9), despite that some *E. coli* proteins were also adsorbed on the silica particles even washed three times. This single step recovery of the proteins makes the upstream process easy, cheap, and fast with the use of widely available, biodegradable, and inexpensive silica particles.

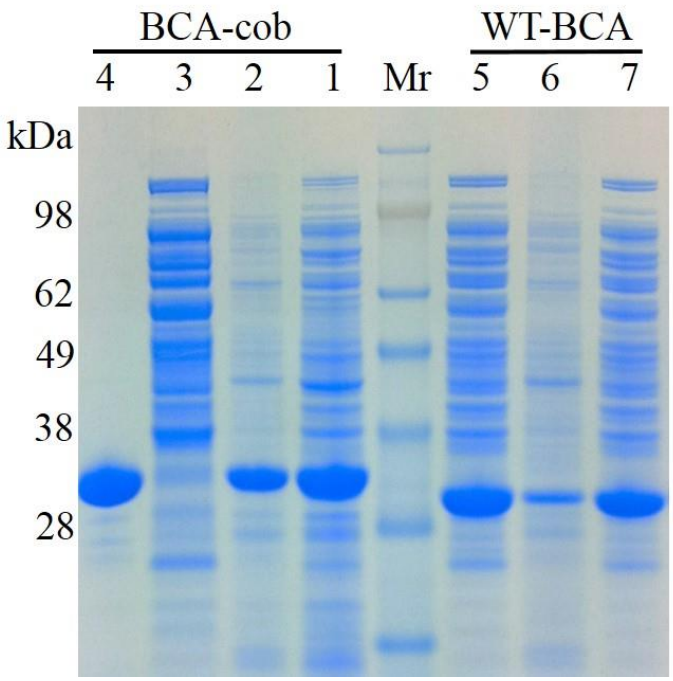

***Figure 4.9**: SDS-PAGE showing the single step recovery of BCA-cob from the crude lysate. Silica particles were suspended on the crude lysates for 1 hour and recovered by centrifugation. The particles and supernatant were analysed by SDS-PAGE. Lane 1: Crude lysate BCA-cob, lane 2: immobilised BCA-cob, lane 3: supernatant BCA-cob, lane 4: BCA-cob purified by Ni-affinity chromatography, lane 5: Crude lysate Wt-BCA, lane 6: immobilised Wt-BCA, lane 6: supernatant Wt-BCA.*

Similarly, the fusion protein Mms6-TmCA was recovered from the crude lysate using IONP and analysed by SDS-PAGE (Figure 4.10). The iron chelating residues in the c-terminal of iron oxide binding protein (Mms6) enabled the facial preparation of Mms6-TmCA bound to iron oxide. Almost all the proteins with the most dominant band were recovered from the crude lysate. However, some *E.coli* non-specific proteins are also adsorbed on the iron oxide, perhaps through nonspecific adsorption.

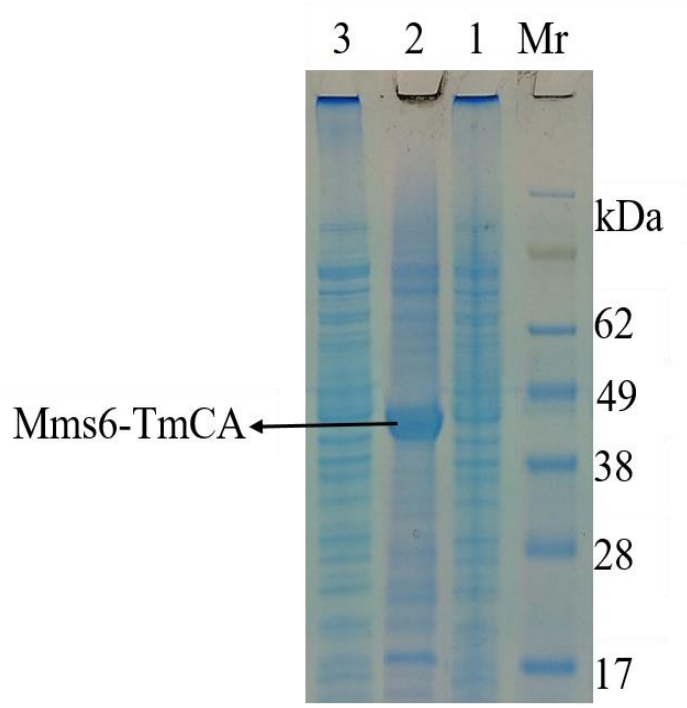

***Figure 4.10**: SDS-PAGE showing the single step recovery of Mms6-TmCA from crude lysate. The IONP were suspended with crude lysate for 20 min then use the magnet to recover the immobilised IONP then loaded into gel. Mr, protein marker; 1, crude lysate; 2, immobilised protein (Mms6-TmCA). A black precipitate on the top of well (P) was due to the gathering of iron oxide nanoparticles. 3; supernatant obtained by using a magnet to the mixture of Mms6-TmCA-IONP.*

4.3.7 Enzymatic Activity

The fusion protein (BCA-cob) was found active to capture and convert carbon dioxide into bicarbonate and hydrogen ion. The enzymatic conversion accelerates the production of H^+ ions that decrease the pH of the working solution. This analysis method showed that the change in pH of the enzymatic reaction mixture substantially drops from 7.85 to 7.5 within 20 secs with 772 WU which accelerated reaction compared to control (without enzyme) presented in Figure 4.11. The highly accelerating capture and conversion of carbon dioxide by BCA-cob will be a useful biocatalyst for carbon dioxide reduction from the flue gas.

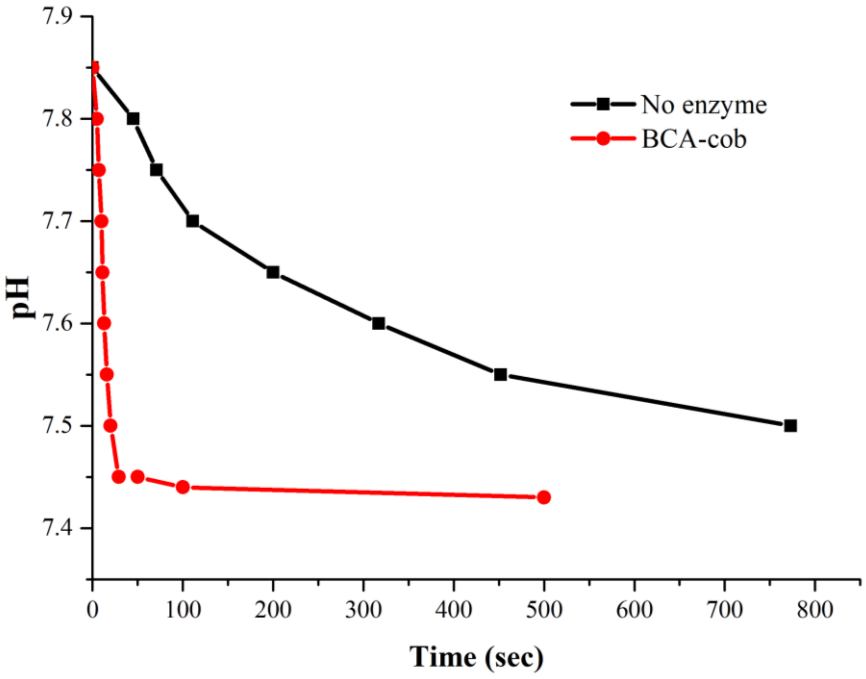

***Figure 4.11**: Carbon dioxide capture by BCA-cob. The capture was studied by the change in pH from 7.85 to 7.45. Buffer was used a control and ran under same condition in the absence of enzyme.*

The catalytic activity of the fusion protein, Mms6-TmCA was determined by pNPA assay, Figure 4.12. Mms6-TmCA was found significantly active in *p*-nitro phenylacetate (*p*NPA) into *p*-nitrophenoxide ions, suggesting that it was renatured after purification. The activity of Mms6-TmCA was compared with monomeric wild-type TmCA (WT-TmCA) and immobilised Mms6-TmCA on IONP. The presence of iron oxide binding peptide on Mms6-TmCA reduced the enzymatic activity to about 53% compared with WT-TmCA. This decrease of activity may be attributed to the partial denaturation of TmCA protein during purification or reducing the access of substrate to its active site. Furthermore, Mms6-TmCA immobilised protein on IONP reduced its catalytic activity to ca. 35%. Nevertheless, Mms6-TmCA-IONP is still enzymatically active.

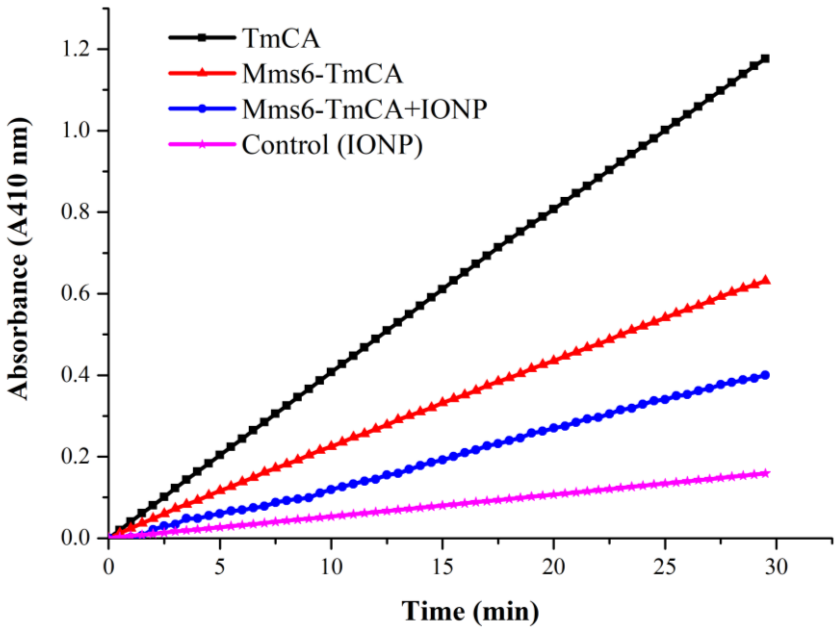

Figure 4.12: *Activity of protein as analysed by the pNPA assay. The assay was performed at room temperature for 30 min. TmCA is the wild-type protein; Mms6-TmCA is a fusion protein that has iron oxide binding peptide; Mms6-TmCA+ IONP, the mixture of fusion protein and iron oxide nanoparticles (IONP); control; IONP nanoparticles without enzyme.*

4.4 Summary

In this chapter, a convenient immobilisation strategy is developed that does not require chemical modification of matrix while delivering a highly stable enzyme in an immobilisation format. The fusion proteins were purified using Ni-affinity column chromatography and attached on the surface nanoparticles through non-covalent affinity immobilisation. MSN and IONP were used for binding while selecting cob and Mms6 that facilitate strong binding of BCA onto silica particles and TmCA onto IONP. The MSN synthesised to have a large pore size of 8.6 nm for easy entries of the enzyme while having a sufficient surface area of 469.3 m^2/g for adsorption of BCA-cob. These particles had maximum adsorption capacity (q_m) 750 ± 30 mg/g and dissociation constant (K_d) 130 ± 20 µg/mL for BCA-cob. Without a purification step, BCA-cob and Mms6-TmCA were efficiently recovered from the crude lysate using MSN and IONP respectively. The immobilised BCA-cob (from crude lysate and pure) were found

active and reused five times without an observed decrease of enzyme activity. The cob peptide facilitates strong binding of the enzyme onto silica particles, and the bound enzymes are not eluted using typical elute conditions such as 2M $MgCl_2$, 2M $CaCl_2$, 5M NaCl or 1M HCl. Mms6-TmCA was found active as analysed by pNPA assay but was found comparatively 50% less active than its monomeric TmCA and on immobilisation to IONP reduced the activity to 35%. The study showed the combination of using affinity binding peptide (cob or Mms6) and carrier molecule (MSN or IONP) have delivered enzymes in immobilised form without using the chemically modified surface nanoparticles. While IONP and Mms6 have only briefly discussed in this chapter, the advantage of affinity peptide will be further utilized in chapter 6 to make protein-IONP nanoclusters.

4.5 References:

Abdelhamid, M.A., Motomura, K., Ikeda, T., Ishida, T., Hirota, R., Kuroda, A. 2014. Affinity purification of recombinant proteins using a novel silica-binding peptide as a fusion tag. *Applied Microbiology and Biotechnology*, **98**(12), 5677-5684.

Arakaki, A., Webb, J., Matsunaga, T. 2003a. A novel protein tightly bound to bacterial magnetic particles in *Magnetospirillum magneticum* Strain AMB-1. *Journal of Biological Chemistry*, **278**(10), 8745-8750.

Arakaki, A., Webb, J., Matsunaga, T. 2003b. A novel protein tightly bound to bacterial magnetic particles in *Magnetospirillum magneticum* strain AMB-1. *J Biol Chem*, **278**(10), 8745-50.

Ding, Y., Yin, G.F., Liao, X.M., Huang, Z.B., Chen, X.C., Yao, Y.D., Li, J. 2013. A convenient route to synthesize SBA-15 rods with tunable pore length for lysozyme adsorption. *Microporous and Mesoporous Materials*, **170**, 45-51.

Fan, J., Lei, J., Wang, L., Yu, C., Tu, B., Zhao, D. 2003. Rapid and high-capacity immobilization of enzymes based on mesoporous silicas with controlled morphologies. *Chemical Communications*(17), 2140-2141.

Feng, S., Wang, L., Palo, P., Liu, X., Mallapragada, S.K., Nilsen-Hamilton, M. 2013a. Integrated self-assembly of the Mms6 magnetosome protein to form an iron-responsive structure. *Int J Mol Sci*, **14**(7), 14594-606.

Feng, S., Wang, L., Palo, P., Liu, X., Mallapragada, S.K., Nilsen-Hamilton, M. 2013b. Integrated self-assembly of the Mms6 magnetosome protein to form an iron-responsive structure. *International journal of molecular sciences*, **14**(7), 14594-14606.

Ikeda, T., Hata, Y., Ninomiya, K.-i., Ikura, Y., Takeguchi, K., Aoyagi, S., Hirota, R., Kuroda, A. 2009. Oriented immobilization of antibodies on a silicon wafer using Si-tagged protein A. *Analytical Biochemistry*, **385**(1), 132-137.

Ikeda, T., Kuroda, A. 2011. Why does the silica-binding protein "Si-tag" bind strongly to silica surfaces? Implications of conformational adaptation of the intrinsically disordered polypeptide to solid surfaces. *Colloids and Surfaces B: Biointerfaces*, **86**(2), 359-363.

Ikeda, T., Ninomiya, K.-i., Hirota, R., Kuroda, A. 2010. Single-step affinity purification of recombinant proteins using the silica-binding Si-tag as a fusion partner. *Protein expression and purification*, **71**(1), 91-95.

Lapresta-Fernández, A., Doussineau, T., Dutz, S., Steiniger, F., Moro, A.J., Mohr, G.J. 2011. Magnetic and fluorescent core–shell nanoparticles for ratiometric pH sensing. *Nanotechnology*, **22**(41), 415501.

Liu, J., Wang, B., Budi Hartono, S., Liu, T., Kantharidis, P., Middelberg, A.P.J., Lu, G.Q., He, L., Qiao, S.Z. 2012. Magnetic silica spheres with large nanopores for nucleic acid adsorption and cellular uptake. *Biomaterials*, **33**(3), 970-978.

Ma, K., Zhao, H., Zheng, X., Sun, H., Hu, L., Zhu, L., Shen, Y., Luo, T., Dai, H., Wang, J. 2017. NMR studies of the interactions between AMB-1 Mms6 protein and magnetosome Fe_3O_4 nanoparticles. *Journal of Materials Chemistry B*, **5**(16), 2888-2895.

Ma, Z., Dosev, D., Nichkova, M., Dumas, R.K., Gee, S.J., Hammock, B.D., Liu, K., Kennedy, I.M. 2009. Synthesis and characterization of multifunctional silica core–shell nanocomposites with magnetic and fluorescent functionalities. *Journal of magnetism and magnetic materials*, **321**(10), 1368-1371.

Ozdemir, E. 2009. Biomimetic CO_2 sequestration: 1. Immobilization of carbonic anhydrase within polyurethane foam. *Energy & Fuels*, **23**(11), 5725-5730.

Shanbhag, B.K., Liu, B., Fu, J., Haritos, V.S., He, L. 2016. Self-assembled enzyme nanoparticles for carbon dioxide capture. *Nano letters*, **16**(5), 3379-3384.

Verpoorte, J.A., Mehta, S., Edsall, J.T. 1967. Esterase activities of human carbonic anhydrases B and C. *Journal of Biological Chemistry*, **242**(18), 4221-4229.

Wang, L., Prozorov, T., Palo, P.E., Liu, X., Vaknin, D., Prozorov, R., Mallapragada, S., Nilsen-Hamilton, M. 2012. Self-assembly and biphasic iron-binding characteristics of Mms6, a

bacterial protein that promotes the formation of superparamagnetic magnetite nanoparticles of uniform size and shape. *Biomacromolecules*, **13**(1), 98-105.
Wanjari, S., Prabhu, C., Satyanarayana, T., Vinu, A., Rayalu, S. 2012. Immobilization of carbonic anhydrase on mesoporous aluminosilicate for carbonation reaction. *Microporous and Mesoporous Materials*, **160**, 151-158.
Wilbur, K.M., Anderson, N.G. 1948. Electrometric and colorimetric determination of carbonic anhydrase. *Journal of Biological Chemistry*, **176**(1), 147-154.
Zhang, Y. 2008. I-TASSER server for protein 3D structure prediction. *BMC Bioinformatics*, **9**(1), 40.

CHAPTER 5

COMPARISONS OF SELF-ASSEMBLY PEPTIDES FOR THE FORMATION OF PROTEIN NANOPARTICLES WITH STIMULI RESPONSIVE ABILITY

This page is intentionally blank

CHAPTER 5
COMPARISIONS OF SELF-ASSEMBLY PEPTIDES FOR THE FORMATION OF PROTEIN NANOPARTICLES WITH STIMULI RESPONSIVE ABILITY

5.1 Introduction

The preparation of functional protein-coated nanoparticles in chapters 3 and 4 relies on using of inorganic nanoparticles such as silica and iron oxide nanoparticles to serve as supporting materials. Is it possible to form protein nanoparticles without inorganic materials? In other words, can one prepare functional nanoparticles that do not utilise solid surface, thereby generating a new form of soft functional nanomaterials?

The scope of this chapter is to explore alternative routes to produce functional nanoparticles that are completely protein-based. Rather than binding proteins onto a solid surface, here we investigate whether careful design and manipulation of peptide sequences allows functional proteins to self-assemble with each other into nanoparticles. There are several reports of peptides with self-assembly features that form different types of nanostructures under specific solution conditions (Zhang, 2003; Zhao et al., 2010). Typically, these peptides require an external stimulus such as pH, temperature, metal ions to initiate self-assemble (Lowik et al., 2010). Although the self-assembly properties of these peptides as individual entities have been well studied, there is little understanding of their assembly when they are linked to other functional proteins.

Fusion of self-assembling peptides to functional proteins have been shown to form protein complexes (Patterson et al., 2011), vesicles (Park & Champion, 2014) and cages (Ross et al., 2017). Alternatively, functional nanofibers have been produced by fusing proteins with the β-

tail peptide and mixing with Q11 peptides at appropriate concentrations (Hudalla et al., 2014). While such strategies have shown significant progress towards producing functional protein nanoparticles, they have limitations. First, multiple fused peptides or components per protein molecule are required to promote self-assembly. Secondly, additional free peptides are required in addition to the fused peptide to achieve the critical peptide concentration that initiates self-assembly and finally self-assembly has been slow and gradual rather than instantaneous. These factors add uncertainty and complexity to production of functional protein nanoparticles and subsequently limits the real-world application of these protein particles.

Alternatively, protein nanoparticles have recently been demonstrated using $P_{11}4$ self-assembling peptide (Aggeli et al., 1997) fused to the enzyme BCA (Shanbhag et al., 2016). The example system BCA-$P_{11}4$ forms nanoparticles instantaneously at reduced pH and are stable under CO_2 capture conditions (Shanbhag et al., 2016). The design strategy employing a single fused peptide that self-assembles rapidly in response to changes in solution pH and offers a simple approach to soft protein nanoparticles (Schematic diagram 5.1).

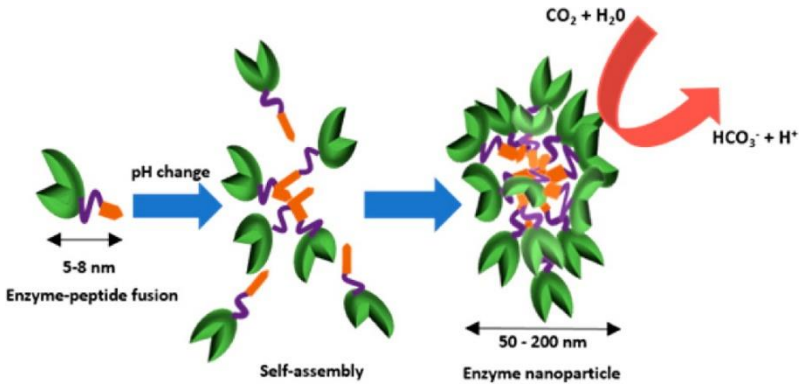

***Scheme 5.1**: Concept of nanoparticles formation driven by self-assembly peptide $P_{11}4$. The nanoparticles are formed at reduced pH. This figure was reproduced from Shanbhag et al. (Shanbhag et al., 2016)*

Built naturally on this concept, this chapter further develops the soft protein nanoparticle concept by focussing on two objectives: (1) evaluating other peptide sequences beyond $P_{11}4$ to

form soft protein nanoparticles and (2) engineering soft nanoparticles with dual functionality by combining two different proteins with unique functions within the single nanoparticle.

For the first part of this chapter, two peptides were chosen: Pep2 (developed as Q11 at University of Chicago (Hudalla et al., 2014) and Pep4, a novel designed peptide. The sequences and properties of Pep2 and Pep4 in comparison with the previously studied peptide $P_{11}4$ are given in Table 5.1.

Table 5.1 *Amino acid sequence and properties of assembly peptides investigated in this study.*

Peptide name	Amino acid Sequence	pI*	Charge at pH 7*	GAVY	Reference
$P_{11}4$	^{N}-QQRFEWEFEQQ-^{C}	4.14	-2.1	-2.209	(Aggeli et al., 1997)
Pep2	^{N}-QQKFQFQFEQQ-^{C}	6.25	-0.1	-1.818	(Hudalla et al., 2014)
Pep4	^{N}-WFRFEWEFEFW-^{C}	4.14	-2.1	-0.591	This study

*- *calculated using Expasy Protparam tool, GAVY: Grand average of hydropathicity*

The purpose of investigating different peptides was to fundamentally understand the influence of amino acid sequence on self-assembly behaviour, which includes factors influencing trigger conditions and exploring alternative trigger mechanisms to generate soft nanoparticles. Furthermore, options for triggering soft nanoparticles under different solution conditions to suit the functional partner protein could be tailored by variation of peptide sequences.

The current knowledge of $P_{11}4$ peptide-driven self-assembly of protein nanoparticles was used to guide the design soft nanoparticle formation using peptides Pep2 and Pep4. It has been demonstrated that pH (Aggeli et al., 2003) and ionic strength of the buffer (Carrick et al., 2007) influence the non-covalent forces involved in the nanofiber formation of $P_{11}4$ peptide. The rationale behind choice of alternative peptide sequences is to exploit various non-covalent

forces to promote soft nanoparticle formation. Specifically, Pep2 was chosen to evaluate the role of ionic interactions in self-assembly. As shown in Table 5.1, Pep2 sequence has four amino acid changes (positions 3, 5, 6 and 7) compared to $P_{11}4$, resulting in a higher pI of 6.25 and a -0.1 charge at pH 7.0, which is anticipated to influence nanoparticle formation at different pH values compared with protein particles designed with $P_{11}4$.

On the other hand, the novel peptide Pep4 was designed specifically to incorporate additional aromatic residues, replacing the glutamate residues in equivalent positions of $P_{11}4$ (Table 5.1). As a result, Pep4 is more hydrophobic compared to the other two peptides as indicated by the increased positive GRAVY score of -0.591 (Table 5.1). Therefore, the Pep4 design is tailored to evaluate the role of aromatic residues, π-π interactions and peptide hydrophobicity in self-assembly of protein nanoparticles.

The second part of this chapter focusses on developing soft nanoparticles with dual functions. In principle if two different proteins are fused with the same self-assembling peptide sequence, then the two fusion systems, when mixed under suitable solution conditions, may self-assemble with each other to form soft nanoparticle with dual functionality. To test this concept, the combination of two fusion systems namely GFP-$P_{11}4$ (green fluorescent protein) and the previously developed system BCA-$P_{11}4$, was investigated. The combination of GFP and BCA proteins allows the evaluation of two distinct functions, which are fluorescence and catalysis, respectively, within the same particle.

In brief, chapter 5 investigates two aspects of soft nanoparticle formation. Part 1 will study the peptide selection in which candidates Pep2 and Pep4 will be examined fusing with BCA and evaluated for self-assembly performance. The individual fusion systems will be studied for

protein expression, purification, self-assembly, and enzyme activity and compared with the previously investigated BCA-P_{11}4. Part 2 will explore the potential of dual functionality by combining BCA-P_{11}4 with the new system GFP-P_{11}4. The expression and purification of the new system GFP-P_{11}4 alongside its wild-type counterpart was investigated. The self-assembly behaviour of the GFP-P_{11}4 exclusively and in combination with BCA-P_{11}4 system is examined to understand the influence of differences in protein sequences and functions. With these two parts, the chapter aims to provide deep knowledge on design strategies for soft nanoparticle formation.

5.2 Materials and Methods

5.2.1 Plasmid Construction and Heterologous Expression in Bacteria

The fusion constructs BCA-Pep2 and BCA-Pep4 were prepared similarly to BCA-P_{11}4, by designing the gene sequence that coded for peptides Pep2 or Pep4 added to the C-terminus of enzyme BCA with an intervening GS-linker sequence. For the GFP system, P_{11}4 peptide was fused to the C-terminus of GFP via the GS-Linker to form GFP-P_{11}4 and as a control protein for comparison; wild-type GFP without the peptide was also constructed. The amino acid sequences of the three constructs are listed below. The gene sequences for each construct were codon optimised, synthesised and ligated into pET28a expression plasmid between *NcoI* and *XhoI* restriction sites by GenScript (Piscataway, NJ, USA). The plasmids were transformed into BL21 (DE3) *E.coli* competent cells using NEB High Efficiency Transformation protocol. Inoculum was prepared by growing 1-2 transformed colonies in terrific broth (TB) medium containing 1%w/v glucose and kanamycin (50 µg/mL) overnight at 37 °C, 250 rpm. Protein expression was carried out using the Auto-Induction method (Studier, 2005). Briefly, TB media containing 2% v/v inoculum, kanamycin (50 µg/mL) and 0.2% w/v lactose was grown at 37°C for 4 h and 250 rpm for the first 4 h, following which each culture was grown at 20 °C overnight.

Amino acid sequences of the fusion proteins investigated in this study.

BCA- $P_{11}4$

GMSHHWGYGKHNGPEHWHKDFPIANGERQSPVDIDTKAVVQDPALKPLALVYGEA
TSRRMVNNGHSFNVEYDDSQDKAVLKDGPLTGTYRLVQFHFHWGSSDDQGSEHTV
DRKKYAAELHLVHWNTKYGDFGTAAQQPDGLAVVGVFLKVGDANPALQKVLDAL
DSIKTKGKSTDFPNFDPGSLLPNVLDYWTYPGSLTTPPLLESVTWIVLKEPISVSSQQM
LKFRTLNFNAEGEPELLMLANWRPAQPLKNRQVRGFPKGGGGSGGGGSQQRFEWE
FEQQ

BCA- Pep2

GMSHHWGYGKHNGPEHWHKDFPIANGERQSPVDIDTKAVVQDPALKPLALVYGEA
TSRRMVNNGHSFNVEYDDSQDKAVLKDGPLTGTYRLVQFHFHWGSSDDQGSEHTV
DRKKYAAELHLVHWNTKYGDFGTAAQQPDGLAVVGVFLKVGDANPALQKVLDAL
DSIKTKGKSTDFPNFDPGSLLPNVLDYWTYPGSLTTPPLLESVTWIVLKEPISVSSQQM
LKFRTLNFNAEGEPELLMLANWRPAQPLKNRQVRGFPKGGGGSGGGGSQQKFQFQF
EQQ

BCA- Pep4

GMSHHWGYGKHNGPEHWHKDFPIANGERQSPVDIDTKAVVQDPALKPLALVYGEA
TSRRMVNNGHSFNVEYDDSQDKAVLKDGPLTGTYRLVQFHFHWGSSDDQGSEHTV
DRKKYAAELHLVHWNTKYGDFGTAAQQPDGLAVVGVFLKVGDANPALQKVLDAL
DSIKTKGKSTDFPNFDPGSLLPNVLDYWTYPGSLTTPPLLESVTWIVLKEPISVSSQQM
LKFRTLNFNAEGEPELLMLANWRPAQPLKNRQVRGFPKGGGGSGGGGSWFRFEWE
FEFW.

GFP- $P_{11}4$

MGHHHHHHTDPMVSKGEELFTGVVPILVELDGDVNGHKFSVSGEGEGDATYGKLT
LKFICTTGKLPVPWPTLVTTLAYGVLCFSRYPDHMKQHDFFKSAMPEGYVQERTIFF
KDDGNYKTRAEVKFEGDTLVNRIELKGIDFKEDGNILGHKLEYNYNSHNVYIMADK
QKNGIKSNFKIRHNIEDGSVQLADHYQQNTPIGDGPVLLPDNHYLSTQSKLSKDPNE
KRDHMVLLEFVTAAGITLGMDELYKGGGGSGGGGSQQRFEWEFEQQ

5.2.2 Cell Harvest and Protein Purification

Cell harvest and purification for all proteins was performed using the similar conditions as described in Chapter 3, section 2.1, with minor modifications with respect to buffers. Purification was performed on a pre-packed 5 mL HisTrapFF (GE Healthcare) immobilised metal-ion affinity chromatography charged with nickel ion using AKTA start™ Chromatography system. The column was equilibrated and washed using binding buffer 10 mM Tris-HCl, 0.5 M NaCl, pH 8 and eluted using 10 mM Tris/HCl, 0.5 M NaCl, 200 mM imidazole, pH 8. The elution condition used for each protein is shown in Table 5.2.

Table 5.2: *Elution conditions for proteins used in this study*

Proteins	Elution type	Elution condition
BCA-$P_{11}4$	Gradient	0 to 200 mM imidazole in 10 mM Tris-HCl, 0.5 M NaCl, pH 8
BCA-Pep2	Gradient	0 to 200 mM imidazole in 10 mM Tris-HCl, 0.5 M NaCl, pH 8
BCA-Pep4	Gradient	0 to 200 mM imidazole in 10 mM phosphate buffer, 0.5 M NaCl, pH 8
WT-GFP **GFP-$P_{11}4$**	Gradient	0 to 200 mM imidazole in 10 mM Tris-HCl, 0.5 M NaCl, pH 8

Eluted protein fractions were pooled based on purity determined by SDS-PAGE 4-12% Bis-Tris Bolt gels and bulk eluate sample was desalted using size exclusion chromatography on a

G25 Sephadex (GE Healthcare) column (17 cm × I.D. 1.5 cm) with 10 mM Tris-HCl, pH 8. Purified samples were stored at 4 °C in desalting buffer for subsequent analysis.

5.2.3 Preparation and Particle Size Measurement of Soft Nanoparticles

Soft nanoparticles were prepared by testing the effect of reduced pH or addition of metal ion as described below. Nanoparticle formation was monitored by Dynamic Light Scattering technique (Zetasizer Nano) and particle sizes determined as triplicate measurements each consisting of 10 cycles of measurement.

To test effect of pH, purified protein samples were diluted to 0.5 mg/mL concentration in 50 mM Tris-HCl pH 8 buffer. The solution pH was reduced stepwise using 5 M or 1 M acetic acid to desired pH, followed by monitoring of particle size using dynamic light scattering with a Zetasizer Nano (Malvern Instruments).

To test the effect of metal ions, purified protein samples were diluted to 0.5 mg/mL concentration in 10 mM Tris-HCl pH 8 buffer and incubated for 10 mins at 25 °C with varying concentration of $MgCl_2$ (5 to 20 mM) in the final solution using 0.5 M $MgCl_2$ stock solution prepared in 10 mM Tris-HCl pH 8 buffer. This was followed by monitoring of particle size using Dynamic Light Scattering.

5.2.4 Dual Functional Nanoparticles

Purified BCA-P_{11}4 and GFP-P_{11}4 samples were diluted to 0.5 mg/mL concentration in 10 mM Tris-HCl pH 8 buffer, separately. GFP-P_{11}4 sample was added into BCA-P_{11}4 sample in different ratios (5, 10, 25, and 50%) with a constant final volume of 1 mL. To each mixture, $MgCl_2$ was added from 0.5 M $MgCl_2$ stock solution prepared in 10 mM Tris-HCl pH 8 buffer

to achieve a final concentration of 20 mM and incubated for 10 mins at 25 °C. Following incubation, particle size was measured using dynamic light scattering method.

5.2.5 Enzyme Activity Assay

The enzyme activities of BCA-P_{11}4, BCA-Pep2, and BCA-Pep4 were measured by esterase assay, as described in chapter 3, section 2.2. Briefly, 0.0125 mg of each protein was mixed with 1 mM concentration of *p*-nitrophenylacetate (*p*NPA) in 50 mM HEPES and 50 mM Na_2SO_4 buffer pH 8. The reaction was performed for 20 mins and *p*-nitrophenol production by the hydrolysis of *p*-nitrophenylacetate (*p*NPA) was measured at 410 nm. A control sample (without enzyme) was monitored under the same condition.

5.2.6 Fluorescent Measurement Assay

Fluorescence measurements of GFP proteins were obtained using the TECAN infinite PRO plater reader. The protein concentration of the samples was set to 0.5 mg/mL prior to measurement. The excitation wavelength was 400 nm and the emission was measured at 450 nm with a bandwidth of 5 nm for each wavelength.

5.2.7 Negative Protein Staining and Transmission Electron Microscopy (TEM)

For the TEM analysis of the protein nanoparticles, 8 µL of protein solution (0.5 mg/mL) was applied on the surface of freshly glow-discharged continuous carbon coated 200 mesh copper grids (GSCu200C, Proscitech, QLD Australia) and incubated for 5 mins. Excess protein was dried using blotting paper then washed with two 25-µL drops of MiliQ water and dried with blotting paper. The grid surface was stained with 2 drops of 2% (v/v) uranyl acetate (negative staining) for 30 sec (Booth et al., 2011). The negatively stained protein particles were observed

under transmission electron microscope at 200 kV and electron micrographs were recorded using CCD camera and Gatan "Digital Micrograph" software.

5.3 Results and Discussion

PART 1 – Effect of Peptide Sequence on Nanoparticle Formation

5.3.1 Structure, Expression and Purification of BCA-Pep2 and BCA-Pep4

The engineered proteins were designed to study the behaviour of self-assembly abilities. The two peptides –Pep2 and –Pep4 and one protein (BCA) were selected for the design. The representative ribbon structures of –Pep2, -Pep4, BCA-Pep2, and BCA-Pep4 is presented in Figure 5.1. The rational design of the fusion proteins enabled the peptides to function efficiently.

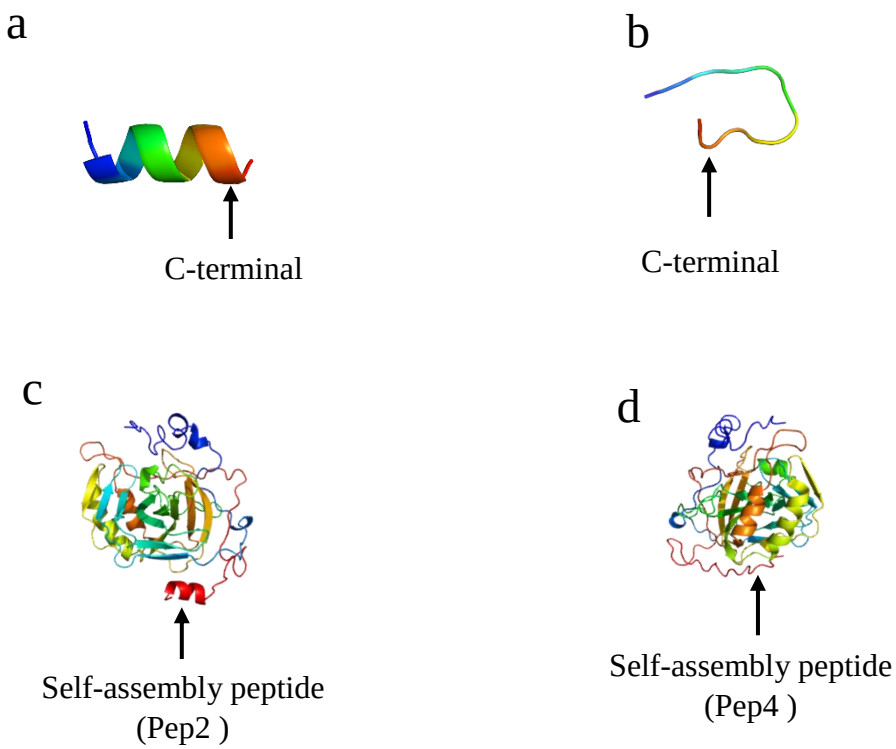

Figure 5.1: *A representative ribbon structure of recombinant protein. a) –Pep2, b) –Pep4, c) BCA-Pep2, and d) BCA-Pep4. The structures presents the self-assembly peptide sites. The structure was produced using I-TASSER server (Zhang, 2008).*

The protein expression for BCA-Pep2 and BCA-Pep4 was performed using the Auto-induction method with lactose as the inducer. The protein expression levels were compared to that of BCA-P_{11}4 expressed under similar conditions as this construct has a high level of soluble protein expression as illustrated in Figure 5.2a.

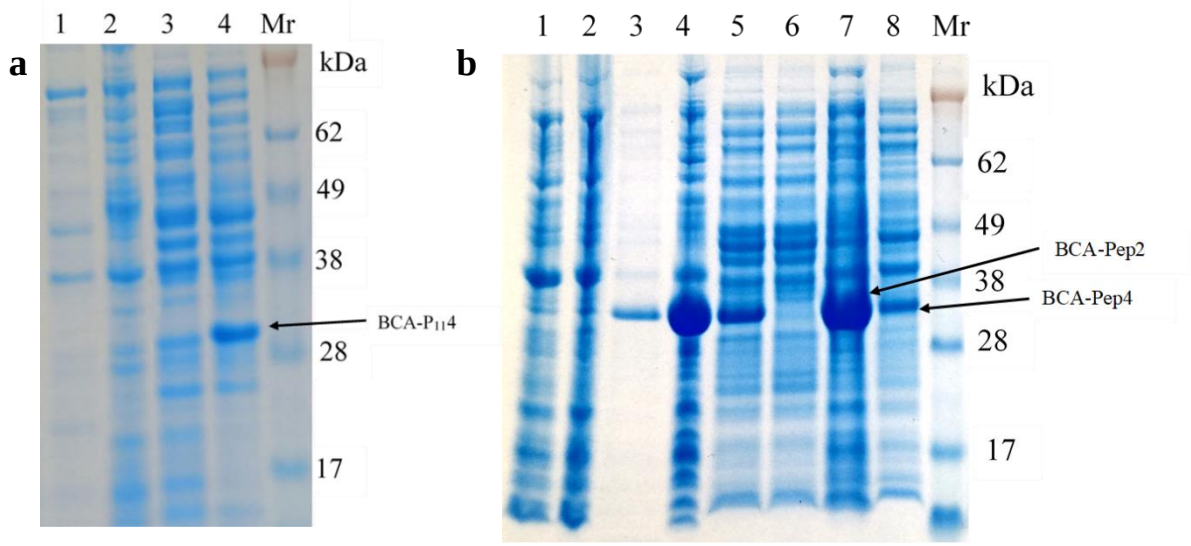

Figure 5.2: *Comparison of protein expression by Auto-Induction method a) Model system BCA-P_{11}4: Lane 1-insoluble seed culture, lane 2-insoluble expression culture, lane 3-soluble seed culture, lane 4-soluble expression culture b) BCA-Pep2: lanes (1,3,5,7)- insoluble seed culture, insoluble expression culture, soluble seed culture, soluble expression culture. BCA-Pep4: lanes (2,4,6,8)- insoluble seed culture, insoluble expression culture, soluble seed culture, soluble expression culture*

The expression levels of BCA-Pep2 in the soluble form was comparable with that of BCA-P_{11}4. However, for the BCA-Pep4 system, the majority of the expressed protein was insoluble as shown in Figure 5.2b. These results illustrate that peptide sequence difference can impact protein expression levels of the fusion system as the remainder of the construct was identical. The peptide Pep4 is more hydrophobic than Pep2 (Table 5.1) and P_{11}-4. The hydrophobic nature of Pep4 could cause easy aggregation of the BCA-Pep4 protein during translation and pose solubility issues within the *E. coli* cytoplasm. Subsequently, the expressed protein forms inclusion bodies. Similar effects of insoluble protein expression due to fusion with self-assembling peptides have been reported (Wu et al., 2011; Zhou et al., 2012).

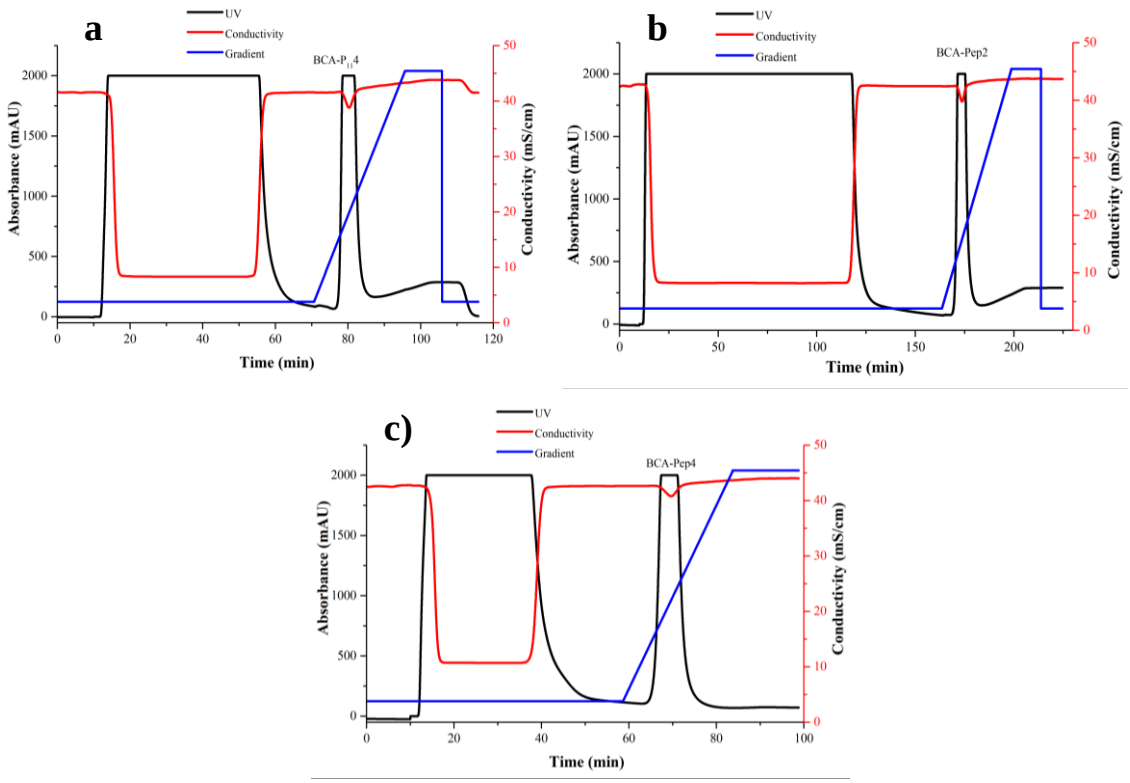

Figure 5.3: *Chromatography profiles of IMAC purification a) BCA-P$_{11}$4 b) BCA-Pep2 c) BCA-Pep4. Proteins in solution were absorbed at 280 nm as presented in the chromatography. The purified proteins were eluted by continuous gradient flow of elution buffer and shown as a peak in the chromatography.*

The soluble fractions from harvested cells of all three-fusion protein systems were purified using the Ni-IMAC process. The purification chromatography profiles of all three fusion proteins are comparable as shown in Figure 5.3 and the SDS-PAGE fractions show that each of the fusion proteins are obtained with high levels of purity, as shown in Figure 5.4. These results demonstrate that once the fusion protein was expressed in the soluble form, the differences in the fused peptide have little or no significant impact on the purification steps. Therefore, the production of such fusion system would be feasible as long as sufficient proteins are expressed in the soluble form.

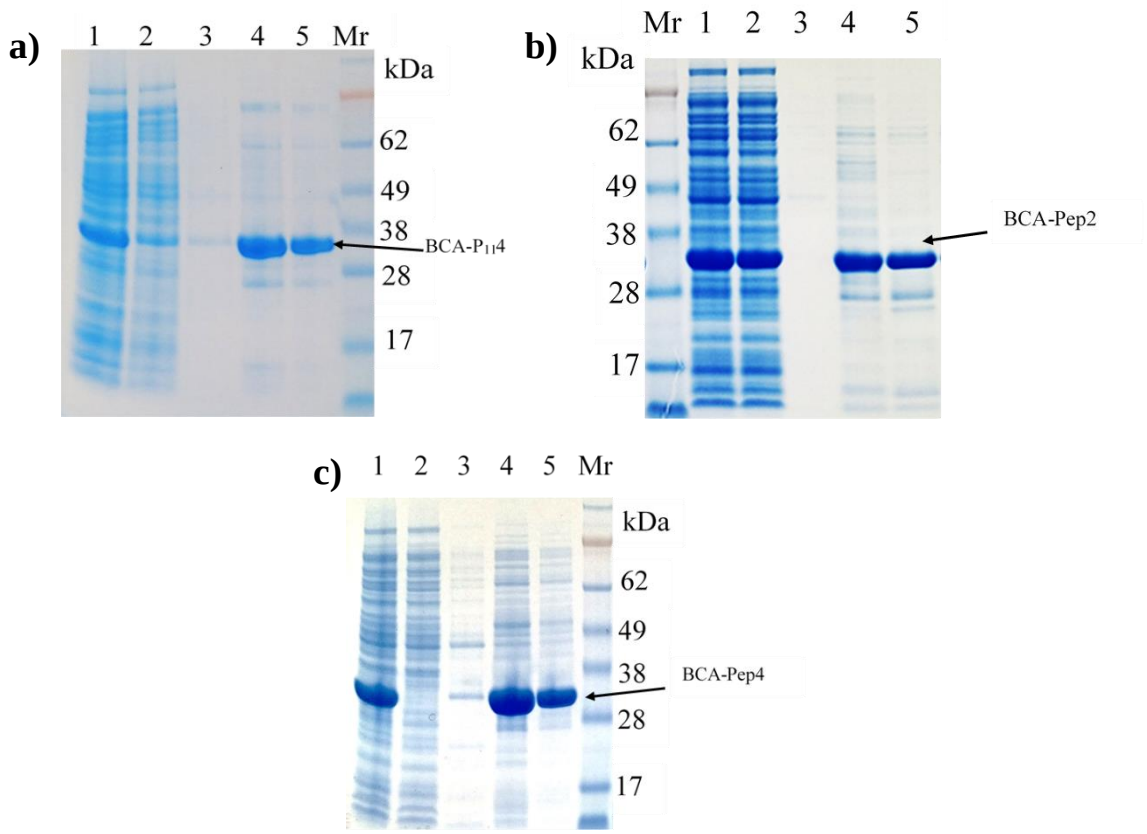

Figure 5.4: *SDS-PAGE gel of IMAC purification samples a) BCA-P$_{11}$4 b) BCA-Pep2 c) BCA-Pep4. Lane 1-Load, lane 2-flow through, lane 3-wash, lane 4-eluate peak in IMAC, and lane 5-eluate after desalting.*

5.3.2 Effect of Buffer Composition on Self-assembly of BCA-Pep2 and BCA-Pep4

The Tris-HCl buffer system was routinely used to test the self-assembly of the model fusion system BCA-P$_{11}$4. At 10 mM Tris-HCl pH 8 condition, the DLS data of BCA-P$_{11}$4 shows a particle size of ~5-7 nm which correlates to the calculated spherical diameter of BCA (~50Å) determined from its crystal structure(Saito et al., 2004). Due to similar sequence length, it was anticipated that both BCA-Pep2 and BCA-Pep4 would have the same particle size as BCA-P$_{11}$4 in the Tris buffer system. Surprisingly, a variation in the particle size was observed for both BCA-Pep2 and BCA-Pep4. Instead of showing a size of ~5-7 nm, BCA-Pep2 showed a particle size of ~15 nm in 10 mM Tris-HCl pH 8 buffer as shown in Figure 5.5. A further increase in particle size to ~30 nm was observed when Tris buffer concentration was increased

to 50 mM as shown in Figure 5.5. It is known that the Tris molecule has hydroxyl groups that is capable of strongly interacting with the peptide backbone (Taha & Lee, 2010) and similar interactions of Tris with BCA-Pep2 are involved in promoting self-assembly.

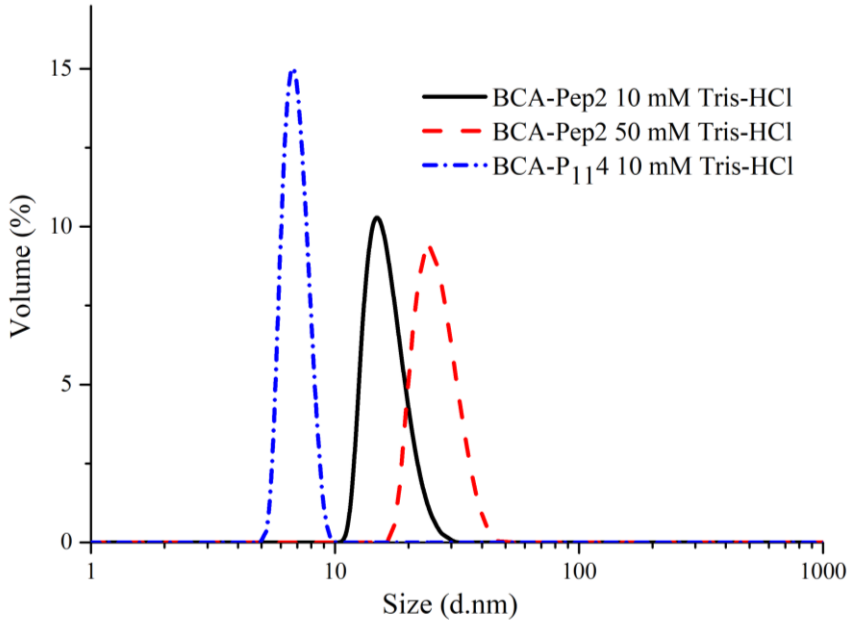

Figure 5.5: *Effect of increasing Tris-HCl buffer concentration on the self-assembly of BCA-Pep2. Here various concentration (0-50 mM) of Tris salt was tested to produce protein nanoparticles at pH 8.*

The absence of such an effect in case of BCA-P_{11}4 may be attributed to the differences in sequence and properties between P_{11}4 and Pep2. As mentioned earlier, Pep2 sequence has two glutamate residues replaced by glutamine and it is slightly more hydrophobic than P_{11}4 (Table 5.1). Due to the absence of repulsive forces from the glutamate residues and the favourable conditions provide by the Tris buffer, the aromatic residues in Pep2 are expected to engage in π-π interaction when two peptide regions come in anti-parallel fashion. Therefore, we hypothesize that the Tris buffer and the lack of glutamate residues in Pep2 sequence contribute towards BCA-Pep2 self-assembly process.

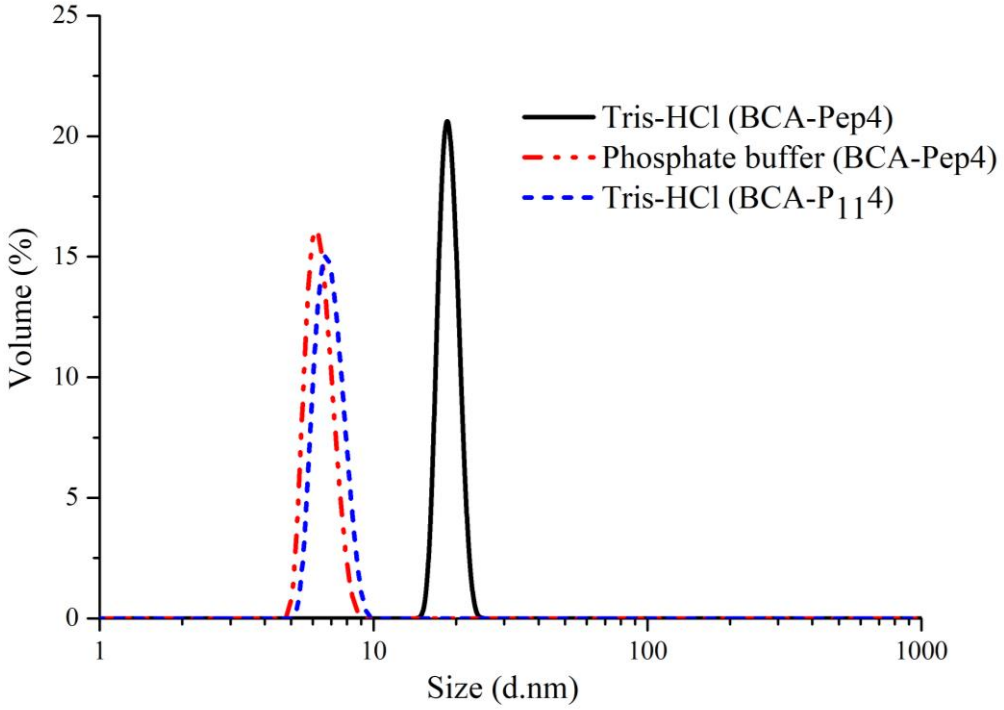

Figure 5.6: *Comparison of BCA-Pep4 particle size in Tris and Phosphate buffer systems. BCA-Pep4 formed the nanoparticles in 10 mM Tris-HCl pH 8, whereas appeared as monomer in 10 mM Phosphate buffer by BCA-Pep4 and 10 mM Tris-HCl by BCA-P$_{11}$4, pH 8.*

Similar increase in particle size (~20 nm) was observed for BCA-Pep4 in 10 mM Tris-HCl pH 8 condition, Figure 5.6. In addition to interaction with the peptide backbone, there is a possibility of Tris to interact with specific amino acids such as glutamic acid (Quan et al., 2008) present in the peptide region of BCA-Pep4 to aid the self-assembly process. To confirm the role of Tris, BCA-Pep4 was purified using phosphate buffer and desalted into the final buffer solution of 10 mM Phosphate pH 8, because phosphate groups are known to bind to neutral glycine residues and do not involve in ion-pair interactions (Collins, 2012), thereby making them poor promoters of self-assembly. Subsequent measurement of the particle size by DLS showed the size of BCA-Pep4 monomer in phosphate buffer is the same as BCA-P$_{11}$4 in Tris buffer pH 8, Figure 5.6. This confirms our hypothesis that the Tris moiety is indeed involved in interactions that promote self-assembly without the change in pH. Therefore, the self-

assembly of BCA-Pep4 is driven by the peptide's overall hydrophobic nature along with favourable conditions provide by Tris for increasing π-π interaction by the additional aromatic residues flanking at either ends of the Pep4 sequence.

Encouraged by these results, the possibility of using Tris buffer as a trigger for self-assembly was explored. To BCA-Pep4 sample prepared with phosphate buffer, Tris-HCl buffer was added at varying concentrations (20 mM to 100 mM). Unfortunately, no self-assembly was observed for BCA-Pep4, Figure 5.7.

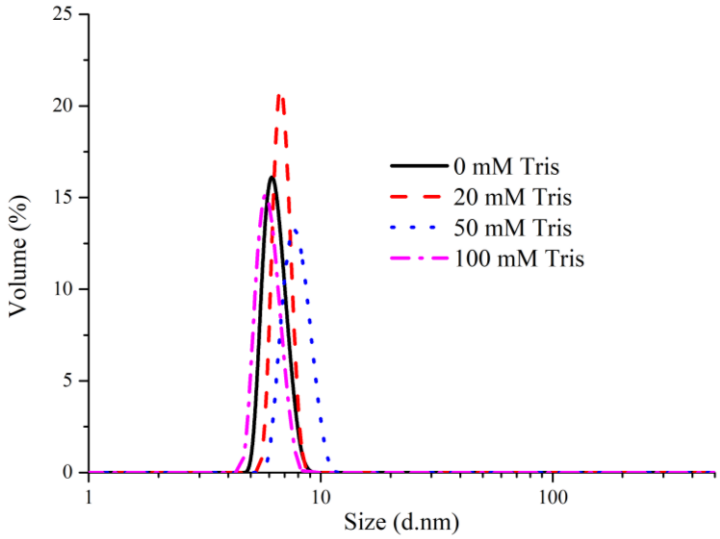

***Figure 5.7**: Effect of varying concentration of Tris-HCl pH 8 buffer on BCA-Pep4 self-assembly. Here, BCA-Pep4 (purified and desalted using phosphate buffer) was tested to study the behaviour of nanoparticles formation at different concentration of Tris-HCl (0-100 mM), pH 8*

The possible explanation for this observation is that the existing of phosphate buffer may prevent formation of nanoparticles. Thus, the ability of Tris to spontaneously trigger self-assembly in a direct fashion is not feasible without removing existing buffer (e.g., phosphate). Therefore, the results suggest that careful consideration of the buffer system is vital to manipulate the self-assembly of BCA-Fusion systems.

5.3.3 Self-assembly Triggered by pH

The nanoparticle formation of BCA-Pep2 system was evaluated by reducing pH using acetic acid. Reduction of pH to 6.0 resulted in instantaneous formation of nanoparticles of large size (>1000 nm) as shown in Figure 5.8. It has been shown that the BCA-P_{11}4 forms nanoparticles at pH 6.8, (Shanbhag et al., 2016) however, this was not observed with the BCA-Pep2 system.

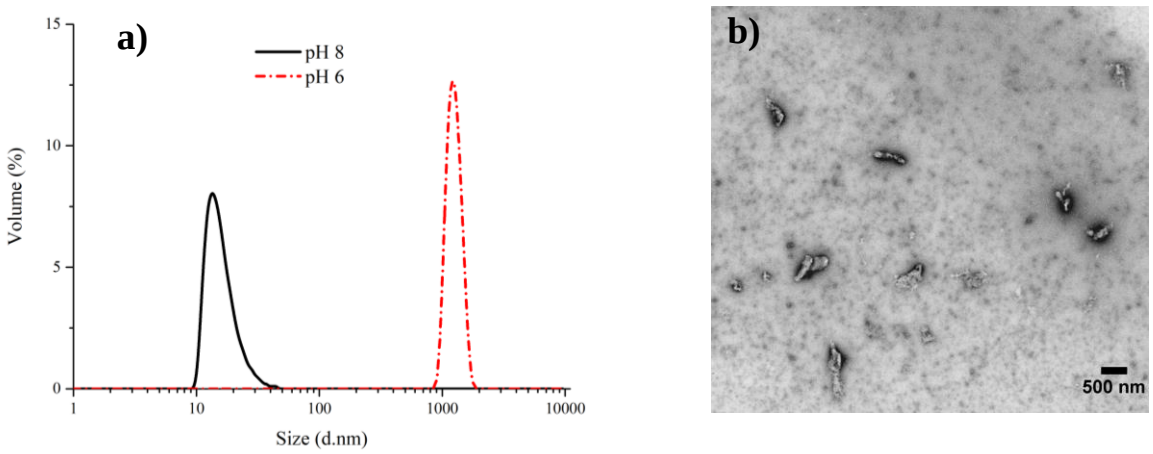

Figure 5.8: *BCA-Pep2 nanoparticles formed using pH as trigger. a) Comparison of particle size distribution of control condition pH 8 and triggered condition pH 6 using dynamic light scattering. The pH of BCA-Pep2 at 10 mM Tris-HCl, pH 8 was adjusted to pH 6 using 5 M acetic acid, incubated for 5 min prior to analysed by DLS. b) TEM image of nanoparticles formed at pH 6. The protein particles were loaded into continuous carbon gird and stained using 2% (v/v) uranyl acetate prior to the analysis under microscopy.*

This due to the difference in pI of the peptides (Table 5.3) that influence the net charge at a particular pH. The difference in the surface charges impact the ionic interactions necessary to promote self-assembly (Aggeli et al., 2003) and subsequently the solution condition required to initiate nanoparticle formation. The difference in particle formation behaviour shows that changes in the peptide sequence can help to tailor the nanoparticle formation under specific conditions or pH values.

Table 5.3. *Estimated charge of peptides $P_{11}4$, Pep2, and Pep4, enzyme BCA, protein GFP, and fusion proteins BCA-$P_{11}4$, BCA-Pep2, BCA-Pep4, and GFP-$P_{11}4$ from pH 4.0 to pH 10.0**

pH	Estimated charges								
	$P_{11}4$	BCA	BCA-$P_{11}4$	GFP	GFP-$P_{11}4$	Pep2	BCA-Pep2	Pep4	BCA-Pep4
4	0.3	29.5	29.7	32.1	32.2	0.8	30.2	0.3	29.7
4.2	-0.1	26.4	26.3	28.5	28.3	0.7	27	-0.1	26.3
4.4	-0.5	23	22.5	24.4	23.9	0.5	23.5	-0.5	22.5
4.6	-0.8	19.5	18.7	20.4	19.5	0.4	19.9	-0.8	18.7
4.8	-1.1	16.3	15.2	16.7	15.5	0.3	16.6	-1.1	15.2
5	-1.4	13.7	12.3	13.6	12.2	0.2	13.9	-1.4	12.3
5.2	-1.6	11.6	10	11.1	9.5	0.1	11.7	-1.6	10
5.4	-1.7	9.9	8.2	9.1	7.4	0.1	10	-1.7	8.2
5.6	-1.8	8.5	6.7	7.4	5.6	0.1	8.6	-1.8	6.7
5.8	-1.9	7.3	5.4	5.8	3.9	0	7.4	-1.9	5.4
6	-1.9	6.1	4.2	4.2	2.3	0	6.1	-1.9	4.2
6.2	-2	4.8	2.8	2.5	0.6	0	4.8	-2	2.8
6.4	-2	3.4	1.4	0.7	-1.3	0	3.4	-2	1.4
6.6	-2	2	0	-1.2	-3.2	0	2	-2	0
6.8	-2	0.7	-1.3	-3	-5	-0.1	0.7	-2	-1.3
7	-2.1	-0.4	-2.4	-4.5	-6.5	-0.1	-0.4	-2.1	-2.4
7.2	-2.1	-1.3	-3.3	-5.7	-7.7	-0.1	-1.3	-2.1	-3.3
7.4	-2.2	-2	-4	-6.7	-8.7	-0.2	-2	-2.2	-4
7.6	-2.3	-2.6	-4.6	-7.5	-9.5	-0.3	-2.6	-2.3	-4.6
7.8	-2.4	-3	-5	-8.2	-10.2	-0.4	-3	-2.4	-5
8	-2.5	-3.4	-5.4	-8.8	-10.8	-0.5	-3.4	-2.5	-5.4

*Estimated using PROTEIN CALCULATOR v3.4

On the contrary, BCA-Pep4 formed nanoparticles at pH 6.8 as shown in Figure 5.9. This illustrates if the peptides have the same pI and net charge at a given pH, the influence of changes in the peptide sequence on pH driven self-assembly is minimum. Here it is observed that the presence of additional aromatic residues in Pep4 did not affect the self-assembly behaviour under reduced pH conditions.

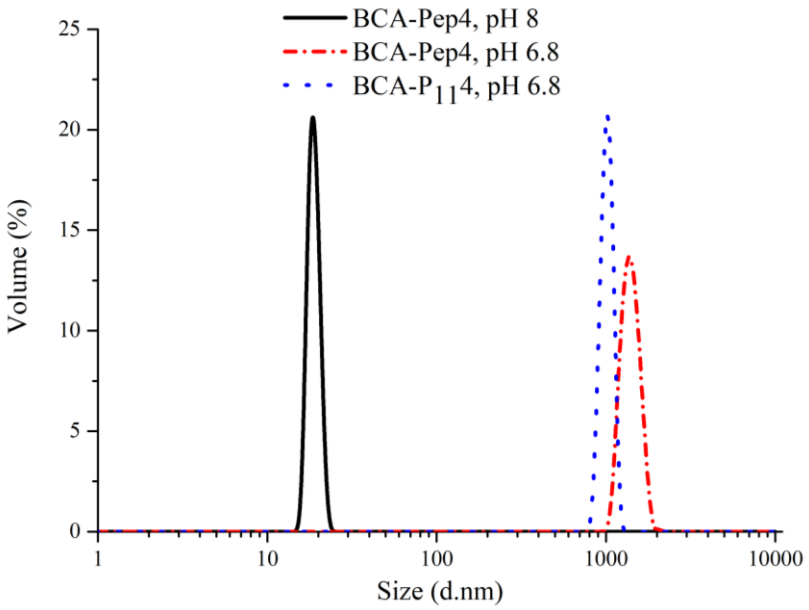

Figure 5.9: *Comparison of particle size distribution of BCA-P$_{11}$4 and BCA-Pep4 at pH 6.8 using dynamic light scattering. The pH of BCA-P$_{11}$4 and BCA-Pep4 at 10 mM Tris-HCl, pH 8 was adjusted to pH 6.8 using 5 M acetic acid, incubated for 5 min prior to analysed by DLS*

5.3.4 Self-assembly Promoted by Metal-ions

Metal ions are known to interact with several biomolecules such as DNA, RNA, protein etc. within in a biological system. Typically, metal-ions are involved in electron sharing and charge-charge interactions in order to stabilise a structure, ligand binding or catalyse a reaction (Jenny P. Glusker, 1999). Furthermore, multi-valent metal ions can form coordination complex with biomolecules with useful consequences, such as calcium driven self-assembly of synthetic peptides to form nanofibers (Stendahl et al., 2006) and protein filaments (Scotter et al., 2007). The speciality of metal-ions is its ability to mediate self-assembly in an independent manner without significant variations required in pH and buffer composition. Based on the learnings from the model system of BCA-P$_{11}$4, it was found understood that Mg^{2+} and NH_4^+ ions have unique properties beneficial for self-assembly of soft protein nanoparticles (Shanbhag, 2016).

In the following sections, the self-assembly of BCA-pep2 and BCA-Pep4 using metal-ions Mg^{2+} and NH_4^+ is presented.

5.3.4.1 Mg^{2+} ions as a Trigger

Magnesium ions have the ability to form coordination complex with negatively charged hydroxyl groups of aspartic acid and glutamic acid (Zheng et al., 2008). When BCA-Pep4 was incubated with $MgCl_2$, self-assembly was observed and the particle size increased with the increase in concentration of magnesium ions shown in Figure 5.10a. Large particles were formed using 20 mM $MgCl_2$ as confirmed by the TEM image shown in Figure 5.10b.

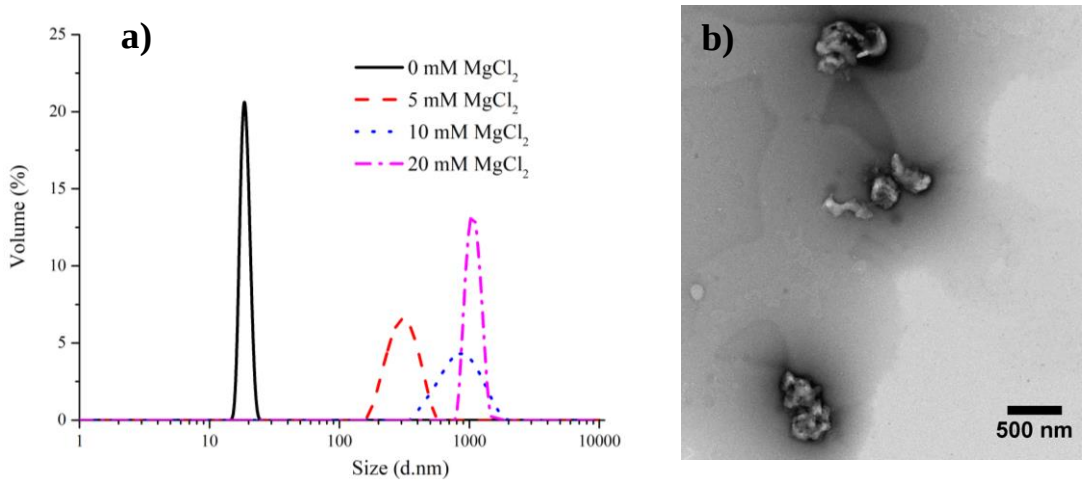

Figure 5.10: *BCA-Pep4 nanoparticles formed using metal-ion as trigger. a) Dynamic light scattering showing effect of varying $MgCl_2$ concentration (0-20 mM) on nanoparticle size. Various concentration of $MgCl_2$ was mixed with BCA-Pep4 and incubated for 5 min prior to analysed by DLS. b) TEM image of nanoparticles formed with 20 mM $MgCl_2$. The protein particles were loaded into continuous carbon gird and stained using 2% (v/v) uranyl acetate prior to the analysis under microscopy.*

This trend is similar to BCA-P_{11}4 nanoparticles formed with $MgCl_2$. Since both P_{11}4 and Pep4 have glutamic acids residues (positions 5 and 7 of the peptide), it can be concluded that the mechanism of self-assembly is the same with both protein which involves Mg^{2+} ions forming

coordination complex with the glutamic acids present in the peptide regions of two fusion monomers (Shanbhag, 2016).

On the other hand, BCA-Pep2 incubated with varying concentration of $MgCl_2$, showed no nanoparticle formation, Figure 5.11.

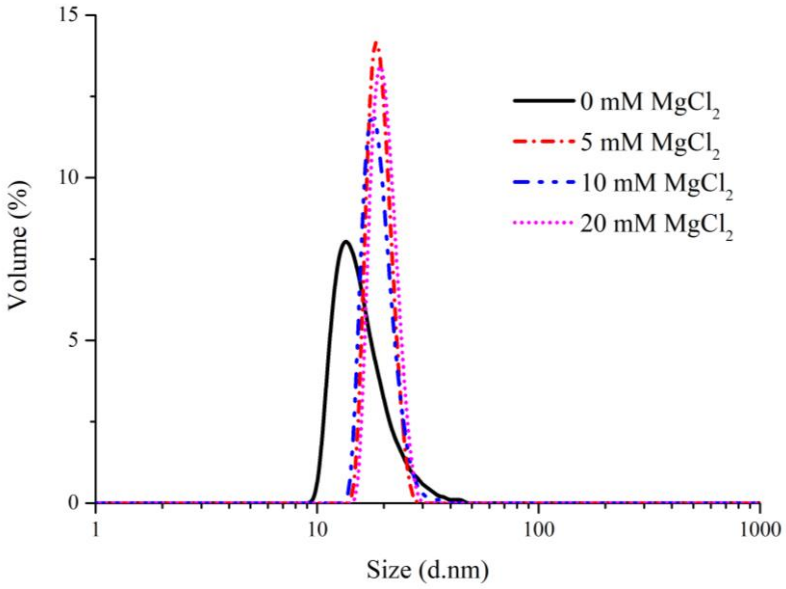

Figure 5.11: *Effect of varying concentration (0-20 mM) of $MgCl_2$ on BCA-Pep2 nanoparticle formation. Various concentration of $MgCl_2$ was mixed with BCA-Pep2 and incubated for 5 min prior to analyse by DLS.*

The absence of self-assembly is attributed to the Pep2 sequence which lacks negatively charged glutamate (E) residues in 5^{th} and 7^{th} positions (replaced with glutamine (Q) residues instead) which is crucial to form coordination complex with Mg^{2+} ions.

5.3.4.2 NH_4^+ ions as a Trigger

The monovalent ammonium ion has a unique property to involve in cation-π interactions with aromatic residues and to play a significant role in protein-protein interactions (Rapp et al.,

2014). For instance, positively charged ammonium groups present in dopamine and acetylcholine can activate G-protein coupled receptors (GPCRs) through cation-π interactions (Torrice et al., 2009). The BCA-Pep4 was designed with additional aromatic groups to exploit this interaction mechanism for soft nanoparticle self-assembly and hence BCA-Pep2 was not evaluated for self-assembly with NH_4^+ ions. As anticipated, BCA-Pep4 formed nanoparticles of average size ranging from ~50 to ~250 nm with 50 mM and 75 mM NH_4Cl respectively, as shown in Figure 5.12.

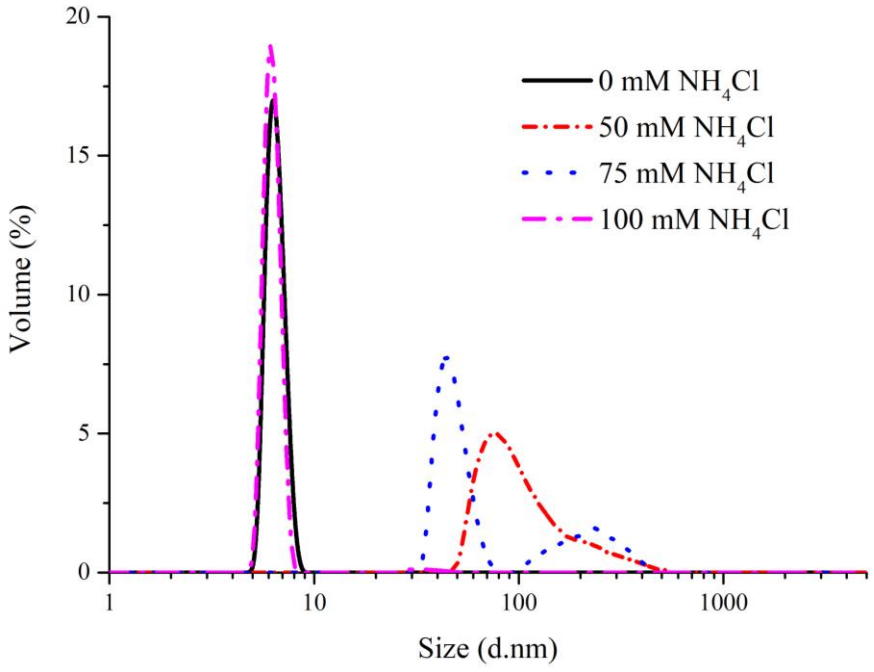

Figure 5.12: *Effect of varying concentration (0-100 mM) of NH_4Cl on BCA-Pep4 nanoparticle formation. Various concentration of NH_4Cl was mixed with BCA-Pep4 and incubated for 5 min prior to analysed by DLS.*

This result suggest that the self-assembly is driven by NH_4^+ ions interacting with the tryptophan and phenylalanine residues present in Pep4 via cation-π interactions (Dougherty, 2007). Increase in NH_4Cl concentration to 100 mM showed no nanoparticle formation. This effect

may be attributed to the high ionic strength contribution from the salt, which interferes with the electrostatic forces required for cation-π interactions.

Therefore, these results establish that peptide sequences may be manipulated to promote or suppress specific self-assembly mechanisms. Different peptide sequences maybe designed to self-assemble specifically in response to certain metal-ions. This strategy opens up many options to design soft protein nanoparticles whose self-assembly may be controlled and tuned using metal-ions for specific application.

5.3.5 Enzyme Activity of BCA-Pep2 and BCA-Pep4

The functionality of BCA fusion systems was determined by testing the catalytic activity of the BCA enzyme. The enzyme activities of all three-fusion systems were tested in their monomeric and particle forms and compared with WT-BCA as a control. The reaction rate profiles in Figure 5.13 showed that both BCA-Pep4 monomer and particle forms had comparable activity to that of BCA-P_{11}4 monomer and particles. On the other hand, BCA-Pep2 showed a reduced activity in both its monomeric and particle forms. This is an interesting observation, since it was anticipated that the hydrophilic nature and high soluble expression of BCA-Pep2 would result in a stable and active enzyme. Instead, the more hydrophobic BCA-Pep4 systems showed a better catalytic performance than BCA-Pep2 system. From these results, it is understood that changes in peptide sequence not only influence the self-assembly behaviour but also impact the function of the protein partner. It is essential to choose the most suited peptide for the intended application in order to obtain the right balance between nanoparticle formation and its functional performance. A general trend of reduced enzyme activity is observed for particle forms in comparison to their monomeric counter-parts (Table 5.4). This may be attributed to

possible mass-transfer limitations that results in slower substrate diffusion from the bulk solution to the active sites within the nanoparticle resulting in lower reaction rates.

Table 5.4: *Relative activity of monomer and particle form*

Construct	%Relative activity	
	Monomer	**Particle**
WT-BCA	100.0	-
BCA-P$_{11}$4	81.0	77.0
BCA-Pep2	62.0	47.0
BCA-Pep4	88.5	67.0

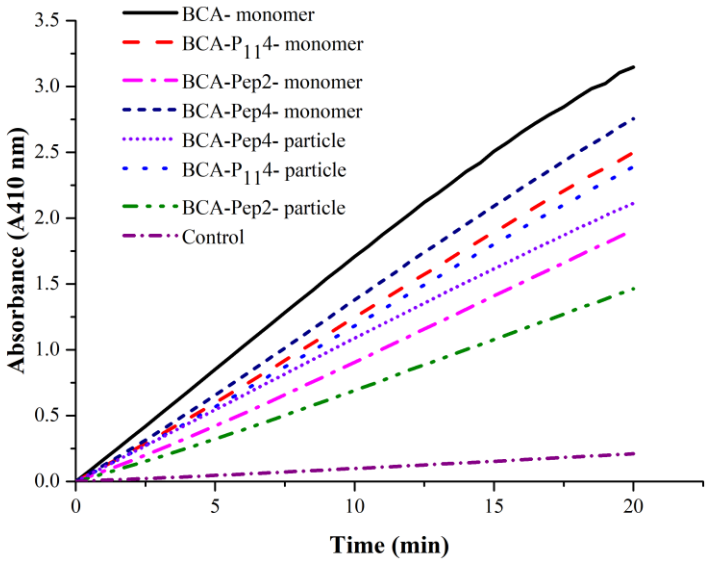

Figure 5.13: *Comparison of initial rates of enzyme-catalysed reactions for monomer and corresponding particle forms of BCA-P$_{11}$4, BCA-Pep2 and BCA-Pep4. The esterase assay was performed using p-NPA as the substrate producing p-nitrophenol and measured at 410 nm*

PART 2 - Development of Soft Nanoparticles with Dual Functionality

5.3.6 Expression and Purification of WT-GFP and GFP-$P_{11}4$

The expression of WT-GFP and GFP-$P_{11}4$ was performed using the auto-induction method. The results show maximum protein expression in the soluble form for both proteins as shown in Figure 5.14.

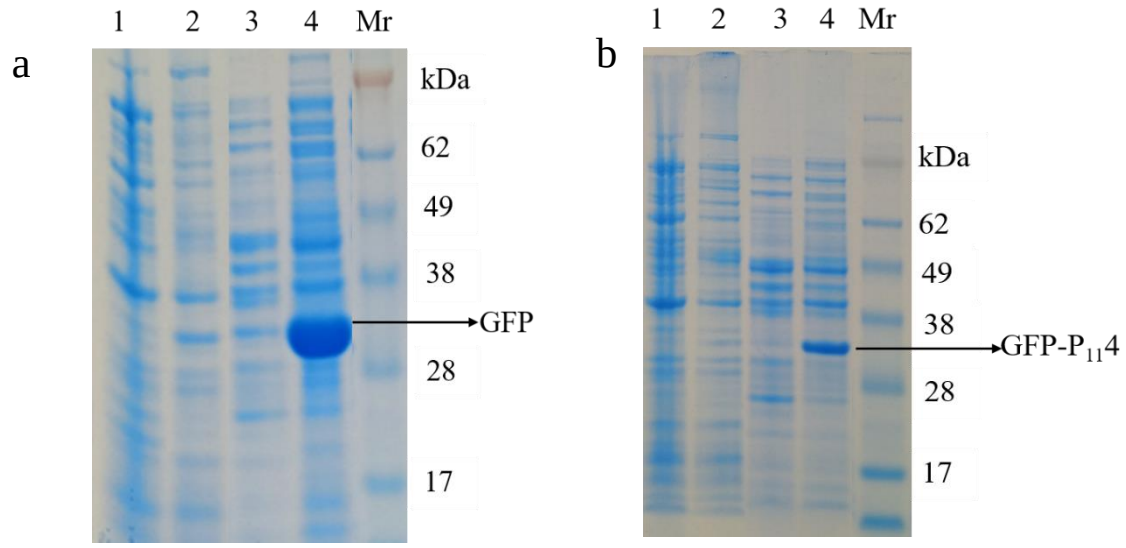

Figure 5.14: *Comparison of protein expression by Auto-Induction method a) WT-GFP: Lane 1-insoluble seed culture, lane 2-insoluble expression culture, lane 3-soluble seed culture, lane 4-soluble expression culture. b) GFP-$P_{11}4$: Lane 1-insoluble seed culture, lane 2-insoluble expression culture, lane 3-soluble seed culture, lane 4-soluble expression culture.*

Similarly, to BCA-$P_{11}4$ system, these results also confirm that fusion of the $P_{11}4$ peptide does not greatly impact the expression levels of the extended protein system. The purification of both WT-GFP and GFP-$P_{11}4$ were comparable, Figure 5.15 in terms of elution profiles and purity of eluate fractions as analysed by SDS-PAGE.

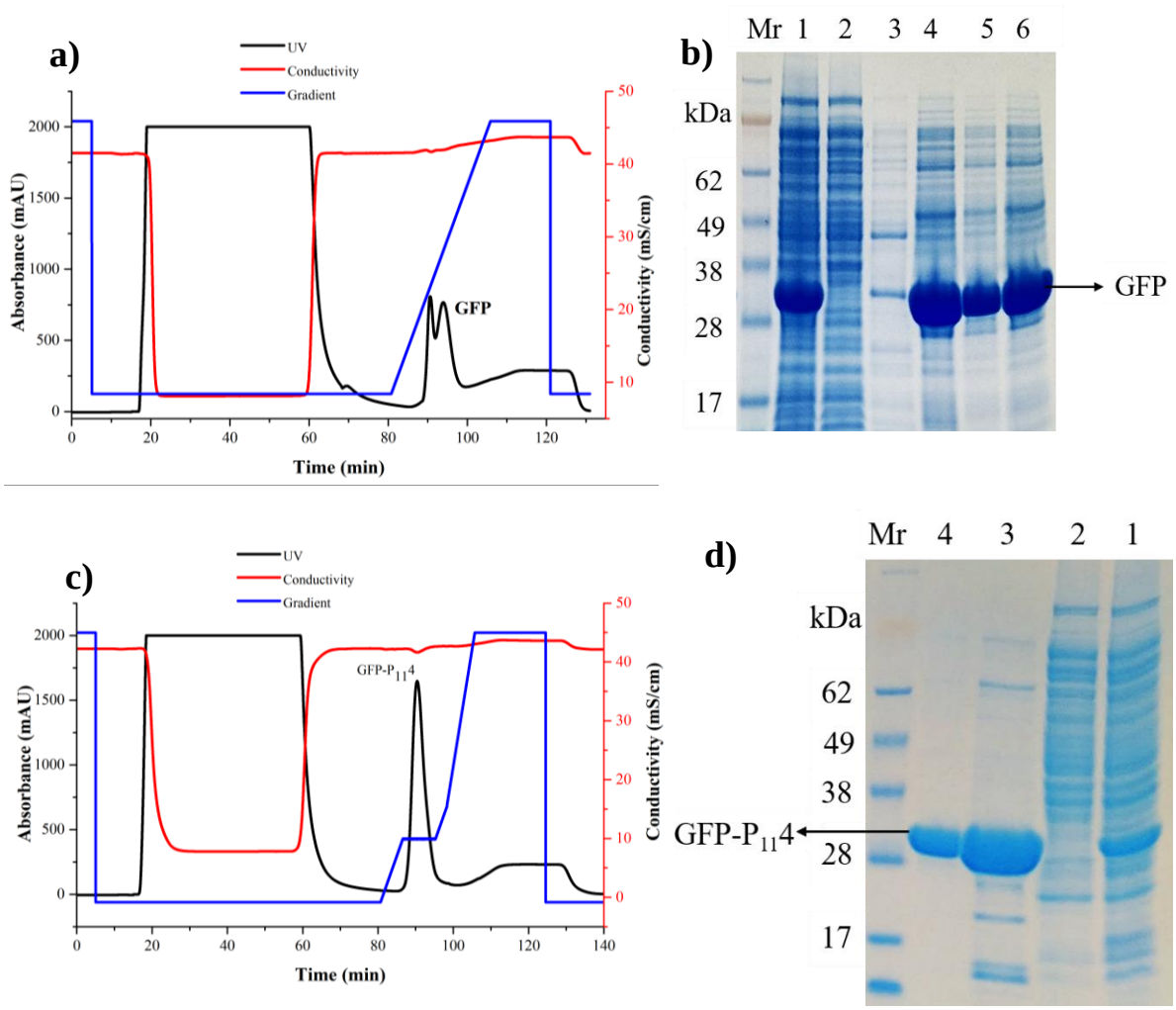

Figure 5.15: *Chromatography profiles and SDS-PAGE gels for IMAC purification. a) WT-GFP chromatogram. Proteins in solution were absorbed at 280 nm as presented in the chromatography. b) WT-GFP-IMAC fractions: Lane 1-Load, lane 2-flow through, lane 3-wash, lane 4-eluate peak 1, and lane 5-eluate peak 2, lane 6-eluate after desalting. c) GFP-P$_{11}$4 chromatogram d) GFP-P$_{11}$4-IMAC fractions: Lane 1-Load, lane 2-flow through, lane 3- eluate, lane 4-eluate after desalting.*

5.3.7 Nanoparticle Formation of GFP-P$_{11}$4

The nanoparticle formation of GFP-P$_{11}$4 was initiated using Mg^{2+} ions and different sized nanoparticles were observed with two different concentrations of Mg^{2+} ions. It is observed that smaller particles of average size 250 nm were formed with 5 mM Mg^{2+} and larger sized particles with average size of 450 nm was formed with 20 mM Mg^{2+} as shown in Figure 5.16.

This trend is similar to that of BCA-$P_{11}4$ and BCA-Pep4 systems where higher concentration of Mg^{2+} ions formed larger particles. This confirms that the mechanism of self-assembly triggered by Mg^{2+} ions is universal and the nature of its interaction does not change with the different proteins as long as the peptide carries residues with ability to coordinate with Mg^{2+} and form a metal ion-peptide complex.

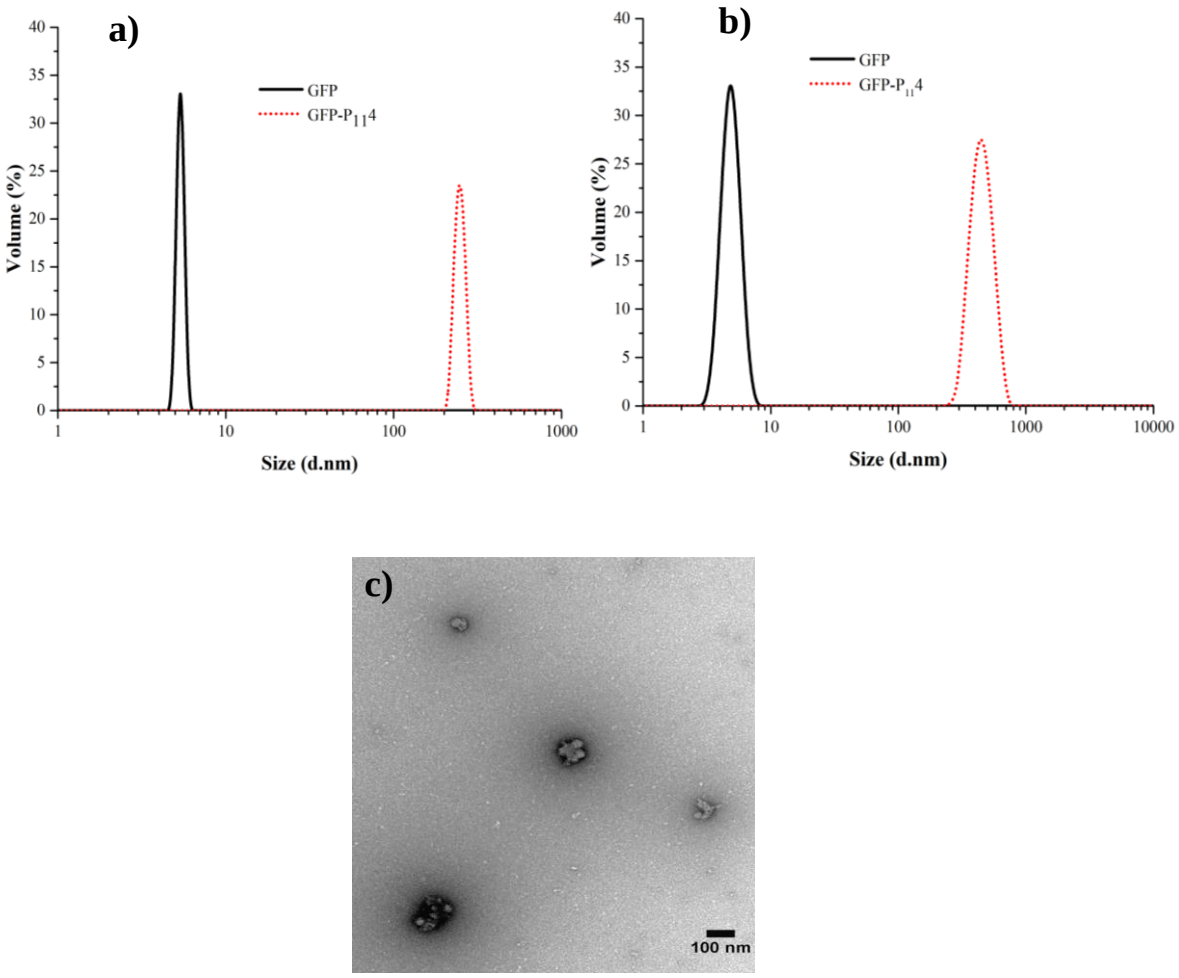

Figure 5.16: *Nanoparticle formation of GFP-$P_{11}4$ with $MgCl_2$ as trigger in comparison to WT-GFP. a) 5 mM $MgCl_2$ b) 20 mM $MgCl_2$. $MgCl_2$ was mixed with GFP and GFP-$P_{11}4$, and incubated for 10 min prior to analysed by DLS. c) TEM image of GFP-$P_{11}4$ nanoparticles formed with 20 mM $MgCl_2$. The protein particles were loaded into continuous carbon gird and stained using 2% (v/v) uranyl acetate prior to the analysis under microscopy.*

With regard to the functional performance of GFP-$P_{11}4$ system, its fluorescence emission scan was determined and compared with WT-GFP. The fluorescence emission and intensity of the fusion system was found to be comparable with the wild type counterpart as shown in Figure 5.17.

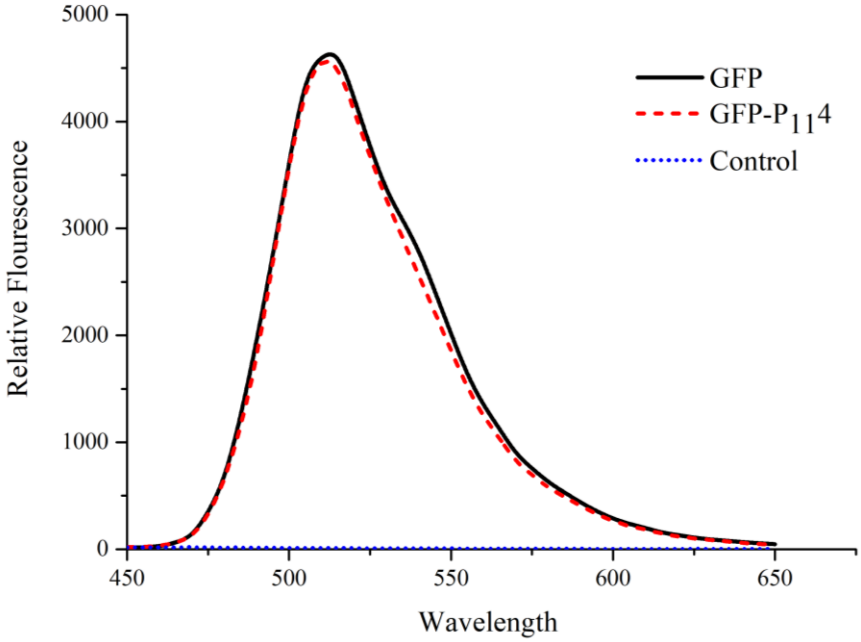

Figure 5.17: *Comparison of fluorescence emission scans of WT-GFP and GFP-$P_{11}4$. The fluorescence scan of the two recombinant proteins at excitation wavelength of 400 nm using Tecan plate ready at room temperature.*

5.3.8 Dual Functional Nanoparticles (GFP-$P_{11}4$ + BCA-$P_{11}4$)

The concept of the dual function nanoparticles was assessed using the fusion systems GFP-$P_{11}4$ and BCA-$P_{11}4$. For this, calculated ratios of GFP-$P_{11}4$ and BCA-$P_{11}4$ proteins were mixed and their fluorescence intensities were measured. It is anticipated that under self-assembly conditions, the mixtures would result in nanoparticles that contain randomly mixed GFP-$P_{11}4$ and BCA-$P_{11}4$ in the same ratios as they were added. Various ratios ranging from 0-100% GFP-$P_{11}4$ were incubated with Mg^{2+} ions to promote self-assembly. Following this the function of

both GFP and BCA proteins were evaluated by fluorescence and enzyme activity assay respectively.

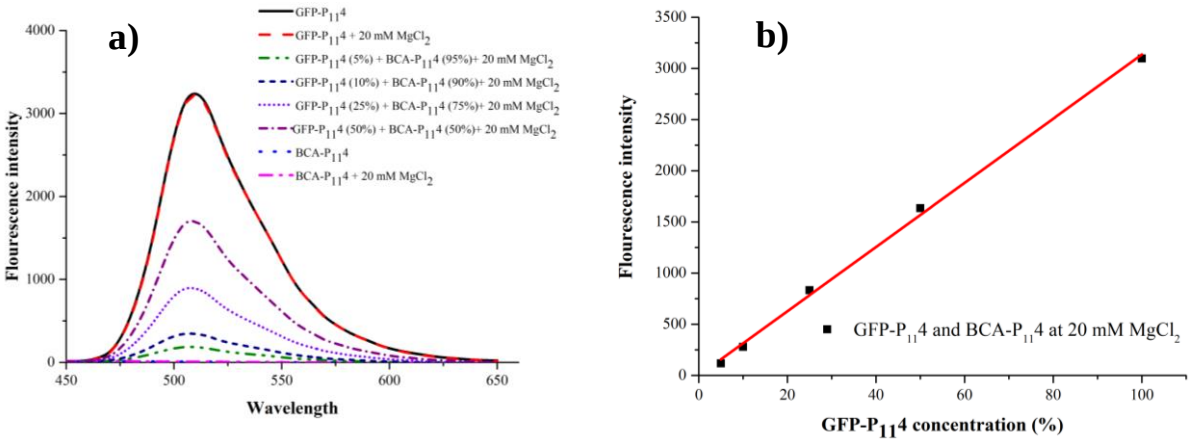

Figure 5.18: *Fluorescence emission data of GFP-P$_{11}$4 + BCA-P$_{11}$4 nanoparticles. a) Fluorescence emission scans for different ratios of GFP-P$_{11}$4 + BCA-P$_{11}$4 nanoparticles. b) Graph showing the fluorescence intensity at different concentration of GFP-P$_{11}$4 and corresponding nanoparticles. Here, different concentration of GFP-P$_{11}$4 and BCA-P$_{11}$4 were mixed with the final concentration of 0.5 mg/mL (protein), incubated for 10 min and fluorescence scan of the solution was performed at excitation wavelength of 400 nm using Tecan plate ready at room temperature.*

Fluorescence measurements of these nanoparticles showed that fluorescence intensity increased proportionally with increasing ratio of GFP-P$_{11}$4 in the mixture as shown in Figure 5.18a. A correlation graph between intensity and ratio of GFP-P$_{11}$4 showed a linear relationship confirming the incorporation of GFP-P$_{11}$4 and BCA-P$_{11}$4 in the same particle (Figure 5.18b). Similar correlation between intensity and number of fused copies of GFP molecules has been reported for icosahedral protein nanoparticles and has been used to differentiate between variations in the nanoparticle structures (Hsia et al., 2016). Therefore peptide based self-assembly approach also has the ability to incorporate GFP-P$_{11}$4 into a mixed protein nanoparticle with no significant impact on its fluorescence efficiency, in a fashion similar to the approach with fusion to the sub-unit of the icosahedral protein. The combination of GFP-P$_{11}$4 with other functional protein fused with P$_{11}$4 will allow one to create functional protein nanoparticles with an in built fluorophore function. This fluorophore function can be exploited

as a tracking or reporting system to monitor the uptake/transport of protein nanoparticles, which would be beneficial in application such as drug delivery.

Next the second function, namely enzyme activity of BCA was evaluated for the mixture samples having same GFP:BCA ratios as used for the fluorescence measurements. A comparison of the reaction rate profiles for monomer and particle samples is shown in Figure 5.19, which illustrate that incorporation of GFP-P_{11}4 into the BCA-P_{11}4, particle had no adverse effect on the enzymatic performance of BCA. This is indicated by the similar reaction rates of BCA-P_{11}4 particles and the 10% GFP-P_{11}4 incorporated BCA-P_{11}4 particles. The 100% GFP-P_{11}4 particles have no significant reaction rate and is similar to the control buffer sample, from which we can conclude that GFP does not influence the enzyme performance in anyway.

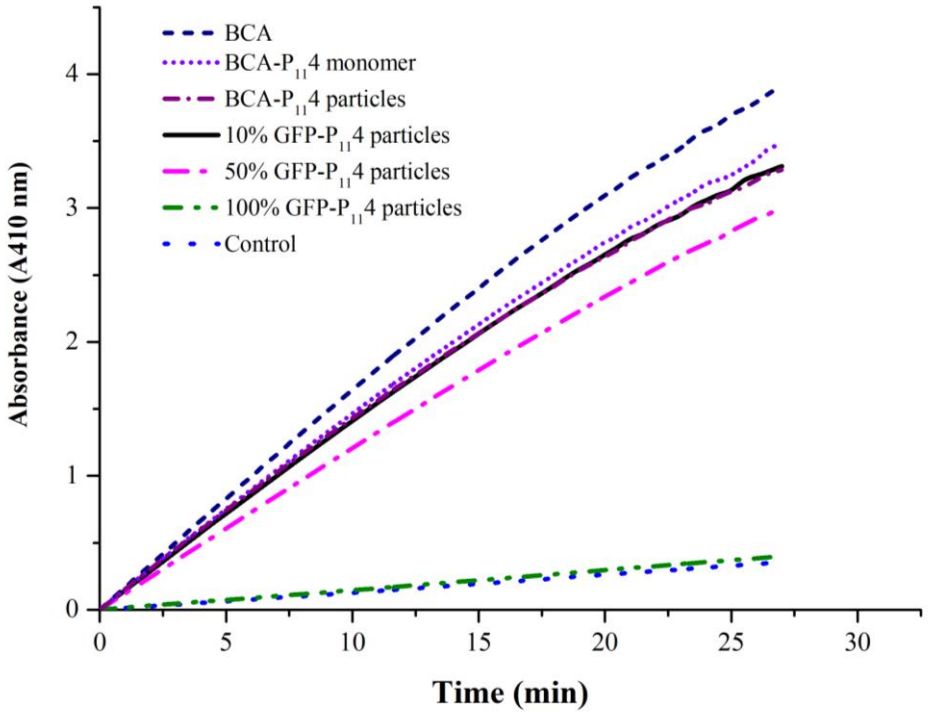

Figure 5.19: *Reaction rate profiles of the esterase assay for BCA. The esterase assay was performed using p-NPA as the substrate producing p-nitrophenol and measured at 410 nm*

Furthermore, the relative activity (%) of 10% GFP-P_{11}4 incorporated BCA-P_{11}4 particles was comparable to 100% BCA-P_{11}4 particles which confirms that the two functional entities GFP and BCA function independently when mixed to form dual system protein nanoparticles (Table 5.5). However, increasing the ratio of GFP with respect to BCA showed a slight reduction in the BCA performance. This may be attributed to the difference on the amount of BCA available for reaction since the volume of protein sample was kept constant resulting in variation on the amount of total protein present in each sample (5.5 µg for 10% particle and 10 µg for 50% particle).

Table 5.5: Relative activity (%) of dual function protein particles in comparison with single function particle and monomers

Protein sample	Relative activity %
BCA	100.00
BCA-P_{11}4 monomer	88.19
BCA-P_{11}4 particles	85.18
GFP-P_{11}4 10%	85.34
GFP-P_{11}4 50%	76.92

These results illustrate that GFP-P_{11}4 and BCA-P_{11}4 can be mixed together to form nanoparticles with no significant impact on the functions of either proteins. This validates that dual function nanoparticle can be prepared by fusing the same peptide to two different proteins and initiating particle formation in the protein mixture. By changing the molar ratios of the proteins, the functionality of these soft protein nanoparticles may be exploited for various applications. For instance, the 10% ratio nanoparticles is advantageous both as a reporting system to obtain quantitative information and as a tracking system to understand spatial information at the nanoscale. On the other hand, the 50% ratio nanoparticles allow equal

mixing of two components, which may be used to create multi-enzyme systems as in cascade reactions. This can be further developed to produce soft protein nanoreactors tuned to produce certain products. In addition, the dual protein nanoparticle reduces the distance between different protein molecules to as small as the length of their individual hydrodynamic diameters (~5 nm for BCA). This feature is beneficial for enzyme cascade reactions or enzymes requiring other protein for co-factor regeneration, where the close proximity of the entities is essential for better reaction rates and enzyme performance.

5.4 Summary

The research in this chapter has investigated a new approach to generate soft nanoparticles driven by peptide self-assembly in the absence of solid supports. Furthermore, this approach does not rely on externally added peptides for self-assembly and the process is instantaneous once being triggered. Since the staring building block is completely made of protein, the approach provides a quick and simple method to generate soft nanoparticles that are biocompatible in nature. The chapter has systematically studied the effect of peptide design, namely Pep2 and Pep4, in comparison to the established system using $P_{11}4$. Firstly, the expression and purification of BCA-Pep2 and BCA-Pep4 systems were evaluated. Differences in the soluble expression levels of the two new systems suggests that peptide sequence and their properties such as overall charge and hydrophobicity may impact soluble expression levels. In this study, auto induction method was used to express the proteins at mild conditions, and further improvement in soluble expression yields may be carried out by using different media conditions (Watson & Kan, 2015). The purification profiles of all fusion systems in this study were comparable and yielded useable quantities of purified fractions. This is an important aspect and is beneficial for large-scale production of the fusion systems for generation of soft nanoparticles for commercial applications.

Regarding nanoparticle formation, designing different peptide sequences offer the flexibility to respond to variable self-assembly initiators. This chapter demonstrated the use of three different types of trigger conditions namely buffer composition, pH and metal-ions to initiate self-assembly of BCA-Pep2 and BCA-Pep4. Various non-covalent forces such as ionic, electrostatic, coordination complex and cation-π interactions have shown to influence self-assembly of these soft protein nanoparticles. Strikingly, BCA-Pep4 forms nanoparticles by one of the three demonstrated methods, which provides the end users with a variety of triggering conditions that suit the specific application. These results also demonstrate that varying peptide sequence can have a significant impact in the self-assembly behaviour. Such peptide sequence may be further tailored to suit the needs of specific applications. The soft nanoparticles formed also showed strong enzyme activity, suggesting that neither the fusion nor the self-assembly process have a negative impact on the enzyme performance.

The second part of this chapter demonstrated another aspect of soft nanoparticle formation that is, incorporating dual functionality in the same nanoparticle. In this case, the $P_{11}4$ peptide was fused to GFP to form a new fusion system. The soluble expression and retention of fluorescence emission was similar to its wild-type counterpart, demonstrating that the peptide-driven approach can be expanded to proteins with different functions beyond enzymes such as BCA. The GFP-BCA combination particle retain both their functions of fluorescence and catalytic activity which is beneficial as a tracking or reporting system for drug delivery purpose and as a platform to create nannoreactor systems based on multi-enzyme cascade reactions.

In summary, this chapter provides a new strategy to form functional nanoparticles that eliminate the need for solid supports or nanomaterial surface. This peptide-driven strategy is simple, biocompatible and can generates nanoparticles instantaneously with triggers. The

method established here may be further explored by tailoring peptide sequences and/or expanded to a wide range of proteins in order to generate soft nanoparticles to suit medical and therapeutic applications.

5.5 References

Aggeli, A., Bell, M., Carrick, L.M., Fishwick, C.W., Harding, R., Mawer, P.J., Radford, S.E., Strong, A.E., Boden, N. 2003. pH as a trigger of peptide β-sheet self-assembly and reversible switching between nematic and isotropic phases. *Journal of the American Chemical Society*, **125**(32), 9619-9628.

Aggeli, b.A., Bell, M., Boden, N., Keen, J., Knowles, P., McLeish, T., Pitkeathly, M., Radford, S. 1997. Responsive gels formed by the spontaneous self-assembly of peptides into polymeric β-sheet tapes. *Nature*, **386**(6622), 259.

Booth, D.S., Avila-Sakar, A., Cheng, Y. 2011. Visualizing proteins and macromolecular complexes by negative stain EM: from grid preparation to image acquisition. *Journal of visualized experiments: JoVE*(58).

Carrick, L.M., Aggeli, A., Boden, N., Fisher, J., Ingham, E., Waigh, T.A. 2007. Effect of ionic strength on the self-assembly, morphology and gelation of pH responsive β-sheet tape-forming peptides. *Tetrahedron*, **63**(31), 7457-7467.

Collins, K.D. 2012. Why continuum electrostatics theories cannot explain biological structure, polyelectrolytes or ionic strength effects in ion–protein interactions. *Biophysical chemistry*, **167**, 43-59.

Dougherty, D.A. 2007. Cation-π interactions involving aromatic amino acids. *The Journal of nutrition*, **137**(6), 1504S-1508S.

Hsia, Y., Bale, J.B., Gonen, S., Shi, D., Sheffler, W., Fong, K.K., Nattermann, U., Xu, C., Huang, P.-S., Ravichandran, R. 2016. Design of a hyperstable 60-subunit protein icosahedron. *Nature*, **535**(7610), 136.

Hudalla, G.A., Sun, T., Gasiorowski, J.Z., Han, H., Tian, Y.F., Chong, A.S., Collier, J.H. 2014. Gradated assembly of multiple proteins into supramolecular nanomaterials. *Nature materials*, **13**(8), 829.

Jenny P. Glusker, A.K.K., Charles W. Bock. 1999. Metal ions in biological systems. *The Rigaku Journal*, **16**, 8-17.

Lowik, D.W., Leunissen, E., van den Heuvel, M., Hansen, M.B., van Hest, J.C. 2010. Stimulus responsive peptide based materials. *Chemical Society Reviews*, **39**(9), 3394-3412.

Park, W.M., Champion, J.A. 2014. Thermally triggered self-assembly of folded proteins into vesicles. *Journal of the American Chemical Society*, **136**(52), 17906-17909.

Patterson, D.P., Desai, A.M., Holl, M.M.B., Marsh, E.N.G. 2011. Evaluation of a symmetry-based strategy for assembling protein complexes. *RSC advances*, **1**(6), 1004-1012.

Quan, L., Wei, D., Jiang, X., Liu, Y., Li, Z., Li, N., Li, K., Liu, F., Lai, L. 2008. Resurveying the Tris buffer solution: the specific interaction between tris (hydroxymethyl) aminomethane and lysozyme. *Analytical biochemistry*, **378**(2), 144-150.

Rapp, C., Goldberger, E., Tishbi, N., Kirshenbaum, R. 2014. Cation–π interactions of methylated ammonium ions: A quantum mechanical study. *Proteins: Structure, Function, and Bioinformatics*, **82**(7), 1494-1502.

Ross, J.F., Bridges, A., Fletcher, J.M., Shoemark, D., Alibhai, D., Bray, H.E., Beesley, J.L., Dawson, W.M., Hodgson, L.R., Mantell, J. 2017. Decorating self-assembled peptide cages with proteins. *ACS nano*, **11**(8), 7901-7914.

Saito, R., Sato, T., Ikai, A., Tanaka, N. 2004. Structure of bovine carbonic anhydrase II at 1.95 Å resolution. *Acta Crystallographica Section D*, **60**(4), 792-795.

Scotter, A.J., Guo, M., Tomczak, M.M., Daley, M.E., Campbell, R.L., Oko, R.J., Bateman, D.A., Chakrabartty, A., Sykes, B.D., Davies, P.L. 2007. Metal ion-dependent, reversible, protein filament formation by designed beta-roll polypeptides. *BMC structural biology*, **7**(1), 63.

Shanbhag, B.K. 2016. Engineering enzyme-peptide fusion systems with self-assembly ability as advanced biocatalysts, Vol. PhD, Monash University.

Shanbhag, B.K., Liu, B., Fu, J., Haritos, V.S., He, L. 2016. Self-assembled enzyme nanoparticles for carbon dioxide capture. *Nano letters*, **16**(5), 3379-3384.

Stendahl, J.C., Rao, M.S., Guler, M.O., Stupp, S.I. 2006. Intermolecular forces in the self-assembly of peptide amphiphile nanofibers. *Advanced Functional Materials*, **16**(4), 499-508.

Studier, F.W. 2005. Protein production by auto-induction in high-density shaking cultures. *Protein expression and purification*, **41**(1), 207-234.
Taha, M., Lee, M.-J. 2010. Interactions of TRIS [tris (hydroxymethyl) aminomethane] and related buffers with peptide backbone: thermodynamic characterization. *Physical Chemistry Chemical Physics*, **12(**39), 12840-12850.
Torrice, M.M., Bower, K.S., Lester, H.A., Dougherty, D.A. 2009. Probing the role of the cation–π interaction in the binding sites of GPCRs using unnatural amino acids. *Proceedings of the National Academy of Sciences*, **106**(29), 11919-11924.
Watson, S.K., Kan, E. 2015. Effects of novel auto-inducible medium on growth, activity and CO_2 capture capacity of Escherichia coli expressing carbonic anhydrase. *Journal of microbiological methods*, **117**, 139-143.
Wu, W., Xing, L., Zhou, B., Lin, Z. 2011. Active protein aggregates induced by terminally attached self-assembling peptide ELK16 in *Escherichia coli*. *Microbial cell factories*, **10**(1), 9.
Zhang, S. 2003. Fabrication of novel biomaterials through molecular self-assembly. *Nature Biotechnology*, **21**, 1171.
Zhang, Y. 2008. I-TASSER server for protein 3D structure prediction. *BMC Bioinformatics*, **9**(1), 40.
Zhao, X., Pan, F., Xu, H., Yaseen, M., Shan, H., Hauser, C.A., Zhang, S., Lu, J.R. 2010. Molecular self-assembly and applications of designer peptide amphiphiles. *Chemical Society Reviews*, **39**(9), 3480-3498.
Zheng, H., Chruszcz, M., Lasota, P., Lebioda, L., Minor, W. 2008. Data mining of metal ion environments present in protein structures. *Journal of inorganic biochemistry*, **102**(9), 1765-1776.
Zhou, B., Xing, L., Wu, W., Zhang, X.-E., Lin, Z. 2012. Small surfactant-like peptides can drive soluble proteins into active aggregates. *Microbial cell factories*, **11**(1), 10.

CHAPTER 6

COMBINING AFFINITY BINDING AND SELF-ASSEMBLY PEPTIDES TO ENGINEER TUNEABLE IRON OXIDE NANOCLUSTERS

This page is intentionally blank

CHAPTER 6
COMBINING AFFINITY BINDING AND SELF-ASSEMBLY PEPTIDES TO ENGINEER TUNEABLE IRON OXIDE NANOCLUSTERS

6.1 Introduction

The work in previous chapters have been focused on formation of individual nanoparticles, including immobilisation of proteins on inorganic nanoparticles (chapters 3 and 4) and protein-only nanoparticles (chapter 5). Two distinct biologic components have been adapted for such tasks, respectively. Affinity binding peptides have been utilized in chapter 4 to noncovalently link proteins with inorganic nanoparticles while self-assembly peptides have been deployed to make protein particles in chapter 5. Built naturally on these achievements, this chapter aims to engineer higher-order structural nanoparticles that have attractive features.

Higher-order structural nanoparticles are of great research interest to produce a new generation of smart nanomaterials. In general, nanoparticles that are assembled into a larger size with hierarchical architecture can confer better properties in comparison to individual nanoparticles. Such higher-order nanomaterials have been increasingly used in optoelectronics, sensors and drug delivery (Edel et al., 2013; Wang & Wang, 2014). To date, there are a variety of higher-order structures such as microcapsules (Evers et al., 2016), super lattices (Han et al., 2018; Udayabhaskararao et al., 2017), and clusters (Casula et al., 2016; Ge et al., 2007; Kralj & Makovec, 2014; Lee et al., 2013; Liao et al., 2016; Qi et al., 2016; Qiu et al., 2010; Yan et al., 2018; Yang et al., 2018; Zhang et al., 2017).

Among these higher-order nanostructure, the clusters of iron oxide nanoparticles (IONP) have attracted particular interests because of their applications in photonics, energy, and biomedicine

(Casula et al., 2016; Han et al., 2018; Kotov, 2017; Lee et al., 2013; Qi et al., 2016). The iron oxide nanoparticle cluster (IONPC) does not only have characteristic properties of individual particles but also new collective functions provided by higher-order structure. For example, IONPC has excellent electrochemistry properties including strong cyclic stability and high rate capability as high-performance anodes (Lee et al., 2013). Although several examples and approaches of IONPC have been reported (Evers et al., 2016; Lee et al., 2013; Udayabhaskararao et al., 2017), they have certain drawbacks, such as ordered structures being devoid of functionality, lacking tuneable structures and poor control over inter-particle space. For example, despite high-performance of self-assembled IONPC as anode for battery application (Lee et al., 2013), the clusters do not have tuneable property and the distance between the nanoparticles was not controlled.

It's still a challenge to control the distance between nanoparticles to form supra-structure such as nanoparticle lattice, particularly for these with an inter-nanoparticle distance ranging from several to several tens of nanometres (Kotov, 2017). At such nanometres of empty space, the high-order structures often collapse because they have poor stabilities. In order to overcome this challenge, Udayabhaskararao *et al*. developed a co-assembles approach that combined gold and iron oxide nanoparticles to form binary nanoparticle lattice first, then transformed them into porous nanomaterials, so called nanoallotropes, by selectively etching away either gold or iron oxide (Udayabhaskararao et al., 2017). Such sacrificial strategy has the potential to make atom-like superlattices with desirable nanoscale architectures. However, fabrication of such nano allotropes is complicated and labour-intensive in addition to harsh conditions of chemical etching. Thus, there is a strong need to develop an innovative way to produce high-order nanostructure with empty space between nanoparticles. Ideally, the new approach should

deliver higher-order functional nanomaterials with a feature of responsiveness to external stimuli, providing better control and tuneability.

The objective of this chapter is to develop such strategy that can produce higher-order cluster structure with improved properties, overcoming the aforementioned limitations of existing methods. The design of a hybrid nanoparticle cluster includes iron oxide nanoparticles (IONP) as the inorganic nanomaterial, two different versions of iron oxide binding protein Mms6, protein carbonic anhydrase, and self-assembly peptide $P_{11}4$ as biologic entities (Figure 6.1). The fusion protein has two important peptide regions: i) a peptide with affinity to iron oxide and ii) the $P_{11}4$ peptide that has an inbuilt self-assembling ability responding to pH alteration or metal ions.

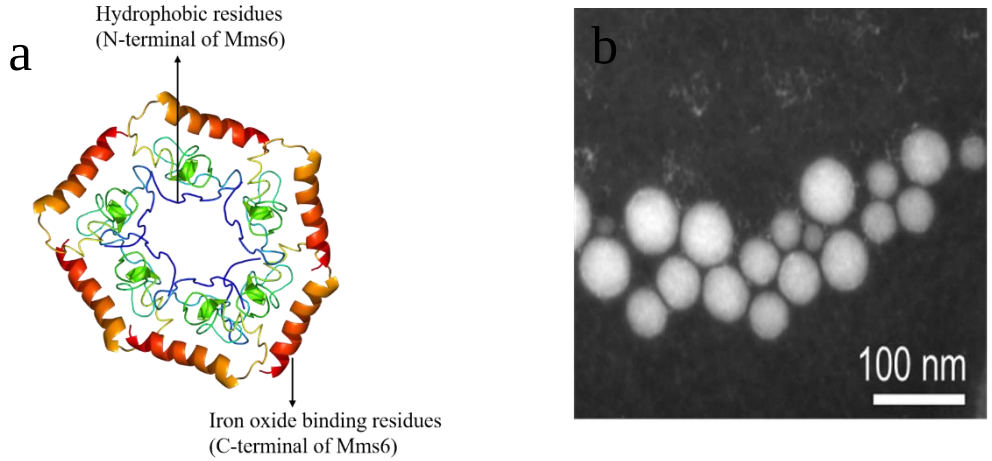

***Scheme 6.1**: Micelles formation by recombinant protein Mms6. a) Schematic micelle structure of Mms6 due to hydrophobic residues in the N-terminal of Mms6. A representative ribbon structure of Mms6 was used to draw the micelles structure; b) high angle annular dark field - scanning transmission electron microscopy (HAADF-STEM) images of micelles by Mms6 (this image was reproduced from Kashyap et al.(Kashyap et al., 2014).*

Mms6 has been found to have an affinity binding with iron oxide. The full length Mms6 forms micelles due to strong hydrophobic residues in N-terminal domain (Scheme 6.1), and they need denaturation conditions to be purified (Ma et al., 2017).

The c-terminal domain, Mms6c, is hydrophilic and has affinity binding with iron oxide (Feng et al., 2013). The second peptide is the stimuli-responsive self-assembly peptide $P_{11}4$ (Aggeli et al., 2003) that has been studied in chapter 5. The fusion protein was designed in a way that either full length Mms6 or its truncated version of Mms6c was fused to the N-terminus of the protein while $P_{11}4$ self-assembly peptides is fused at C-terminus of the protein.

The enzyme carbonic anhydrase from two sources namely *Thiomicrospira crunogena* (TmCA) and bovine have been used to design a series of fusion proteins in this study (Table 6.1). Fusion of the enzymes with Mms6/Mms6c protein and $P_{11}4$ are linked with a GS linker to maintain sufficient space and improve flexibility. A representation of the fusion protein and the conceptualisation of the higher-order functional cluster is illustrated in Figure 6.1. The self-assembly and iron binding properties of the these engineered fusion proteins were evaluated first, followed by examing whether they can form functional nanoclusters of higher-order, using two complementary approaches as detailed in the following sections.

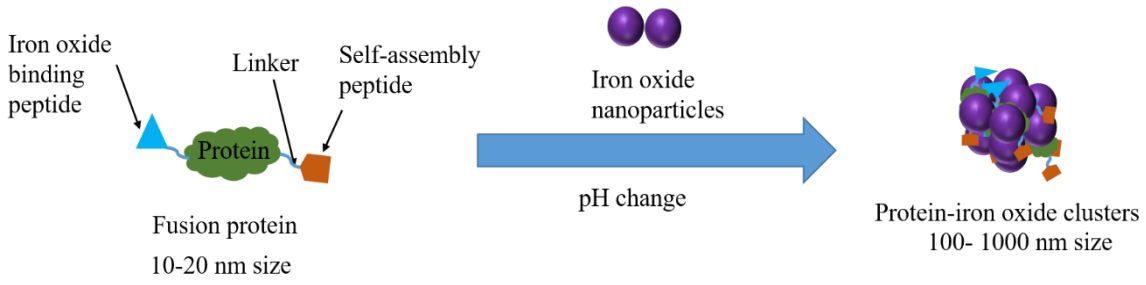

Figure 6.1: *Design and engineering of affinity and self-assembly protein for the fabrication of multifunctional IONPC*

6.2 Materials and Methods

6.2.1 Materials

E. coli BL21 (DE3) competent cells were purchased from New England Bio labs Inc.-NEB (Wilbury Way Hitchin, UK). The pET28a vectors encoding all constructs in Table 6.1 were

synthesized by GenScript (Piscataway, NJ 08854, USA). Iron oxide nanoparticles (IONP) (SOR-COMO-3) of size 5, 10, 20, and 30 nm were purchased from Ocean Nanotech, San Diego, CA 92126.

6.2.2 Protein Design

In this work, seven different protein constructs, Mms6, Mms6-TmCA, Mms6-TmCA-P_{11}4, Mms6-BCA, Mms6-BCA-P_{11}4, Mms6c-BCA-P_{11}4, and BCA-P_{11}4 were designed (Table 6.1). TmCA and BCA were selected as model enzymes that have different surface charges and thermal stabilities (Warden et al., 2015). The N-terminal of Mms6 are rich of hydrophobic amino acids and have the ability to form into micelles structure. The c-terminal of Mms6 have iron oxide binding property due to the presence of amino acids capable of complexation with iron (Aspartic acid, Glutamic acid).

In the first design strategy, the fusion of the full-length protein Mms6 on the N-terminal of either BCA or TmCA yielding two constructs, Mms6-BCA and Mms6-TmCA. The full length Mms6 protein has the self-assembly and iron binding functionality, but there is no control over the particle sizes formed. Therefore the second design strategy was developed by introducing the self-assembly peptide P_{11}4 (Aggeli et al., 2003). For this purpose, three constructs have been designed, including Mms6-TmCA-P_{11}4, Mms6-BCA-P_{11}4, and Mms6c-BCA-P_{11}4. As a control, BCA-P_{11}4 was also included in this chapter. For all designs, the GS linker (amino acid sequences: GGGGSGGGGS) has been used as a linking sequence to provide a flexible region between the fusion peptides and the enzyme for better self-assembly and binding.

***Table 6.1**: Summary of design and functionalities of engineered proteins*

Construct	**Design**	**Structure and Functionality**	**Sequences**
Mms6	Full-length iron oxide binding protein.	Self-assembly forming micelles due to hydrophobic residues in N-terminal. C-terminal binds with iron oxide	MVGGTIWTGKGLGLGLGLGLGAWGPIILGVVGAGAVYAYMKSRDIES AQSDEEVELRDALAHHHHHH
Mms6-TmCA	Full-length protein (Mms6) was fused at N-terminus of TmCA GS linker is kept between them for better flexibility and functionality	The fusion protein has self-assembly (micelles) and iron oxide-binding properties due to Mms6 and carbon dioxide capturing enzyme TmCA. No size controlled	MGSSHHHHHHSSGLVPRGSHMVGGTIWTGKGLGLGLGLGLGAWGPIIL GVVGAGAVYAYMKSRDIESAQSDEEVELRDALAGGGGSGGGGSANN VAAPLIDLGAEAKKQAQKSAATQSAVPEKESATKVAEKQKEPEEKAKP EPKKPPHWGYFGEEGPQYWGELAPEFSTCKTGKNQSPINLKPQTAVGT TSLPGFDVYYRETALKLINNGHTLQVNIPLGSYIKINGHRYELLQYHFHT PSEHQRDGFNYPMEMHLVHKDGDGNLAVIAILFQEGEENETLAKLMSF LPQTLKKQEIHESVKIHPAKFFPADKKFYKYSGSLTTPPCSEGVYWMVF KQPIQASVTQLEKMHEYLGSNARPVQRQNARTLLKSWPDRNRANTVY EFY
Mms6-BCA	Full-length protein (Mms6) was fused with BCA. GS linker is kept between peptide and enzyme.	Mms6 causes self-assembly (micelles) and binds with iron oxide. BCA, carbon dioxide capture enzyme, No size control	MVGGTIWTGKGLGLGLGLGLGAWGPIILGVVGAGAVYAYMKSRDIES AQSDEEVELRDALAGGGGSGGGGSSHHWGYGKHNGPEHWHKDFPIA NGERQSPVDIDTKAVVQDPALKPLALVYGEATSRRMVNNGHSFNVEY DDSQDKAVLKDGPLTGTYRLVQFHFHWGSSDDQGSEHTVDRKKYAAE LHLVHWNTKYGDFGTAAQQPDGLAVVGVFLKVGDANPALQKVLDAL DSIKTKGKSTDFPNFDPGSLLPNVLDYWTYPGSLTTPPLLESVTWIVLKE PISVSSQQMLKFRTLNFNAEGEPELLMLANWRPAQPLKNRQVRGFPK

Mms6-TmCA-$P_{11}4$	Full-length protein (Mms6) and self-assembly peptide ($P_{11}4$) were fused on bN- and C- termini of enzyme TmCA. GS linker was kept between peptides and enzyme	This fusion protein forms micelles and iron oxide binding due to Mms6. However, the self-assembly (size) can be controlled due to peptide $P_{11}4$ (change in pH). TmCA, carbon dioxide capture enzyme.	MGSSHHHHHHSSGMVGGTIWTGKGLGLGLGLGLGAWGPIILGVVGAG AVYAYMKSRDIESAQSDEEVELRDALAGGGGSGGGGSANNVAAPLIDL GAEAKKQAQKSAATQSAVPEKESATKVAEKQKEPEEKAKPEPKKPPH WGYFGEEGPQYWGELAPEFSTCKTGKNQSPINLKPQTAVGTTSLPGFD VYYRETALKLINNGHTLQVNIPLGSYIKINGHRYELLQYHFHTPSEHQR DGFNYPMEMHLVHKDGDGNLAVIAILFQEGEENETLAKLMSFLPQTLK KQEIHESVKIHPAKFFPADKKFYKYSGSLTTPPCSEGVYWMVFKQPIQA SVTQLEKMHEYLGSNARPVQRQNARTLLKSWPDRNRANTVYEFYGGG GSGGGGSQQRFEWEFEQQ
Mms6-BCA-$P_{11}4$	The fusion protein has full-length protein (Mms6) and $P_{11}4$ on N- and C-terminus of BCA. GS linker was kept between them	This protein self-assembly forming micelles and have iron oxide binding property (Mms6). The size can be controlled due to peptide $P_{11}4$ (pH change). BCA, carbon dioxide capture enzyme	MVGGTIWTGKGLGLGLGLGLGAWGPIILGVGAGAVYAYMKSRDIESA QSDEEVELRDALAGGGGSGGGGSSHHWGYGKHNGPEHWHKDFPIAN GERQSPVDIDTKAVVQDPALKPLALVYGEATSRRMVNNGHSFNVEYD DSQDKAVLKDGPLTGTYRLVQFHFHWGSSDDQGSEHTVDRKKYAAEL HLVHWNTKYGDFGTAAQQPDGLAVVGVFLKVGDANPALQKVLDALD SIKTKKSTDFPNFDPGSLLPNVLDYWTYPGSLTTPPLLESVTWIVLKEPIS VSSQQMLKFRTLNFNAEGEPELLMLANWRPAQPLKNRQVRGFPKGGG GSGGGGSQQRFEWEFEQQ
Mms6c-BCA-$P_{11}4$	The C-terminal of Mms6 (Mms6c) and $P_{11}4$ on N- and C-terminus of BCA. GS linker was kept	The fusion protein has iron oxide binding property due to Mms6c and self-assembly property due to $P_{11}4$. The size can be controlled by the change	MYAYMKSRDIESAQSDEEVELRDALAGGGGSGGGGSSHHWGYGKHN GPEHWHKDFPIANGERQSPVDIDTKAVVQDPALKPLALVYGEATSRRM VNNGHSFNVEYDDSQDKAVLKDGPLTGTYRLVQFHFHWGSSDDQGSE HTVDRKKYAAELHLVHWNTKYGDFGTAAQQPDGLAVVGVFLKVGDA NPALQKVLDALDSIKTKGKSTDFPNFDPGSLLPNVLDYWTYPGSLTTPP

	between the peptide and protein	in pH. BCA, carbon dioxide capture enzyme	LLESVTWIVLKEPISVSSQQMLKFRTLNFNAEGEPELLMLANWRPAQPL KNRQVRGFPKGGGGSGGGGSQQRFE WEFEQQ
BCA-P_{11}4	Self-assembly peptide (P_{11}4) attached to the C-terminal of BCA	This fusion protein self-assembly due to peptide P_{11}4. BCA, carbon dioxide capture enzyme. This protein lacks iron oxide binding peptide	GMSHHWGYGKHNGPEHWHKDFPIANGERQSPVDIDTKAVVQDPALKP LALVYGEATSRRMVNNGHSFNVEYDDSQDKAVLKDGPLTGTYRLVQF HFHWGSSDDQGSEHTVDRKKYAAELHLVHWNTKYGDFGTAAQQPDG LAVVGVFLKVGDANPALQKVLDALDSIKTKGKSTDFPNFDPGSLLPNV LDYWTYPGSLTTPPLLESVTWIVLKEPISVSSQQMLKFRTLNFNAEGEPE LLMLANWRPAQPLKNRQVRGFPKGGGGSGGGGSQQRFE WEFEQQ

6.2.3 Expression and Purification

The gene sequences encoding proteins Mms6, Mms6-TmCA, Mms6-TmCA-P_{11}4, Mms6-BCA, Mms6-BCA-P_{11}4, Mms6c-BCA-P_{11}4, and BCA-P_{11}4 were codon optimised and synthesised between *NcoI* and *XhoI* restriction sites into pET28a expression plasmids by GenScript. The transformation and expression were performed under same conditions as described in chapter 3. The recombinant proteins were purified using Ni-affinity column chromatography. HiTrap FF (5 mL) (GE Healthcare). Briefly, Mms6, Mms6-TmCA, Mms6-TmCA-P_{11}4, Mms6-BCA, Mms6-BCA-P_{11}4, were purified under denaturation condition in the presence of 1% SDS in the lysis buffer (50 mM Tris-HCl pH 8.0, 50 mM NaCl, 1 mM EDTA, 0.5% Triton-X 100) and elution buffer (10 mM Tris/HCl, 0.5 M NaCl, 200 mM imidazole, pH 8). However, Mms6c-BCA-P_{11}4 and BCA-P_{11}4 were purified without using SDS. The purified proteins were desalted into 10 mM phosphate buffer pH 8 using Sephadex G-25 (16.7 cm × I.D. 1.7 cm).

6.2.3 Protein concentration and Enzyme Activity

Proteins concentration were determined by absorbance at 280 nm using the extinction coefficient calculated from amino acid sequence. The enzymatic activity of recombinant proteins was measured by esterase assay (Verpoorte et al., 1967), as described in chapter 3.

6.2.4 Self-assembly and Characterisation of Protein Nanoparticles

The self-assembly of recombinant fusion proteins with self-assembly peptide (P_{11}4) was evaluated using pH and Mg^{2+} ions triggers. Briefly, purified fusion proteins (0.5 mg/mL) in desalting buffer was adjusted to pH 6.8, using acetic acid. Alternatively, protein nanoparticles were produced by addition of $MgCl_2$ (20 mM). Protein nanoparticles were analysed through dynamic light experiment (DLS, Zetasizer Nano, Malvern Instruments) and transmission electron microscopy (TEM, FEI, Tecnai G2 T20).

For the DLS, 1 mL of the nanoparticles sample was taken in the disposable cuvette, equilibrate for 30 sec, and nanoparticles were measured using Zetasizer software. The experiments were conducted at 25 °C and measurement data were collected from three independent runs with each comprising 10 cycles. The protein nanoparticles were analysed using TEM using the same protocol used in chapter 5, section 5.2.7.

6.2.5 Fabrication and Characterisation of Protein-iron Oxide Clusters

The protein-iron oxide cluster (PIONC) were formed through two different routes: 1) mix Mms6c-BCA-P_{11}4 and IONP at pH 8 then decrease the pH to 6.8, 2) form protein particles of Mms6c-BCA-P_{11}4 first at pH 6.8, then add IONP to protein particles (Figure 6.2). In route 1, 0.5 mg of IONP (4 µL of 25 mg/mL) was mixed with 200 µL of acetone and sonicated for 5 minutes for proper suspension of the oleic acid-coated iron oxide. Then, 800 µL Mms6c-BCA-P_{11}4 (0.36 mg) in desalting buffer was incubated with the IONP solution to produce IONPC. The pH of the mixture solution was adjusted to 6.8 to produce supercluster, as presented in route 1, Figure 6.2.

The route 2 started with formation of Mms6c-BCA-P_{11}4 protein nanoparticles (soft particles) by pH adjustment, followed by the addition of the IONP for cluster formation. First, 1 mL of Mms6c-BCA-P_{11}4 (0.45 mg) in desalting buffer was adjusted to pH 6.8 by using 5 M acetic acid, and then 800 µL of protein particles (0.36 mg) was mixed with sonicated 200 µL of IONP (0.5 mg) in acetone to produce cluster nanoparticles. A control (BCA-P_{11}4) was run for both routes 1 and 2. The higher-order IONC were characterized using TEM using the same protocol used in chapter 5, section 5.2.7.

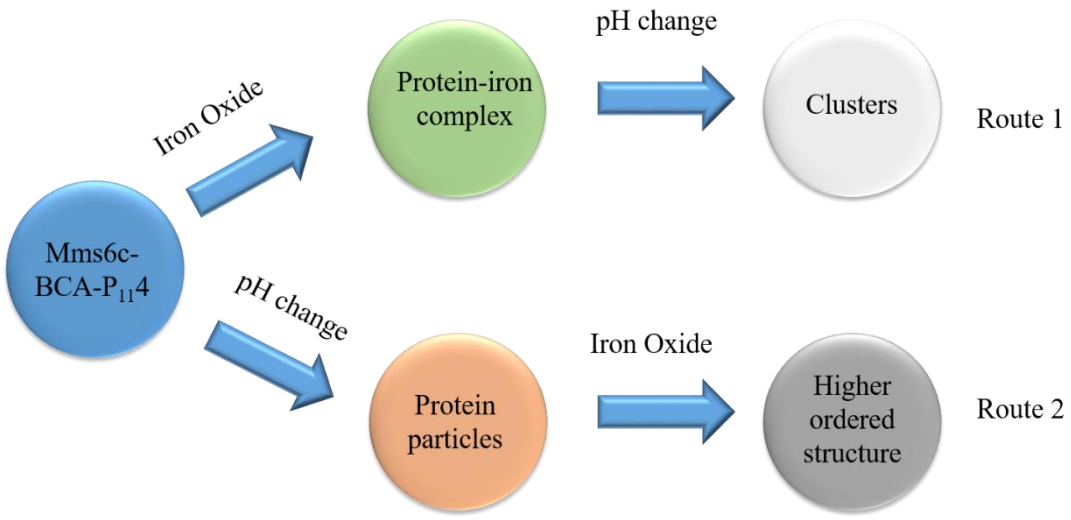

Figure 6.2: *Combination of self-assembly of $P_{11}4$and affinity binding of Mms6c to fabricate protein-iron oxide clusters. In route 1, Mms6c-BCA-P114 first binds iron oxide to form protein-iron complex, followed by alteration of pH change to form clusters. In route 2, Mms6c-BCA-P114 form the protein-only nano-particles first, followed by addition of iron oxide to form higher order structure.*

6.3 Result and Discussion

6.3.1 Structure, Expression, and Purification of Proteins

The engineered proteins were designed to include self-assembly and iron binding abilities. Two versions of iron binding proteins – Mm6 and Mm6c, two enzymes – TmCA and BCA, and one self-assembly peptide – $P_{11}4$ have been selected as biologic elements in the design. Representative ribbon structure of Mms6, Mms6-TmCA-$P_{11}4$, Mms6-BCA, and Mms6c-BCA-$P_{11}4$ is presented in Figure 6.3. The rational design of the fusion proteins made the both peptides readily available to undertake their functions such as self-assembly and affinity binding on iron oxide. For example, Mms6c-BCA-$P_{11}4$ have Mms6c and $P_{11}4$ peptides localised in opposite positions to minimize clashes between two peptides.

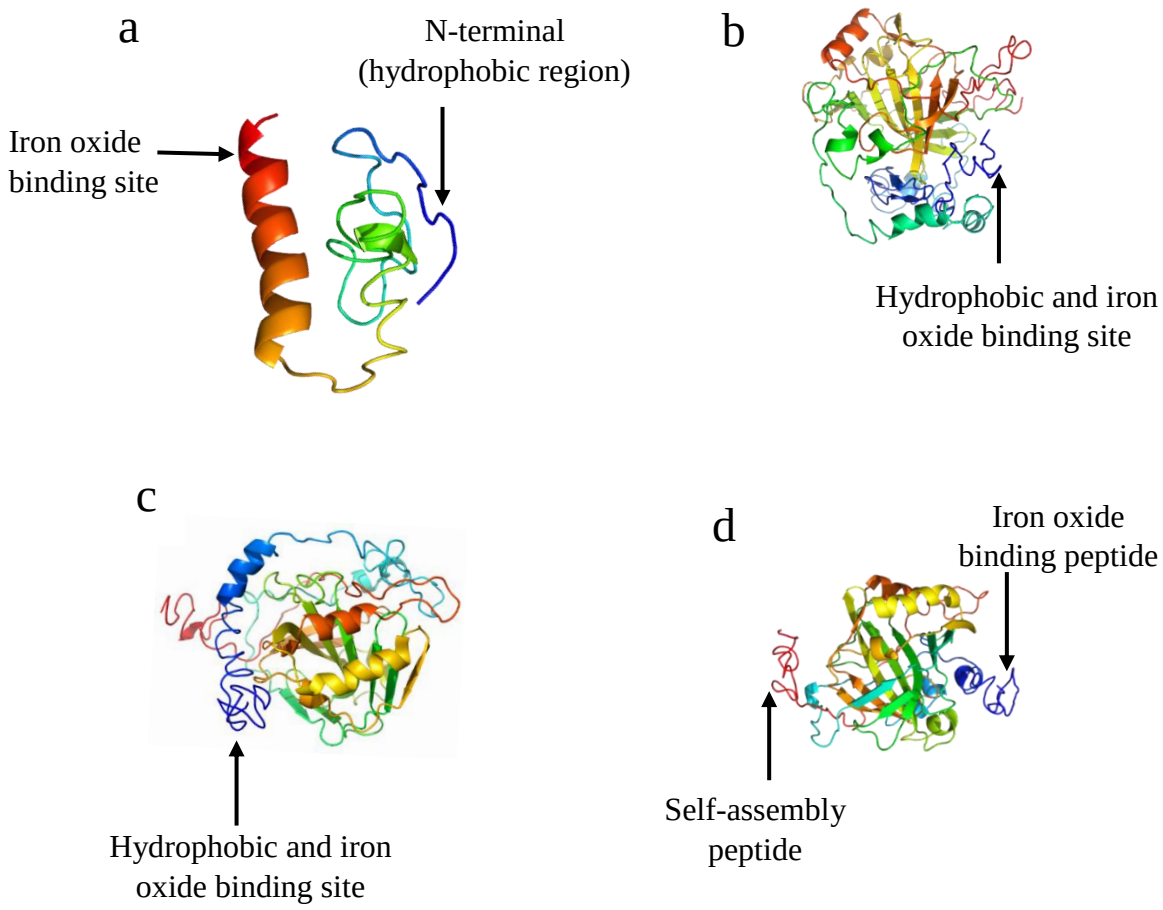

Figure 6.3: *A representative ribbon structure of recombinant protein. a, Mms6, b) Mms6-TmCA-P$_{11}$4, c) Mms6-BCA, and d) Mms6c-BCA-P$_{11}$4. The structures presents the iron oxide binding peptide and/or self-assembly peptide sites. The structure was produced using I-TASSER server (Zhang, 2008).*

The engineering proteins were expressed in *E. coli BL21* (DE3) cells and analysed by SDS-PAGE as shown in Figure 6.4. Although soluble proteins were visible for most proteins, insoluble proteins were dominated for Mms6-BCA (B), Mms6-BCA-P$_{11}$4 (C), and Mms6-TmCA-P$_{11}$4 (D). This protein solubility issue may be attributed to the presence of a hydrophobic micelle forming region in the N-terminus of the full-length protein (Mms6). The phenomenon of micelles formation (300 kDa) was previously reported (Wang et al., 2012). In contrast, Mms6c-BCA-P$_{11}$4 (E) in which the truncated Mms6C lacks the micelle forming hydrophobic region were mostly expressed in a soluble form. This suggests that the micelle

forming region of Mms6 promotes uncontrolled aggregation leading to insoluble protein expression of the constructs.

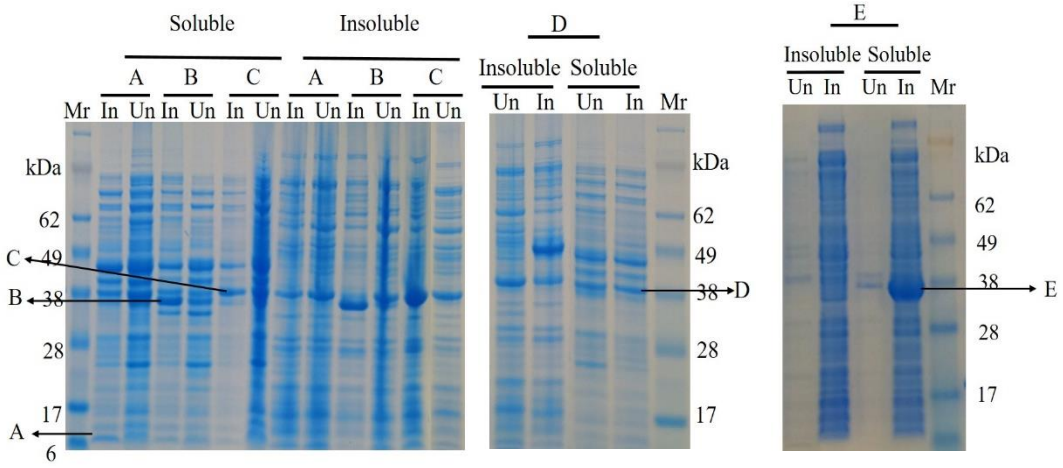

Figure 6.4: *Expression of recombinant protein analysed by SDS-PAGE. A: Mms6, B: Mms6-BCA, C: Mms6-BCA-P$_{11}$4, D: Mms6-TmCA-P$_{11}$4, E: Mms6c-BCA-P$_{11}$4. Un, uninduced cells; In, induced cells; soluble, soluble fraction; insoluble, insoluble fraction..*

The recombinant proteins were purified using Ni-affinity column chromatography. The fusion proteins with full-length sequence of Mms6 (Mms6, Mms6, Mms6-BCA, and Mms6-TmCA-P$_{11}$4) were purified under mild denaturing condition using 1% SDS in both lysis and purification buffers. It was anticipated that these conditions might decrease or minimize aggregation of the Mms6, thus allowing binding and elution in purification process. However, the purification of Mms6-BCA-P$_{11}$4 was still not as effective as BCA-P$_{11}$4 (data not shown). In contrast, Mms6c-BCA-P$_{11}$4 simplifies the purification procedure and was purified without 1% SDS. Also, Mms6c-BCA-P$_{11}$4 purified has the highest purity in comparison to other constructs as shown in Figure 6.5.

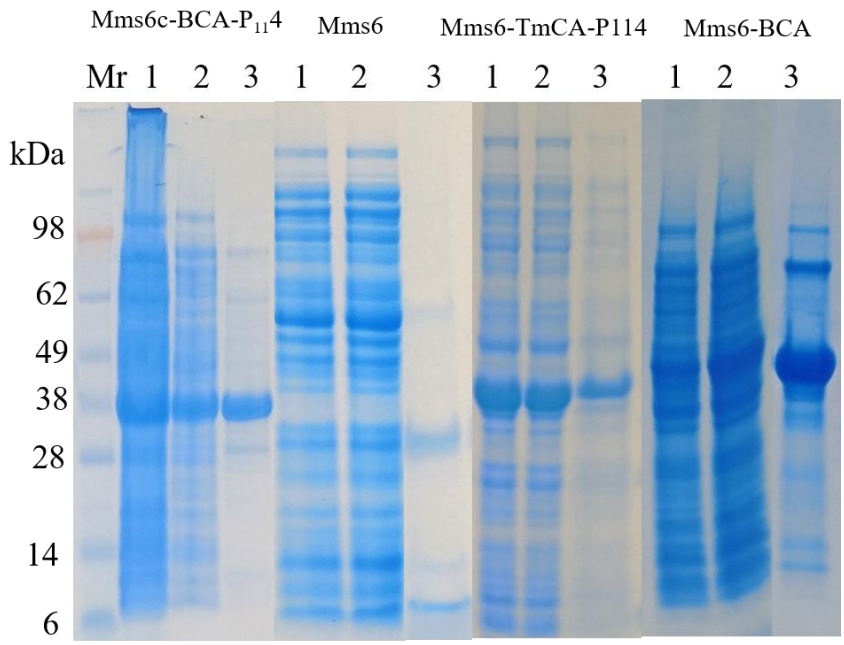

Figure 6.5*: SDS-PAGE showing the purification of proteins. Here, 1: crude lysate, 2: flow through, and 3: purified protein.*

In the SDS-PAGE results, Mms6-BCA, Mms6-TmCA-P114, and Mms6c-BCA-P114 appeared as a single band with molecular weight of 35, 43, and 34 kDa respectively. However, the unstructured protein Mms6 (6 kDa) appeared at multiple places when analysed by SDS-PAGE, and all bands were confirmed to be Mms6 by mass spectrometry, suggesting Mms6 can form aggregates even in denaturing conditions.

6.3.2 Self-assembly of Protein Nanoparticles

The hydrophobic residues at N-termini of Mms6 is responsible for the self-assembly of Mms6 protein into micelle as reported previously in literature (Kashyap et al., 2014; Wang et al., 2012). Our results showed that Mms6 forms nanoparticles with size around 100 nm (Figure 6.6a), similar to that reported in literature (25-100 nm). However, these particles cannot be controlled or tuned to a desirable size by using external stimuli.

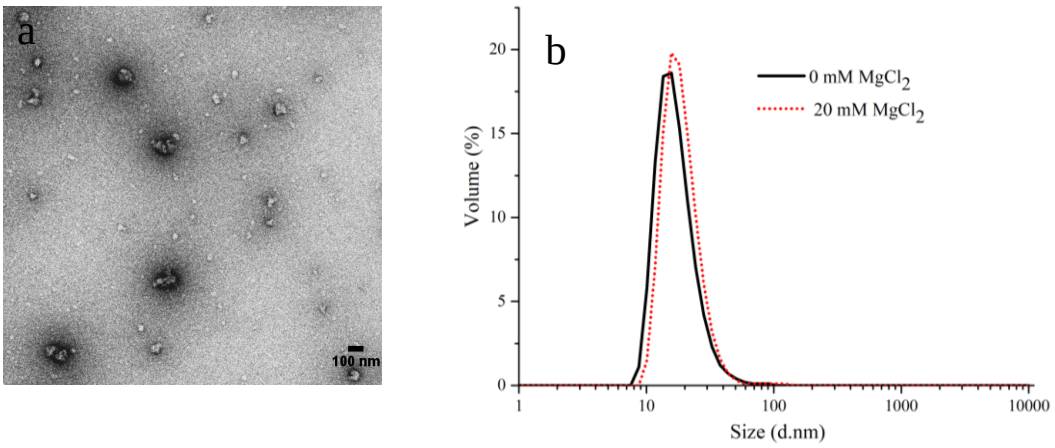

Figure 6.6: *Self-assembly of protein particles, a) TEM image of Mms6, and b) Dynamic light scattering (DLS) results of Mms6-TmCA-P$_{11}$4 particles (0.5 mg/mL) at pH 8. The TEM samples were negative stained using 2% (v/v) uranyl acetate.*

The protein construct Mms6-TmCA-P$_{11}$4 was designed to incorporate the self-assembly peptide (P$_{11}$4) on the C-terminus of TmCA while Mms6 was fused at N-terminus. It is known that P$_{11}$4 peptide assists fused protein-peptide to form protein nanoparticles by alteration of the pH and/or by addition of Mg^{2+} as we have shown in Chapter 5. Mms6-TmCA-P$_{11}$4 appeared in small nanoparticle format (20 nm) as shown Figure 6.6b. However, it did not respond to addition of the Mg^{+2} ion to increase its size. This may be due to the micelles formation driven by the N-terminal region of Mms6, preventing effective interactions between P$_{11}$4 peptides for self-assembly.

Mms6c-BCA-P$_{11}$4 is expected to minimize micelle formation of full length Mms6 by truncating its N-terminal domain. Indeed, Mms6c-BCA-P$_{11}$4 forms protein nanoparticles and the sizes are tuneable using pH and Mg^{2+} ion as shown in Figure 6.7. The monomeric Mms6c-BCA-P$_{11}$4 protein formed nanoparticles of 140 ± 6 nm when pH was reduced to 6.8 as

confirmed by the DLS and TEM images. The TEM images of nanoparticles showed the well-structured protein nanoparticles as shown in Figure 6.7b. The addition of 20 mM $MgCl_2$ to the monomeric proteins led to protein particles formation of 750 ± 120 nm, as illustrated in Figure 6.7c.

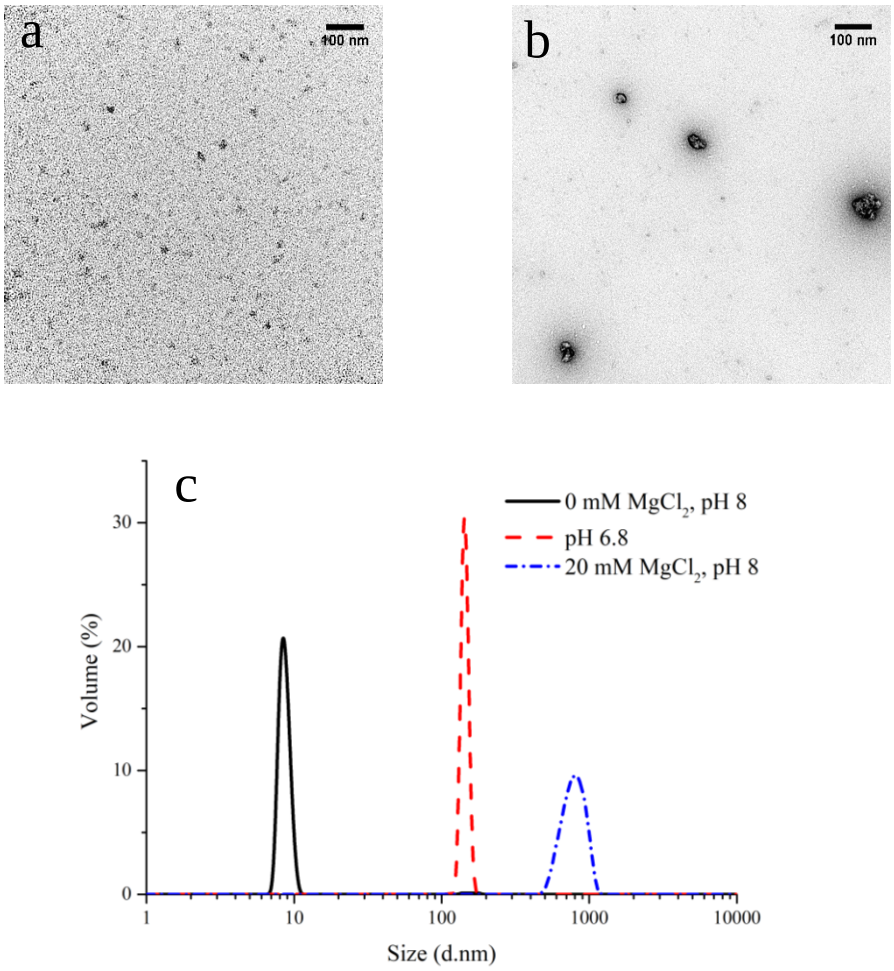

Figure 6.7: *Formation of protein nanoparticle by Mms6c-BCA-P_{11}4. a) TEM image of monomeric Mms6c-BCA-P_{11}4 at 10 mM phosphate buffer pH 8, b) TEM image of Mms6c-BCA-P_{11}4 protein nanoparticles at pH 6.8, and c) DLS of Mms6c-BCA-P_{11}4 nanoparticles tuned by change in pH or addition of $MgCl_2$. The TEM samples were negative stained using 2% (v/v) uranyl acetate.*

6.3.3 Fabrication of Iron Oxide Nanoclusters

The IONP, when mixed with Mms6 and Mms6-BCA, formed high-ordered materials as shown in Figure 6.8. The 10 nm size IONP were attached by the iron-oxide binding peptides present in the proteins forming nanoclusters of size about 100 nm. However, these nanoclusters have irregular shape and lack defined size and tuneable/switchable properties which are highly desirable for biomedical applications (Ankamwar, 2012).

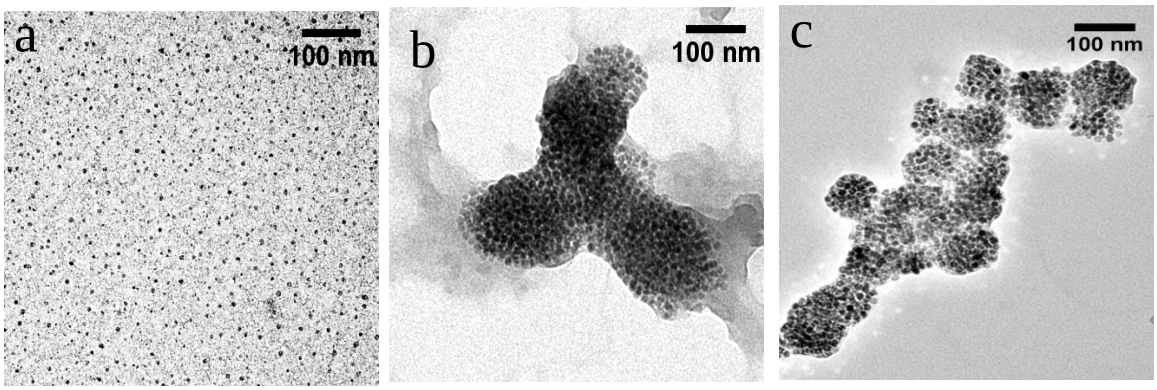

Figure 6.8: *TEM images of IONP under different conditions. a) IONP (10 nm size) in10 mM phosphate buffer pH 8; b) IONP (10 nm) with Mms6 at pH 8; c) IONP (10 nm) with Mms6-BCA. Note the TEM samples were not negatively stained.*

In contrast, IONPC with a regular and defined shape were achieved using Mms6c-BCA-P_{11}4 through two different routes. In the first route, IONP (10 nm) was incubated with Mms6c-BCA-P_{11}4 at 10 mM Phosphate buffer pH 8 to form protein-iron oxide complex (about 130 nm) as shown in Figure 6.9a. Then, they were turned into a larger size when the pH was decreased to 6.8 (Figure 6.9b). The protein-mediated nano-clusters of iron oxide was confirmed with the image from the TEM without negative staining, for which electron signals from iron oxide are dominated.

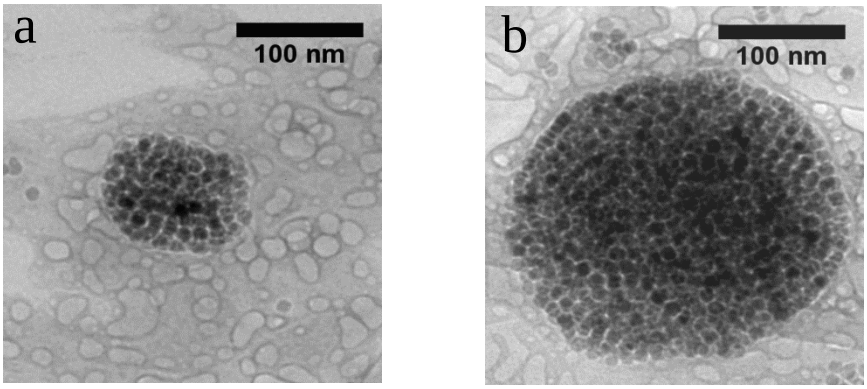

Figure 6.9: *TEM images of IONPC of Mms6c-BCA-P_{11}4 prepared by Route 1. a) IONP (10 nm size) and Mms6c-BCA-P_{11}4 in10 mM phosphate buffer pH 8; b) IONP (10 nm) and Mms6c-BCA-P_{11}4 at pH 6.8. Note the TEM samples were not negatively stained.*

The route 2 of fabricating IONPC was carried out by forming protein nanoparticles first, followed by additions of IONP. The self-assemble peptide (P_{11}4) mediated the formation of protein particles (Figure 6.10a) when pH was adjusted to 6.8. Then the addition of the IONP produced the clusters with a size around 200 nm as shown in Figure 6.10b.

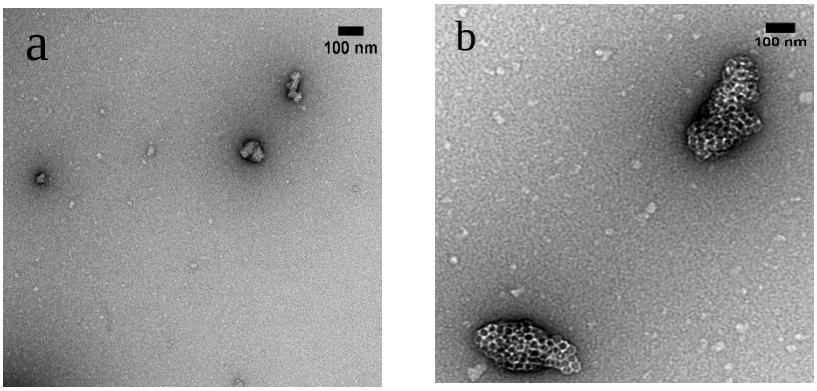

Figure 6.10: *TEM images of IONPC by Mms6c-BCA-P_{11}4 through route 2., a) Mms6c-BCA-P_{11}4 nanoparticles in10 mM phosphate buffer pH 6.8; b) IONP (10 nm) and Mms6c-BCA-P_{11}4 in10 mM phosphate buffer pH 6.8. The TEM samples were negative stained using 2% (v/v) uranyl acetate.*

In this route, it is likely that the clusters have a soft core of protein nanoparticles, with iron oxide nanoparticles surrounding the protein core. However, further research in future is needed to verify whether this is the case.

The nano-cluster formation was further explored by using different sizes of IONP (5, 20 and 30 nm). When Mms6c-BCA-P_{11}4 in 10 mM at phosphate buffer pH 8 was incubated with IONP of different sizes, varying cluster sizes were formed, with cluster structure proportional to the size of their individual IONP as shown in Figure 6.11.

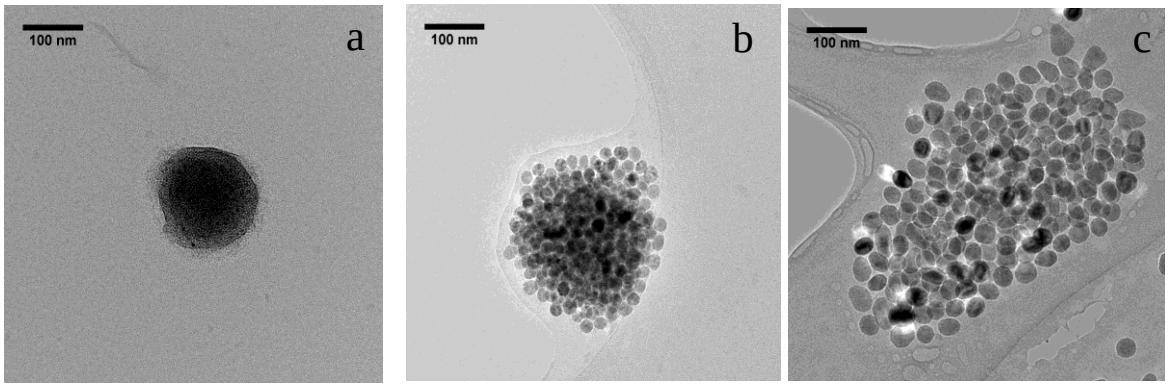

Figure 6.11*: Different size IONP used to produce clusters using protein Mms6c-BCA-P_{11}4. Here, a) IONP (5 nm); b) IONP (20 nm); c), IONP (30 nm) + Mms6c-BCA-P_{11}4 at pH 8 in 10 mM phosphate buffer pH 8; Note the TEM samples were not negatively stained.*

The protein-mediated clusters produced in this study may serve as a platform to produce higher-order structures under mild conditions. With further development, it may be able to address the challenge of controlling space between inorganic nanoparticles with desirable functionalities (Kotov, 2017).

6.3.4 Functionality of Cluster Particles

The enzymatic functionality of protein-mediated IONPC were determined by pNPA assay as shown in Figure 6.12. The IONPC showed slightly lower activity compared to monomeric

Mms6c-BCA-P$_{11}$4. Nevertheless, it confirmed that IONPC has the intended enzymatic functionality. Regardless the route used for preparation, IONPC formed with 10 nm IONP have the similar enzyme activities (Figure 6.12a). Also, the different size of IONP (5, 20 and 30 nm) does not show significant effect on enzymatic activity of IONPC (Figure 6.12b). Thus, the approaches developed here can make nanoclusters without negatively impacting biological elements.

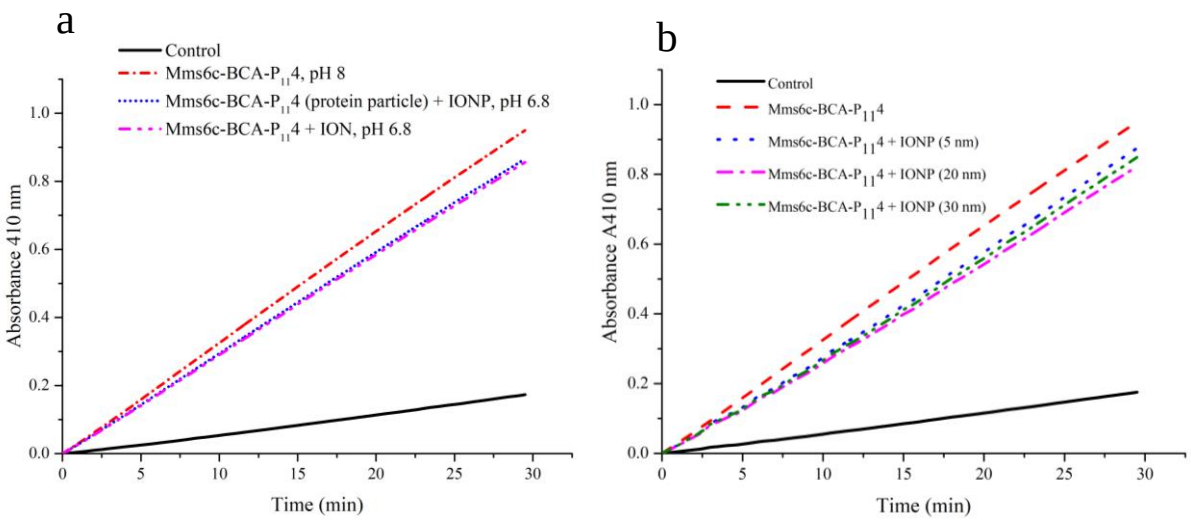

Figure 6.12: *pNPA assay of the protein-IONPC. a) comparison of enzyme activities of iron clusters produced from two different routes by using 10 nm iron oxide and Mms6c-BCA-P$_{11}$4 at pH 6.8, b) comparison of enzymatic activities of iron clusters formed by 5, 20, and 30 nm iron oxide and Mms6c-BCA-P$_{11}$4 at pH 8.*

6.4 Summary

This chapter has developed new strategies to engineer higher-order structure of iron oxide nanoparticles, demonstrating formation of nanoclusters using two different routes. A panel of protein constructs have been designed to combine iron oxide-binding peptides (Mms6 and Mms6c) and the self-assembling peptide P$_{11}$4 with two enzymes, BCA and TmCA. By fusing two peptides to N- and C- termini of enzymes, multifunctional proteins were created to have three distinct functions: enzyme activity, iron oxide binding and self-assembly ability. Comparison of these constructs have identified Mms6c-BCA-P$_{11}$4 as the most promising

candidate to facilitate formation of iron oxide nanoclusters. Importantly, the nature of the clusters can be varied by selectively activating either iron binding or self-assembly peptide of Mms6c-BCA-P_{11}4 using different preparation routes. In route one, BCA bound to IONPs via Mms6 and then self-assembled into larger structures through P_{11}4 after alteration of pH. In route two, self-assembled proteins particles (via pH alteration) were attached to IONPs to create a larger structure. These findings showed that the formation of nano-clusters could be controlled or triggered with the added advantage that the structural details could be determined by the components present in the mixture at different stages in the formation of the nanoclusters. Also, the demonstrated functionality of the nanoclusters suggests it can have potential applications in different sections such as medicine, biotechnology, and energy because the biological components can retain their bioactivities.

6.5 References

Aggeli, A., Bell, M., Carrick, L.M., Fishwick, C.W., Harding, R., Mawer, P.J., Radford, S.E., Strong, A.E., Boden, N. 2003. pH as a trigger of peptide β-sheet self-assembly and reversible switching between nematic and isotropic phases. *Journal of the American Chemical Society*, **125**(32), 9619-9628.

Ankamwar, B. 2012. Size and shape effect on biomedical applications of nanomaterials. in: *Biomedical Engineering-Technical Applications in Medicine*, Intech.

Casula, M.F., Conca, E., Bakaimi, I., Sathya, A., Materia, M.E., Casu, A., Falqui, A., Sogne, E., Pellegrino, T., Kanaras, A.G. 2016. Manganese doped-iron oxide nanoparticle clusters and their potential as agents for magnetic resonance imaging and hyperthermia. *Physical Chemistry Chemical Physics*, **18**(25), 16848-16855.

Edel, J.B., Kornyshev, A.A., Urbakh, M. 2013. Self-assembly of nanoparticle arrays for use as mirrors, sensors, and antennas. *ACS Nano*, **7**(11), 9526-9532.

Evers, C.H., Luiken, J.A., Bolhuis, P.G., Kegel, W.K. 2016. Self-assembly of microcapsules via colloidal bond hybridization and anisotropy. *Nature*, **534**(7607), 364.

Feng, S., Wang, L., Palo, P., Liu, X., Mallapragada, S.K., Nilsen-Hamilton, M. 2013. Integrated self-assembly of the Mms6 magnetosome protein to form an iron-responsive structure. *International journal of molecular sciences*, **14**(7), 14594-14606.

Ge, J., Hu, Y., Biasini, M., Beyermann, W.P., Yin, Y. 2007. Superparamagnetic magnetite colloidal nanocrystal clusters. *Angewandte Chemie International Edition*, **46**(23), 4342-4345.

Han, D., Guo, G., Yan, Y., Li, T., Wang, B., Dong, A. 2018. Pomegranate-like, carbon-coated Fe_3O_4 nanoparticle superparticles for high-performance lithium storage. *Energy Storage Materials*, **10**, 32-39.

Kashyap, S., Woehl, T.J., Liu, X., Mallapragada, S.K., Prozorov, T. 2014. Nucleation of iron oxide nanoparticles mediated by Mms6 protein in situ. *Acs Nano*, **8**(9), 9097-9106.

Kotov, N.A. 2017. The art of empty space. *Science*, **358**(6362), 448-448.

Kralj, S., Makovec, D. 2014. The chemically directed assembly of nanoparticle clusters from superparamagnetic iron-oxide nanoparticles. *RSC Advances*, **4**(25), 13167-13171.

Lee, S.H., Yu, S.-H., Lee, J.E., Jin, A., Lee, D.J., Lee, N., Jo, H., Shin, K., Ahn, T.-Y., Kim, Y.-W. 2013. Self-assembled Fe_3O_4 nanoparticle clusters as high-performance anodes for lithium ion batteries via geometric confinement. *Nano letters*, **13**(9), 4249-4256.

Liao, N., Wu, M., Pan, F., Lin, J., Li, Z., Zhang, D., Wang, Y., Zheng, Y., Peng, J., Liu, X. 2016. Poly (dopamine) coated superparamagnetic iron oxide nanocluster for noninvasive labeling, tracking, and targeted delivery of adipose tissue-derived stem cells. *Scientific Reports*, **6**, 18746.

Ma, K., Zhao, H., Zheng, X., Sun, H., Hu, L., Zhu, L., Shen, Y., Luo, T., Dai, H., Wang, J. 2017. NMR studies of the interactions between AMB-1 Mms6 protein and magnetosome Fe_3O_4 nanoparticles. *Journal of Materials Chemistry B*, **5**(16), 2888-2895.

Qi, H., Liu, C., Long, L., Ren, Y., Zhang, S., Chang, X., Qian, X., Jia, H., Zhao, J., Sun, J. 2016. Blood exosomes endowed with magnetic and targeting properties for cancer therapy. *ACS nano*, **10**(3), 3323-3333.

Qiu, P., Jensen, C., Charity, N., Towner, R., Mao, C. 2010. Oil phase evaporation-induced self-assembly of hydrophobic nanoparticles into spherical clusters with controlled surface chemistry in an oil-in-water dispersion and comparison of behaviors of individual and clustered iron oxide nanoparticles. *Journal of the American Chemical Society*, **132**(50), 17724-17732.

Udayabhaskararao, T., Altantzis, T., Houben, L., Coronado-Puchau, M., Langer, J., Popovitz-Biro, R., Liz-Marzán, L.M., Vuković, L., Král, P., Bals, S. 2017. Tunable porous nanoallotropes prepared by post-assembly etching of binary nanoparticle superlattices. *Science*, **358**(6362), 514-518.

Verpoorte, J.A., Mehta, S., Edsall, J.T. 1967. Esterase activities of human carbonic anhydrases B and C. *Journal of Biological Chemistry*, **242**(18), 4221-4229.

Wang, E.C., Wang, A.Z. 2014. Nanoparticles and their applications in cell and molecular biology. *Integrative Biology*, **6**(1), 9-26.

Wang, L., Prozorov, T., Palo, P.E., Liu, X., Vaknin, D., Prozorov, R., Mallapragada, S., Nilsen-Hamilton, M. 2012. Self-assembly and biphasic iron-binding characteristics of Mms6, a bacterial protein that promotes the formation of superparamagnetic magnetite nanoparticles of uniform size and shape. *Biomacromolecules*, **13**(1), 98-105.

Warden, A.C., Williams, M., Peat, T.S., Seabrook, S.A., Newman, J., Dojchinov, G., Haritos, V.S. 2015. Rational engineering of a mesohalophilic carbonic anhydrase to an extreme halotolerant biocatalyst. *Nature Communications*, **6**, 10278.

Yan, L., Amirshaghaghi, A., Huang, D., Miller, J., Stein, J.M., Busch, T.M., Cheng, Z., Tsourkas, A. 2018. Protoporphyrin IX (PpIX)-coated superparamagnetic iron oxide nanoparticle (SPION) nanoclusters for magnetic resonance imaging and photodynamic therapy. *Advanced Functional Materials*.

Yang, Z., Wei, J., Sobolev, Y.I., Grzybowski, B.A. 2018. Systems of mechanized and reactive droplets powered by multi-responsive surfactants. *Nature*.

Zhang, Q., Wei, W., Wang, P., Zuo, L., Li, F., Xu, J., Xi, X., Gao, X., Ma, G., Xie, H.-y. 2017. Biomimetic magnetosomes as versatile artificial antigen-presenting cells to potentiate T-cell-based anticancer therapy. *ACS nano*, **11**(11), 10724-10732.

Zhang, Y. 2008. I-TASSER server for protein 3D structure prediction. *BMC Bioinformatics*, **9**(1), 40.

This page is intentionally blank

CHAPTER 7

CONCLUSION AND FUTURE WORK

This page is intentionally blank

CHAPTER 7
CONCLUSION AND FUTURE WORK

7.1 Conclusions

Nanomaterials are incredibly versatile structures with a multitude of applications and functions, which are largely determined by their chemical composition and architecture. In broad terms, nanomaterials can be built from molecules of inorganic, organic or biological origin and these molecules impact not only on the properties of materials but also the methods used for production and assembly. The incorporation of biological molecules into nanomaterial presents many advantages including highly specific binding, reaction catalysis, bio-compatibility, and biodegradability. The application of biological molecules as nanomaterials also presents challenges due to their relative instability, requirement of hydration environment, and resistance to the formation of larger higher-order structures. Blending the benefits of biological materials with the utility of other compounds such as inorganic materials presents a remarkable opportunity to develop new nanomaterials with improved properties and functionality broadening applications for this highly useful group of materials.

This research focused on the development of new hybrid nanomaterials that are a combination of inorganic and biological components and methods for their production, which provides low-cost nanomaterials that, are readily customisable for specific applications. Carbonic anhydrase (CA) and green fluorescent protein (GFP) were used as model proteins for the biological component of the nanoparticles. CA catalyses the conversion of carbon dioxide to carbonic acid – an important reaction that may find application in carbon capture to reduce atmospheric greenhouse gases. Due to its fluorescence, GFP is suitable for imaging and has applications in research and disease diagnosis.

Mesoporous silica nanoparticles (MSN) have found wide application in nanomaterials research and after chemical functionalisation; proteins can be covalently linked to the silica providing highly specific biological functions. In this work, Bovine carbonic anhydrase (BCA) was covalently attached to MSN and activity of immobilised BCA was significantly improved by "dilution" of the number binding sites using a competing chemistry. When BCA was "diluted" on the surface of MSN presumably steric hindrance was reduced by avoiding overcrowding of the immobilised enzymes. Dilution also resulted in improved thermal stability of the enzyme and the immobilised enzyme could be re-used further highlighting improved stability and utility. Whilst covalent modification provided a useful and convenient method of immobilisation, the lack of orientation control (covalent attachment can occur anywhere on the protein surface) has a negative impact on protein function and the chemical reactions used can cause inactivation of protein functions. To solve this problem attachment via affinity immobilisation was evaluated as a method to immobilise BCA on the surface of MSN as well as carbonic anhydrase from *Thiomicrospira crunogena* (TmCA) on the surface of iron oxide nanoparticles (IONPs). An affinity binding approach has a further advantage as the binding can be reversed and controlled providing a mechanism to trigger self-assembly of hybrid nanomaterials that contain such biological components. By engineering a silica-binding peptide (cob) into BCA and iron oxide-binding (Mms6) peptide into TmCA protein, affinity binding of proteins to both MSN and IONP were achieved. Affinity immobilisation to either inorganic material did not compromise enzyme activity and the affinity binding was strong, as the BCA-cob was not released when the MSN were suspended in high ionic strength buffers. Furthermore, the affinity-immobilised enzymes could be re-used to the same extent as the covalently immobilised enzyme highlighting the robustness of the affinity binding and its potential in industrial situations where enzyme costs are considerable.

Whilst affinity binding proved suitable for immobilisation, this approach required and inorganic support for the formation of a nanoparticle. An alternative approach is to produce nanoparticles that are comprised exclusively of protein. There are several peptides which can be incorporated into protein sequences and can facilitate self-assembly via a range of different mechanisms. One such peptide is $P_{11}4$, which can self-assemble when magnesium ions are present in solution. Although unproven, it was hypothesized that the self-assembly of $P_{11}4$ is mediated through a complex of four glutamic acid residues with magnesium. To test this hypothesis, a peptide with an amino acid sequence similar (aromatic amino acids; tryptophan and phenylalanine) to $P_{11}4$ (denoted Pep2) but missing one glutamic acid residue was tested for self-assembly in the presence of magnesium and self-assembly did not occur. This provided clear evidence as to the mechanism of $P_{11}4$ self-assembly. It appears that two glutamic acid residues align in anti-parallel fashion forming Mg^{2+}coordinate complex resulting in self-assembly. Interestingly, Pep2 self-assembly was triggered when the pH was reduced to pH 6. These two peptides ($P_{11}4$ and Pep2) provided two different methods that can be used to trigger self-assembly – addition of magnesium and pH change. A third peptide (Pep4) was also tested. This peptide was rich in aromatic amino acid residues and was shown to self-assemble at low ionic strength through π-π interaction. When fused to either BCA or GFP, self-assembling nanoparticles were produced that retained the protein's functionality, that is conversion of CO_2 to carbonic acid (BCA) or fluorescence (GFP). The GFP nanoparticles could be further customised with regard to fluorescence intensity by dilution with BCA-$P_{11}4$ demonstrating the flexibility of protein-based molecules as a platform for biologically active nanoparticles. These findings demonstrated that through thoughtful design of self-assembling peptides a range of potential triggers could be engineered into protein sequences providing on-demand assembly of nanoparticles with biological functions.

Peptides that bind to inorganic materials or self-assemble with changes to physical or chemical conditions are useful tools in the formation of biologically based nanomaterials. This coupled with the ready manipulation of proteins sequences provides a pathway to create functional proteins with multiple peptide sequences that can be used to engineer unique and controlled molecular architectures. A combination of an iron-binding peptide (Mms6) and the self-assembling peptide $P_{11}4$ is an example of such an approach because both peptides had been shown to facilitate the formation of nanoparticles. By fusing each of the two peptides to the termini of BCA, a multifunctional protein was created which not only retained its enzyme activity but could also be used to create different types of nano-clusters. The nature of the clusters was varied depending on which peptide property was activated and the sequence of activation routes developed. In route one, BCA bound to IONPs via Mms6 and then self-assembled into larger structures through $P_{11}4$ after alteration of pH. In route two, self-assembled proteins particles (via pH alteration) were attached to IONPs to create a larger superstructure. These findings showed that the formation the nano-superstructures could be controlled or triggered with the added advantage that the structural details could be determined by the components present in the mixture at different stages in the formation of the nanoclusters. The engineered larger structures provide the platform technology in developing protein-based functional nanomaterials to use in medicine, biotechnology, and energy.

The research described herewith demonstrates the merits of combining the versatility of biological molecules with the robustness and physical properties of inorganic materials to create a suite of interesting and useful nanomaterials with broad applicability in a diverse array of medical and industrial situations. Retained function, improved stability, and greater flexibility offered by hybrid nanomaterials are expected to broaden their application and provide a pathway for greater exploitation in research and commercial activities.

7.2 Future work

The work reported in this PhD research have established complementary strategies to engineer protein-based functional nanomaterials and opened an avenue to explore them as advanced nanomaterials with attractive functions. Built on these achievements, the following research are recommended for future work in order to understand the assembly mechanism of nanoclusters and explore advanced applications of protein-based hybrid nanomaterials.

1. *Structure of iron oxide clusters and assembly mechanism*

While the work in chapter 6 has clearly demonstrated the formation of nano-clusters by TEM imaging, it is not yet clear what internal structure such clusters may have. Such information is critical for future design of advanced nanoclusters and exploring their applications. Also, it's important to understand the mechanism of assembly of nanoparticles into highly ordered clusters. It would be highly valuable to compare internal structure of nano-clusters that are formed at different assembly conditions, particularly for those prepared by two different routes described in chapter 6. Advanced Focused Ion Beam Scanning Electron Microscopes (FIB/SEM imaging) and cryo-TEM may be useful to provide such valuable structure information.

2. *Applications of protein-mediated iron oxide nano-clusters*

Iron oxide clusters preparing by conventional methods has already been used for interesting applications such as high-performance anodes. The protein-aided iron oxide nano-clusters developed in this thesis may offer unique structure properties such as controllable distances between individual iron oxide nanoparticles. Future work should be carried out to explore whether such physical properties can be turned into attractive functions and applications, such as surface catalysis and tandem reactions. For example, one can use iron oxide nanoparticles

as chemical catalyst while using enzyme as biocatalysts and integrate both components into nano-clusters to better catalyse sequential reactions.

3. Cell imaging and tracking using fluorescence protein nanoparticles

The florescent protein nanoparticles demonstrated in Chapter 5 have potential applications in biomedical and health sector. Particularly, the size of such fluorescent nanoparticles can be tuned for imaging and tracking. Also, the fluorescent intensity can be varied by dilution with a second molecules such as BCA-P_{11}4. The mixture system of nanoparticles containing two or more proteins may be used to offer multifunctionalities, for example, targeting delivery with antibody and tracking by fluorescence. Future application will also benefit from fundamental knowledge of nanoparticle structure using advanced fluorescence imaging tools such as Stochastic Optical Reconstruction Microscopy (STORM).

APPENDIX

This page is intentionally blank

MASCOT Search Results

Protein View: BCA_cob|BCA_cob

gi|BCA_cob|BCA_cob

Database:	inhouse
Score:	1386
Nominal mass (M,):	31394
Calculated pI:	8.64

Sequence similarity is available as **an NCBI BLAST search of BCA_cob|BCA_cob against nr**.

Search parameters

MS data file:	C:\Users\mascot\Desktop\david mgf's\2016_057\BCA_cob_1-B,8_01_12103.mgf
Enzyme:	Trypsin: cuts C-term side of KR unless next residue is P
Fixed modifications:	**Carbamidomethyl (C)**

Protein sequence coverage: 74%

Matched peptides shown in ***bold red***.

```
  1 GMSHHWGYGK HNGPEHWHKD FPIANGERQS PVDIDTKAVV QDPALKPLAL
 51 VYGEATSRRM VNNGHSFNVE YDDSQDKAVL KDGPLTGTYR LVQFHFHWGS
101 SDDQGSEHTV DRKKYAAELH LVHWNTKYGD FGTAAQQPDG LAVVGVFLKV
151 GDANPALQKV LDALDSIKTK GKSTDFPNFD PGSLLPNVLD YWTYPGSLTT
201 PPLLESVTWI VLKEPISVSS QQMLKFRTLN FNAEGEPELL MLANWRPAQP
251 LKNRQVRGFP KGGGGSGGGG SGSGRARAQR QSSRGR
```

Unformatted sequence string: **286 residues** (for pasting into other applications).

Sort peptides by (•) Residue Number ( ) Increasing Mass ( ) Decreasing Mass

Show predicted peptides also

Query	Start – End	Observed	Mr(expt)	Mr(calc)	ppm	M	Score	Expect	Rank	U	Peptide
230	1 – 10	387.1692	1158.4856	1158.5029	-14.9	0	13	0.8	1	U	-.GMSHHWGYGK.H
206	11 – 19	381.1738	1140.4996	1140.5213	-19.0	0	10	2.5	1	U	K.HNGPEHWHK.D
207	11 – 19	571.2580	1140.5014	1140.5213	-17.4	0	29	0.037	1	U	K.HNGPEHWHK.D
208	11 – 19	571.2580	1140.5015	1140.5213	-17.4	0	28	0.038	1	U	K.HNGPEHWHK.D
209	11 – 19	381.1746	1140.5018	1140.5213	-17.1	0	7	5.7	1	U	K.HNGPEHWHK.D
211	11 – 19	571.7519	1141.4893	1140.5213	849	0	6	4.5	1	U	K.HNGPEHWHK.D
159	20 – 28	509.7430	1017.4715	1017.4879	-16.1	0	48	0.00078	1	U	K.DFPIANGER.Q
160	20 – 28	510.2359	1018.4571	1017.4879	953	0	11	3.4	2	U	K.DFPIANGER.Q
139	29 – 37	501.7485	1001.4824	1001.5029	-20.5	0	49	0.00072	1	U	R.QSPVDIDTK.A
142	29 – 37	501.7568	1001.4990	1001.5029	-3.91	0	54	0.00029	1	U	R.QSPVDIDTK.A
572	38 – 58	733.4026	2197.1861	2197.2106	-11.2	0	64	1.2e-005	1	U	K.AVVQDPALKPLALVYGEATSR.R
573	38 – 58	733.4061	2197.1965	2197.2106	-6.42	0	79	3.4e-007	1	U	K.AVVQDPALKPLALVYGEATSR.R
575	38 – 58	733.7499	2198.2280	2197.2106	463	0	92	1e-008	1	U	K.AVVQDPALKPLALVYGEATSR.R
576	38 – 58	733.7507	2198.2303	2197.2106	464	0	81	1.4e-007	1	U	K.AVVQDPALKPLALVYGEATSR.R
535	60 – 77	700.2931	2097.8574	2097.8698	-5.90	0	104	2.5e-010	1	U	R.MVNNGHSFNVEYDDSQDK.A
536	60 – 77	1049.9360	2097.8574	2097.8698	-5.90	0	70	6.6e-007	1	U	R.MVNNGHSFNVEYDDSQDK.A
537	60 – 77	700.6161	2098.8264	2097.8698	456	0	77	7.9e-008	1	U	R.MVNNGHSFNVEYDDSQDK.A
539	60 – 77	700.6267	2098.8582	2097.8698	471	0	79	9.1e-008	1	U	R.MVNNGHSFNVEYDDSQDK.A
540	60 – 77	1050.4377	2098.8609	2097.8698	472	0	68	1.2e-006	1	U	R.MVNNGHSFNVEYDDSQDK.A
123	82 – 90	979.4719	978.4646	978.4771	-12.7	0	19	0.82	1	U	K.DGPLTGTYR.L
124	82 – 90	490.2433	978.4721	978.4771	-5.11	0	56	0.00016	1	U	K.DGPLTGTYR.L
651	91 – 112	862.0558	2583.1456	2583.1528	-2.78	0	117	3.2e-011	1	U	R.LVQFHFHWGSSDDQGSEHTVDR.K
652	91 – 112	517.6368	2583.1474	2583.1528	-2.09	0	23	0.087	1	U	R.LVQFHFHWGSSDDQGSEHTVDR.K
653	91 – 112	646.7941	2583.1474	2583.1528	-2.08	0	69	2e-006	1	U	R.LVQFHFHWGSSDDQGSEHTVDR.K
411	115 – 127	527.9351	1580.7834	1580.8099	-16.8	0	36	0.015	1	U	K.YAAELHLVHWNTK.Y
412	115 – 127	527.9436	1580.8090	1580.8099	-0.61	0	54	0.00023	1	U	K.YAAELHLVHWNTK.Y
602	128 – 149	1127.0819	2252.1491	2252.1478	0.61	0	124	1.7e-011	1	U	K.YGDFGTAAQQPDGLAVVGVFLK.V
603	128 – 149	751.7237	2252.1492	2252.1478	0.62	0	85	1.3e-007	1	U	K.YGDFGTAAQQPDGLAVVGVFLK.V
144	150 – 159	506.7621	1011.5097	1011.5349	-24.9	0	46	0.0016	1	U	K.VGDANPALQK.V
149	150 – 159	506.7700	1011.5254	1011.5349	-9.38	0	58	0.00011	1	U	K.VGDANPALQK.V
151	150 – 159	506.7785	1011.5425	1011.5349	7.50	0	58	9.6e-005	1	U	K.VGDANPALQK.V
112	160 – 168	487.2715	972.5284	972.5491	-21.3	0	3	48	1	U	K.VLDALDSIK.T
113	160 – 168	487.2717	972.5288	972.5491	-20.9	0	47	0.0018	1	U	K.VLDALDSIK.T
118	160 – 168	973.5453	972.5381	972.5491	-11.4	0	58	0.00017	1	U	K.VLDALDSIK.T
120	160 – 168	487.2810	972.5474	972.5491	-1.83	0	50	0.001	1	U	K.VLDALDSIK.T
121	160 – 168	487.2834	972.5523	972.5491	3.25	0	50	0.001	1	U	K.VLDALDSIK.T
701	173 – 213	1149.0788	4592.2861	4592.3407	-11.9	0	24	0.036	1	U	K.STDFPNFDPGSLLPNVLDYWTYPGSLTTPPLLESVTWIVLK.E
327	214 – 225	673.8573	1345.7000	1345.6911	6.57	0	61	6.2e-005	1	U	K.EPISVSSQQMLK.F
330	214 – 225	674.3527	1346.6909	1345.6911	743	0	49	0.0011	1	U	K.EPISVSSQQMLK.F

MASCOT Search Results

Protein View: GFP-P114

gi|GFP-P114|GFP-P114

Database: inhouse
Score: 23386
Nominal mass (M,): 30340
Calculated pI: 5.81

Sequence similarity is available as **an NCBI BLAST search of GFP-P114 against nr**.

Search parameters

MS data file: C:\Users\mascot\Desktop\david mgf's\2017_127\P220170711_DSteer_2017127_GFPP114.mgf
Enzyme: semiTrypsin: cuts C-term side of KR unless next residue is P
Cleavage is semi-specific. (Peptide can be non-specific at one terminus only)
Fixed modifications: **Carbamidomethyl (C)**

Protein sequence coverage: 94%

Matched peptides shown in ***bold red***.

```
  1 HHHHHHTDPM VSKGEELFTG VVPILVELDG DVNGHKFSVS GEGEGDATYG
 51 KLTLKFICTT GKLPVPWPTL VTTLAYGVLC FSRYPDHMKQ HDFFKSAMPE
101 GYVQERTIFF KDDGNYKTRA EVKFEGDTLV NRIELKGIDF KEDGNILGHK
151 LEYNYNSHNV YIMADKQKNG IKSNFKIRHN IEDGSVQLAD HYQQNTPIGD
201 GPVLLPDNHY LSTQSKLSKD PNEKRDHMVL LEFVTAAGIT LGMDELYKGG
251 GGSGGGGSQQ RFEWEFEQQ
```

Unformatted sequence string: **269 residues** (for pasting into other applications).

Sort peptides by ◉ Residue Number ○ Increasing Mass ○ Decreasing Mass

Query	Start – End	Observed	Mr(expt)	Mr(calc)	ppm	M	Score	Expect	Rank	U	Peptide
2288	5 – 13	526.2540	1050.4934	1050.4917	1.67	0	51	0.017	1	U	H.HHTDPMVSK.G
783	6 – 13	457.7245	913.4345	913.4328	1.88	0	26	4	1	U	H.HTDPMVSK.G
9994	9 – 36	745.8958	2979.5541	2978.5423	340	1	34	0.25	1	U	D.PMVSKGEELFTGVVPILVELDGDVNGHK.F
9697	11 – 36	917.8182	2750.4328	2750.4491	-5.93	1	13	40	1	U	M.VSKGEELFTGVVPILVELDGDVNGHK.F
9698	11 – 36	688.6230	2750.4627	2750.4491	4.95	1	40	0.069	1	U	M.VSKGEELFTGVVPILVELDGDVNGHK.F
9704	11 – 36	918.4990	2752.4752	2750.4491	737	1	56	0.0017	1	U	M.VSKGEELFTGVVPILVELDGDVNGHK.F
9524	12 – 36	884.8015	2651.3827	2651.3807	0.76	1	9	1e+002	1		V.SKGEELFTGVVPILVELDGDVNGHK.F
9525	12 – 36	663.8530	2651.3831	2651.3807	0.92	1	26	2	1		V.SKGEELFTGVVPILVELDGDVNGHK.F
9526	12 – 36	884.8030	2651.3872	2651.3807	2.48	1	42	0.053	1		V.SKGEELFTGVVPILVELDGDVNGHK.F
9528	12 – 36	885.1165	2652.3277	2651.3807	357	1	17	16	1		V.SKGEELFTGVVPILVELDGDVNGHK.F
9530	12 – 36	885.1196	2652.3370	2651.3807	361	1	53	0.0047	1		V.SKGEELFTGVVPILVELDGDVNGHK.F
9531	12 – 36	664.1032	2652.3837	2651.3807	378	1	43	0.04	1		V.SKGEELFTGVVPILVELDGDVNGHK.F
9532	12 – 36	885.4620	2653.3642	2651.3807	748	1	63	0.00046	1		V.SKGEELFTGVVPILVELDGDVNGHK.F
9533	12 – 36	885.4713	2653.3921	2651.3807	759	1	54	0.0034	1		V.SKGEELFTGVVPILVELDGDVNGHK.F
9018	13 – 36	642.0903	2564.3321	2564.3486	-6.45	1	12	58	1		S.KGEELFTGVVPILVELDGDVNGHK.F
9079	13 – 36	856.1244	2565.3514	2564.3486	391	1	60	0.00082	1		S.KGEELFTGVVPILVELDGDVNGHK.F
9080	13 – 36	642.3462	2565.3557	2564.3486	393	1	47	0.017	1		S.KGEELFTGVVPILVELDGDVNGHK.F
9081	13 – 36	642.3472	2565.3597	2564.3486	394	1	20	8.5	1		S.KGEELFTGVVPILVELDGDVNGHK.F
7975	14 – 35	770.3961	2308.1665	2308.1587	3.36	0	68	0.00018	1		K.GEELFTGVVPILVELDGDVNGH.K
7976	14 – 35	770.3965	2308.1677	2308.1587	3.90	0	91	7.7e-007	1		K.GEELFTGVVPILVELDGDVNGH.K
7977	14 – 35	1155.0923	2308.1700	2308.1587	4.87	0	85	3.2e-006	1		K.GEELFTGVVPILVELDGDVNGH.K
7978	14 – 35	1155.0959	2308.1772	2308.1587	8.00	0	24	3.8	1		K.GEELFTGVVPILVELDGDVNGH.K
8394	14 – 36	813.0814	2436.2225	2436.2537	-12.8	0	50	0.011	1		K.GEELFTGVVPILVELDGDVNGHK.F
8395	14 – 36	813.0830	2436.2272	2436.2537	-10.9	0	37	0.19	1		K.GEELFTGVVPILVELDGDVNGHK.F
8396	14 – 36	1219.1225	2436.2305	2436.2537	-9.53	0	16	27	1		K.GEELFTGVVPILVELDGDVNGHK.F
8397	14 – 36	813.0842	2436.2307	2436.2537	-9.45	0	59	0.0011	1		K.GEELFTGVVPILVELDGDVNGHK.F
8399	14 – 36	813.0895	2436.2467	2436.2537	-2.88	0	25	2.9	1		K.GEELFTGVVPILVELDGDVNGHK.F
8400	14 – 36	813.0896	2436.2470	2436.2537	-2.75	0	20	9.2	1		K.GEELFTGVVPILVELDGDVNGHK.F
8401	14 – 36	813.0896	2436.2471	2436.2537	-2.71	0	62	0.00064	1		K.GEELFTGVVPILVELDGDVNGHK.F
8402	14 – 36	1219.1311	2436.2476	2436.2537	-2.49	0	72	5.8e-005	1		K.GEELFTGVVPILVELDGDVNGHK.F
8403	14 – 36	610.0696	2436.2492	2436.2537	-1.84	0	56	0.0025	1		K.GEELFTGVVPILVELDGDVNGHK.F
8404	14 – 36	813.0905	2436.2496	2436.2537	-1.69	0	70	0.0001	1		K.GEELFTGVVPILVELDGDVNGHK.F
8405	14 – 36	488.2572	2436.2496	2436.2537	-1.67	0	48	0.014	1		K.GEELFTGVVPILVELDGDVNGHK.F
8406	14 – 36	1219.1324	2436.2502	2436.2537	-1.41	0	81	6.9e-006	1		K.GEELFTGVVPILVELDGDVNGHK.F
8407	14 – 36	813.0917	2436.2533	2436.2537	-0.17	0	51	0.0077	1		K.GEELFTGVVPILVELDGDVNGHK.F
8408	14 – 36	1219.1340	2436.2534	2436.2537	-0.094	0	76	2.6e-005	1		K.GEELFTGVVPILVELDGDVNGHK.F
8409	14 – 36	1219.1341	2436.2536	2436.2537	-0.029	0	80	9.9e-006	1		K.GEELFTGVVPILVELDGDVNGHK.F
8410	14 – 36	813.0923	2436.2551	2436.2537	0.57	0	18	14	1		K.GEELFTGVVPILVELDGDVNGHK.F
8411	14 – 36	610.0712	2436.2557	2436.2537	0.82	0	20	9	1		K.GEELFTGVVPILVELDGDVNGHK.F
8412	14 – 36	610.0713	2436.2561	2436.2537	0.98	0	1	8.3e+002	1		K.GEELFTGVVPILVELDGDVNGHK.F
8413	14 – 36	813.0928	2436.2567	2436.2537	1.24	0	52	0.0055	1		K.GEELFTGVVPILVELDGDVNGHK.F
8414	14 – 36	813.0929	2436.2568	2436.2537	1.29	0	70	9.3e-005	1		K.GEELFTGVVPILVELDGDVNGHK.F
8415	14 – 36	1219.1358	2436.2570	2436.2537	1.38	0	69	0.00012	1		K.GEELFTGVVPILVELDGDVNGHK.F
8416	14 – 36	610.0716	2436.2573	2436.2537	1.49	0	43	0.046	1		K.GEELFTGVVPILVELDGDVNGHK.F
8417	14 – 36	813.0931	2436.2573	2436.2537	1.50	0	66	0.00024	1		K.GEELFTGVVPILVELDGDVNGHK.F
8418	14 – 36	1219.1361	2436.2577	2436.2537	1.67	0	98	1.6e-007	1		K.GEELFTGVVPILVELDGDVNGHK.F
8419	14 – 36	1219.1362	2436.2578	2436.2537	1.69	0	77	2.1e-005	1		K.GEELFTGVVPILVELDGDVNGHK.F
8420	14 – 36	1219.1363	2436.2581	2436.2537	1.82	0	51	0.0081	1		K.GEELFTGVVPILVELDGDVNGHK.F
8421	14 – 36	813.0934	2436.2585	2436.2537	1.97	0	109	1.1e-008	1		K.GEELFTGVVPILVELDGDVNGHK.F

MASCOT Search Results

Protein View: Mms6

gi|Mms6|Mms6 (up and low)

Database:	inhouse
Score:	1580
Nominal mass (M_r):	7010
Calculated pI:	6.00

Sequence similarity is available as **an NCBI BLAST search of Mms6 against nr**.

Search parameters

MS data file:	C:\Users\mascot\Desktop\david mgf's\2017_127\P220170711_DSteer_2017127_MMS6100.mgf
Enzyme:	semiTrypsin: cuts C-term side of KR unless next residue is P. Cleavage is semi-specific. (Peptide can be non-specific at one terminus only.)
Fixed modifications:	**Carbamidomethyl (C)**

Protein sequence coverage: 100%

Matched peptides shown in ***bold red***.

```
  1 MVGGTIWTGK GLGLGLGLGL GAWGPIILGV VGAGAVYAYM KSRDIESAQS
 51 DEEVELRDAL AHHHHHH
```

Unformatted sequence string: **67 residues** (for pasting into other applications).

Sort peptides by ◉ Residue Number ○ Increasing Mass ○ Decreasing Mass

Query	Start – End	Observed	Mr(expt)	Mr(calc)	ppm	M	Score	Expect	Rank	U	Peptide
1318	1 – 10	525.2768	1048.5390	1048.5376	1.37	0	43	0.11	1		-.MVGGTIWTGK.G
433	2 – 10	459.7554	917.4962	917.4971	-1.00	0	57	0.0055	1		M.VGGTIWTGK.G
81	3 – 10	410.2217	818.4289	818.4287	0.31	0	40	0.26	1		V.GGTIWTGK.G
6256	11 – 39	895.5101	2683.5086	2683.5102	-0.58	0	38	0.1	1		K.GLGLGLGLGLGAWGPIILGVVGAGAVYAY.M
893	33 – 41	487.2446	972.4747	972.4739	0.88	0	10	2.2e+002	2		G.AGAVYAYMK.S
190	35 – 41	423.2160	844.4174	844.4153	2.51	0	25	7.3	1		G.AVYAYMK.S
4575	42 – 57	931.9395	1861.8644	1861.8653	-0.47	1	49	0.017	1		K.SRDIESAQSDEEVELR.D
4576	42 – 57	621.6289	1861.8650	1861.8653	-0.20	1	55	0.0047	1		K.SRDIESAQSDEEVELR.D
4577	42 – 57	621.6299	1861.8679	1861.8653	1.37	1	46	0.038	1		K.SRDIESAQSDEEVELR.D
4580	42 – 57	621.9578	1862.8516	1861.8653	530	1	44	0.057	1		K.SRDIESAQSDEEVELR.D
3248	44 – 56	732.3253	1462.6360	1462.6311	3.38	0	3	6.4e+002	7		R.DIESAQSDEEVEL.R
3761	44 – 57	810.3568	1618.6991	1618.7322	-20.4	0	52	0.0074	1		R.DIESAQSDEEVELR.D
3762	44 – 57	810.3709	1618.7272	1618.7322	-3.07	0	97	2.8e-007	1		R.DIESAQSDEEVELR.D
3763	44 – 57	810.3718	1618.7290	1618.7322	-1.97	0	32	0.95	1		R.DIESAQSDEEVELR.D
3764	44 – 57	540.5838	1618.7296	1618.7322	-1.63	0	76	3.7e-005	1		R.DIESAQSDEEVELR.D
3765	44 – 57	405.6898	1618.7300	1618.7322	-1.38	0	42	0.09	1		R.DIESAQSDEEVELR.D
3767	44 – 57	810.3727	1618.7308	1618.7322	-0.89	0	30	1.4	1		R.DIESAQSDEEVELR.D
3768	44 – 57	810.3728	1618.7311	1618.7322	-0.66	0	40	0.13	1		R.DIESAQSDEEVELR.D
3770	44 – 57	810.3734	1618.7322	1618.7322	0.015	0	25	4.5	1		R.DIESAQSDEEVELR.D
3771	44 – 57	810.3737	1618.7329	1618.7322	0.45	0	42	0.1	1		R.DIESAQSDEEVELR.D
3772	44 – 57	810.3738	1618.7331	1618.7322	0.55	0	110	1.6e-008	1		R.DIESAQSDEEVELR.D
3773	44 – 57	810.3740	1618.7335	1618.7322	0.84	0	53	0.0071	1		R.DIESAQSDEEVELR.D
3774	44 – 57	810.3742	1618.7338	1618.7322	0.97	0	56	0.0035	1		R.DIESAQSDEEVELR.D
3775	44 – 57	810.3742	1618.7339	1618.7322	1.07	0	56	0.0041	1		R.DIESAQSDEEVELR.D
3776	44 – 57	540.5853	1618.7340	1618.7322	1.10	0	55	0.0048	1		R.DIESAQSDEEVELR.D
3777	44 – 57	810.3744	1618.7343	1618.7322	1.31	0	103	7.1e-008	1		R.DIESAQSDEEVELR.D
3778	44 – 57	540.5854	1618.7344	1618.7322	1.35	0	39	0.19	1		R.DIESAQSDEEVELR.D
3779	44 – 57	540.5854	1618.7344	1618.7322	1.36	0	60	0.0016	1		R.DIESAQSDEEVELR.D
3780	44 – 57	810.3746	1618.7347	1618.7322	1.56	0	49	0.017	1		R.DIESAQSDEEVELR.D
3781	44 – 57	810.3747	1618.7348	1618.7322	1.58	0	41	0.13	1		R.DIESAQSDEEVELR.D
3782	44 – 57	810.3747	1618.7348	1618.7322	1.59	0	103	7.9e-008	1		R.DIESAQSDEEVELR.D
3783	44 – 57	540.5856	1618.7349	1618.7322	1.70	0	58	0.0022	1		R.DIESAQSDEEVELR.D
3784	44 – 57	810.3748	1618.7350	1618.7322	1.76	0	106	3.6e-008	1		R.DIESAQSDEEVELR.D
3785	44 – 57	810.3748	1618.7350	1618.7322	1.76	0	2	1e+003	1		R.DIESAQSDEEVELR.D
3786	44 – 57	810.3750	1618.7354	1618.7322	2.01	0	100	1.6e-007	1		R.DIESAQSDEEVELR.D
3787	44 – 57	810.3751	1618.7357	1618.7322	2.18	0	27	3.1	1		R.DIESAQSDEEVELR.D
3789	44 – 57	810.3753	1618.7361	1618.7322	2.40	0	98	2.4e-007	1		R.DIESAQSDEEVELR.D
3790	44 – 57	810.3753	1618.7361	1618.7322	2.43	0	102	8.4e-008	1		R.DIESAQSDEEVELR.D
3791	44 – 57	810.3754	1618.7362	1618.7322	2.46	0	90	1.5e-006	1		R.DIESAQSDEEVELR.D
3792	44 – 57	810.3757	1618.7368	1618.7322	2.82	0	64	0.00061	1		R.DIESAQSDEEVELR.D
3793	44 – 57	810.3757	1618.7368	1618.7322	2.86	0	103	8e-008	1		R.DIESAQSDEEVELR.D
3794	44 – 57	810.3757	1618.7368	1618.7322	2.88	0	53	0.0083	1		R.DIESAQSDEEVELR.D
3795	44 – 57	540.5866	1618.7380	1618.7322	3.60	0	43	0.076	1		R.DIESAQSDEEVELR.D
3796	44 – 57	810.3765	1618.7384	1618.7322	3.86	0	13	77	1		R.DIESAQSDEEVELR.D
3797	44 – 57	810.3766	1618.7386	1618.7322	3.98	0	87	2.8e-006	1		R.DIESAQSDEEVELR.D
3798	44 – 57	810.3768	1618.7390	1618.7322	4.19	0	84	6.4e-006	1		R.DIESAQSDEEVELR.D

MASCOT Search Results

Protein View: Mms6-TmCA_rec|Mms6-TmCA

gi|Mms6-TmCA_rec|Mms6-TmCA recombinant

Database:	inhouse
Score:	26976
Nominal mass (M_r):	42571
Calculated pI:	7.81

Sequence similarity is available as an NCBI BLAST search of Mms6-TmCA_rec|Mms6-TmCA against nr.

Search parameters

MS data file:	C:\Users\mascot\Desktop\david mgf's\2017_057\C20170407_DSteer_2017057_PIMS6.mgf
Enzyme:	semiTrypsin: cuts C-term side of KR unless next residue is P. Cleavage is semi-specific. (Peptide can be non-specific at one terminus only.)
Fixed modifications:	**Carbamidomethyl (C)**
Variable modifications:	**Oxidation (M)**

Protein sequence coverage: 90%

Matched peptides shown in ***bold red***.

```
  1 MGSSHHHHHH SSGLVPRGSH MVGGTIWTGK GLGLGLGLGL GAWGPIILGV
 51 VGAGAVVAYM KSRDIESAQS DEEVELRDAL AGGGGSGGGG SANNVAAPLI
101 DLGAEAKKQA QKSAATQSAV PEKESATKVA EKQKEPEEKA KPEPKKPPHW
151 GYPGEEGPQY WGELAPEFST CKTGKNQSPI NLKPQTAVGT TSLPGFDVYY
201 RETALKLINN GHTLQVNIPL GSYIKINGHR YELLQYHFHT PSEHQRDGFN
251 YPMEMHLVHK DGDGNLAVIA ILFQEGEENE TLAKLMSFLP QTLKKQEIHE
301 SVKIHPAKFF PADKKFYKYS GSLTTPPCSE GVYWMVFKQP IQASVTQLEK
351 MHEYLGSNAR PVQRQNARTL LKSWPDRNRA NTVYEFY
```

Unformatted sequence string: **387 residues** (for pasting into other applications).

Sort peptides by ◉ Residue Number ○ Increasing Mass ○ Decreasing Mass

Query	Start – End	Observed	Mr(expt)	Mr(calc)	ppm	M	Score	Expect	Rank	U	Peptide
3202	7 – 17	632.3252	1262.6359	1262.6381	-1.76	0	19	9.4	1		H.HHHSSGLVPR.G
1931	8 – 17	563.7950	1125.5754	1125.5792	-3.35	0	24	2.6	1		H.HHSSGLVPR.G
1057	9 – 17	495.2671	988.5196	988.5203	-0.72	0	26	1.9	1		H.HSSGLVPR.G
1058	9 – 17	495.2672	988.5199	988.5203	-0.36	0	7	1.5e+002	1		H.HSSGLVPR.G
420	10 – 17	426.7371	851.4596	851.4613	-2.07	0	40	0.047	1		H.SSGLVPR.G
421	10 – 17	426.7376	851.4606	851.4613	-0.84	0	30	0.53	1		H.SSGLVPR.G
3679	18 – 30	665.8292	1329.6438	1329.6500	-4.64	0	39	0.079	1	U	R.GSHMVGGTIWTGK.G
3680	18 – 30	665.8333	1329.6520	1329.6500	1.49	0	64	0.00029	1	U	R.GSHMVGGTIWTGK.G
3681	18 – 30	444.2247	1329.6521	1329.6500	1.63	0	40	0.071	1	U	R.GSHMVGGTIWTGK.G
3682	18 – 30	665.8337	1329.6529	1329.6500	2.20	0	66	0.00018	1	U	R.GSHMVGGTIWTGK.G
3683	18 – 30	665.8338	1329.6531	1329.6500	2.32	0	67	0.00014	1	U	R.GSHMVGGTIWTGK.G
3684	18 – 30	444.2250	1329.6531	1329.6500	2.37	0	42	0.039	1	U	R.GSHMVGGTIWTGK.G
3685	18 – 30	665.8341	1329.6536	1329.6500	2.75	0	38	0.11	1	U	R.GSHMVGGTIWTGK.G
3686	18 – 30	444.2252	1329.6538	1329.6500	2.91	0	42	0.037	1	U	R.GSHMVGGTIWTGK.G
3687	18 – 30	444.2253	1329.6542	1329.6500	3.15	0	41	0.048	1	U	R.GSHMVGGTIWTGK.G
3688	18 – 30	444.2254	1329.6543	1329.6500	3.24	0	35	0.22	1	U	R.GSHMVGGTIWTGK.G
3689	18 – 30	665.8345	1329.6545	1329.6500	3.37	0	60	0.00062	1	U	R.GSHMVGGTIWTGK.G
3690	18 – 30	665.8347	1329.6548	1329.6500	3.60	0	64	0.00029	1	U	R.GSHMVGGTIWTGK.G
3691	18 – 30	444.2256	1329.6549	1329.6500	3.67	0	34	0.24	1	U	R.GSHMVGGTIWTGK.G
3692	18 – 30	665.8348	1329.6551	1329.6500	3.89	0	59	0.00082	1	U	R.GSHMVGGTIWTGK.G
3693	18 – 30	665.8350	1329.6555	1329.6500	4.17	0	35	0.21	1	U	R.GSHMVGGTIWTGK.G
3694	18 – 30	665.8352	1329.6558	1329.6500	4.39	0	42	0.039	1	U	R.GSHMVGGTIWTGK.G
3695	18 – 30	444.2259	1329.6559	1329.6500	4.47	0	38	0.096	1	U	R.GSHMVGGTIWTGK.G
3696	18 – 30	665.8353	1329.6560	1329.6500	4.49	0	29	0.76	1	U	R.GSHMVGGTIWTGK.G
3698	18 – 30	444.2261	1329.6564	1329.6500	4.80	0	23	3.5	1	U	R.GSHMVGGTIWTGK.G
3699	18 – 30	665.8356	1329.6567	1329.6500	5.06	0	29	0.92	1	U	R.GSHMVGGTIWTGK.G
3700	18 – 30	665.8358	1329.6570	1329.6500	5.27	0	42	0.042	1	U	R.GSHMVGGTIWTGK.G
3701	18 – 30	665.8363	1329.6581	1329.6500	6.08	0	42	0.039	1	U	R.GSHMVGGTIWTGK.G
3702	18 – 30	665.8364	1329.6582	1329.6500	6.21	0	26	1.9	1	U	R.GSHMVGGTIWTGK.G
3703	18 – 30	665.8364	1329.6582	1329.6500	6.22	0	32	0.45	1	U	R.GSHMVGGTIWTGK.G
3704	18 – 30	665.8380	1329.6614	1329.6500	8.60	0	37	0.15	1	U	R.GSHMVGGTIWTGK.G
3834	18 – 30	673.8292	1345.6438	1345.6449	-0.82	0	11	46	1	U	R.GSHMVGGTIWTGK.G + Oxidation (M)
3837	18 – 30	673.8305	1345.6465	1345.6449	1.17	0	41	0.049	1	U	R.GSHMVGGTIWTGK.G + Oxidation (M)
3838	18 – 30	673.8305	1345.6465	1345.6449	1.18	0	64	0.00029	1	U	R.GSHMVGGTIWTGK.G + Oxidation (M)
3840	18 – 30	449.5562	1345.6469	1345.6449	1.50	0	17	13	1	U	R.GSHMVGGTIWTGK.G + Oxidation (M)
3841	18 – 30	673.8307	1345.6469	1345.6449	1.52	0	68	0.00011	1	U	R.GSHMVGGTIWTGK.G + Oxidation (M)
3842	18 – 30	673.8309	1345.6473	1345.6449	1.76	0	42	0.04	1	U	R.GSHMVGGTIWTGK.G + Oxidation (M)
3843	18 – 30	449.5564	1345.6474	1345.6449	1.87	0	57	0.0013	1	U	R.GSHMVGGTIWTGK.G + Oxidation (M)
3844	18 – 30	673.8310	1345.6474	1345.6449	1.88	0	4	2.8e+002	2	U	R.GSHMVGGTIWTGK.G + Oxidation (M)
3845	18 – 30	449.5565	1345.6478	1345.6449	2.14	0	50	0.0062	1	U	R.GSHMVGGTIWTGK.G + Oxidation (M)
3846	18 – 30	673.8312	1345.6478	1345.6449	2.15	0	47	0.012	1	U	R.GSHMVGGTIWTGK.G + Oxidation (M)
3847	18 – 30	673.8314	1345.6483	1345.6449	2.53	0	58	0.0011	1	U	R.GSHMVGGTIWTGK.G + Oxidation (M)
3848	18 – 30	673.8315	1345.6484	1345.6449	2.57	0	56	0.0017	1	U	R.GSHMVGGTIWTGK.G + Oxidation (M)
3849	18 – 30	449.5568	1345.6485	1345.6449	2.70	0	45	0.021	1	U	R.GSHMVGGTIWTGK.G + Oxidation (M)
3850	18 – 30	449.5568	1345.6487	1345.6449	2.80	0	41	0.055	1	U	R.GSHMVGGTIWTGK.G + Oxidation (M)

MASCOT Search Results

Protein View: Mms6-TmCA-P114

gi|Mms6-TmCA-P114|Mms6-TmCA-P114

Database: inhouse
Score: 24134
Nominal mass (M,): 43991
Calculated pI: 6.79

Sequence similarity is available as **an NCBI BLAST search of Mms6-TmCA-P114 against nr**.

Search parameters

MS data file: C:\Users\mascot\Desktop\david mgf's\2017_127\P220170711_DSteer_2017127_MMS6TmCAP114.mgf
Enzyme: semiTrypsin: cuts C-term side of KR unless next residue is P.
Cleavage is semi-specific. (Peptide can be non-specific at one terminus only.)
Fixed modifications: **Carbamidomethyl (C)**

Protein sequence coverage: 90%

Matched peptides shown in ***bold red***.

```
  1 MGSSHHHHHH SSGMVGGTIW TGKGLGLGLG LGLGAWGPII LGVVGAGAVY
 51 AYMKSRDIES AQSDEEVELR DALAGGGGSG GGGSANNVAA PLIDLGAEAK
101 KQAQKSAATQ SAVPEKESAT KVAEKQKEPE EKAKPEPKKP PHWGYFGEEG
151 PQYWGELAPE FSTCKTGKNQ SPINLKPQTA VGTTSLPGFD VYYRETALKL
201 INNGHTLQVN IPLGSYIKIN GHRYELLQYH FHTPSEHQRD GFNYPMEMHL
251 VHKDGDGNLA VIAILFQEGE ENETLAKLMS FLPQTLKKQE IHESVKIHPA
301 KFFPADKKFY KYSGSLTTPP CSEGVYWMVF KQPIQASVTQ LEKMHEYLGS
351 NARPVQRQNA RTLLKSWPDR NRANTVYEFY GGGGSGGGGS QQRFEWEFEQ
401 Q
```

Unformatted sequence string: **401 residues** (for pasting into other applications).

Sort peptides by ◉ Residue Number ○ Increasing Mass ○ Decreasing Mass

Query	Start – End	Observed	Mr(expt)	Mr(calc)	ppm	M	Score	Expect	Rank	U	Peptide
1547	14 – 23	525.2775	1048.5404	1048.5376	2.71	0	46	0.055	1		G.MVGGTIWTGK.G
419	15 – 23	459.7561	917.4976	917.4971	0.55	0	51	0.018	1		M.VGGTIWTGK.G
58	16 – 23	410.2216	818.4287	818.4287	0.084	0	34	1.1	1		V.GGTIWTGK.G
257	24 – 33	435.2774	868.5403	868.5382	2.42	0	16	26	1		K.GLGLGLGLGL.G
535	24 – 34	463.7886	925.5627	925.5597	3.26	0	22	6.9	1		K.GLGLGLGLGLG.A
1349	24 – 35	499.3069	996.5992	996.5968	2.45	0	7	2.5e+002	8		K.GLGLGLGLGLGA.W
9955	24 – 52	1342.7613	2683.5081	2683.5102	-0.79	0	29	0.91	1		K.GLGLGLGLGLGAWGPIILGVVGAGAVYAY.M
9956	24 – 52	895.5117	2683.5134	2683.5102	1.19	0	34	0.26	1		K.GLGLGLGLGLGAWGPIILGVVGAGAVYAY.M
10425	24 – 54	981.8957	2942.6654	2942.6456	6.72	0	96	1.2e-007	1		K.GLGLGLGLGLGAWGPIILGVVGAGAVYAYMK.S
10699	24 – 56	1062.9412	3185.8017	3185.7787	7.22	1	86	1.2e-006	1		K.GLGLGLGLGLGAWGPIILGVVGAGAVYAYMKSR.D
2956	43 – 54	614.8262	1227.6378	1227.6322	4.57	0	74	7e-005	1		G.VVGAGAVYAYMK.S
1084	46 – 54	487.2459	972.4773	972.4739	3.52	0	65	0.00075	1		G.AGAVYAYMK.S
139	48 – 54	423.2157	844.4169	844.4153	1.87	0	17	46	1		G.AVYAYMK.S
6303	55 – 70	621.6291	1861.8655	1861.8653	0.078	1	65	0.00041	1		K.SRDIESAQSDEEVELR.D
6304	55 – 70	621.6291	1861.8655	1861.8653	0.10	1	46	0.035	1		K.SRDIESAQSDEEVELR.D
6305	55 – 70	931.9406	1861.8667	1861.8653	0.75	1	98	2.2e-007	1		K.SRDIESAQSDEEVELR.D
6306	55 – 70	621.6296	1861.8670	1861.8653	0.88	1	86	3.6e-006	1		K.SRDIESAQSDEEVELR.D
6307	55 – 70	466.4740	1861.8670	1861.8653	0.89	1	88	2.1e-006	1		K.SRDIESAQSDEEVELR.D
6308	55 – 70	931.9408	1861.8671	1861.8653	0.94	1	17	25	1		K.SRDIESAQSDEEVELR.D
6309	55 – 70	621.6302	1861.8689	1861.8653	1.92	1	63	0.00071	1		K.SRDIESAQSDEEVELR.D
6310	55 – 70	931.9423	1861.8700	1861.8653	2.54	1	10	1.4e+002	9		K.SRDIESAQSDEEVELR.D
6311	55 – 70	931.9423	1861.8701	1861.8653	2.57	1	83	6.2e-006	1		K.SRDIESAQSDEEVELR.D
6312	55 – 70	621.6310	1861.8713	1861.8653	3.21	1	81	1.1e-005	1		K.SRDIESAQSDEEVELR.D
6313	55 – 70	621.6313	1861.8720	1861.8653	3.60	1	48	0.022	1		K.SRDIESAQSDEEVELR.D
6314	55 – 70	621.6313	1861.8721	1861.8653	3.63	1	87	2.6e-006	1		K.SRDIESAQSDEEVELR.D
6315	55 – 70	931.9437	1861.8728	1861.8653	4.04	1	21	11	1		K.SRDIESAQSDEEVELR.D
6324	55 – 70	932.4317	1862.8489	1861.8653	528	1	20	14	1		K.SRDIESAQSDEEVELR.D
6325	55 – 70	621.9577	1862.8513	1861.8653	530	1	56	0.0035	1		K.SRDIESAQSDEEVELR.D
6327	55 – 70	622.2711	1863.7914	1861.8653	1034	1	39	0.13	1		K.SRDIESAQSDEEVELR.D
5915	56 – 70	592.6198	1774.8377	1774.8333	2.48	1	55	0.0046	1		S.RDIESAQSDEEVELR.D
5916	56 – 70	888.4272	1774.8398	1774.8333	3.64	1	47	0.029	1		S.RDIESAQSDEEVELR.D
4770	57 – 70	810.3477	1618.6808	1618.7322	-31.7	0	19	15	1		R.DIESAQSDEEVELR.D
4771	57 – 70	810.3570	1618.6994	1618.7322	-20.2	0	55	0.0043	1		R.DIESAQSDEEVELR.D
4773	57 – 70	810.3709	1618.7273	1618.7322	-3.03	0	67	0.00032	1		R.DIESAQSDEEVELR.D
4774	57 – 70	810.3723	1618.7301	1618.7322	-1.31	0	58	0.0024	1		R.DIESAQSDEEVELR.D
4776	57 – 70	810.3731	1618.7317	1618.7322	-0.29	0	34	0.62	1		R.DIESAQSDEEVELR.D
4777	57 – 70	810.3733	1618.7321	1618.7322	-0.066	0	8	2.4e+002	5		R.DIESAQSDEEVELR.D
4778	57 – 70	810.3734	1618.7322	1618.7322	0.025	0	89	2e-006	1		R.DIESAQSDEEVELR.D
4779	57 – 70	810.3739	1618.7332	1618.7322	0.63	0	38	0.24	1		R.DIESAQSDEEVELR.D
4780	57 – 70	540.5850	1618.7333	1618.7322	0.69	0	92	9.7e-007	1		R.DIESAQSDEEVELR.D
4781	57 – 70	405.6907	1618.7336	1618.7322	0.86	0	39	0.18	1		R.DIESAQSDEEVELR.D
4782	57 – 70	810.3745	1618.7345	1618.7322	1.40	0	103	8.3e-008	1		R.DIESAQSDEEVELR.D
4783	57 – 70	540.5854	1618.7345	1618.7322	1.43	0	87	2.8e-006	1		R.DIESAQSDEEVELR.D
4784	57 – 70	810.3746	1618.7346	1618.7322	1.46	0	103	7.9e-008	1		R.DIESAQSDEEVELR.D
4785	57 – 70	810.3748	1618.7350	1618.7322	1.76	0	94	5.4e-007	1		R.DIESAQSDEEVELR.D

MASCOT Search Results

Protein View: Mms6-BCA

gi|Mms6-BCA|Mms6-BCA

Database: inhouse
Score: 578
Nominal mass (M_r): 35764
Calculated pI: 5.99

Sequence similarity is available as **an NCBI BLAST search of Mms6-BCA against nr**.

Search parameters

MS data file: C:\Users\mascot\Desktop\david mgf's\2017_127\P220170711_DSteer_2017127_MMS6up.mgf
Enzyme: semiTrypsin: cuts C-term side of KR unless next residue is P.
Cleavage is semi-specific. (Peptide can be non-specific at one terminus only.)
Fixed modifications: **Carbamidomethyl (C)**

Protein sequence coverage: 81%

Matched peptides shown in ***bold red***.

```
  1 MVGGTIWTGK GLGLGLGLGL GAWGPIILGV VGAGAVYAYM KSRDIESAQS
 51 DEEVELRDAL AGGGGSGGGG SSHHWGYGKH NGPEHWHKDF PIANGERQSP
101 VDIDTKAVVQ DPALKPLALV YGEATSRRMV NNGHSFNVEY DDSQDKAVLK
151 DGPLTGTYRL VQFHFHWGSS DDQGSEHTVD RKKYAAELHL VHWNTKYGDF
201 GTAAQQPDGL AVVGVFLKVG DANPALQKVL DALDSIKTKG KSTDFPNFDP
251 GSLLPNVLDY WTYPGSLTTP PLLESVTWIV LKEPISVSSQ QMLKFRTLNF
301 NAEGEPELLM LANWRPAQPL KNRQVRGFPK
```

Unformatted sequence string: **330 residues** (for pasting into other applications).

Sort peptides by ◉ Residue Number ○ Increasing Mass ○ Decreasing Mass

Query	Start – End	Observed	Mr(expt)	Mr(calc)	ppm	M	Score	Expect	Rank	U	Peptide
5524	11 – 39	895.5107	2683.5103	2683.5102	0.060	0	69	8.7e-005	1		K.GLGLGLGLGLGAWGPIILGVVGAGAVYAY.M
5797	11 – 41	981.8973	2942.6702	2942.6456	8.36	0	88	7.6e-007	1		K.GLGLGLGLGLGAWGPIILGVVGAGAVYAYMK.S
6049	11 – 43	1063.2753	3186.8041	3185.7787	322	1	19	5.9	1		K.GLGLGLGLGLGAWGPIILGVVGAGAVYAYMKSR.D
4103	42 – 57	621.6312	1861.8716	1861.8653	3.39	1	31	1	1		K.SRDIESAQSDEEVELR.D
3297	44 – 57	810.3735	1618.7324	1618.7322	0.10	0	43	0.074	1		R.DIESAQSDEEVELR.D
3298	44 – 57	810.3743	1618.7340	1618.7322	1.13	0	101	1.2e-007	1		R.DIESAQSDEEVELR.D
3299	44 – 57	540.5854	1618.7342	1618.7322	1.26	0	54	0.0062	1		R.DIESAQSDEEVELR.D
3300	44 – 57	810.8665	1619.7184	1618.7322	609	0	11	1.2e+002	2		R.DIESAQSDEEVELR.D
4261	58 – 79	986.4381	1970.8616	1970.8620	-0.20	0	7	2.2e+002	1	U	R.DALAGGGGSGGGGSSHHWGYGK.H
4262	58 – 79	657.9615	1970.8625	1970.8620	0.29	0	17	24	1	U	R.DALAGGGGSGGGGSSHHWGYGK.H
1586	80 – 88	571.2679	1140.5213	1140.5213	0.018	0	23	8.8	1		K.HNGPEHWHK.D
1156	89 – 97	509.7514	1017.4882	1017.4879	0.30	0	16	62	1	U	K.DFPIANGER.Q
1157	89 – 97	509.7523	1017.4900	1017.4879	2.05	0	26	5.3	1	U	K.DFPIANGER.Q
1107	98 – 106	501.7587	1001.5028	1001.5029	-0.18	0	40	0.26	1	U	R.QSPVDIDTK.A
4583	107 – 127	733.4099	2197.2079	2197.2106	-1.26	0	41	0.071	1	U	K.AVVQDPALKPLALVYGEATSR.R
4584	107 – 127	733.4115	2197.2127	2197.2106	0.93	0	24	4.2	1	U	K.AVVQDPALKPLALVYGEATSR.R
940	151 – 159	490.2450	978.4754	978.4771	-1.65	0	21	17	1	U	K.DGPLTGTYR.L
4466	160 – 177	704.9784	2111.9133	2111.9086	2.21	0	11	76	2	U	R.LVQFHFHWGSSDDQGSEH.T
5413	160 – 181	862.0583	2583.1531	2583.1528	0.12	0	55	0.0027	1	U	R.LVQFHFHWGSSDDQGSEHTVDR.K
5414	160 – 181	517.6379	2583.1531	2583.1528	0.14	0	7	1.5e+002	1	U	R.LVQFHFHWGSSDDQGSEHTVDR.K
5416	160 – 181	646.7958	2583.1543	2583.1528	0.59	0	2	5e+002	1	U	R.LVQFHFHWGSSDDQGSEHTVDR.K
3689	183 – 196	855.9584	1709.9022	1708.9049	584	1	19	19	1		K.KYAAELHLVHWNTK.Y
3690	183 – 196	570.9751	1709.9035	1708.9049	584	1	32	0.96	1		K.KYAAELHLVHWNTK.Y
3110	184 – 196	527.9439	1580.8100	1580.8099	0.023	0	21	12	1		K.YAAELHLVHWNTK.Y
3111	184 – 196	396.2098	1580.8101	1580.8099	0.10	0	12	1.1e+002	1		K.YAAELHLVHWNTK.Y
3112	184 – 196	527.9443	1580.8110	1580.8099	0.67	0	5	5e+002	1		K.YAAELHLVHWNTK.Y
3113	184 – 196	791.4132	1580.8118	1580.8099	1.18	0	56	0.0043	1		K.YAAELHLVHWNTK.Y
3114	184 – 196	791.4135	1580.8125	1580.8099	1.61	0	30	1.7	1		K.YAAELHLVHWNTK.Y
4766	197 – 218	751.7230	2252.1472	2252.1478	-0.26	0	5	3.6e+002	1	U	K.YGDFGTAAQQPDGLAVVGVFLK.V
4767	197 – 218	751.7254	2252.1544	2252.1478	2.94	0	29	1.2	1	U	K.YGDFGTAAQQPDGLAVVGVFLK.V
4768	197 – 218	1127.0898	2252.1650	2252.1478	7.67	0	39	0.14	1	U	K.YGDFGTAAQQPDGLAVVGVFLK.V
4774	197 – 218	752.3950	2254.1632	2252.1478	895	0	47	0.022	1	U	K.YGDFGTAAQQPDGLAVVGVFLK.V
6094	197 – 228	1083.2296	3246.6670	3245.6721	307	1	12	32	1	U	K.YGDFGTAAQQPDGLAVVGVFLKVGDANPALQK.V
6095	197 – 228	812.6747	3246.6697	3245.6721	307	1	4	2.2e+002	1	U	K.YGDFGTAAQQPDGLAVVGVFLKVGDANPALQK.V
1110	209 – 218	501.8223	1001.6301	1001.6274	2.75	0	38	0.17	1	U	D.GLAVVGVFLK.V
1135	219 – 228	506.7754	1011.5362	1011.5349	1.24	0	8	3.3e+002	3	U	K.VGDANPALQK.V
913	229 – 237	487.2818	972.5490	972.5491	-0.11	0	20	19	1	U	K.VLDALDSIK.T
914	229 – 237	487.2819	972.5492	972.5491	0.059	0	41	0.17	1	U	K.VLDALDSIK.T
915	229 – 237	487.2822	972.5498	972.5491	0.65	0	25	7	1	U	K.VLDALDSIK.T
916	229 – 237	487.2825	972.5504	972.5491	1.29	0	23	11	1	U	K.VLDALDSIK.T
7505	242 – 282	1149.1017	4592.3775	4592.3407	8.01	0	35	0.08	1	U	K.STDFPNFDPGSLLPNVLDYWTYPGSLTTPPLLESVTWIVLK.E
7506	242 – 282	1532.4686	4594.3840	4592.3407	445	0	64	9.2e-005	1	U	K.STDFPNFDPGSLLPNVLDYWTYPGSLTTPPLLESVTWIVLK.E
5871	257 – 282	998.5507	2992.6303	2990.6045	677	0	12	37	1	U	N.VLDYWTYPGSLTTPPLLESVTWIVLK.E
4644	297 – 315	740.3716	2218.0930	2217.0888	453	0	36	0.28	1	U	R.TLNFNAEGEPELLMLANWR.P
4645	297 – 315	1110.0551	2218.0956	2217.0888	454	0	49	0.013	1	U	R.TLNFNAEGEPELLMLANWR.P
5708	297 – 321	951.8307	2852.4703	2851.4690	351	0	32	0.46	1	U	R.TLNFNAEGEPELLMLANWRPAQPLK.N

MASCOT Search Results

Protein View: Mms6-BCA-P114

gi|Mms6-BCA-P114|Mms6-BCA-P114

Database: inhouse
Score: 31326
Nominal mass (M_r): 37930
Calculated pI: 5.77

Sequence similarity is available as **an NCBI BLAST search of Mms6-BCA-P114 against nr**.

Search parameters

MS data file: C:\Users\mascot\Desktop\david mgf's\2017_127\P220170711_DSteer_2017127_MMS6BCAP114.mgf
Enzyme: semiTrypsin: cuts C-term side of KR unless next residue is P.
Cleavage is semi-specific. (Peptide can be non-specific at one terminus only.)
Fixed modifications: **Carbamidomethyl (C)**

Protein sequence coverage: 98%

Matched peptides shown in ***bold red***.

```
  1 MVGGTIWTGK GLGLGLGLGL GAWGPIILGV VGAGAVYAYM KSRDIESAQS
 51 DEEVELRDAL AGGGGSGGGG SSHHWGYGKH NGPEHWHKDF PIANGERQSP
101 VDIDTKAVVQ DPALKPLALV YGEATSRRMV NNGHSFNVEY DDSQDKAVLK
151 DGPLTGTYRL VQFHFHWGSS DDQGSEHTVD RKKYAAELHL VHWNTKYGDF
201 GTAAQQPDGL AVVGVFLKVG DANPALQKVL DALDSIKTKG KSTDFPNFDP
251 GSLLPNVLDY WTYPGSLTTP PLLESVTWIV LKEPISVSSQ QMLKFRTLNF
301 NAEGEPELLM LANWRPAQPL KNRQVRGFPK GGGGSGGGGS QQRFEWEFEQ
351 Q
```

Unformatted sequence string: **351 residues** (for pasting into other applications).

Sort peptides by ◉ Residue Number ○ Increasing Mass ○ Decreasing Mass

Query	Start – End	Observed	Mr(expt)	Mr(calc)	ppm	M	Score	Expect	Rank	U	Peptide
1867	1 – 10	525.2759	1048.5373	1048.5376	-0.27	0	48	0.036	1		-.MVGGTIWTGK.G
514	2 – 10	459.7564	917.4983	917.4971	1.31	0	62	0.0015	1		M.VGGTIWTGK.G
314	11 – 20	435.2779	868.5412	868.5382	3.48	0	23	4.8	1		K.GLGLGLGLGL.G
1482	11 – 22	499.3075	996.6005	996.5968	3.69	0	13	53	3		K.GLGLGLGLGLGA.W
7055	11 – 33	1030.6192	2059.2239	2059.2194	2.18	0	15	22	1		K.GLGLGLGLGLGAWGPIILGVVGA.G
9145	11 – 37	817.4770	2449.4093	2449.4097	-0.18	0	52	0.0041	1		K.GLGLGLGLGLGAWGPIILGVVGAGAVY.A
9146	11 – 37	1225.7140	2449.4135	2449.4097	1.52	0	14	24	1		K.GLGLGLGLGLGAWGPIILGVVGAGAVY.A
10141	11 – 39	1342.7652	2683.5158	2683.5102	2.08	0	58	0.001	1		K.GLGLGLGLGLGAWGPIILGVVGAGAVYAY.M
10142	11 – 39	895.5133	2683.5182	2683.5102	2.99	0	16	17	1		K.GLGLGLGLGLGAWGPIILGVVGAGAVYAY.M
10143	11 – 39	895.5140	2683.5203	2683.5102	3.78	0	11	48	1		K.GLGLGLGLGLGAWGPIILGVVGAGAVYAY.M
10144	11 – 39	895.5143	2683.5212	2683.5102	4.11	0	0	6e+002	3		K.GLGLGLGLGLGAWGPIILGVVGAGAVYAY.M
10160	11 – 39	896.1789	2685.5149	2683.5102	747	0	42	0.045	1		K.GLGLGLGLGLGAWGPIILGVVGAGAVYAY.M
11103	11 – 41	981.8912	2942.6516	2942.6456	2.05	0	77	1.2e-005	1		K.GLGLGLGLGLGAWGPIILGVVGAGAVYAYMK.S
11107	11 – 41	982.2232	2943.6478	2942.6456	341	0	8	92	1		K.GLGLGLGLGLGAWGPIILGVVGAGAVYAYMK.S
5992	24 – 41	889.9984	1777.9823	1777.9801	1.27	0	10	1.4e+002	1		W.GPIILGVVGAGAVYAYMK.S
6278	42 – 57	931.9374	1861.8603	1861.8653	-2.71	1	41	0.12	1		K.SRDIESAQSDEEVELR.D
6279	42 – 57	931.9398	1861.8650	1861.8653	-0.15	1	96	3.7e-007	1		K.SRDIESAQSDEEVELR.D
6280	42 – 57	466.4736	1861.8652	1861.8653	-0.087	1	74	5.1e-005	1		K.SRDIESAQSDEEVELR.D
6281	42 – 57	931.9402	1861.8659	1861.8653	0.33	1	78	2.3e-005	1		K.SRDIESAQSDEEVELR.D
6282	42 – 57	621.6297	1861.8674	1861.8653	1.10	1	59	0.0015	1		K.SRDIESAQSDEEVELR.D
6283	42 – 57	621.6298	1861.8677	1861.8653	1.27	1	79	1.6e-005	1		K.SRDIESAQSDEEVELR.D
6284	42 – 57	931.9417	1861.8688	1861.8653	1.86	1	69	0.00019	1		K.SRDIESAQSDEEVELR.D
6285	42 – 57	621.6303	1861.8692	1861.8653	2.06	1	66	0.00034	1		K.SRDIESAQSDEEVELR.D
6286	42 – 57	621.6303	1861.8692	1861.8653	2.07	1	78	2.2e-005	1		K.SRDIESAQSDEEVELR.D
6287	42 – 57	621.6303	1861.8692	1861.8653	2.09	1	72	9.2e-005	1		K.SRDIESAQSDEEVELR.D
6290	42 – 57	621.9572	1862.8496	1861.8653	529	1	41	0.12	1		K.SRDIESAQSDEEVELR.D
6292	42 – 57	932.4327	1862.8508	1861.8653	529	1	32	0.88	1		K.SRDIESAQSDEEVELR.D
5103	44 – 57	810.3471	1618.6797	1618.7322	-32.5	0	12	64	1		R.DIESAQSDEEVELR.D
5104	44 – 57	810.3720	1618.7295	1618.7322	-1.66	0	96	3.3e-007	1		R.DIESAQSDEEVELR.D
5105	44 – 57	810.3725	1618.7304	1618.7322	-1.14	0	74	5.4e-005	1		R.DIESAQSDEEVELR.D
5106	44 – 57	810.3727	1618.7308	1618.7322	-0.86	0	102	8.6e-008	1		R.DIESAQSDEEVELR.D
5107	44 – 57	405.6900	1618.7309	1618.7322	-0.80	0	56	0.0038	1		R.DIESAQSDEEVELR.D
5108	44 – 57	810.3728	1618.7310	1618.7322	-0.72	0	89	1.9e-006	1		R.DIESAQSDEEVELR.D
5109	44 – 57	540.5845	1618.7317	1618.7322	-0.33	0	79	1.9e-005	1		R.DIESAQSDEEVELR.D
5110	44 – 57	810.3731	1618.7317	1618.7322	-0.33	0	89	1.8e-006	1		R.DIESAQSDEEVELR.D
5111	44 – 57	540.5845	1618.7318	1618.7322	-0.24	0	75	5.2e-005	1		R.DIESAQSDEEVELR.D
5112	44 – 57	810.3732	1618.7319	1618.7322	-0.16	0	97	2.8e-007	1		R.DIESAQSDEEVELR.D
5113	44 – 57	540.5846	1618.7321	1618.7322	-0.083	0	78	2.1e-005	1		R.DIESAQSDEEVELR.D
5114	44 – 57	810.3734	1618.7322	1618.7322	-0.00062	0	91	1.1e-006	1		R.DIESAQSDEEVELR.D
5115	44 – 57	810.3734	1618.7323	1618.7322	0.056	0	89	1.9e-006	1		R.DIESAQSDEEVELR.D
5116	44 – 57	810.3735	1618.7324	1618.7322	0.10	0	92	1e-006	1		R.DIESAQSDEEVELR.D
5118	44 – 57	810.3737	1618.7328	1618.7322	0.39	0	102	8.8e-008	1		R.DIESAQSDEEVELR.D
5120	44 – 57	810.3737	1618.7329	1618.7322	0.43	0	103	7.7e-008	1		R.DIESAQSDEEVELR.D
5121	44 – 57	810.3738	1618.7330	1618.7322	0.47	0	100	1.4e-007	1		R.DIESAQSDEEVELR.D
5122	44 – 57	810.3738	1618.7330	1618.7322	0.49	0	103	8e-008	1		R.DIESAQSDEEVELR.D
5123	44 – 57	540.5850	1618.7331	1618.7322	0.53	0	31	1.1	1		R.DIESAQSDEEVELR.D
5124	44 – 57	810.3739	1618.7332	1618.7322	0.62	0	103	7.8e-008	1		R.DIESAQSDEEVELR.D

MASCOT Search Results

Protein View: MMS6C-BCA-P114|MMS6C-BCA-P114

gi|MMS6C-BCA-P114|MMS6C-BCA-P114

Database: inhouse
Score: 2472
Nominal mass (M_r): 34762
Calculated pI: 5.66

Sequence similarity is available as an NCBI BLAST search of MMS6C-BCA-P114|MMS6C-BCA-P114 against nr.

Search parameters

MS data file: C:\Users\mascot\Desktop\david mgf's\2016_086\BCA_1-B,8_01_12584.mgf
Enzyme: semiTrypsin: cuts C-term side of KR unless next residue is P.
Cleavage is semi-specific. (Peptide can be non-specific at one terminus only.)
Fixed modifications: Carbamidomethyl (C)

Protein sequence coverage: 86%

Matched peptides shown in ***bold red***.

```
  1 MYAYMKSRDI ESAQSDEEVE LRDALAGGGG SGGGGSSHHW GYGKHNGPEH
 51 WHKDFPIANG ERQSPVDIDT KAVVQDPALK PLALVYGEAT SRRMVNNGHS
101 FNVEYDDSQD KAVLKDGPLT GTYRLVQFHF HWGSSDDQGS EHTVDRKKYA
151 AELHLVHWNT KYGDFGTAAQ QPDGLAVVGV FLKVGDANPA LQKVLDALDS
201 IKTKGKSTDF PNFDPGSLLP NVLDYWTYPG SLTTPPLLES VTWIVLKEPI
251 SVSSQQMLKF RTLNFNAEGE PELLMLANWR PAQPLKNRQV RGFPKGGGGS
301 GGGGSQQRFE WEFEQQ
```

Unformatted sequence string: **316 residues** (for pasting into other applications)

Sort peptides by ◉ Residue Number ○ Increasing Mass ○ Decreasing Mass

Query	Start - End	Observed	Mr(expt)	Mr(calc)	ppm	M	Score	Expect	Rank	U	Peptide
468	9 - 22	810.3722	1618.7299	1618.7322	-1.44	0	85	2.6e-006	1	U	R.DIESAQSDEEVELR.D
469	9 - 22	810.3757	1618.7369	1618.7322	2.93	0	112	5e-009	1	U	R.DIESAQSDEEVELR.D
208	14 - 22	552.7833	1103.5520	1103.5095	38.5	0	18	36	1	U	A.QSDEEVELR.D
313	23 - 38	622.2682	1242.5219	1242.5225	-0.47	0	45	0.017	1	U	R.DALAGGGGSGGGGSSH.H
377	23 - 39	690.7992	1379.5839	1379.5815	1.78	0	59	0.00064	1	U	R.DALAGGGGSGGGGSSHH.W
513	23 - 42	893.8807	1785.7468	1785.7456	0.72	0	36	0.094	1	U	R.DALAGGGGSGGGGSSHHWGY.G
557	23 - 44	986.4523	1970.8900	1970.8620	14.2	0	49	0.0091	1	U	R.DALAGGGGSGGGGSSHHWGYGK.H
558	23 - 44	657.9706	1970.8900	1970.8620	14.2	0	98	1.1e-007	1	U	R.DALAGGGGSGGGGSSHHWGYGK.H
512	25 - 44	595.9388	1784.7946	1784.7979	-1.86	0	70	6.5e-005	1	U	A.LAGGGGSGGGGSSHHWGYGK.H
244	45 - 53	381.1783	1140.5131	1140.5213	-7.23	0	10	80	2	U	K.HNGPEHWHK.D
245	45 - 53	571.2667	1140.5188	1140.5213	-2.22	0	26	2.2	1	U	K.HNGPEHWHK.D
248	45 - 53	571.7579	1141.5012	1140.5213	859	0	23	3.4	1	U	K.HNGPEHWHK.D
170	54 - 62	509.7487	1017.4828	1017.4879	-5.07	0	48	0.021	1	U	K.DFPIANGER.Q
156	63 - 71	501.7642	1001.5138	1001.5029	10.8	0	51	0.012	1	U	R.QSPVDIDTK.A
256	72 - 82	575.8441	1149.6736	1149.6758	-1.83	0	39	0.074	1	U	K.AVVQDPALKPL.A
257	72 - 82	575.8456	1149.6766	1149.6758	0.73	0	38	0.093	1	U	K.AVVQDPALKPL.A
348	72 - 84	667.9089	1333.8033	1333.7969	4.80	0	54	0.0011	1	U	K.AVVQDPALKPLAL.V
626	72 - 92	733.4069	2197.1988	2197.2106	-5.37	0	4	2.3e+002	1	U	K.AVVQDPALKPLALVYGEATSR.R
628	72 - 92	733.4227	2197.2463	2197.2106	16.2	0	89	4.3e-007	1	U	K.AVVQDPALKPLALVYGEATSR.R
483	77 - 92	562.6567	1684.9482	1684.9512	-1.76	0	68	0.0001	1	U	D.PALKPLALVYGEATSR.R
326	81 - 92	638.8438	1275.6730	1275.6823	-7.24	0	11	1.1e+002	2	U	K.PLALVYGEATSR.R
327	81 - 92	638.8484	1275.6822	1275.6823	-0.026	0	63	0.00062	1	U	K.PLALVYGEATSR.R
197	83 - 92	533.7783	1065.5420	1065.5455	-3.20	0	66	0.00032	1	U	L.ALVYGEATSR.R
114	85 - 92	441.7170	881.4195	881.4243	-5.38	0	42	0.081	1	U	L.VYGEATSR.R
592	94 - 111	1049.9423	2097.8701	2097.8698	0.13	0	57	0.0006	1	U	R.MVNNGHSFNVEYDDSQDK.A
593	94 - 111	700.2980	2097.8723	2097.8698	1.20	0	93	1.5e-007	1	U	R.MVNNGHSFNVEYDDSQDK.A
594	94 - 111	700.6280	2098.8620	2097.8698	473	0	71	1.9e-005	1	U	R.MVNNGHSFNVEYDDSQDK.A
595	94 - 111	1050.4394	2098.8642	2097.8698	474	0	29	0.33	1	U	R.MVNNGHSFNVEYDDSQDK.A
506	97 - 111	877.8646	1753.7147	1753.7180	-1.88	0	22	1.8	1	U	N.NGHSFNVEYDDSQDK.A
401	100 - 111	723.8033	1445.5920	1445.5947	-1.82	0	55	0.0011	1	U	H.SFNVEYDDSQDK.A
145	116 - 124	490.2508	978.4870	978.4771	10.1	0	53	0.0072	1	U	K.DGPLTGTYR.L
95	125 - 130	395.7120	789.4094	789.4174	-10.1	0	19	24	1	U	R.LVQFHF.H
96	125 - 130	790.4169	789.4096	789.4174	-9.87	0	16	47	1	U	R.LVQFHF.H
126	125 - 131	464.2430	926.4714	926.4763	-5.27	0	27	2.6	1	U	R.LVQFHFH.W
695	125 - 146	646.7950	2583.1511	2583.1528	-0.66	0	72	3.3e-005	1	U	R.LVQFHFHWGSSDDQGSEHTVDR.K
696	125 - 146	517.6431	2583.1789	2583.1528	10.1	0	28	0.95	1	U	R.LVQFHFHWGSSDDQGSEHTVDR.K
697	125 - 146	646.8023	2583.1800	2583.1528	10.6	0	109	7.8e-009	1	U	R.LVQFHFHWGSSDDQGSEHTVDR.K
698	125 - 146	862.0673	2583.1800	2583.1528	10.6	0	134	2.3e-011	1	U	R.LVQFHFHWGSSDDQGSEHTVDR.K
690	126 - 146	824.3646	2470.0720	2470.0687	1.33	0	77	7.5e-006	1	U	L.VQFHFHWGSSDDQGSEHTVDR.K
691	126 - 146	618.5253	2470.0720	2470.0687	1.33	0	63	0.00022	1	U	L.VQFHFHWGSSDDQGSEHTVDR.K
651	128 - 146	748.6564	2242.9475	2242.9417	2.60	0	20	3.4	1	U	Q.FHFHWGSSDDQGSEHTVDR.K
652	128 - 146	561.7442	2242.9475	2242.9417	2.60	0	19	4.1	1	U	Q.FHFHWGSSDDQGSEHTVDR.K
590	129 - 146	524.9795	2095.8888	2095.8733	7.40	0	75	1.2e-005	1	U	F.HFHWGSSDDQGSEHTVDR.K
591	129 - 146	699.6369	2095.8888	2095.8733	7.40	0	105	1.3e-008	1	U	F.HFHWGSSDDQGSEHTVDR.K
550	130 - 146	980.4226	1958.8307	1958.8144	8.37	0	43	0.019	1	U	H.FHWGSSDDQGSEHTVDR.K
551	130 - 146	653.9510	1958.8313	1958.8144	8.63	0	105	1.3e-008	1	U	H.FHWGSSDDQGSEHTVDR.K
519	131 - 146	604.9227	1811.7463	1811.7459	0.18	0	69	3.8e-005	1	U	F.HWGSSDDQGSEHTVDR.K
482	132 - 146	559.2362	1674.6868	1674.6870	-0.15	0	64	0.00012	1	U	H.WGSSDDQGSEHTVDR.K